Trace element cycling in Bangladesh shrimp aquaculture systems: Implications for food and water security

By

Matthew John Dietrich

Dissertation

Submitted to the Faculty of the

Graduate School of Vanderbilt University

in partial fulfillment of the requirements

for the degree of

DOCTOR OF PHILOSOPHY

in

Earth and Environmental Sciences

June 30, 2021

Nashville, Tennessee

Approved:

John C. Ayers, Ph.D.
Steven L. Goodbred, Ph.D.
Jessica L. Oster, Ph.D.
Alan R. Bowers, Ph.D.
Jonathan M. Gilligan, Ph.D.

ACKNOWLEDGEMENTS

I owe so many people thanks for their support on this wild PhD journey. Obviously, whatever I write here will not fully capture my gratitude, but I'll give it a shot.

First, I owe my family everything for supporting me on this journey. They always supported my educational endeavors, and for that, I couldn't be more grateful. I particularly thank my Grandpa, Dr. Dietrich for serving as a "PhD role model" regarding how to be a family man, man of strong Christian faith, man of the outdoors, man of good health, and a man of science. You and Grandma Dietrich have been an inspiration to me through your support and kindness. To my Grandma and Grandpa Prominski, I will miss you forever, and your support of all my endeavors meant so much to me. To my parents and brother Josh, you have always been there when I needed you and have helped keep me going when the going gets tough. I couldn't have done this without you. I love you all, now and forever.

I am also so thankful for all my friends and colleagues in Nashville who have provided camaraderie and support on this journey. To my friends in the department, both past and present, thank you for the Kay Bob's adventures and fun chats in the grad room and around Stevenson. Thanks especially to Chris, Moyo, David, Cam, and Jess, for letting me bombarde you with questions and send random research papers. I am also extremely thankful for the running community I have found in Nashville, which has helped keep me sane, particularly during the times of COVID-19. Joey, Ricky, Matt, Brent, Yuri, Nick, Steven… the list goes on. Thank you for giving me a life outside of graduate school. And lastly, to my roommates over the years in Nashville. Carsen, Alan, Eric, thank you for being great company and helping me grind through the PhD even during Covid when we were all stuck at home.

I deeply owe the Earth and Environmental Science Department at Vanderbilt. Thank you for providing me the opportunity to explore so many different research avenues and feed my intellectual curiosity. I have learned more in my four years here than I have ever learned before. Special thanks to my advisor, John. You have helped me grow so much as a scientist and have been a great example of how to be an amazing researcher. My trips to Bangladesh would not have been possible without you. I also need to thank my committee, Steve, Jessica, Alan, and Jonathan, for their great support and advice during my PhD, as well as all the staff in the department who have helped my PhD come to fruition over the years. Gale, Dallas, Chantry, and Jewell, thank you so much for your tireless support, especially when there were times I was ordering lab materials every other day it seemed. Lastly, none of my work would have been possible without the laboratory assistance of Rossane, Richard, Sunny, and James. Thank you for helping process so many of my samples and dealing with my unending abundance of questions.

Lastly, I owe all of my Bangladeshi friends, colleagues, and Coastal SEES collaborators a deep debut of gratitude. None of my research would have been possible without them. I owe Jess and Kelsea much thanks for not only helping me gather samples, but falling in a shrimp pond for me! I particularly owe all my sampling success in Bangladesh to Zahid, who not only proved to be the most helpful field assistant, translator, and guide, but a good friend as well. Much appreciation goes out to the great crew at Pugmark Tours, particularly Bachchu, for taking great care of our research teams and making sure I always got to the sampling locations that I needed

to get to. Lastly, to my friends at Dhaka University, Saddam and Abrar, I thank you so much for your kindness and hospitality that allowed me to both feel welcome and be able to process my samples before heading back to the United States.

My work was supported through the National Science Foundation NSF Coastal SEES Collaborative Research Grant OCE-1600319.

Table of Contents

LIST OF TABLES

LIST OF FIGURES

CHAPTER I

INTRODUCTION

1.1 Background

Bangladesh is one of the most densely populated countries in the world, but has serious concerns in regards to water security. Specifically, Bangladesh sits within the Ganges—Brahmaputra—Meghna delta and supports more than 160 million people, which is anticipated to approach 180 million in 2025 (Uddin et al., 2019 and the references therein). However, particularly in Southwest Bangladesh (Fig. 1), both groundwater and surface water quality are threatened by arsenic (As), manganese (Mn), and high salinity due to saltwater influence from the Bay of Bengal (e.g., Ayers et al., 2017, 2016; Hasan & Ashraf Ali, 2010). Additionally, Southwest Bangladesh is particularly vulnerable to stresses on water security from climatic changes and surface water chemistry/quality routinely fluctuates between seasons because of Bangladesh's monsoonal climate (e.g., Benneyworth et al., 2016; Roy et al., 2018), where approximately 80% of the total annual rainfall in Bangladesh occurs from June to September (e.g., Chowdhury, 2010).

Although a significant amount of research has been done in Southwest Bangladesh and Bangladesh in general regarding trace element contamination (primarily As) of groundwater (e.g., Anawar et al., 2003; Ayers et al., 2016; Neumann et al., 2009), relatively little comprehensive research has been performed on Southwest Bangladesh surface water chemistry (e.g., Akter & Ahmed, 2019; Roy et al., 2018; Shammi et al., 2017), particularly near the Bay of Bengal (BoB) and the Sundarbans mangrove forest. Only one published study has completed a detailed geochemical examination of multiple trace elements in Southwest Bangladesh surface waters over multiple seasons (Ayers et al., 2017).

In coastal Southwest Bangladesh, rice agriculture and shrimp aquaculture are prevalent (e.g., Barai et al., 2019; Kabir et al., 2016). Shrimp farming has increased in the region within the last 10-15 years (Barai et al., 2019), with the practice of rotational farming popular in Southwest Bangladesh, where shrimp are raised in ponds during the dry season, and rice is grown in paddies during the wet season when tidal channel waters are less saline (e.g., Ayers et al., 2017; Azad et al., 2009). Water is essential to agriculture and aquaculture, and surface water from tidal channels is commonly used for irrigation of both rice paddies and shrimp farms in Southwest Bangladesh (Ayers et al., 2017), although there is local variation in farming practices. Thus, the concentrations of trace elements as well as other ions in surface water used for irrigation is relevant to the health of local agriculture and aquaculture systems.

Trace elements such as As and Mn of are particular concern because of their known adverse human health effects when consumed in excess quantities. For example, As is very well categorized as a toxin to humans (e.g., Bowell et al., 2014; Hughes, 2002), and overexposure to Mn can affect the central nervous system, resulting in symptoms similar to that of Parkinson's disease or cognitive impairment in children (e.g., Frisbie et al., 2012; Rahman et al., 2017). Trace elements can also adversely affect ecosystems. For example, excess selenium (Se) bioaccumulation in fish and birds can lead to toxic effects such as teratogenesis and reduced

growth (e.g., Hamilton, 2004), and excess As bioaccumulation is toxic to biota as well (e.g., Eisler, 1994). Although predominantly found in groundwater in Bangladesh, high levels of As and Mn can still be found in surface waters, particularly during the dry season within tidal channels (As) and shrimp ponds (As and Mn) in Southwest Bangladesh (Ayers et al., 2017). Because of the prevalence of arsenic in Bangladesh (e.g., Anawar et al., 2003), the detailed documentation of both its acute and chronic toxicity (e.g., Hughes, 2002), and the inadequate study of arsenic in surface waters, arsenic is one of the elements of focus in this dissertation.

Elevated levels of As in surface waters can come from a variety of sources, such as from geothermal springs, arsenic-rich groundwaters, mine waste, or industrial waste discharge (Smedley and Kinniburgh, 2002). However, in Bangladesh, there is some debate about the underlying causes of enriched As in surface waters. Ayers et al., 2017 attributes elevated surface water As in Southwest Bangladesh to several possible causes (i.e., groundwater exfiltration; groundwater irrigation from upstream; remobilization of As from sediments after transport from the Himalayas via Fe-oxyhydroxides), albeit no explanations entail anthropogenically derived As.

Bhuiyan et al., 2015 attributes high levels of As in the Buriganga River near Dhaka, Bangladesh to be primarily from anthropogenic sources, with 48% of the variability in As concentrations likely coming from municipal wastes and phosphate fertilizers. Saha et al., 2017 looked at several metals (and As) and how their concentrations varied spatially from a major industrial zone just north of Dhaka. Saha et al., 2017 found significant decreases in the concentrations of Pb, Ni, Cr, Zn, Cu and Cd away from the industrial zone, but not for As or Mn. They ascribed As and Mn to geogenic sourcing because of the lack of spatial trends and separate grouping in principle component analysis (PCA) results, although did not elaborate further on this hypothesis. Part of this dissertation will therefore focus on trying to better constrain the transport and nature of As as a pollutant in Bangladesh waterways, in addition to other trace elements that may be of health concern, such as Se.

Understanding the partitioning between the solid and aqueous phase of trace elements is essential in interpreting the mobility and transport of these elements in the environment. A partition coefficient (Kd) represents the ratio between the concentration of an element in the solid phase over the concentration of an element in the aqueous phase: $Kd_{solid/aqueous} = C_{solid}/C_{aqueous}$. Kd values can be used to describe partitioning between suspended sediments and surface water or between deposited surface sediments and surface water, with the surface water element concentrations essentially representing the more bio accessible/mobile fraction of elements in a system (aqueous phase). Kd values can be influenced by a variety of factors, such as pH, dissolved organic carbon (DOC) and cation-exchange capacity (CEC) of sediment (Gooddy et al., 1995; Janssen et al., 1997; Van den Hoop, 1995). Thus, evaluating geochemical properties of sediment and water in a system is paramount to understanding possible effects on element partitioning and thus element transport and mobility.

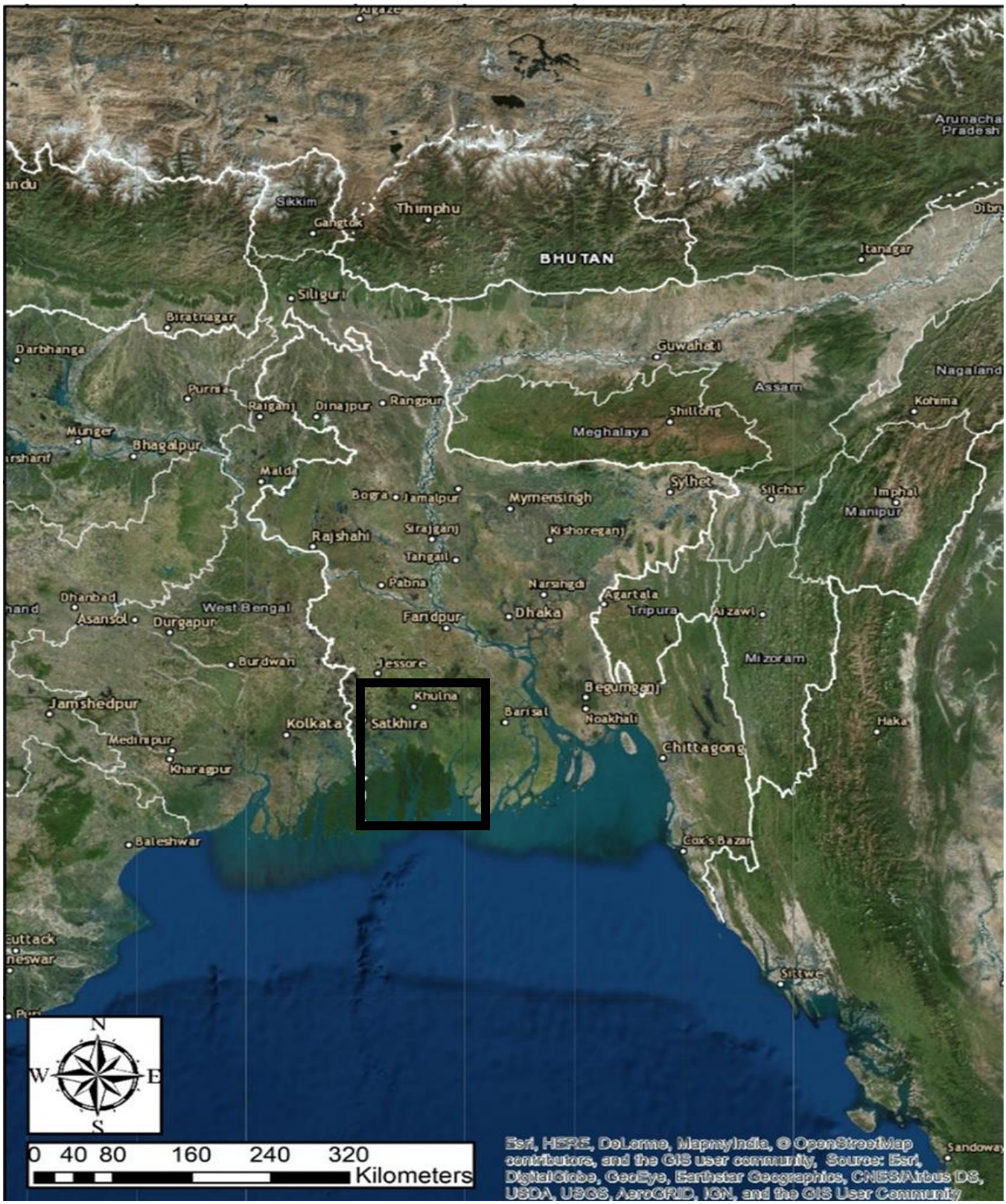

Figure 1: Location of Southwest Bangladesh outlined in black.

1.2 Research objectives and overview

The overall prevailing theme of this dissertation is to holistically characterize the geochemical system in Southwest Bangladesh to get a better grasp on the transport, mobility and fate of trace elements such as As. One must fully understand the passive (stationary, geochemical processes) and active (mixing and physical transport) processes (Fig. 2) at work in Southwest Bangladesh in order to prevent or mitigate potentially harmful accumulation of trace elements in the environment. The primary research objectives by chapter include:

II. Characterize the surface water chemistry in Southwest Bangladesh (particularly aquaculture shrimp ponds) and assess the effects of seasonal variation, irrigation, evaporation, dilution, mixing, and pollution; identify the geochemical controls on trace metal(loid)s such as As and Se.

III. Characterize the main input system of shrimp ponds in Southwest Bangladesh, tidal channels, using in situ field measurements, GIS to evaluate potential pollutant sources (e.g., Khulna City), geochemical/mineralogical analysis of suspended sediment, and comparison of elemental compositions in the suspended load to the dissolved load during seawater mixing.

IV. Investigate element partitioning between important environmental media within aquaculture shrimp ponds, including the sediment, pond water and shrimp, particularly to assess whether shrimp are accumulating toxic trace elements, which may pose a health hazard to consumers.

Chapter II looks at statistically predicting aquaculture shrimp pond and tidal channel water trace element concentrations. With only 3-4 independent variables, Se and As dissolved concentrations can be moderately predicted. Furthermore, this chapter examines how certain processes are essential to water chemistry, such as seasonal water dilution, evaporation, and irrigation source. It is shown how even early wet season monsoonal rains begin to dilute most element concentrations, but this is more pronounced in tidal channel waters compared to shrimp ponds. Furthermore, As and Se may have an important relationship in regard to toxicity, which is discussed. This work preludes the importance of looking at other components of the shrimp pond system, sediment and the shrimp, to gain a better understanding of geochemical partitioning in the natural environment.

Chapter III focuses on the main input into shrimp ponds in Southwest Bangladesh, tidal channels. Suspended sediment and the dissolved load of water samples taken along a transect from Khulna, Bangladesh down to the Sundarbans near the coast of the Bay of Bengal were analyzed. We found that several trace elements increase in dissolved concentrations along the transect because of desorption processes (i.e. Ni and Co), while Se decreases in concentration, likely because of conservative mixing/dilution with seawater after nonconservative anthropogenic sourcing upstream. Arsenic does not show a clear mixing trend along the transect and is likely largely geogenic in origin.

Chapter IV focuses more holistically on the relationship between pond water, sediment, feed, and shrimp within shrimp ponds. This is essential for understanding the entire impact

trace elements may have on the aquaculture system in Southwest Bangladesh. Data show that shrimp elemental composition is more related to fish feed composition than water, sediment, or sediment pore waters (represented by batch experiment sediment extracts). Partition coefficients and concentration relationships between sediment extracts and sediment suggest that while chemical steady state may happen quickly, chemical equilibrium takes much longer due to the highly weathered sediments and high mineral saturation indices of the waters. Aquaculture shrimp were also found not to contain measurable Se or As despite elevated water concentrations of Se and As, but did contain elevated thallium (Tl) concentrations, which poses a significant health risk to consumers.

Chapter V holistically ties together the importance of the dynamic geochemical system in Southwest Bangladesh, and the implications this has for both Southwest Bangladesh and consumers of agricultural products from the region. Additionally, this chapter points out possible future research directions for better understanding of elemental partitioning in the region.

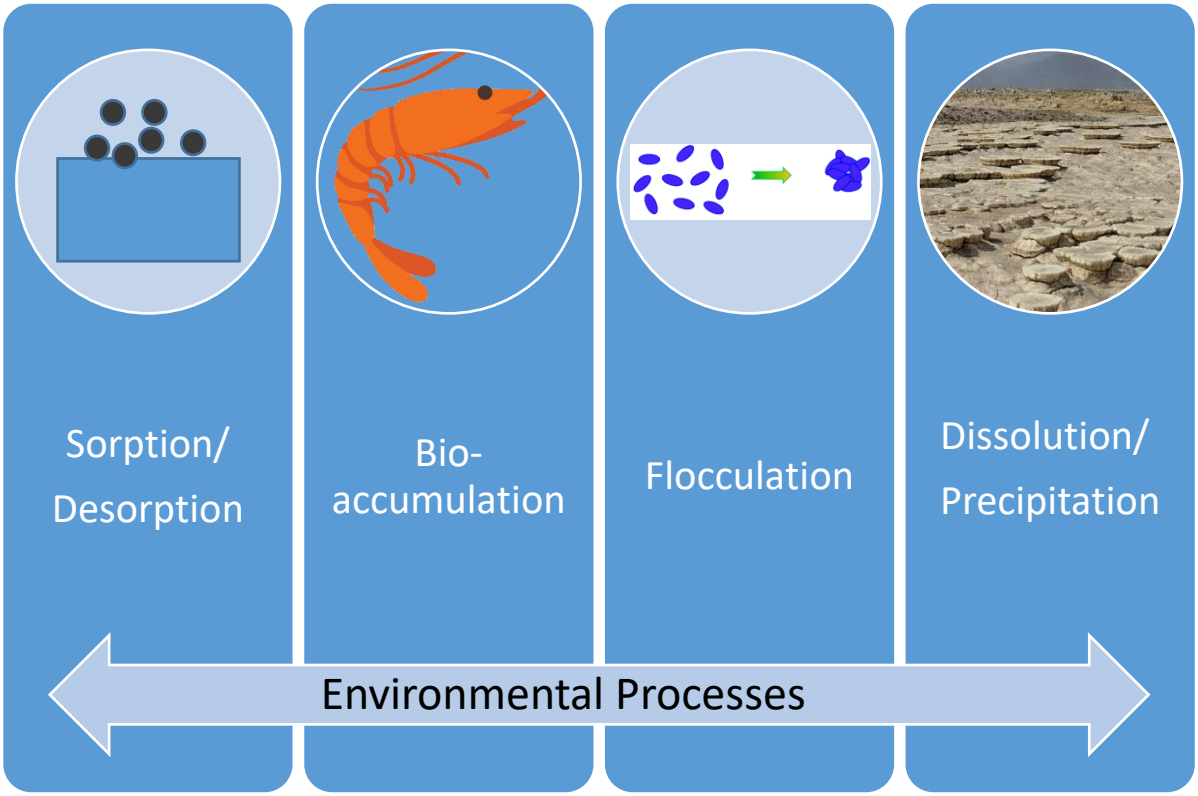

Figure 2: Several different processes possibly affecting element transport, fate, and mobility in the Southwest Bangladesh environment.

CHAPTER II

INFLUENCES ON TIDAL CHANNEL AND AQUACULTURE SHRIMP POND WATER CHEMICAL COMPOSITION IN SOUTHWEST BANGLADESH[1]

Abstract:

Detailed geochemical studies of both major and minor elements in Bangladesh surface waters are sparse, particularly in shrimp aquaculture pond environments. Therefore, water samples from shrimp aquaculture ponds and tidal channels were collected in high precipitation (July) and low precipitation (May) months from 2018-2019 in Southwest Bangladesh and analyzed for complete water chemistry. Selenium (Se) and arsenic (As) were elevated above WHO guidelines in 50% and ~87% of samples, respectively, but do not show any recognizable spatial patterns. Shrimp pond and tidal channel water compositions in the dry season (May) are similar, illustrating their connectivity and minimal endogenous effects within shrimp ponds. Tidal channels are less saline in July than shrimp ponds still irrigated by tidal channels, suggesting that either farmers limit irrigation to continue farming saltwater shrimp, or the irrigation flux is low and leads to a lag in aquaculture-tidal channel compositional homogenization. $\delta^{18}O$ and $\delta^{2}H$ isotopic compositions from samples in May of 2019 reveal tidal channel samples are closer to the local meteoric water line (LMWL) than shrimp pond samples, because of less evaporation. However, evaporation in May shrimp ponds has a minimal effect on water composition, likely because of regular drainage/exchange of pond waters. Dissolved organic carbon (DOC) is positively correlated with both $\delta^{18}O$ and $\delta^{2}H$ in shrimp ponds, suggesting that as evaporation increases, DOC becomes enriched. Multiple linear regression reveals that As and Se can be moderately predicted (adjusted R^2 values between 0.4-0.7, $p < 0.01$) in surface waters of our study with only 3-4 independent predictor variables (e.g., Ni, V and DOC for Se prediction; Cu, V, Ni and P for As prediction). Thus, this general approach should be followed in other regions throughout the world when measurements for certain hazardous trace elements such as Se and As may be lacking in several samples from a dataset.

Keywords: *Trace elements, arsenic, selenium, surface water chemistry, aquaculture*

1 Introduction

Although there has been much research in Bangladesh on groundwater and contaminants such as arsenic (As) (e.g., Anawar et al., 2003; Ayers et al., 2016; Charlet and Polya, 2006; Knappett et al., 2016; Neumann et al., 2009; Nickson et al., 2000), less emphasis has been placed on surface water chemistry, especially in Southwest Bangladesh. Multiple studies in Bangladesh have geochemically examined tidally dominated rivers (hereafter called tidal channels) and adjacent waterways in both temporal and spatial ways (e.g., Akter et al., 2020; Akter and

[1] Chapter published open access in "Geochemical Transactions" and reproduced with the permission of the publisher (Springer Nature) and my co-author (Dr. John Ayers): Dietrich, M., & Ayers, J. C. (2021). Influences on tidal channel and aquaculture shrimp pond water chemical composition in Southwest Bangladesh. *Geochemical Transactions*, 22(1), 1-22. https://doi.org/10.1186/s12932-021-00074-2

Ahmed, 2019; Datta et al., 2020; Haldar et al., 2020; Roy et al., 2018; Shammi et al., 2017). Studies have also looked at trace element concentrations in aquaculture ponds near the coastal region of Bangladesh (Das et al., 2017; Guhathakurta and Kaviraj, 2000; Sarkar et al., 2016) or in coastal Bangladesh rivers (Islam et al., 2020; Proshad et al., 2020) and nonspecified lakes/ponds (Ahmed et al., 2020). However, these studies have focused more on risk assessment, general reporting of trace element or major element concentrations, and overall water quality. While reporting concentrations and changes in water chemistry is useful for preliminary work, more detailed understanding of surface water geochemical relationships is imperative for predicting where waters may have elevated concentrations of certain hazardous elements such as As or selenium (Se), and what ultimately controls the element concentrations.

Studies thus far also have not thoroughly researched the relationship of tidal channel waters with aquaculture shrimp ponds, which are often irrigated with tidal channel water during the dry season in Southwest Bangladesh instead of groundwater (Ayers et al., 2017) (Fig. 1). Recent studies indicate that tidal channel waters often have elevated arsenic, especially in the dry season (Ayers et al., 2017; Dietrich and Ayers, under review), so there is concern that shrimp ponds and the shrimp grown in them may also have high arsenic.

Particularly reliant upon surface water in Southwest Bangladesh (e.g., Satkhira and Khulna districts) are aquaculture and agriculture, where rice farming, fishing, and shrimp farming are the primary sources of income for people in the area (e.g. Benneyworth et al., 2016) and shrimp farming in particular has increased dramatically since the 1980s (Azad et al., 2009). Shrimp ponds (bottom left of Fig. 1) are typically 1m or less in depth on average and vary largely in area, although averaging around 3 ha, while the tidal channels irrigating them have variable depths ranging up to several meters.

In general, critically understanding relationships between trace elements in surface waters in Bangladesh is particularly needed because trace element chemistry in Asian rivers is poorly understood (Gaillardet et al., 2014), and the aquaculture shrimp ponds and tidal channels in Southwest Bangladesh are an innate offshoot of the large Ganges River system. Additionally, better understanding of water chemistry in Bangladesh aquaculture environments has worldwide applicability to coastal aquaculture systems in other countries such as India and Taiwan. Thus, this study aims to holistically examine possible influences (i.e., precipitation, evaporation, irrigation) on the composition of tidal channel and shrimp pond water in Southwest Bangladesh, and to use multivariate techniques to assess whether As and Se concentrations can be predicted in surface waters. The main research questions are: 1) Do early monsoonal rains affect water compositions of shrimp ponds and tidal channels differently? 2) Are any elements or other geochemical parameters sensitive to endogenous changes within shrimp ponds following tidal channel irrigation? and 3) Can Se and As surface water concentrations be reasonably explained and modeled by a small subset of other variables through multiple linear regression modeling?

2 Methods and study area

2.1 Study area

Southwest Bangladesh is a tidally influenced area near the coast of the Bay of Bengal (Fig. 2), with the tidal influence extending just north of Khulna City in the dry season (e.g., Brammer, 2014). Studies in the area have shown that tidal influence on tidal channel water composition varies by season and the amount of freshwater discharge from upstream (Rahaman et al., 2014, 2013). Specifically, salinity ranges between 0-2 parts per thousand (ppt) between the tides, and pH ranges 0-0.4 units between tides throughout the year depending on location within the Sundarbans (Rahaman et al., 2014, 2013). This tidal area has not been as extensively studied as the northern floodplains in the G-B-M delta or the Himalayan foothills, where river water and sediment compositions were previously researched (e.g., Bickle et al., 2018; Lupker et al., 2012; Sarin et al., 1989; Singh et al., 2003). The tidal region includes part of the Sundarbans mangrove forest, although much of this forest was converted to agricultural islands back in the 1960s-1970s (e.g., Peters et al., 2019 and the references cited therein). These agricultural islands are also known as "polders," and are surrounded by embankments, shielding these islands from storm surges or tidal inundation (Auerbach et al., 2015; Peters et al., 2019).

Bangladesh experiences a strong monsoonal climate, where biseasonal precipitation causes approximately 80% of yearly rainfall to occur between the months of June to September (e.g., Benneyworth et al., 2016; Chowdhury, 2010; Peters et al., 2019). This large seasonal difference in precipitation can lead to vast changes in surface water chemistry during different seasons, particularly in coastal regions (e.g., Akter and Ahmed, 2019; Roy et al., 2018; Shammi et al., 2017).

2.2 Sample collection

Surface water samples were collected in both the early monsoon season in July of 2018 and 2019, and during the end of the dry season in May of 2019. July average precipitation in Khulna is ~363mm, while May average precipitation is ~180mm (BARC, 2020). All samples were taken within the general vicinity of Southwest Bangladesh, and predominantly within the Khulna District (Fig. 2). All but one shrimp pond aquaculture sample (KA-10) were irrigated with tidal channel water.

Samples were collected as follows:

- **July**: 11 shrimp ponds + 5 tidal channel samples + 1 rainwater sample (n=17)
- **May**: 10 shrimp ponds + 4 tidal channel samples (n=14)

May and July shrimp pond samples were taken in the same relative locations to avoid differences in tidal influence and thus allow more direct comparison. Tidal channel samples were taken at different locations between seasons, but those used for dissolved ion concentration comparison in spider diagrams (P32-TC, P32-1 and P32-2 in July; MD-TC-16, MD-TC-18, MD-TC-19, and MD-TC-22 in May) were collected in channels that irrigated the studied shrimp ponds in both seasons. One rainwater sample was collected in July of 2018 from a tin roof collection device.

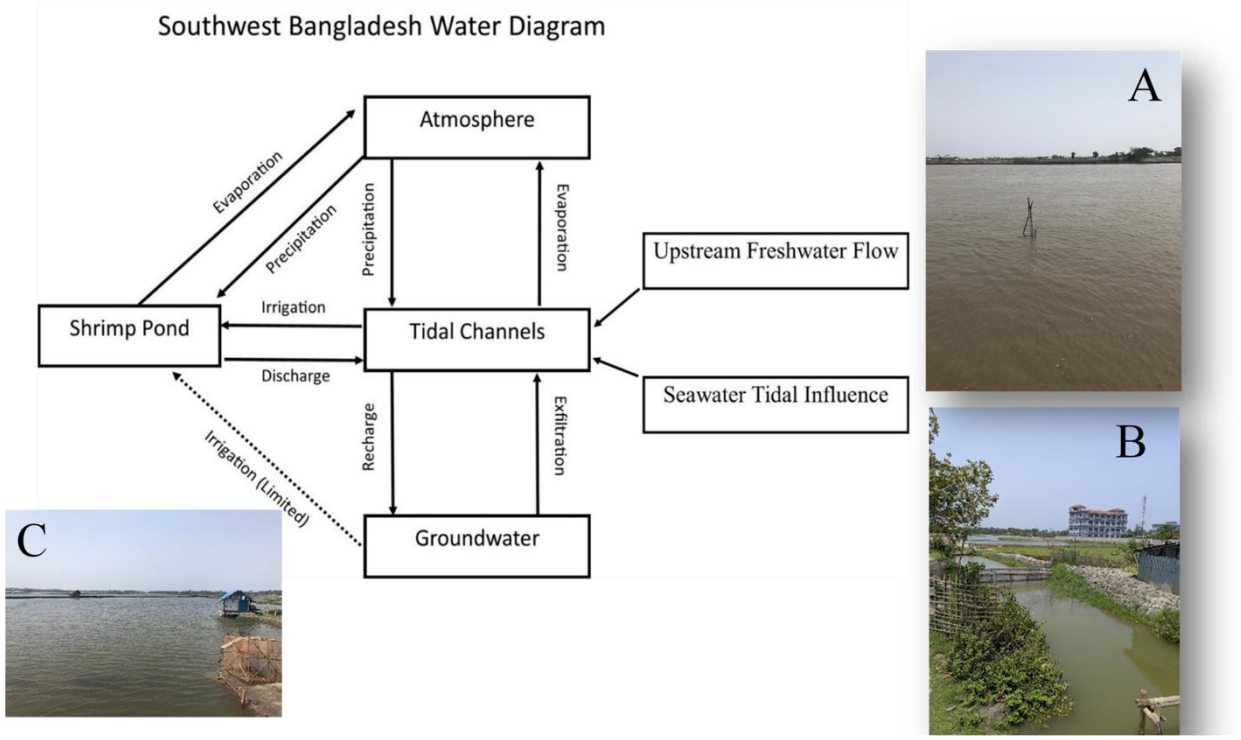

Figure 1: Conceptual diagram of the water cycle within Southwest Bangladesh and example images of tidal channels that irrigate shrimp ponds (both a typical main channel like that sampled in this study (A) and an inlet from a smaller, connective channel (B). A typical shrimp pond (C). A video of tidal channel irrigation to a shrimp pond is provided at: https://doi.org/10.1186/s12932-021-00074-2.

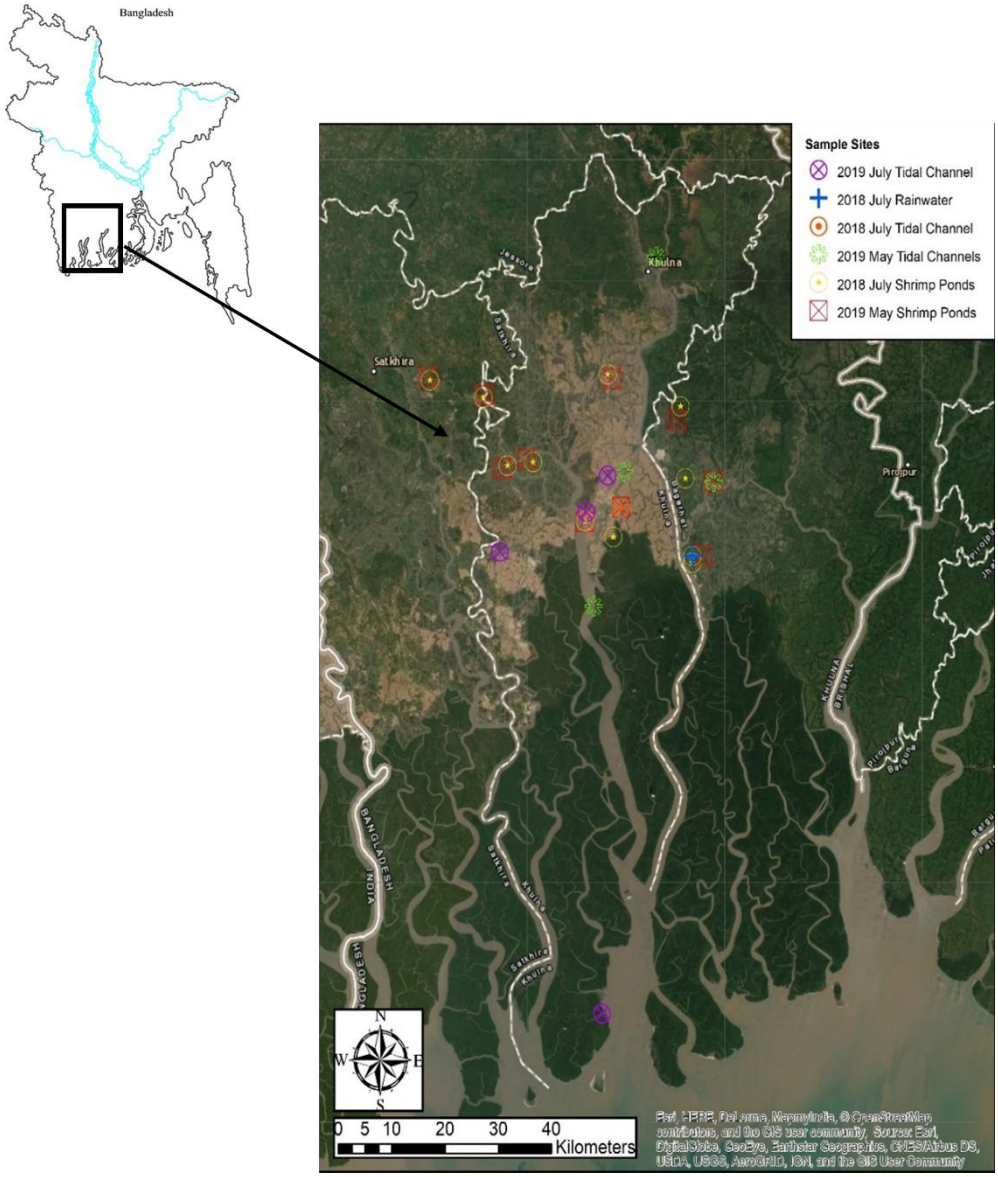

Figure 2: Map of the study area and the sample sites in Southwest Bangladesh, with the dark green area representing the Sundarbans natural mangrove forest.

Surface water samples were collected with plastic syringes and buckets from the upper 1m of the water column and were rinsed at least once between each sample. Samples were filtered in the field with a syringe and 0.45µm polypropylene filter into 60- and 125-mL bottles. May 2019 and July 2019 samples were all filtered into 60 mL bottles until the bottles were completely filled to prevent oxygen and hydrogen isotope exchange with headspace before analysis. Only 2019 samples were collected for isotopic analysis because in our lab, analytical

capabilities for oxygen and hydrogen isotopes were not yet available in 2018. The July 2018 tidal channel and rainwater samples were placed in 500 mL bottles, with the tidal channel sample filtered in the laboratory with a 0.45μm polypropylene filter (not filtered in the field).

2.3 Field measurements

A Hach Hydrolab DS5 was used to gather in situ surface water measurements of pH, oxidation-reduction potential (ORP) in millivolts (mV), specific conductivity (SpC) in microsiemens per centimeter (μS/cm), and temperature in degrees Celsius (˚C) for July 2018 shrimp pond, May 2019 shrimp pond, and May 2019 tidal channel samples following the methods of Ayers et al. (2017). July 2018 tidal channel SpC was measured with a hand-held SpC Hanna probe while one July 2018 shrimp pond sample (KA-1) SpC value was estimated through total ion summation.

ORP measurements from the Hach Hydrolab DS5 were used for distinguishing oxic and anoxic conditions for surface water samples, as described in Ayers et al., 2017, 2016. ORP (relative to the Ag/AgCl redox couple) was converted to Eh (relative to the standard hydrogen electrode (SHE)) in Table 1 by adding 187 mV to each field measurement.

2.4 Sample preparation and analyses

2-10 mL of each filtered sample was acidified with a drop of concentrated nitric acid (HNO_3) in the laboratory for inductively coupled plasma (ICP) analysis, while approximately 20-30 mL of sample was left unacidified and used for ion chromatography (IC) and total organic carbon analysis (TOC). Approximately 2 mL of filtered, unacidified May and July 2019 samples were transferred to glass vials via plastic pipette immediately upon opening the 60 mL bottles for $\delta^{18}O$ and $\delta^{2}H$ isotope analysis.

All acidified water samples were analyzed on a Perkin Elmer NexION 2000B ICP-MS in both standard and kinetic energy discrimination (KED) modes using EPA Method 6020B at Vanderbilt University for the elements As, Be, Cd, Co, Cr, Cu, Fe, Mn, Mo, Ni, Pb, Sb, Se, Ti, Tl, V, and Zn. All acidified surface water samples were also analyzed on an Agilent 5110 VDV ICP-OES using EPA Method 6010D at Vanderbilt University to report the ions: Al, As, B, Ba, Ca, Fe, K, Mg, Na, P, S, Si, and Sr. All 2018 filtered, unacidified surface water samples were analyzed for inorganic and organic carbon content with a Shimadzu model TOC-V CPH/CPN using ASTM Method D-7573-09 at Vanderbilt University, as described in Ayers et al., 2017, 2016, while samples from 2019 were all analyzed via a Shimadzu model TOC-LCPH using EPA Method 9060A. Unacidified water samples were also analyzed for Cl, F, Br, NO_3, PO_4, and SO_4 with a Metrohm 881 Compact IC Pro using SW-846 EPA Method 9056. NO_3, PO_4 and F were omitted from the reported results because nearly all values were <MDL.

May and July 2019 water samples were run on a Picarro L2130-i isotope and gas concentration analyzer at Vanderbilt University to provide $\delta^{18}O$ and $\delta^{2}H$ isotope values relative to Vienna Standard Mean Ocean Water (VSMOW). Each sample was run twice, with the mean of four measured injections (following four preparatory injections) used to generate $\delta^{18}O$ and $\delta^{2}H$ isotope values for each sample run. Average values of the two sample runs are reported.

Average precision (1σ) between replicate sample runs was ~0.1‰ for δ^2H and ~0.02‰ for $\delta^{18}O$. Salt liners were used to prevent damage from salt precipitates. USGS standards USGS45, USGS49 and USGS50 were used to correct measured sample values through the USGS LIMS for Lasers data reduction scheme.

More details on sample preparation are included in the Supplementary Document.

2.5 Quality control

Method blanks of samples were taken with deionized water in the field in July 2018 and May 2019 and analyzed for complete chemical analysis (IC, TOC, ICP-MS, ICP-OES), and routinely show concentrations at or below method detection limits (Table 2). For samples run on the ICP-MS, ICP-OES, IC and TOC analyzers, periodically measured concentrations in standards were required to be within 15% of the known value and blanks were required to be below the method detection limit (MDL). A duplicate shrimp pond sample from May 2019 showed all concentrations except Mn in very close alignment with one another (3.0% average difference in concentrations for all reported elements (including DIC and DOC) that had concentrations >10ppb), illustrating the representative nature of each sample. Method detection limits are listed in Table 2. Average charge-balance error was 4.6%, similar to the average charge-balance error in Ayers et al., 2017 of 3.9%.

2.6 Data reduction

Maps were generated using ArcGIS 10.6.1 and QGIS 3.10, while RStudio and Microsoft Excel were used for figure generation and statistical analyses. Multiple linear regression subset selection used the "leaps" package in R, with 8 variables used as the max number of subsets (Lumley, 2020). The Geochemist's Workbench 14.0 was used to generate a Piper diagram and an evaporation model in the React program, using sample MD-TC-22 as the input basis. HCO_3^- concentrations (from measured dissolved inorganic carbon (DIC)), charge imbalance, and mineral saturation indices were calculated using SpecE8 software in The Geochemist's Workbench 14.0 with the default thermo.dat database (Bethke, 2007). Uncertainties are reported as sample standard deviation (1σ).

3 Results

3.1 Geochemical concentrations

Dissolved concentrations tend to be lognormally distributed, so they are summarized using the geometric mean. Element concentrations reflect relatively saline waters in shrimp ponds regardless of season, shown by high conservative ion concentrations approaching average seawater concentrations (Table 2). Tidal channel waters show more variability in conservative ion concentrations between sampling months compared to shrimp ponds. Eh values in both sampling months are generally consistent and positive in surface waters, indicative of oxidizing conditions (422 ± 48 mV). Including both sampling months (because of minimal seasonal variability in DOC), the mean shrimp pond DOC concentration is 7.3 ± 4.3 mg.L-1, while the

mean tidal channel DOC concentration is 3.1 ± 1.0 mg.L-1, compared to a river world average of 5.8 mg.L-1 and 12 mg.L-1 median value in the world's eutrophic lakes (Ayers et al., 2017 and the references therein). pH values show relatively little variability regardless of sampling month, although shrimp pond waters at 8.4 ± 0.4 are markedly more alkaline than tidal channel waters at 7.6 ± 0.1. Out of elements with known adverse health outcomes in excessive quantities, Cr (6.6 ± 3.6 μg.L-1) and Mn (3 ± 17 μg.L-1) overall surface water values are all well below levels of health concern (World Health Organization, 2017), while Pb, Be, Cd, and Tl were either close to detection limit or below detection limit and thus not reported. Ti, Sb, Fe and Mo values are also not reported because of either low values (e.g., nearly all May samples had negative reported Fe values) or concerns with interference on the ICP. However, both As (25 ± 19 μg.L-1) and Se (45 ± 45 μg.L-1) are at levels of potential health concern across both sampling months based on WHO and EPA drinking water guidelines, which are 10 μg.L-1 for As for both the EPA and WHO, and 50 μg.L-1 and 40 μg.L-1, respectively, for Se EPA and WHO guidelines (U.S. EPA, 2009; World Health Organization, 2017).

3.2 Element and geochemical parameter correlations

Concentrations of most conservative elements are strongly correlated, indicative of their similar mobilities in solution (Fig. A1). Concentrations of many elements that tend to behave nonconservatively such as As and Se do not show strong correlations, indicative of redox conditions and sorption/desorption mechanisms possibly affecting concentrations. However, pH and Eh measured in shrimp ponds do not correlate well with any elements (Fig. A2). DOC, important in groundwater chemical reactions in Bangladesh, does not show strong correlations with any elements (Fig. A1).

3.3 Monthly composition differences and element enrichment relative to seawater

In general, lower element concentrations are seen in July tidal channel waters relative to May tidal channel waters (Fig. 3). Concentrations in July tidal channel waters, however, show much more variance, although nonconservative elements have less consistency in variation. July and May shrimp ponds show slight differences in average compositions, albeit with most overlap contained within 1σ error bars (Fig. 4a). However, Se, Cu, Cr, and Co are all elevated in July shrimp ponds relative to May shrimp ponds outside of 1σ variation. July shrimp ponds are slightly less saline on average than May shrimp ponds (Fig. A3). When normalizing shrimp pond (Fig. 4b) and tidal channel (Fig. A4) concentrations to that of seawater (values from literature; Table A1), several elements are clearly enriched, such as Ba, As, Se, and Zn. Additionally, DOC is well enriched in shrimp ponds relative to values typically seen in the Indian Ocean (Ogawa and Tanoue, 2003), shown through DOC plotting well above 0 in Figure 4a.

Table 1: Sample location information, in-situ measurements, and saturated minerals in solution

Sample	Type	Latitude	Longitude	Date-Time[a]	CIB (%)[b]	Saturated minerals[d]	pH	SpC (µS/cm)[e]	Eh (mV)[g]
KA-1	Shrimp Pond July	22.47861853	89.47911456	7/6/2018	0.65%	Kfs, kln, Ms, Dol, Cal, Ilt	8.09	28403.0	399.0
KA-2	Shrimp Pond July	22.50075958	89.43157628	7/7/2018	-3.61%	Kfs, Ms, Dol, Cal, Ilt	8.50	20200.0	357.0
KA-3	Shrimp Pond July	22.69571769	89.16967095	7/8/2018	-3.41%	Ms, Dol, Cal	9.00	6541.0[f]	377.0
KA-4	Shrimp Pond July	22.67178417	89.25978431	7/8/2018	-2.54%	Kfs, kln, Ms, Dol, Cal, Ilt	8.26	20398.0	407.0
KA-5	Shrimp Pond July	22.57789021	89.30023656	7/9/2018	1.63%	Ms, Dol, Cal	8.61	29595.0	390.0
KA-6	Shrimp Pond July	22.58252190	89.34350180	7/9/2018	2.03%	Kfs, kln, Ms, Dol, Cal, Ilt	8.44	28264.0	391.0
KA-7	Shrimp Pond July	22.44306661	89.61203278	7/10/2018	-3.90%	Dol	8.08	12203.0	600.0
KA-8	Shrimp Pond July	22.45236994	89.61284144	7/10/2018	-3.87%	Kfs, kln, Ms, Dol, Cal, Ilt	8.38	9053.0	445.0
KA-9	Shrimp Pond July	22.55983540	89.60069553	7/10/2018	-1.71%	Ms, Dol, Cal	8.19	16466.0	437.0
KA-10	Shrimp Pond July	22.65947095	89.59243177	7/11/2018	-1.44%	Dol, Cal	9.28	1505.0	389.0
KA-11	Shrimp Pond July	22.70397053	89.46984816	7/11/2018	-0.83%	Dol, Cal	8.41	22440.0	436.0
P32-TC	Tidal Channel July	22.51957700	89.49199400	7/6/2018	8.00%			6990.0	
KA-8RW	Rainwater	22.45236994	89.61284144	7/10/2018	-1.16%				
KA- 12	Shrimp Pond May	22.49975329	89.43115749	5/6/19 15:42	7.48%	Kfs, Ms, Dol, Cal, Ilt	8.65	27731.0	390.0
KA- 13	Shrimp Pond May	22.51984753	89.49248609	5/7/19 9:37	8.46%	Kfs, kln, Ms, Dol, Cal, Ilt	8.05	31367.0	431.0
KA- 14	Shrimp Pond May	22.45304998	89.62798504	5/8/19 10:00	4.34%	Kfs, kln, Ms, Dol, Cal, Ilt	7.97	26077.0	414.0
KA- 15	Shrimp Pond May	22.55608476	89.64831928	5/8/19 12:30	4.33%	Kfs, kln, Ms, Dol, Cal, Ilt	8.15	25749.0	418.0
MD-TC-22	Tidal Channel May	22.55505854	89.64806772	5/8/19 12:50	3.33%	Kfs, kln, Ms, Dol, Ilt	7.67	25339.0	454.0
KA- 16	Shrimp Pond May	22.57374567	89.29286777	5/9/19 10:10	4.66%	Ms, Dol, Cal	8.77	28851.0	404.0

KA- 17	Shrimp Pond May	22.58665928	89.33286479	5/9/19 11:25	6.70%	Kfs, kln, Ms, Dol, Cal, Ilt	7.96	33034.0	443.0
KA- 18	Shrimp Pond May	22.67498980	89.26152243	5/9/19 14:00	4.79%	Kfs, kln, Ms, Dol, Cal, Ilt	8.55	11285.0	403.0
KA- 19	Shrimp Pond May	22.69974406	89.16632039	5/10/19 10:10	7.03%	Kfs, Ms, Dol, Cal	8.86	17557.0	359.0
KA- 20	Shrimp Pond May	22.69793983	89.47640710	5/11/19 9:00	3.90%	Kfs, kln, Ms, Dol, Cal, Qz, Ilt	7.77	32046.0	474.0
KA- 21	Shrimp Pond May	22.64063033	89.58598250	5/11/19 11:00	6.41%	Kfs, Ms, Dol, Cal, Ilt	8.61	26270.0	430.0
MD-TC-16	Tidal Channel May	22.38292227	89.44586719	5/6/2019 10:55	4.18%	Kfs, kln, Ms, Dol, Ilt	7.56	36334.0	450.0
MD-TC-18	Tidal Channel May	22.56935935	89.49654172	5/7/2019 10:55	4.07%	Kfs, kln, Ms, Dol, Ilt	7.64	29662.0	458.0
MD-TC-19	Tidal Channel May	22.86607737	89.55133013	5/7/2019 15:27	4.13%	Kfs, kln, Ms, Dol, Ilt	7.63	25837.0	445.0
Hiron Point	Tidal Channel July	21.81744000	89.46000000	7/22/2019 10:05	10.53%				
Site-1	Tidal Channel July	22.45839000	89.28765000	7/25/2019 19:55	9.34%				
P32-1	Tidal Channel July	22.51326000	89.43369000	7/26/2019 8:10	10.47%				
P32-2	Tidal Channel July	22.56404000	89.46957000	7/26/2019 14:50	3.74%				
Pond and Tidal Channel Geometric Mean					4.60%[c]		8.27	19842.57	421.69
Pond and Tidal Channel Std Dev							0.45	8959.77	48.00

[a]Bangladesh Standard Time (BST or GMT+6).

[b]Charge imbalance error (%) between major ionic species in solution.

[c]Arithmetic mean of absolute value (%).

[d]Saturated minerals have saturation index >0 (log(Q/K)) - *Kfs* K-feldspar; *Kln* kaolinite; *Ms* muscovite;

Dol dolomite; *Cal* calcite; *Qz* quartz; *Ilt* illite (Note: No Fe-minerals because of no reported Fe).

[e]Acronym represents specific conductivity (SpC).

[f]Field measurement likely inaccurate based on major ion concentrations.

[g]Eh is relative to the standard hydrogen electrode (SHE).

Table 2: Measured geochemical parameters

MDL (mg/L)		0.0034	0.00013	0.00026	0.00016	0.00011	0.00026	0.00020
Sample	**Type**	**Al[1]**	**V**	**Cr**	**Mn**	**Co**	**Ni**	**Cu**
KA-5-Blank	**Blank**	0.004	0.000	0.001	0.000			
KA-7-Blank	**Blank**	0.001	0.000	0.000	0.000			
KA-17-Blank	**Blank**		0.000	0.004	0.003	0.0003	0.005	
KA-20-Blank	**Blank**		0.000	0.003	0.000		0.000	
KA-1	**Shrimp Pond July**	0.160	0.008	0.010	0.006	0.0013	0.011	0.018
KA-2	**Shrimp Pond July**	0.152	0.008	0.009	0.001	0.0009	0.009	0.016
KA-3	**Shrimp Pond July**	0.250	0.013	0.008	0.007	0.0009	0.007	0.016
KA-4	**Shrimp Pond July**	0.145	0.016	0.010	0.005	0.0011	0.011	0.021
KA-5	**Shrimp Pond July**	0.242	0.021	0.013	0.002	0.0016	0.024	0.019
KA-6	**Shrimp Pond July**	0.228	0.020	0.013	0.013	0.0018	0.024	0.013
KA-7	**Shrimp Pond July**	0.134	0.004	0.008	0.003	0.0008	0.006	0.012
KA-8	**Shrimp Pond July**	0.073	0.007	0.006	0.049	0.0005	0.000	0.019
KA-9	**Shrimp Pond July**	0.121	0.009	0.008	0.000	0.0008	0.009	0.017
KA-10	**Shrimp Pond July**	0.066	0.005	0.004	0.001	0.0002	0.007	0.009
KA-11	**Shrimp Pond July**	0.155	0.007	0.010	0.001	0.0011	0.014	0.018
P32-TC	**Tidal Channel July**	0.016			0.000	0.0001	0.002	0.010

KA-8RW	**Rainwater**	0.003	0.000		0.004			
KA- 12	**Shrimp Pond May**	0.093	0.022	0.004	0.005	0.0004	0.006	0.008
KA- 13	**Shrimp Pond May**	0.092	0.021	0.003	0.004	0.0003	0.004	0.007
KA- 14	**Shrimp Pond May**	0.093	0.017	0.006	0.004	0.0004	0.006	0.005
KA- 15	**Shrimp Pond May**	0.093	0.017	0.005	0.002	0.0003	0.006	0.007
MD-TC-22	**Tidal Channel May**	0.094	0.018	0.004	0.004	0.0004	0.006	0.006
KA- 16	**Shrimp Pond May**	0.093	0.019	0.005	0.004	0.0003	0.006	0.004
KA- 17	**Shrimp Pond May**	0.094	0.019	0.004	0.004	0.0004	0.006	0.007
KA- 18	**Shrimp Pond May**	0.085	0.011	0.005	0.004	0.0004	0.007	0.004
KA- 19	**Shrimp Pond May**	0.086	0.018	0.004	0.004	0.0002	0.003	0.005
KA- 20	**Shrimp Pond May**	0.100	0.020	0.004	0.003	0.0003	0.004	0.005
KA- 21	**Shrimp Pond May**	0.092	0.019	0.005	0.084	0.0004	0.000	0.003
MD-TC-16	**Tidal Channel May**	0.104	0.021	0.004	0.003	0.0003	0.006	0.005
MD-TC-18	**Tidal Channel May**	0.114	0.019	0.005	0.002	0.0004	0.007	0.005
MD-TC-19	**Tidal Channel May**	0.090	0.018	0.005	0.004	0.0004	0.007	0.006
Hiron Point	**Tidal Channel July**	0.140	0.017	0.013	0.005	0.0009	0.013	0.017
Site-1	**Tidal Channel July**	0.182	0.023	0.018	0.003	0.0016	0.019	0.026
P32-1	**Tidal Channel July**	0.039	0.004	0.009	0.001	0.0002	0.000	0.016
P32-2	**Tidal Channel July**	0.039	0.001	0.009	0.000	0.0001	0.002	0.021

Pond and Tidal Channel Geometric Mean		0.101	0.012	0.0066	0.003	0.0005	0.005	0.010
Pond and Tidal Channel Std Dev		0.056	0.007	0.004	0.017	0.0005	0.006	0.006

MDL (mg/L)	0.00045	0.00018	0.00031	0.0023	0.0016	0.0065	0.0032	0.0035	0.0056
Sample	**Zn**	**As**	**Se**	**B**	**Ba**	**Ca**	**K**	**Mg**	**Na**
KA-5-Blank	0.003	0.000	0.005	0.171			0.096	0.389	2.27
KA-7-Blank	0.003			0.085	0.002	0.16	0.093	0.189	2.65
KA-17-Blank	0.002	0.004		0.503	0.002		0.032	0.037	1.93
KA-20-Blank	0.003	0.006		0.500	0.000		0.024	0.029	0.60
KA-1	0.007	0.034	0.076	2.43	0.16	174.62	279.68	541.62	5279.52
KA-2	0.006	0.043	0.076	1.83	0.22	168.61	186.15	407.08	3798.48
KA-3	0.006	0.036	0.073	1.56	0.27	143.92	149.33	366.38	3388.44
KA-4	0.005	0.095	0.095	1.68	0.28	178.91	179.83	415.85	3812.76
KA-5	0.006	0.015	0.091	2.28	0.25	212.77	289.88	622.51	6033.30
KA-6	0.005	0.018	0.198	1.57	0.19	227.05	218.08	609.45	5270.34
KA-7	0.005	0.017	0.074	0.89	0.16	119.44	91.32	228.58	1976.76
KA-8	0.006	0.059	0.069	0.56	0.11	93.10	58.21	176.56	1414.74
KA-9	0.004	0.007	0.119	1.16	0.25	122.30	137.19	330.07	2929.44
KA-10	0.004	0.001	0.060	0.12	0.10	40.87	12.46	31.79	146.68
KA-11	0.006	0.003	0.168	1.58	0.14	176.36	205.94	468.59	4312.56
P32-TC	0.000	0.019	0.014	0.47	0.07	70.25	54.13	124.34	1375.98
KA-8RW	0.760	0.000	0.004		0.00	1.54	0.42	0.72	6.41
KA- 12	0.007	0.039	0.035	3.40	0.24	237.80	293.90	631.90	5781.00
KA- 13	0.003	0.033	0.034	3.56	0.19	247.80	342.60	703.80	6546.00
KA- 14	0.003	0.033	0.031	2.90	0.26	232.70	271.80	594.30	5532.00
KA- 15	0.004	0.030	0.015	2.94	0.30	214.40	283.00	597.80	5501.00
MD-TC-22	0.004	0.043	0.012	2.50	0.25	198.60	278.20	567.00	5405.00
KA- 16	0.004	0.032	0.029	3.10	0.26	221.90	311.60	662.30	6091.00
KA- 17	0.007	0.025	0.034	3.54	0.22	249.60	372.20	778.10	7148.00
KA- 18	0.003	0.027	0.035	1.47	0.24	122.30	101.30	244.10	2353.00

KA- 19	0.003	0.049	0.037	2.15	0.19	141.80	175.50	368.80	3741.00
KA- 20	0.004	0.041	0.054	3.29	0.22	266.80	351.30	763.90	7007.00
KA- 21	0.004	0.026	0.029	2.52	0.25	219.50	265.10	630.70	5718.00
MD-TC-16	0.018	0.038	0.056	3.69	0.11	264.70	422.80	865.10	7938.00
MD-TC-18	0.011	0.042	0.015	2.85	0.25	223.00	331.20	668.80	6378.00
MD-TC-19	0.010	0.039	0.030	2.57	0.30	204.60	291.10	589.90	5492.00
Hiron Point	0.014	0.020	0.101	3.48	0.07	184.21	240.62	571.61	7481.70
Site-1	0.029	0.041	0.055	3.56	0.09	267.85	383.72	877.00	10726.32
P32-1	0.008	0.054	0.039	0.82	0.06	44.55	22.37	71.70	817.12
P32-2	0.006	0.006	0.008	0.41	0.03	25.72	3.01	7.15	23.04
Pond and Tidal Channel Geometric Mean	0.005	0.025	0.045	1.75	0.17	155.51	158.16	361.47	3254.04
Pond and Tidal Channel Std Dev	0.006	0.019	0.045	1.09	0.08	70.12	118.31	243.64	2498.31

MDL (mg/L)	0.0068	0.0058	0.0038	0.0037	0.0101	0.0064	0.0254		0.15	0.18
Sample	**P**	**S**	**Si**	**Sr**	**Cl**	**Br**	**SO_4**	**HCO_3**	**DIC***	**DOC***
KA-5-Blank	0.075	0.539		0.002	0.768		0.93		0.450	2.85
KA-7-Blank	0.032	0.252			0.915		1.23		0.470	2.09
KA-17-Blank	0.012			0.019					0.272	0.47
KA-20-Blank									0.225	0.58
KA-1	0.089	450.94	0.95	3.66	9250.22	35.42	1108.30	151.60	29.84	5.71
KA-2	0.100	352.72	0.70	2.84	7321.86	29.82	860.10	152.90	30.10	8.42
KA-3	0.112	284.38	0.57	2.55	6516.78	28.48	707.86	137.60	27.09	10.30
KA-4	0.070	335.78	2.01	2.91	7224.22	30.46	830.56	193.00	38.01	8.38
KA-5	0.021	525.91	0.28	4.32	10412.60	38.84	1251.36	93.76	18.46	9.10
KA-6	0.086	461.14	1.38	3.91	9182.44	36.72	1108.48	167.50	32.98	22.0
KA-7	0.080	202.47		1.59	3920.46	22.42	515.96	41.29	8.13	6.56
KA-8	0.326	122.60	1.40	1.17	2798.86	20.58	306.78	193.00	38.00	11.82
KA-9	0.067	252.14	0.22	2.22	5463.42	26.82	614.10	169.20	33.32	8.15
KA-10	0.032	21.93	1.59	0.29	283.54	14.92	50.80	131.90	25.97	8.58

KA-11	0.059	396.27		3.18	7885.82	31.98	925.68	138.30	27.24	7.20
P32-TC	0.013	94.68	1.95	0.86	1980.40		258.52	176.60	34.78	5.70
KA-8RW	0.012	0.63	0.25		9.34		1.99	7.97	1.57	2.60
KA- 12	0.035	498.20	1.43	4.05	8721.00	51.54	1518.00	122.10	24.04	8.02
KA- 13	0.052	551.30	0.91	4.52	9562.00	64.54	1793.00	159.90	31.49	3.77
KA- 14	0.026	442.10	1.94	3.76	8895.00	48.85	1444.00	162.20	31.93	4.73
KA- 15	0.038	448.10	1.21	3.84	8916.00	45.87	1341.00	157.80	31.07	4.11
MD-TC-22	0.054	436.30	2.12	3.65	8869.00	44.86	1337.00	146.40	28.82	2.86
KA- 16	0.050	501.30	0.60	4.22	9755.00	56.42	1544.00	122.30	24.08	5.28
KA- 17	0.030	589.20	1.75	4.98	10920.00	61.37	1872.00	148.70	29.28	3.19
KA- 18	0.049	171.70	2.34	1.64	3733.00	11.14	531.30	179.70	35.38	6.91
KA- 19	0.238	231.00	1.00	2.38	5674.00	22.88	724.70	181.60	35.75	15.62
KA- 20	0.036	560.00	2.89	4.76	11380.00	70.65	1822.00	196.20	38.64	5.55
KA- 21	0.021	445.20	1.55	3.76	8926.00	48.64	1347.00	94.31	18.57	7.60
MD-TC-16	0.065	671.00	1.48	5.52	12810.00	88.36	2081.00	143.80	28.31	2.36
MD-TC-18	0.027	518.40	1.91	4.28	10250.00	62.98	1649.00	145.60	28.67	3.14
MD-TC-19	0.048	453.30	2.29	3.76	8837.00	47.60	1457.00	150.80	29.69	3.20
Hiron Point		440.44	2.24	3.69	10285.90	30.60	1165.50	114.60	22.57	2.74
Site-1	0.014	663.41	1.35	5.52	15269.20	48.40	1765.20	137.40	27.05	3.05
P32-1		51.26	2.90	0.52	1116.12	3.84	137.68	100.70	19.83	3.12
P32-2		4.98	3.16	0.11	32.09	0.13	13.50	95.03	18.71	2.80
Pond and Tidal Channel Geometric Mean	0.050	275.20	1.34	2.47	5350.28	28.51	766.12	138.10	27.19	5.67
Pond and Tidal Channel Std Dev	0.068	187.98	0.77	1.52	3724.62	20.35	587.11	34.91	6.87	4.25

[1]All measurements in $mg.L^{-1}$, including method detection limits (MDL). Omitted values are negative reported values.

*Acronyms represent dissolved inorganic carbon (DIC) and dissolved organic carbon (DOC).

3.4 Tidal channel versus shrimp pond composition

May tidal channels and shrimp ponds have similar average compositions, although there is more variability in the nonconservative elements such as Zn and Ni (Fig. 5a). In July however, tidal channel and shrimp pond compositions are not as similar, although it is noted that there is high variability within July tidal channel samples (Fig. 5a). In general, July shrimp ponds have higher average concentrations of elements and DOC compared to July tidal channels.

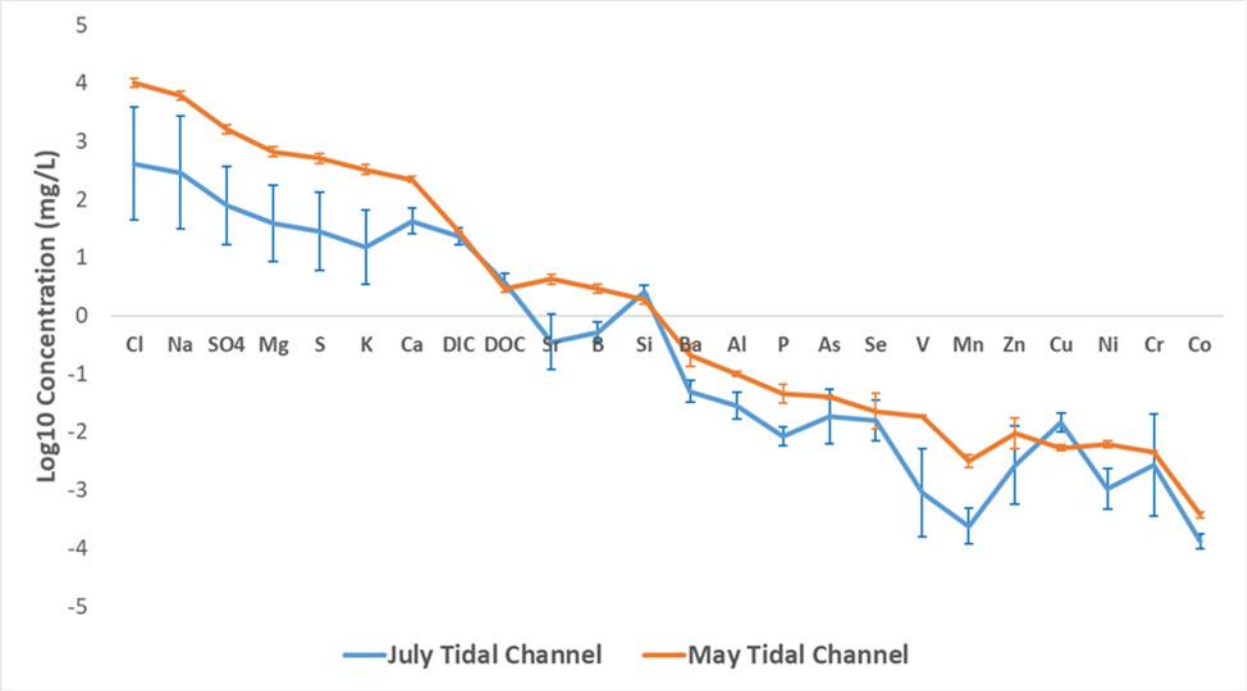

Figure 3: Spider diagram of tidal channel arithmetic mean log10 concentrations, arranged from left to right with decreasing concentrations in seawater. 1σ error bars are given. Illustrates the seasonality between tidal channel samples, with larger variation in July because of early monsoonal rains coupled with tidal influence. July tidal channel samples P32-TC, P32-1 and P32-2 were averaged instead of other July tidal channel samples because of proximity to the shrimp ponds they were irrigating.

3.5 Oxygen and hydrogen isotopes specific trends

$\delta^{18}O$ and $\delta^{2}H$ from tidal channel samples (Table 3) plot relatively close to the local meteoric water line (LMWL) (Fig. 6). Furthermore, they plot linearly between the LMWL and the expected value for seawater. Shrimp ponds plot farther off the LMWL than tidal channel samples and their stable isotope values are heavier (more positive) than tidal channel isotope values.

$\delta^{18}O$ and $\delta^{2}H$ show a strong positive correlation with DOC in shrimp ponds ($\delta^{18}O$ and DOC; Spearman $\rho = 0.92$, $p = 0.00047$) (Fig. 7). As shrimp ponds become more enriched in both ^{18}O and ^{2}H isotopes, DOC increases. Tidal channel samples do not show this same relationship ($\delta^{18}O$ and DOC; Spearman $\rho = 0.095$, $p = 0.84$), with DOC values remaining quite stable as $\delta^{18}O$ and $\delta^{2}H$ increase.

Table 3: Isotopic measurements relative to VSMOW

Sample	Type	$\delta^{18}O$ (‰)^{VSMOW}	$\delta^{2}H$ (‰)^{VSMOW}
KA- 12	Shrimp Pond May	1.9	9.1
KA- 13	Shrimp Pond May	-0.1	-3.6
KA- 14	Shrimp Pond May	0.1	-2.3
KA- 15	Shrimp Pond May	-1.2	-10.3
MD-TC-22	Tidal Channel May	-2.2	-15.5
KA- 16	Shrimp Pond May	0.6	0.8
KA- 17	Shrimp Pond May	-0.9	-7.3
KA- 18	Shrimp Pond May	2.8	13.8
KA- 19	Shrimp Pond May	3.7	21.8
KA- 20	Shrimp Pond May	1.0	2.4
KA- 21	Shrimp Pond May	2.7	13.3
MD-TC-16	Tidal Channel May	-1.4	-9.2
MD-TC-18	Tidal Channel May	-1.5	-11.4
MD-TC-19	Tidal Channel May	-1.6	-12.1
Hiron Point	Tidal Channel July	-2.6	-15.6
Site-1	Tidal Channel July	-1.0	-7.0
P32-1	Tidal Channel July	-6.7	-44.0
P32-2	Tidal Channel July	-7.2	-46.8

^{VSMOW}Isotope values are delta values relative to VSMOW (Vienna Standard Mean Ocean Water)

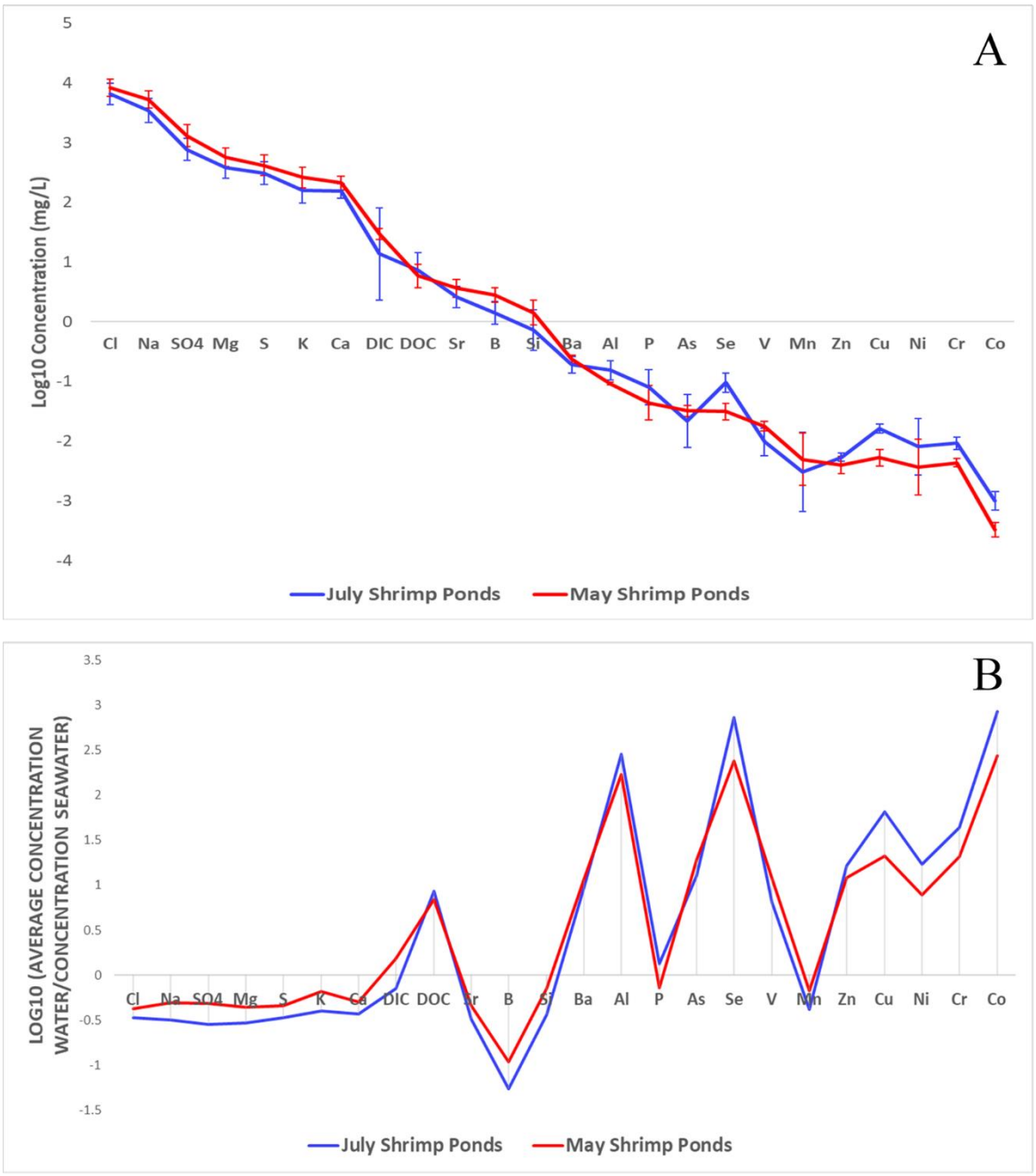

Figure 4: Spider diagrams of arithmetic mean log10 concentrations in July (excluding KA-10) and May shrimp ponds. Slight seasonality is apparent between July and May shrimp ponds irrigated with tidal channels (A), albeit with overlap within 1σ error bars. Concentrations in shrimp ponds normalized to seawater (B), with log10(geometric mean/seawater) instead of arithmetic mean of log10 concentrations, with points above 0 showing relative enrichment and points below 0 showing relative depletion compared to seawater. Two Si values are omitted from the July shrimp pond data because of anomalous negative values.

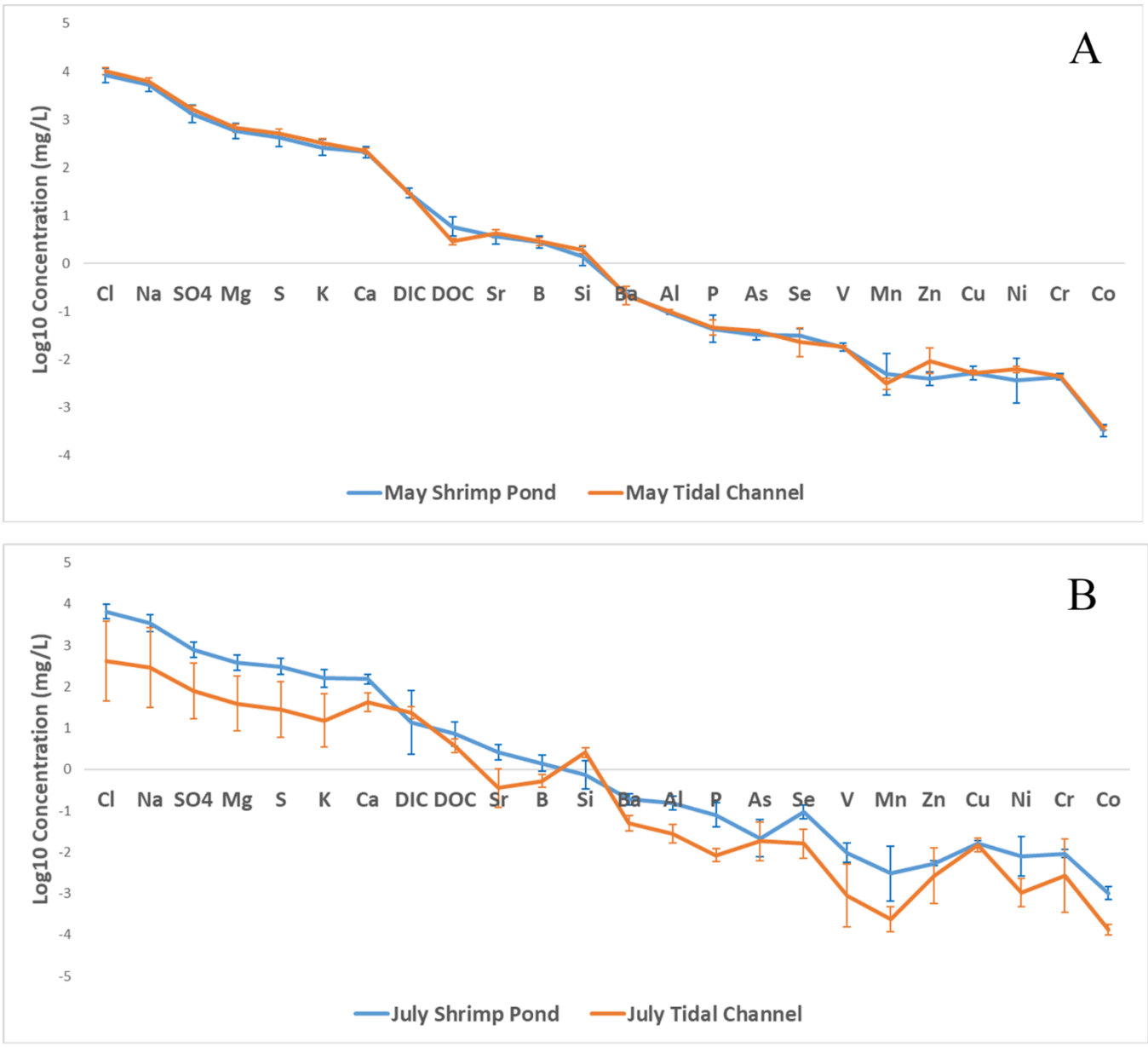

Figure 5: Spider diagrams showing arithmetic mean log10 concentrations in shrimp ponds (excluding KA-10) and tidal channel waters. Strong similarity is seen between May shrimp ponds and the tidal channels irrigating them (A). Less similarity is seen in July (B), with large variance seen in July tidal channels and lack of overlap between the two water types. Two Si values are omitted from the July shrimp pond data because of anomalous negative values.

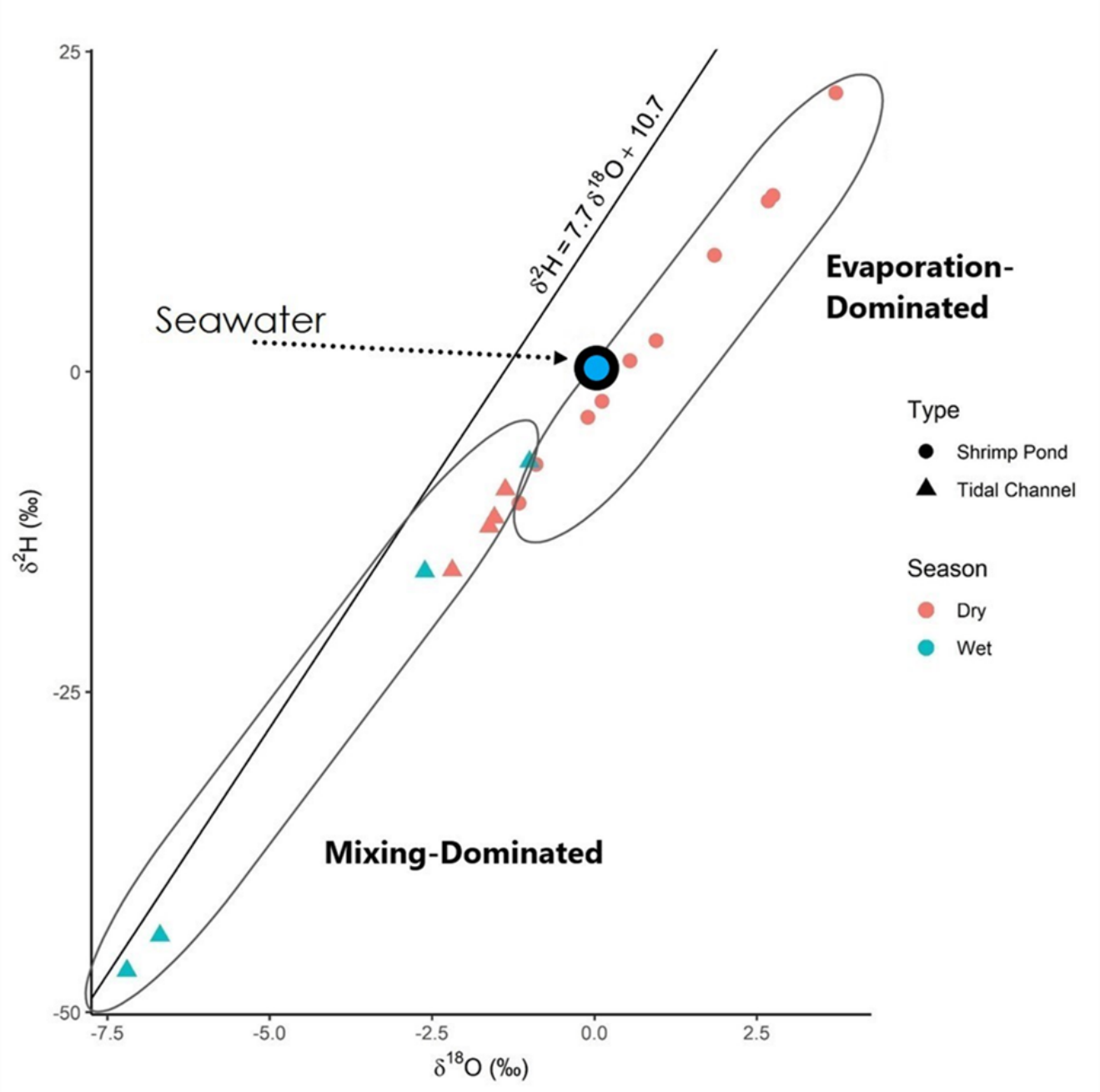

Figure 6: Bivariate plot of $\delta^{18}O$ and $\delta^{2}H$ isotopes from May shrimp ponds and May/July tidal channels. Dry season represents samples collected in May, wet season in July. Local meteoric water line (LMWL) taken from Majumder et al., 2011. "Seawater" is theoretical seawater at 0‰ $\delta^{18}O$ and $\delta^{2}H$, with a large symbol plotted to represent deviation from exact 0‰ isotopic values in the Bay of Bengal.

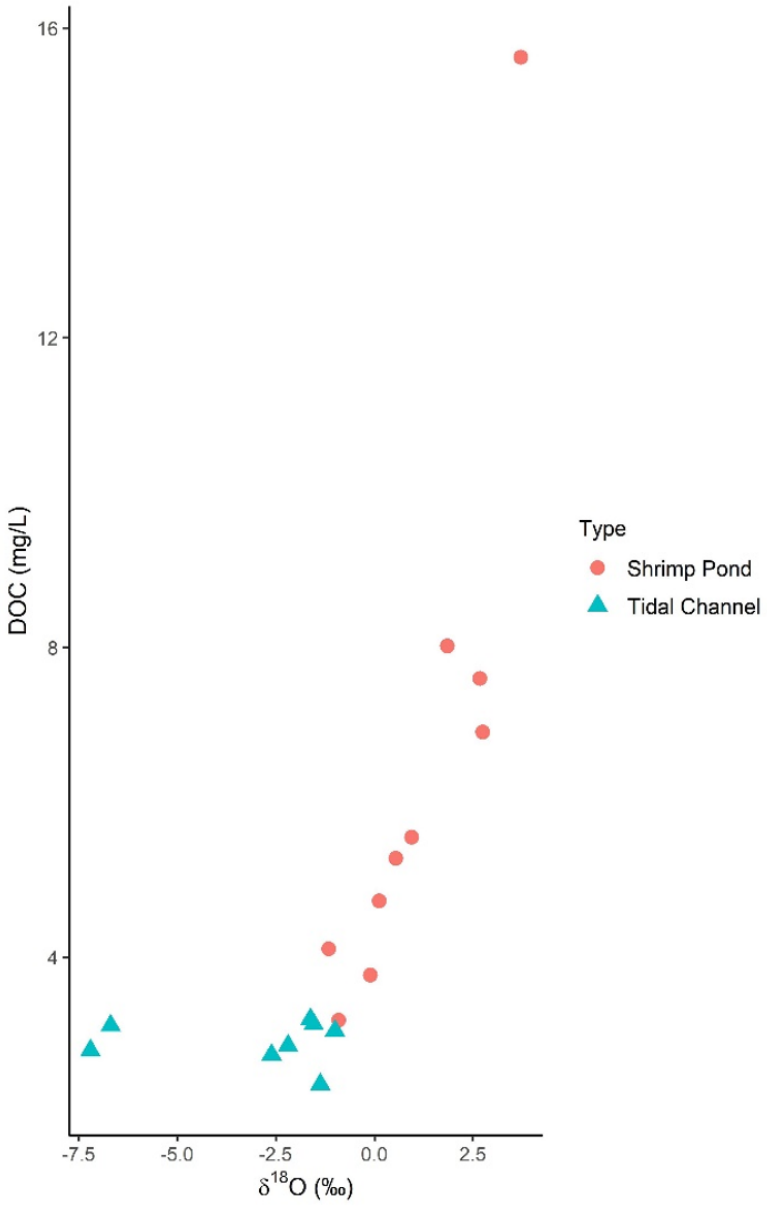

Figure 7: Bivariate plot of $\delta^{18}O$ from May shrimp ponds and May/July tidal channels showing DOC increasing with enrichment of isotopes in shrimp ponds. Spearman correlation coefficients (DOC is non-normally distributed) of 0.92 between $\delta^{18}O$ and DOC in shrimp ponds ($p = 0.00047$) and 0.095 in tidal channels ($p = 0.84$).

3.6 Surface water evaporation models

Through the React program in Geochemist's Workbench (GWB), a simple evaporation model was performed (Table A2) from the initial 1kg solution of sample MD-TC-22 to estimate

the amount of water evaporation that would yield the concentrations of conservative elements in the irrigated shrimp pond (KA-15) directly adjacent to sample MD-TC-22.

The model estimates that only a relatively small fraction of water evaporation (~0.5-10%) is needed to concentrate non-reactive major conservative ions in solution to the concentrations observed in the irrigated shrimp pond (KA-15). When looking at modeled salinity (essentially grouping all major seawater ions together), 1.5-2% evaporation of water can explain the relative increase in salinity observed from tidal channel to shrimp pond water (Fig. A5), which is close to intersample variability.

In addition to the aforementioned mass-balance focused geochemical model, relatively straightforward isotopic equations can be used to estimate the amount of evaporation in a shrimp pond after tidal channel input. Using several simplifying assumptions such as thermodynamic equilibrium and an equilibrium fractionation factor (α (l/v)) of 1.0098 at 20˚C (even though sampling temperatures were ~30-35˚C) for $^{18}O/^{16}O$ exchange (Majoube, 1971), a Rayleigh distillation equation may be used to estimate the residual fraction of water (f) left in a system (Eq. 1; Gat, 1996):

$$R = R_0 * f^{(1/\alpha - 1)} \quad (1)$$

Where R is the isotopic ratio of the residual water and R_0 is the isotopic ratio of the initial water. In a system where water is evaporating and the liquid phase is known to be more enriched in the heavier stable isotope (i.e., ^{18}O), the term for the fractionation factor (α) becomes <1 (1/α), causing isotopic enrichment in the residual liquid phase as f decreases. After converting the $\delta^{18}O$ value of the irrigating tidal channel (MD-TC-22) to an $^{18}O/^{16}O$ ratio and employing the Raleigh equation, ~10% of evaporation of the initial amount of material can explain the more enriched $^{18}O/^{16}O$ ratio of the directly irrigated shrimp pond (KA-15). However, this also assumes no other influences on stable isotopes in the shrimp pond, such as precipitation, and assumes that all water was derived from the tidal channel. These are reasonable assumptions, as during the sampling period in May 2019 no measurable precipitation was observed, and the impermeable clays lining most of the ponds prevents groundwater exfiltration or seepage from other water sources (Ayers et al., 2017, 2016).

The discrepancy between the estimated 2% evaporation based on salinity and 10% evaporation based on isotopes may be in part due to slight non-conservative processes occurring in ponds such as ion exchange that affect saltwater ions, and our isotopic evaporation model is merely an estimate, as we assume an open system with Rayleigh fractionation. In reality, the system is likely somewhere between an ideal open and ideal closed system. Additionally, if assuming fractionation between the liquid-vapor phased predominantly occurred at the surface water interface in our water samples, a temperature of ~30˚C would change the evaporative estimate to ~11% because of a different α value.

3.7 Selenium and arsenic spatial and seasonal variability

Arsenic concentrations in shrimp ponds and tidal channels are close to or above WHO drinking water guidelines (10 μg.L-1) in both May and July samples throughout SW Bangladesh

(Fig. A6). There does not appear to be any spatial correlation between measured arsenic values in both shrimp ponds and tidal channels. Additionally, selenium values are close to or above WHO drinking water guidelines (40 μg.L-1) throughout SW Bangladesh in tidal channels and shrimp ponds, with seemingly random spatial concentration trends (Fig. A7). In general, spatial heterogeneity in surface water trace element compositions appears to be the norm.

While both Se and As are within 1σ variation in May and July tidal channels (Fig. 3), Se is greater in July shrimp ponds compared to May shrimp ponds outside of 1σ variation (Fig. 4a). Arsenic is within 1σ variation when comparing May and July shrimp ponds (Fig. 4a).

3.8 Multiple linear regression

Best subsets multiple linear regression (details on variable selection in the Supplementary Document) suggests that the variables Cu, P, V and Ni can explain most As variance (Fig. 8), with an adjusted R^2 of 0.39 ($p = 0.006$) (Table A3). Their significance is supported by V, Ni, and Cu each having p-values <0.05 when looking at those four variables together as a linear regression fit for As (Table A3). For Se, linear regression using the concentrations of only V, Ni, DOC, and Cl result in one of the best adjusted R^2 values (0.74) (Table A4; Fig. 8), and each variable has a p-value <0.01 (Table A4). When removing Cl from the predictive model, the adjusted R^2 becomes 0.67 ($p < 0.0001$) with each variable (V, Ni and DOC) having a p-value <0.01 (Table A5)

Details of other models and violations of multiple linear regression assumptions are provided in the Supplementary Document.

4 Discussion

4.1 Trace element enrichment in surface waters

Trace elements of initial focus in this study were Mn and As, because of their known elevated concentrations in groundwater in the region (and potential to enter surface water through groundwater irrigation upstream or exfiltration) and known adverse health effects in excessive quantities (e.g., Frisbie et al., 2002; Harvey et al., 2002; Rahman et al., 2017; Rodrigues et al., 2016). Furthermore, Ayers et al., 2017 measured elevated As >10 μg.L-1 (WHO drinking water guideline; World Health Organization, 2017) in 78% of shrimp ponds on Polder 32 in SW Bangladesh (several samples in this present study are from/around the same polder), with 71% of May tidal channels around Polder 32 containing As >10 μg.L-1 as well. Ayers et al., 2017 also measured Mn >400 μg.L-1 (WHO health-based value; World Health Organization, 2017) in 6% of surface water samples.

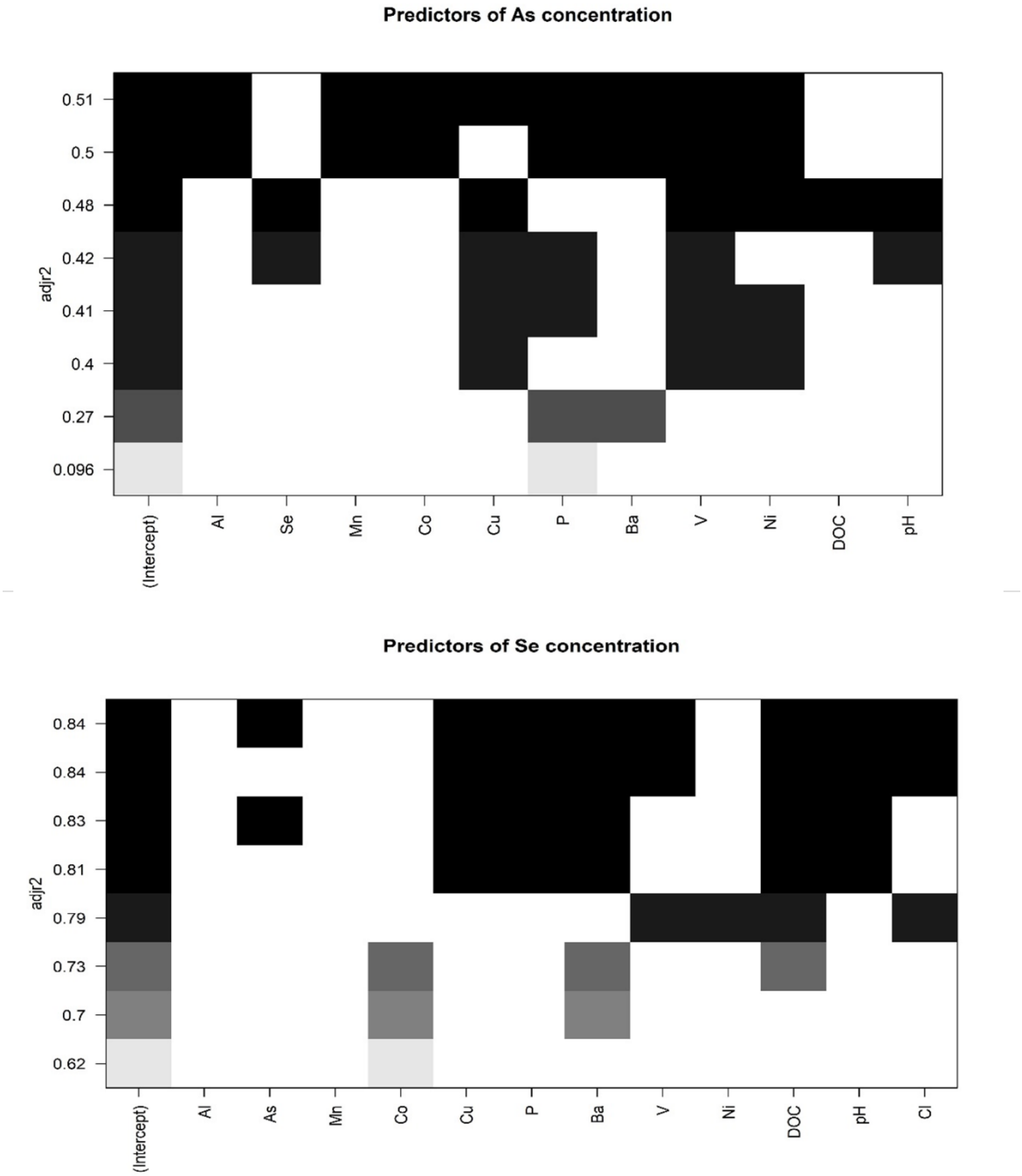

Figure 8: Multiple linear regression models for grouped variables initially selected for Se and As, with adjusted R^2 values along the y-axis. The best model was computed for each subset size (e.g., each amount of predictor variables utilized in the overall model). n = 25 because of some samples missing predictive variable measurements and thus being omitted, which also explains the slight discrepancy between multiple linear regression analyses completed with more samples (i.e., Table A4).

In this study, however, no dissolved Mn concentrations were above the WHO health-based value of 400 μg.L-1 (World Health Organization, 2017) in either shrimp ponds or tidal channels, which is expected based on Mn solubility decreasing when pH is >6, due to the formation of solid-phase Mn oxides and hydroxides (e.g., Holloway et al., 2016). Thus, elevated Mn values were reported in some of Ayers et al., 2017's shrimp pond samples despite similar pH and redox conditions. Arsenic was elevated above the WHO standard in almost all shrimp pond and tidal channel samples regardless of season, with ~87% containing As >10 μg.L-1 (Table 2). This supports data from Ayers et al., 2017 where elevated As in SW Bangladesh surface waters was also reported. However, dissolved As is not expected to be as elevated in near-neutral pH, oxidizing conditions such as those seen in surface waters (e.g., Ayers et al., 2017; Smedley and Kinniburgh, 2002), and thus more research on As cycling at the groundwater-surface water interface in Bangladesh is needed (e.g., Berube et al., 2018).

Arsenic values were >10 μg.L-1 in 75% of July samples (shrimp pond and tidal channels) during the early monsoon in this study, while Ayers et al., 2017 measured only 11% of tidal channels in October with As > 10 μg.L-1. This suggests that the monsoon rainfall has not yet reached a high enough continuous level in July to thoroughly dilute the source of surface water As compared to October. In Khulna the average precipitation in the preceding four months were ~1,261mm in October, only ~142mm in May, and ~627mm in July (BARC, 2020).

Because there were no previous reports of high Se in SW Bangladesh surface waters, it was not an initial element of concern going into this study. Furthermore, Se has been reported as low in Bangladesh groundwater (e.g., Frisbie et al., 2009, 2002; Rahman et al., 2015), so even if heavy groundwater irrigation or exfiltration could affect surface water concentrations, Se was not expected to be elevated. However, dissolved Se was found to be >50 μg.L-1 (EPA MCL; U.S. EPA, 2009) in 50% of all samples and > 40 μg.L-1 (WHO guideline; World Health Organization, 2017) in 50% of all samples (Table 2), with substantially higher average concentrations in the July shrimp ponds compared to May shrimp ponds (Fig. 4a). While low levels of Se intake can lead to nutritional deficiencies in humans such as impaired growth, or thyroid function abnormalities (e.g., Winkel et al., 2012), excessive Se intake can be toxic for humans and animals, particularly for inorganic species of Se (Spallholz et al., 2004). However, when shrimp ponds are often converted to rice paddies in the wet season in SW Bangladesh, the chemically reducing paddy sediment likely leads to the formation of insoluble elemental Se (Winkel et al., 2012).

When normalized to average concentrations in seawater, As, Se and Mn are all enriched in shrimp ponds (Fig. 4b), while As and Se are also enriched in tidal channels (Fig. A4). Thus, the sourcing of these "enriched" elements cannot be explained by seawater from the Bay of Bengal alone, and must have outside sources such as riverine flow, direct anthropogenic input (fertilizers or other chemical supplements), or groundwater flow. The higher Se concentrations in July shrimp ponds versus May shrimp ponds is difficult to explain (Fig. 4a), particularly because the same distinct seasonality is not seen in tidal channels (Fig. 3). A possible explanation is that desorption mechanisms are at work in the July shrimp ponds, although there are no correlations between Se and Eh or pH to suggest this is redox or pH influenced (Fig. A2). Because colloids can have an important influence on trace elements in solution (e.g., Gaillardet et al., 2014),

future spectroscopy and speciation analyses may help identify whether they play an important role in enrichment and seasonality in Bangladesh.

4.2 Tidal channel and shrimp pond connectivity

Strong compositional similarities were seen between May shrimp ponds and the tidal channel sources irrigating them (Fig. 5a). This suggests that there is little compositional change within the shrimp ponds after irrigation, although there is more variance between nonconservative elements, suggesting that sorption/desorption reactions may be occurring after shrimp ponds have been irrigated. This may particularly be true for cation species like Ni and Zn, which may undergo desorption in more saline waters due to competition for sorption sites with salt cations such as Ca and Na (e.g., de Souza Machado et al., 2016; Samanta and Dalai, 2018). Across all dissolved water samples in this current study, moderate positive correlations between metal cations such as Co, Ni, and Cu (Fig. A1) suggest similar geochemical processes occurring in the natural environment, such as sorption/desorption effects. July shrimp ponds show much less compositional overlap with July tidal channels (Fig. 5b). However, there is high variance of dissolved ion concentrations within July tidal channel samples (Fig. 3), which could be indicative of salinity fluctuation closely tied to rainfall and river discharge. July shrimp ponds and tidal channels may not be as similar compositionally because of shrimp farmers limiting irrigation of less saline waters to prolong harvest of brackish water shrimp varieties, or because of slow mixing rates between the irrigation source (tidal channels) and the shrimp ponds, which may not become complete until late in the monsoon season (i.e., late August or September). Future work analyzing water fluxes in and out of shrimp ponds over time would help better quantify the mixing of pond water and irrigation source.

4.3 Enrichment of As and Se

Arsenic and selenium concentrations vary widely throughout the region. However, they are both ubiquitously elevated >WHO drinking water guidelines in May and July shrimp ponds and tidal channels (Figs. A6 &A7). The widespread occurrence of high As and Se concentrations throughout the region suggests that As and Se are predominantly not locally point-sourced.

Arsenic may be sourced from arsenic-rich groundwater in the region (often >10 μg.L-1) as previously suggested (Ayers et al., 2017), upstream weathering in the Himalayas, or anthropogenic effluent run-off from cities upstream such as Khulna. Because As shows little to no correlation with conservative ions found in seawater and tends to behave nonconservatively (Fig. A1), it is difficult to deduce whether As increases as more groundwater is present in the system, particularly because there are two possible lower salinity end-members (riverine flow from upstream and groundwater flow) with potentially different As concentrations. It is noted that a January (dry season) freshwater river sample in the nearby Meghna River (where groundwater As concentrations are >10 μg.L-1) had As < 10 μg.L-1 (Berube et al., 2018), although this river has a different drainage basin.

Arsenic concentrations in this study are also much greater than surface waters sampled in 2016 in the same geographic region (Ayers et al., 2020). The differences in As concentrations between Ayers et al., 2020 and both this study and Ayers et al., 2017 may be attributed to small

sample size, overall less saline (and thus potentially more diluted) samples in Ayers et al. (2020), and sample location heterogeneity, as all three studies used similar methodology. For example, if groundwater exfiltration is a possible source of As to surface waters, sampling locations from Ayers et al., 2020 may receive different exfiltration rates of groundwater because of widespread geologic heterogeneity in the area (e.g., Ayers et al., 2016).

Selenium concentrations higher than average seawater in estuaries can be caused by conservative mixing of polluted/enriched Se river water and relatively Se-depleted seawater, such as in the Solent area in mid-southern England (Measures and Burton, 1978) or the Rhone river delta off the Mediterranean Sea (Guan and Martin, 1991). Anthropogenic input of Se was documented in the San Francisco Bay estuary from both sewage treatment plants and oil refineries, albeit the concentrations in the mixed estuary samples were much lower than those seen here (Cutter, 1989; Cutter and San Diego-McGlone, 1990). Selenium was also elevated relative to natural background in agricultural irrigation drainage in central California in the mid-1980s (Lemly, 2004). Thus, Se may be sourced from sewage, oil refineries, or agricultural runoff in the area. It is also interesting that Se concentrations are much higher in our samples from 2018 and 2019 (regardless of season) compared to results from surface waters in the same general study area in 2016 analyzed using the same methods (Ayers et al., 2020). One possible explanation for this is that Se is anthropogenic and the source of its release into the dissolved load began after sampling in 2016, potentially from industrial centers in Khulna (Dietrich and Ayers, under review), while another possible explanation is that the overall less saline samples taken in 2016 were more diluted with rainwater or other sources than ours in 2018 and 2019, thus lowering Se concentrations.

Recently, in the Ganges River system, "hot spots" of elevated trace element concentrations (relative to "background" in the study) were observed near large urban and industrial areas, but these concentrations became diluted by other river tributaries downstream (Boral et al., 2020). Thus, a city like Khulna could be a source of Se or other trace elements, and dilution is limited until either the tidal channels empty into the Bay of Bengal or it becomes peak monsoon season. Regardless of the source, a dramatic increase in Se input would be necessary for an increase in surface water concentrations from ~0.5-2 μg.L-1 in 2016 to ~10-200 μg.L-1 in 2018-2019.

4.4 Surface water isotopic composition, trends, and evaporative effects

$\delta^{18}O$ and $\delta^{2}H$ isotopes in surface waters can be useful proxies for illustrating mixing or evaporative processes. Any samples plotting on the local meteoric water line (LMWL) are theoretically local precipitation, while samples plotting to the right of the LMWL have undergone fractionation, which can be interpreted as evaporation (Gat, 1996), or mixing with isotopically enriched water such as seawater. All tidal channel samples plot close to the LMWL and trend towards the isotopic value of seawater as they become heavier or more enriched, suggesting they have undergone minimal evaporation and represent mixing between rainwater and seawater (Fig. 6). Dry season (May) shrimp pond samples are heavier in $\delta^{18}O$ and $\delta^{2}H$ and plot farther off the LMWL compared to tidal channel samples, suggesting they have undergone more evaporation and are not simply depicting mixing between rainwater and seawater.

However, even though shrimp ponds are likely undergoing more evaporation, there is not a positive correlation with isotope values and salinity (SpC) (Fig. A8). A positive correlation would be expected, because as water evaporates, conservative ions should stay in solution and become more concentrated. The lack of an observed positive correlation is likely a consequence of each shrimp pond having different starting salinities following irrigation from tidal channels, with concentration variations in the tidal channel irrigation source "masking" the relatively minor effects of evaporation on conservative salt ions. However, when looking at a shrimp pond and irrigating tidal channel directly adjacent to it, slight evaporative enrichment occurs with conservative elements, while several nonconservative elements are depleted in shrimp ponds (i.e., Mn and P; those less likely to desorb from saltwater cation exchange), possibly due to mineral precipitation or sorption onto sediment surfaces (Fig. A9).

Evaporative models further illustrate the aforementioned point that although evaporation is likely occurring in the shrimp ponds more than the irrigating tidal channels, the amount of evaporation has little overall influence on major element concentrations in solution (Fig. A5). Evaporation appears low in May (≤10%) and does not significantly affect element concentrations in shrimp ponds. This is likely a result of regular shrimp pond drainage of wastes and replenishment from new tidal channel water, which would reduce water residence time and the effects of evaporation. However, the evaporation models were based on a sample close to high tide and are thus minimum estimates of evaporation, although in the nearby Bangladesh Sundarbans, salinity changes between high and low tide in the dry season tidal channels are often around ~1ppt or less, with some tidal channels seeing practically no salinity change between tides at all (Rahaman et al., 2014, 2013).

Trace elements of interest, such as As and Se, also do not show any clear trends with stable isotopes (Fig. A10). Weak to moderate relationships are seen with all other elements as well (Fig. A11). Essentially, evaporation is not great enough to overcome the large variance in starting compositions of the shrimp pond water, or the effects of nonconservative element behavior are larger than the effects of evaporation, effectively erasing any possible correlation between stable isotopes and nonconservative behaving elements.

DOC shows a strong positive relationship with stable isotopes (Fig. 7). As $\delta^{18}O$ and $\delta^{2}H$ isotopes become heavier in shrimp ponds, DOC increases as well, likely because these variables are affected by endogenous processes in shrimp ponds (e.g., biological processes or evaporation), while other geochemical parameters are more affected by exogenous processes (e.g., upstream rock weathering, seawater mixing). For example, as shrimp pond waters undergo more evaporation, they become more stagnant with lower flow conditions, algae-rich, and produce DOC through algal photosynthetic activity (e.g., Cole et al., 1982). Additionally, all shrimp ponds have similar DOC concentrations in their irrigation source (as seen with little variation in tidal channel DOC values in Fig. 7), which allows identification of the small changes caused by evaporation. DOC values do not show a relationship with isotopes in tidal channels because tidal channel isotopic values are predominantly influenced by rainwater-seawater mixing instead of evaporation.

Lastly, it must be noted that expanding isotopic analysis of shrimp pond waters to other months/seasons may be useful for helping determine geochemical relationships as well,

particularly because when excluding isotopes, multidimensional scaling (MDS) shows July shrimp ponds are distinct from other samples (Fig. A12).

4.5 Multiple linear regression and predictors of As and Se

Nearly all our samples plotted similarly to seawater in a Piper diagram (Fig. A13), and were thus collectively used in multiple linear regression to assess important predictor variables for As and Se, even though most elements showed large variability in concentration.

Multiple linear regression illustrates that Ni, P and V are important predictor variables for Se and/or As in most water samples (Fig. 8). Phosphorus is regarded as a "chemical analog" to As, and like As (as pentavalent arsenate) in oxidized aqueous environments, P is mainly in an oxyanion form (as PO_4^{3-}) (Strawn, 2018). However, in the main predictive model for As, P is positively correlated (Table A3), which would suggest that even though both elements are likely negatively charged species in solution, their concentrations are not explained by competitive adsorption. Vanadium is likely predominantly an oxyanion as well given the pH and oxidizing conditions of the surface water samples, with the most common ion of V being $H_2VO_4^-$ in natural waters (Crans and Tracey, 1998). Because V is positively correlated with As in the predictive model (Table A3), it may also behave similarly in solution but not compete directly for sorption sites. However, Ni is most often a cation species with a valence of +2 in natural waters (Langmuir et al., 2004). When analyzing primary influencing variables for As (Cu, V, Ni and P), it is clear that only Ni is negatively correlated, illustrating that Ni may improve the model because of different chemical behaviors (i.e., sorption affinities) as a cation in solution (Table A3).

Selenium also exists as oxyanions in oxidizing environments such as surface waters (Winkel et al., 2012). When looking at the predictive variables V, Ni, and DOC for Se; V has a negative coefficient in the model while Ni has a positive coefficient (Table A5). This is opposite that of the main As model (Table A3). Thus, for Se, even though V is likely an anion in solution and Ni a cation, the anion is associated with a decrease in Se in the model. This may be due to competitive sorption properties of Se and V on solid particle surfaces (particularly with selenite on Fe-oxyhydroxides or clay minerals), which would increase V in solution as Se sorbs. Ni may complex with aqueous species that behave similarly to Se but do not compete with sorption sites.

pH is important to include in modeling because of its known effects on speciation and mobility of Se and As (e.g., Strawn, 2018; Winkel et al., 2012). However, models that include pH do not significantly improve As or Se prediction (Fig. 8), potentially due to relatively small variance in pH values (Table 1). Thus, pH does not likely have a large, statistically significant influence on either Se or As concentrations in these surface waters, although it is acknowledged that pH is important in speciation of these elements and thus their chemical characteristics in solution.

When adding isotopes to predictive modeling to determine whether evaporation/mixing may affect Se and As predictability, the adjusted R^2 values for both Se and As increase to both 0.70 ($p = 0.016$) and 0.90 ($p = 0.0041$), respectively (Tables A6 & A7), but only 14 samples are included in the analysis, omitting all July shrimp ponds. The influence of isotopes must be taken with care, as clear bivariate relationships between Se, As and $\delta^{18}O$ (and $\delta^{2}H$) are not apparent

(Fig. A10), and the inclusion of both isotopes ($\delta^{18}O$ and $\delta^{2}H$) in the Se model (Table A7) clearly violate the multiple linear regression assumption of no multicollinearity among predictor variables. However, future work investigating the predictive nature of stable isotopes for trace elements in surface water or groundwater modeling may be warranted because as proxies of mixing or evaporation, O and H isotopes may provide additional insight as to where certain elements originated from or if evaporation concentrated elements in solution.

Additionally, because organic matter such as DOC can affect trace elements in multiple ways, such as complexing with As species or competing for sorption sites (e.g., Lin et al., 2017; Williams et al., 2011), it was another geochemical parameter worth examining. For Se, it was found that the predictor variables DOC, V, and Ni resulted in an adjusted R^2 of 0.67 ($p < 0.0001$) (Table A5). Thus, Se may also be affected by DOC, such as by surface water reoxidation of biogenic elemental Se (BioSe) that originated from microbes (Winkel et al., 2012) in high DOC waters. More research in shrimp pond elemental cycling would help shed insight on this. Lastly, it is apparent that adding Cl as a representative saltwater ion to the variables DOC, V and Ni improves the predictive model (Table A4), which may be indicative of slight seawater mixing or seasonality effects on aqueous Se. However, it is noted that Cl does have a strong positive correlation with V (Fig. A1), and thus violates the assumption of no multicollinearity for multiple linear regression.

4.6 Applicability of Se and As models

While these models do not identify the mechanisms that control As and Se concentrations in shrimp ponds and tidal channel waters, they are very useful in gauging what elements/geochemical parameters are most important in influencing As and Se concentrations in surface waters. This extends to upstream (non-headwaters) Ganges River samples (Boral et al., 2020; their Table S4), where Cu, Vi, and Ni result in a great multiple linear predictive model fit for As (adjusted $R^2 = 0.64$, $p = 7.2e\text{-}15$) (Table A8). Additionally, when examining tidal channel samples from Ayers et al. (2020), predicting As with Cu, V, Ni, and P results in a great overall fit as well (adjusted $R^2 = 0\ .74$, $p = 0.024$) (Table A9). However, Se predictive modeling for tidal channels in Ayers et al. (2020) is much poorer, with DOC, V, and Ni only resulting in an adjusted R^2 of 0.24 ($p = 0.17$). Nevertheless, the general approach of multiple linear regression with several important predictor variables such as Ni and V or other geochemical analogues appears to be applicable to other surface water bodies, particularly rivers, and can be especially useful in better understanding and predicting the concentration of As in solution. Further research in quantifying Se in surface waters will help in understanding what controls/predicts its geochemical variability.

These models also provide a way to estimate As and Se concentrations in Bangladesh surface waters without direct measurements of As or Se. Model validation using other published datasets indicates that the model parameters obtained in this study do not produce model predictions that agree well with observed As and Se concentrations (i.e., Fig. A14). However, the general approach used here can help improve predictions and measurements in other regions throughout the world, particularly when several geochemical parameters may be missing from samples within an area. For example, if a study has only analyzed As or Se in 15% of samples,

but the remaining samples contain potentially important predictor variables such as Ni or V, a modeling solution can be applied to estimate As or Se in the remaining samples.

Although this study assumed linear relationships in predictive modeling, future work involving nonlinear predictive modeling techniques such as machine learning techniques (i.e., boosted regression trees) is warranted, as these techniques have been shown to outperform multiple linear regression predictive modeling in groundwater (Nolan et al., 2015).

4.7 Selenium and arsenic antagonistic relationship

Se is known to combat the toxic effects of As, and As is known to inhibit Se toxicity (e.g., George et al., 2013; Spallholz et al., 2008, 2004). Elevated Se and As can be taken up by biological organisms, and may eventually sorb onto soils/sediment. This is particularly relevant for As in the area, as many shrimp ponds are utilized for rice farming in the wet season (Ayers et al., 2017), where flooded soils could remobilize sorbed As through reductive dissolution of Fe oxyhydroxides (e.g., Roberts et al., 2011). However, even if Se becomes elevated in soils from tidal channel irrigation, the reducing conditions in flooded rice paddy soils could lead to immobile elemental selenium being formed, which is not bioavailable (Winkel et al., 2012). Thus, rice could potentially take up arsenic, but not selenium, with humans therefore lacking the detoxifying effects of selenium when ingesting the rice. Further work is needed to explore the cycling and antagonistic relationship between Se and As in Southwest Bangladesh, such as identifying if sediments in contact with Se and As-rich waters are elevated in both those elements, what fraction is bioavailable, and if Se concentrations in tidal channel waters in the peak monsoon season become heavily diluted. Although much research in Bangladesh has examined As in crops such as rice (e.g., Khan et al., 2010; Williams et al., 2011, 2006), crop/aquaculture Se should be more heavily researched in Southwest Bangladesh as well, particularly where Se water concentrations are high.

5 Conclusion

Through examining surface water chemistry in Southwest Bangladesh in two different months over a wide spatial area, it was deduced that: 1) Monthly precipitation differences between May and July has a greater effect on tidal channel water composition compared to shrimp pond composition; 2) There is a large compositional difference between shrimp ponds and the tidal channels irrigating them in the early monsoon (July), but not in May; 3) Evaporation in shrimp ponds and endogenous pond effects in general have a relatively minimal impact on surface water trace element and major ion chemistry based on May pond data, although DOC has a strong positive correlation with $\delta^{18}O$ and $\delta^{2}H$ isotopes and thus evaporation; 4) Arsenic and selenium concentrations are elevated above WHO drinking water guidelines in the majority of surface water samples and are correlated with other trace elements in solution such as Ni and V; and 5) Predictive modeling of hazardous trace elements in surface waters may prove useful in future studies throughout the world when measurements of certain toxic elements cannot always be easily made.

Acknowledgements:

We thank the two anonymous reviewers and the handling editor, Jeremy Fein for their thoughtful and thorough comments that improved the quality of this manuscript. Funding supported by the NSF Coastal SEES Collaborative Research Grant OCE-1600319. Special thanks to Md. Zahidul Haque, Jess Raff and Kelsea Best for their immense help in the field; Md. Saddam Hossain and Abrar Hossain for general assistance in Bangladesh; Carol Wilson and Michael Steckler for sample collection assistance, and thanks to many others from the University of Dhaka, Khulna University and Pugmark Tours (Md Nazrul Islam (Bachchu)) who have helped with this ongoing research project. Thanks also goes out to Rossane DeLapp and Richard Bradshaw for analytical assistance, and Jessica Oster for fruitful discussion.

References:

Ahmed, A., Ghosh, P.K., Hasan, M., Rahman, A., 2020. Surface and groundwater quality assessment and identification of hydrochemical characteristics of a south-western coastal area of Bangladesh. Environ. Monit. Assess. 192. https://doi.org/10.1007/s10661-020-8227-0

Akter, S., Ahmed, K.R., 2019. Water chemistry and water quality of a tidal river system in relation with riverbank land use pattern and regional climate in the southwest Bengal Delta of Bangladesh. Sustain. Water Resour. Manag. 1–21. https://doi.org/10.1007/s40899-019-00308-3

Akter, S., Ahmed, K.R., Marandi, A., Schüth, C., 2020. Possible factors for increasing water salinity in an embanked coastal island in the southwest Bengal Delta of Bangladesh. Sci. Total Environ. https://doi.org/10.1016/j.scitotenv.2020.136668

Anawar, H.M., Akai, J., Komaki, K., Terao, H., Yoshioka, T., Ishizuka, T., Safiullah, S., Kato, K., 2003. Geochemical occurrence of arsenic in groundwater of Bangladesh: Sources and mobilization processes. J. Geochemical Explor. 77, 109–131. https://doi.org/10.1016/S0375-6742(02)00273-X

Auerbach, L.W., Goodbred Jr, S.L., Mondal, D.R., Wilson, C. a., Ahmed, K.R., Roy, K., Steckler, M.S., Small, C., Gilligan, J.M., Ackerly, B. a., 2015. Flood risk of natural and embanked landscapes on the Ganges–Brahmaputra tidal delta plain. Nat. Clim. Chang. 5, 153–157. https://doi.org/10.1038/nclimate2472

Ayers, J.C., George, G., Fry, D., Benneyworth, L., Wilson, C., Auerbach, L., Roy, K., Karim, M.R., Akter, F., Goodbred, S., 2017. Salinization and arsenic contamination of surface water in southwest Bangladesh. Geochem. Trans. 18, 4. https://doi.org/10.1186/s12932-017-0042-3

Ayers, J.C., George, G., Fry, D., Benneyworth, L., Wilson, C., Wallace Auerbach, L., Roy, K., Karim, M.R., Akhter, F., Goodbred, S., 2016. Sources of Salinity and Arsenic in groundwater in Southwest Bangladesh. Geochem. Trans. 1–22. https://doi.org/10.1186/s12932-016-0036-6

Ayers, J. C., Patton, B., & Dietrich, M. (2020). Preliminary Evidence of Transport-Limited Chemical Weathering and Element Immobility in the Ganges Tidal Delta Plain of Bangladesh. *Geochemistry, Geophysics, Geosystems*, *21*(8), e2020GC009029.

Azad, A.K., Jensen, K.R., Lin, C.K., 2009. Coastal Aquaculture Development in Bangladesh: Unsustainable and Sustainable Experiences. Environ. Manage. 44, 800–809. https://doi.org/10.1007/s00267-009-9356-y

Bangladesh Agricultural Research Council (BARC), 2020. Climate Data – Rainfall (1950-2018). Accessed March 31, 2020. http://climate.barcapps.gov.bd/rainfall

Benneyworth, L., Gilligan, J., Ayers, J.C., Goodbred, S., George, G., Carrico, A., Karim, M.R., Akter, F., Fry, D., Donato, K., Piya, B., 2016. Drinking water insecurity: water quality and access in coastal south-western Bangladesh. Int. J. Environ. Health Res. 3123, 1–17. https://doi.org/10.1080/09603123.2016.1194383

Berube, M., Jewell, K., Myers, K. D., Knappett, P. S., Shuai, P., Hossain, A., ... & Datta, S. (2018). The fate of arsenic in groundwater discharged to the Meghna River, Bangladesh. *Environ. Chem.*, *15*, 29.

Bethke, C. M. (2007). Geochemical and biogeochemical reaction modeling. Cambridge University Press.

Bickle, M.J., Chapman, H.J., Tipper, E., Galy, A., De La Rocha, C.L., Ahmad, T., 2018. Chemical weathering outputs from the flood plain of the Ganga. Geochim. Cosmochim. Acta 225, 146–175. https://doi.org/10.1016/j.gca.2018.01.003

Boral, S., Sen, I.S., Tripathi, A., Sharma, B., Dhar, S., 2020. Tracking dissolved trace and heavy metals in the Ganga River from source to sink: A baseline to judge future changes. Geochemistry, Geophys. Geosystems 1–22. https://doi.org/10.1029/2020GC009203

Brammer, H., 2014. Bangladesh's dynamic coastal regions and sea-level rise. Clim. Risk Manag. 1, 51–62. https://doi.org/10.1016/j.crm.2013.10.001

Charlet, L., Polya, D.A., 2006. Arsenic in shallow, reducing groundwaters in southern Asia: an environmental health disaster. Elements 2, 91.

Chowdhury, N.T., 2010. Water management in Bangladesh: An analytical review. Water Policy 12, 32–51. https://doi.org/10.2166/wp.2009.112

Cole, J.J., Likens, G.E., Strayer, D.L., 1982. Photosynthetically produced dissolved organic carbon: An important carbon source for planktonic bacteria. Limnol. Oceanogr. 27, 1080–1090. https://doi.org/10.4319/lo.1982.27.6.1080

Crans, D. C., & Tracey, A. S. (1998). The chemistry of vanadium in aqueous and nonaqueous

solution. ACS Symp Ser 711:2–29. https://doi.org/10.1021/bk-1998-0711.ch001

Cutter, G.A., 1989. The estuarine behaviour of selenium in San Francisco Bay. Estuar. Coast. Shelf Sci. https://doi.org/10.1016/0272-7714(89)90038-3

Cutter, G.A., San Diego-McGlone, M.L.C., 1990. Temporal variability of selenium fluxes in San Francisco Bay. Sci. Total Environ. https://doi.org/10.1016/0048-9697(90)90243-N

Das, P.R., Hossain, K., Sarker, B.S., Parvin, A., Das, S.S., Moniruzzaman, M., Saha, B., 2017. Heavy Metals in Farm Sediments , Feeds and Bioaccumulation of Some Selected Heavy Metals in Various Tissues of Farmed Pangasius hypophthalmus in Bangladesh 8. https://doi.org/10.4172/2150-3508.1000218

Datta, D., Ghosh, P., Karim, R., Rahman, M., 2020. Geochemical Options for Water Security in a Coastal Urban Agglomerate of Lower Bengal Delta , Bangladesh. J. Geochemical Explor. 209, 106440. https://doi.org/10.1016/j.gexplo.2019.106440

Dietrich, M.., Ayers, J. (under review). Element transport and partitioning along tidal channels in Southwest Bangladesh. Environ. Sci.: Process. Impacts.

Frisbie, S.H., Mitchell, E.J., Mastera, L.J., Maynard, D.M., Yusuf, A.Z., Siddiq, M.Y., Ortega, R., Dunn, R.K., Westerman, D.S., Bacquart, T., Sarkar, B., 2009. Public health strategies for western Bangladesh that address arsenic manganese, uranium, and other toxic elements in drinking water. Environ. Health Perspect. 117, 410–416. https://doi.org/10.1289/ehp.11886

Frisbie, S.H., Ortega, R., Maynard, D.M., Sarkar, B., 2002. The concentrations of arsenic and other toxic elements in Bangladesh's drinking water. Environ. Health Perspect. 110, 1147–1153. https://doi.org/10.1289/ehp.021101147

Gaillardet, J., Viers, J., Dupré, B., 2014. Trace Elements in River Waters in: Surface and Ground Water, Weathering and Soils, Treatise on Geochemistry. https://doi.org/10.1016/B978-0-08-095975-7.00507-6

Gat, J.R., 1996. Oxygen and Hydrogen Isotopes in the Hydrologic Cycle. Annu. Rev. Earth Planet. Sci. 24, 225–262. https://doi.org/10.1146/annurev.earth.24.1.225

George, C.M., Gamble, M., Slavkovich, V., Levy, D., Ahmed, A., Ahsan, H., Graziano, J., 2013. A cross-sectional study of the impact of blood selenium on blood and urinary arsenic concentrations in Bangladesh. Environ. Heal. A Glob. Access Sci. Source 12, 1–7. https://doi.org/10.1186/1476-069X-12-52

Guan, D.M., Martin, J.M., 1991. Selenium distribution in the Rhône delta and the Gulf of Lions. Mar. Chem. https://doi.org/10.1016/S0304-4203(09)90068-8

Guhathakurta, H., Kaviraj, A., 2000. Heavy metal concentration in water, sediment, shrimp

(Penaeus monodon) and Mullet (Liza parsia) in some brackish water ponds of Sunderban, India. Mar. Pollut. Bull. 40, 914–920. https://doi.org/10.1016/S0025-326X(00)00028-X

Haldar, K., Kujawa-Roeleveld, K., Dey, P., Bosu, S., Datta, D.K., Rijnaarts, H.H.M., 2020. Spatio-temporal variations in chemical-physical water quality parameters influencing water reuse for irrigated agriculture in tropical urbanized deltas. Sci. Total Environ. 708, 134559. https://doi.org/10.1016/j.scitotenv.2019.134559

Harvey, C.F., Swartz, C.H., Badruzzaman, A.B.M., Keon-Blute, N., Yu, W., Ali, M.A., Jay, J., Beckie, R., Niedan, V., Brabander, D., Oates, P.M., Ashfaque, K.N., Islam, S., Hemond, H.F., Ahmed, M.F., 2002. Arsenic mobility and groundwater extraction in Bangladesh. Science (80-.). 298, 1602–1606. https://doi.org/10.1126/science.1076978

Holloway, C.J., Santos, I.R., Tait, D.R., Sanders, C.J., Rose, A.L., Schnetger, B., Brumsack, H.J., Macklin, P.A., Sippo, J.Z., Maher, D.T., 2016. Manganese and iron release from mangrove porewaters: A significant component of oceanic budgets? Mar. Chem. 184, 43–52. https://doi.org/10.1016/j.marchem.2016.05.013

Islam, A.R.M.T., Islam, H.M.T., Mia, M.U., Khan, R., Habib, M.A., Bodrud-Doza, M., Siddique, M.A.B., Chu, R., 2020. Co-distribution, possible origins, status and potential health risk of trace elements in surface water sources from six major river basins, Bangladesh. Chemosphere 249. https://doi.org/10.1016/j.chemosphere.2020.126180

Khan, M.A., Stroud, J.L., Zhu, Y.-G., McGrath, S.P., Zhao, F.-J., 2010. Arsenic Bioavailability to Rice Is Elevated in Bangladeshi Paddy Soils. Environ. Sci. Technol. 44, 8515–8521. https://doi.org/10.1021/es101952f

Knappett, P.S.K., Mailloux, B.J., Choudhury, I., Khan, M.R., Michael, H.A., Barua, S., Mondal, D.R., Steckler, M.S., Akhter, S.H., Ahmed, K.M., Bostick, B., Harvey, C.F., Shamsudduha, M., Shuai, P., Mihajlov, I., Mozumder, R., van Geen, A., 2016. Vulnerability of low-arsenic aquifers to municipal pumping in Bangladesh. J. Hydrol. https://doi.org/10.1016/j.jhydrol.2016.05.035

Langmuir, D., Chrostowski, P., Vigneault, B., & Chaney, R. (2004). Issue paper on the environmental chemistry of metals. US-EPA Risk Assessment Forum: Papers Addressing Scientific Issues in the Risk Assessment of Metals, p 114. http://cfpub.epa.gov/ncea/raf/recordisplay.cfm?deid=59052

Lemly, A. D. (2004). Aquatic selenium pollution is a global environmental safety issue. *Ecotoxicology and environmental safety*, *59*(1), 44-56.

Lin, T. Y., Hafeznezami, S., Rice, L., Lee, J., Maki, A., Sevilla, T., ... & Badruzzaman, A. B. M. (2017). Arsenic oxyanion binding to NOM from dung and aquaculture pond sediments in Bangladesh: importance of site-specific binding constants. Applied Geochemistry, 78, 234-240.

Lumley, T. (2020). Package 'leaps': Regression Subset Selection. CRAN – Package. https://cran.r-project.org/web/packages/leaps/leaps.pdf

Lupker, M., France-Lanord, C., Galy, V., Lavé, J., Gaillardet, J., Gajurel, A.P., Guilmette, C., Rahman, M., Singh, S.K., Sinha, R., 2012. Predominant floodplain over mountain weathering of Himalayan sediments (Ganga basin). Geochim. Cosmochim. Acta. https://doi.org/10.1016/j.gca.2012.02.001

Majoube, M. (1971). Fractionnement en oxygene 18 et en deuterium entre l'eau et sa vapeur. J. Chim. Phys., 68, 1423-1436.

Majumder, R.K., Halim, M.A., Saha, B.B., Ikawa, R., Nakamura, T., Kagabu, M., Shimada, J., 2011. Groundwater flow system in Bengal Delta , Bangladesh revealed by environmental isotopes. Environ. Earth Sci. 64, 1343–1352. https://doi.org/10.1007/s12665-011-0959-2

Measures, C.I., Burton, J.D., 1978. Behaviour and speciation of dissolved selenium in estuarine waters. Nature 273.

Neumann, R.B., Ashfaque, K.N., Badruzzaman, a. B.M., Ashraf Ali, M., Shoemaker, J.K., Harvey, C.F., 2009. Anthropogenic influences on groundwater arsenic concentrations in Bangladesh. Nat. Geosci. 3, 46–52. https://doi.org/10.1038/ngeo685

Nickson, R.T., McArthur, J.M., Ravenscroft, P., Burgess, W.G., Ahmed, K.M., 2000. Mechanism of arsenic release to groundwater, Bangladesh and West Bengal. Appl. Geochemistry 15, 403–413.

Nolan, B. T., Fienen, M. N., & Lorenz, D. L. (2015). A statistical learning framework for groundwater nitrate models of the Central Valley, California, USA. Journal of Hydrology, 531, 902-911.

Ogawa, H., Tanoue, E., 2003. Dissolved Organic Matter in Freshwaters. J. Oceanogr. 59, 129–147. https://doi.org/10.1016/B0-08-043751-6/05080-5

Peters, C.N., Baroud, H., Hornberger, G.M., 2019. Multicriteria Decision Analysis of Drinking Water Source Selection in Southwestern Bangladesh. J. Water Resour. Plan. Manag. 145, 05019004. https://doi.org/10.1061/(ASCE)WR.1943-5452.0001029

Proshad, R., Islam, S., Tusher, T.R., Zhang, D., Khadka, S., Gao, J., Kundu, S., 2020. Appraisal of heavy metal toxicity in surface water with human health risk by a novel approach: a study on an urban river in vicinity to industrial areas of Bangladesh. Toxin Rev. 0, 1–17. https://doi.org/10.1080/15569543.2020.1780615

Rahaman, S.M.B., Sarder, L., Rahaman, M.S., Ghosh, A.K., Biswas, S.K., Siraj, S.M.S., Huq, K.A., Hasanuzzaman, A.F.M., Islam, S.S., 2013. Nutrient dynamics in the Sundarbans mangrove estuarine system of Bangladesh under different weather and tidal cycles. Ecol. Process. 2, 1–13. https://doi.org/10.1186/2192-1709-2-29

Rahaman, S.M.B., Biswas, S.K., Rahaman, M.S., Ghosh, A.K., Sarder, L., Siraj, S.M.S., Islam, S.S., 2014. Seasonal nutrient distribution in the Rupsha-Passur tidal river system of the Sundarbans mangrove forest, Bangladesh. Ecol. Process. 3, 1–11. https://doi.org/10.1186/s13717-014-0018-5

Rahman, M.M., Dong, Z., Naidu, R., 2015. Concentrations of arsenic and other elements in groundwater of Bangladesh and West Bengal, India: Potential cancer risk. Chemosphere 139, 54–64. https://doi.org/10.1016/j.chemosphere.2015.05.051

Rahman, S.M., Kippler, M., Tofail, F., Bölte, S., Hamadani, J.D., Vahter, M., 2017. Manganese in drinking water and cognitive abilities and behavior at 10 years of age: A prospective cohort study. Environ. Health Perspect. 125, 1–8. https://doi.org/10.1289/EHP631

Roberts, L.C., Hug, S.J., Voegelin, A., Dittmar, J., Kretzschmar, R., Wehrli, B., Saha, G.C., Badruzzaman, A.B.M., Ali, M.A., 2011. Arsenic dynamics in porewater of an intermittently irrigated paddy field in Bangladesh. Environ. Sci. Technol. 45, 971–976. https://doi.org/10.1021/es102882q

Rodrigues, E.G., Bellinger, D.C., Valeri, L., Hasan, M.O.S.I., Quamruzzaman, Q., Golam, M., Kile, M.L., Christiani, D.C., Wright, R.O., Mazumdar, M., 2016. Neurodevelopmental outcomes among 2- to 3-year-old children in Bangladesh with elevated blood lead and exposure to arsenic and manganese in drinking water. Environ. Heal. 15, 44. https://doi.org/10.1186/s12940-016-0127-y

Roy, K., Karim, M.R., Akter, F., Islam, M.S., Ahmed, K., Rahman, M., Datta, D.K., Khan, M.S.A., 2018. Hydrochemistry, water quality and land use signatures in an ephemeral tidal river: implications in water management in the southwestern coastal region of Bangladesh. Appl. Water Sci. 8, 78. https://doi.org/10.1007/s13201-018-0706-x

Samanta, S., Dalai, T.K., 2018. Massive production of heavy metals in the Ganga (Hooghly) River estuary, India: Global importance of solute-particle interaction and enhanced metal fluxes to the oceans. Geochim. Cosmochim. Acta 228, 243–258. https://doi.org/10.1016/j.gca.2018.03.002

Sarin, M.M., Krishnaswami, S., Dilli, K., Somayajulu, B.L.K., Moore, W.S., 1989. Major ion chemistry of the Ganga-Brahmaputra river system: Weathering processes and fluxes to the Bay of Bengal. Geochim. Cosmochim. Acta. https://doi.org/10.1016/0016-7037(89)90205-6

Sarkar, T., Alam, M.M., Parvin, N., Fardous, Z., Chowdhury, A.Z., Hossain, S., Haque, M.E., Biswas, N., 2016. Assessment of heavy metals contamination and human health risk in shrimp collected from different farms and rivers at Khulna-Satkhira region, Bangladesh. Toxicol. Reports 3, 346–350. https://doi.org/10.1016/j.toxrep.2016.03.003

Shammi, M., Rahman, M.M., Islam, M.A., Bodrud-Doza, M., Zahid, A., Akter, Y., Quaiyum, S., Kurasaki, M., 2017. Spatio-temporal assessment and trend analysis of surface water salinity

in the coastal region of Bangladesh. Environ. Sci. Pollut. Res. 24, 14273–14290. https://doi.org/10.1007/s11356-017-8976-7

Singh, M., Müller, G., Singh, I.B., 2003. Geogenic distribution and baseline concentration of heavy metals in sediments of the Ganges River, India. J. Geochemical Explor. https://doi.org/10.1016/S0375-6742(03)00016-5

Smedley, P.L., Kinniburgh, D.G., 2002. Source and behaviour of arsenic in natural waters. Appl. Geochemistry 17, 517–568.

de Souza Machado, A., Spencer, K., Kloas, W., Toffolon, T., Zarfl, C., 2016. Metal fate and effects in estuaries: A review and conceptual model forbetter understanding of toxicity. Sci. Total Environ. 541, 268–281. https://doi.org/.1037//0033-2909.I26.1.78

Spallholz, J.E., Boylan, L.M., Rahman, M.M., Katz, D., Robertson, J.D., Zakaria, A.B.M., Khan, A.H., Alauddin, M., Bhattacharjee, M., Sultana, S., Khanam, S., Choucair, Z., 2008. Selenium content of rice, mixed plant foods and fish from Bangladesh. Toxicol. Environ. Chem. 90, 211–220. https://doi.org/10.1080/02772240701419404

Spallholz, J.E., Boylan, L.M., Rhaman, M.M., 2004. Environmental hypothesis: Is poor dietary selenium intake an underlying factor for arsenicosis and cancer in Bangladesh and West Bengal, India? Sci. Total Environ. 323, 21–32. https://doi.org/10.1016/j.scitotenv.2003.09.034

Strawn, D.G., 2018. Review of interactions between phosphorus and arsenic in soils from four case studies. Geochem. Trans. 19, 10. https://doi.org/10.1186/s12932-018-0055-6

U.S. EPA [U.S. Environmental Protection Agency]. (2009). National Primary Drinking Water Regulations. https://www.epa.gov/sites/production/files/2016-06/documents/npwdr_complete_table.pdf

Williams, P.N., Islam, M.R., Adomako, E.E., Raab, A., Hossain, S.A., Zhu, Y.G., Feldmann, J., Meharg, A.A., 2006. Increase in rice grain arsenic for regions of Bangladesh irrigating paddies with elevated arsenic in groundwaters. Environ. Sci. Technol. 40, 4903–4908. https://doi.org/10.1021/es060222i

Williams, P.N., Zhang, H., Davison, W., Meharg, A.A., Hossain, M., Norton, G.J., Brammer, H., Islam, M.R., 2011. Organic matter-solid phase interactions are critical for predicting arsenic release and plant uptake in Bangladesh paddy soils. Environ. Sci. Technol. 45, 6080–6087. https://doi.org/10.1021/es2003765

Winkel, L.H.E., Johnson, C.A., Lenz, M., Grundl, T., Leupin, O.X., Amini, M., Charlet, L., 2012. Environmental selenium research: From microscopic processes to global understanding. Environ. Sci. Technol. 46, 571–579. https://doi.org/10.1021/es203434d

World Health Organization, 2017. WHO Guidelines for Drinking-water Quality: Fourth Edition

Incorporating the First Addendum. https://www.who.int/publications/i/item/9789241549950

CHAPTER III

ELEMENT TRANSPORT AND PARTITIONING ALONG TIDAL CHANNELS IN SOUTHWEST BANGLADESH[2]

Abstract:

Studies of element partitioning between suspended sediment and water with increased seawater mixing are sparse, particularly in Bangladesh. However, these studies are important for understanding elemental cycling and inorganic pollution transport because of the large amount of water and sediment discharge to the oceans and abundance of life in estuarine environments, such as the Sundarbans mangrove forest in Southwest Bangladesh. Thus, water samples collected within the upper 1m of the water column along a tidal channel transect in Southwest Bangladesh during the dry season were analyzed for dissolved and suspended sediment element concentrations and other geochemical parameters. While most elements in the suspended load were close to or depleted relative to upper continental crust (UCC), several trace elements such as Sb, As, Cd and Se were slightly enriched. Additionally, most trace elements in the dissolved load were well above world average riverine concentrations, particularly Se and As, which were also above World Health Organization (WHO) drinking water guidelines. Dissolved load Ba and Se displayed mostly conservative mixing trends with seawater after nonconservative sourcing, with Ba likely originally sourced from sediment desorption in addition to groundwater exfiltration, while Se may have been anthropogenically sourced from the city of Khulna or farther upstream. Dissolved As did not display conservative mixing trends, and may ultimately be geogenic in origin, possibly from groundwater. Ni and Co show trends consistent with desorption from competitive seawater cation exchange along the transect, similar to a study in the nearby Hooghly Estuary in West Bengal. Because humans and other organisms are sensitive to anthropogenic perturbations and fluctuations of trace elements due to their limited natural abundance in the environment, monitoring of trace elements in coastal riverine systems is imperative for protection of natural areas and agriculture many people depend on. This is particularly true for Se, which is likely anthropogenically sourced from effluent discharge upstream near Khulna city, which only environmental controls and monitoring can effectively limit.

Keywords: Estuary mixing; element partitioning; trace metals; suspended sediment transport; Southwest Bangladesh

1 Introduction

Estuarine environments can have important water-particle reactions due to the mixing of upstream freshwater and seawater.[1,2] These interactions are important to quantify because of their profound impacts on the riverine fluxes of both solid-phase and dissolved phase elements to the oceans. Specifically, changes in pH or the influence of seawater ions in an estuarine environment can affect elements through processes such as sorption, flocculation, or ion

[2] Chapter under review for publication in the journal "Environmental Science: Processes & Impacts" with Dr. John Ayers as coauthor.

exchange.[1,3–6] For example, desorption from suspended sediment due to competitive sorption with Na can increase some element concentrations in the dissolved load and decrease their concentrations in the suspended load.[1] Additionally, changes in pH and dissolved oxygen due to seawater mixing can cause certain elements such as Mn to precipitate from solution.[6] Research in estuarine environments throughout the world have shown how changes in river chemistry with increasing amounts of seawater mixing are often more complex than simple conservative mixing processes,[1,2,6,7] and thus these dynamic environments require thorough investigation.

Although previous work has analyzed geochemical changes in the dissolved and suspended load directly to the west of Bangladesh in the Hooghly Estuary in India,[1,8] there have been no detailed geochemical examinations of elements in the dissolved and suspended load in Bangladesh rivers during seawater mixing besides Ba and Ra.[9,10] It is imperative to quantify these geochemical changes and understand the underlying mechanisms behind them, not only for improving general knowledge of riverine-ocean elemental fluxes and elemental cycling within global estuaries, but because potentially harmful metals (in excess amounts) such as Ni and Co may have increased mobility in some pristine estuary environments due to competition with seawater cations for adsorption.[1,5] Coastal Bangladesh is an ideal natural laboratory for these detailed geochemical investigations because of the large influx of sediment, abundance of river tributaries, and profound tidal influence from the ocean. It is also analogous to other deltaic systems throughout the world, such as the Mississippi River or Red River deltas, making research findings here relevant to other coastal settings.

Bangladesh lies between India and Myanmar (Burma), with the Bay of Bengal along its southern coastline (Fig. 1). Bangladesh mostly sits in a low-elevation deltaic environment, filled with alluvial deposits from the Himalayas carried by the Ganges and Brahmaputra (G-B) rivers, and experiences a strong seasonal monsoon climate, with about 80% of annual rainfall occurring between the months of June to September.[11] This strong seasonality leads to large differences in surface water chemistry in coastal areas, with tidally-influenced rivers experiencing vastly lower levels of salinity during the monsoon season compared to the drier months.[12,13]

Southwest Bangladesh (Fig. 1) is in a tidal delta and its tributaries stem from the Ganges River, originating in the western Himalayas. These river tributaries experience a large inundation of seawater during the dry season with the tidal influence extending just north past Khulna,[14] and are hereafter called tidal channels. These tidal channels experience semi-diurnal tides[15] and in the wet season tidal channels encounter highly saline waters near the coast, although the salinity front extends much less inland compared to the dry season. Tidal cycle influence on water composition in the dry season in Southwest Bangladesh tends to be relatively minimal, with salinity in the dry season often changing ~1ppt or less between high and low tide in Sundarbans tidal channels near our study area.[16,17]

Hale et al.[15] extensively examined the properties of several tidal channels in this region. They found that one of the larger tidal channels sampled in our study, the Shibsa, has widths of ~1-2 km and depths up to 20m in some locations, while one of the smaller tidal channels in our study, the Bhadra, only has widths of 0.15–0.3 km. The differences between the larger (e.g., Rupsha and Shibsa rivers) and smaller channels (e.g., Bhairab and Bhadra rivers) in our study has an important influence on suspended sediment loads, for even though tidal channels in the

region generally contain more suspended sediment and greater suspended sediment concentrations in the wet season than the dry season, smaller channels experience more seasonality in suspended sediment concentrations compared to larger channels whose sediment loads are predominantly influenced by tidal variability. Most of the water exchanged through the tidal channels in this area is tidally reworked, with estimates suggesting that within our study area in the Shibsa River, nearly 2×10^{11} m^3 of water is moved through the channel each year.[15]

Southwest Bangladesh also contains the largest mangrove forest in the world, the Sundarbans (dark green in southern extent of Fig. 1), which is susceptible and sensitive to anthropogenic pollution.[18,19] A potential anthropogenic pollutant source upstream of the Sundarbans is the city of Khulna along the Bhairab and Rupsha rivers, which is the third most populated urban center in Bangladesh with ~1.5 million people.[20] Khulna holds several industrial and municipal sources that may contribute effluent discharge to the surrounding rivers, such as oil refineries, power companies, and jute mills.[21]

This study aims to utilize measured data of the suspended and dissolved loads from a tidal channel transect (Bhairab-Rupsha-Bhadra-Shibsa rivers) in Southwest Bangladesh (Fig. 1) to examine geochemical changes with increasing seawater mixing along the transect (Fig. 2), as well as identify whether any toxic elements (i.e., Se and As) that may prove hazardous to the Sundarbans/rural agricultural areas are sourced from the city of Khulna. Of focus are Ba, Ni and Co because of previous research of these elements near the study area,[1,8–10] as well as As and Se because of the relatively limited research of these potentially toxic elements in Southwest Bangladesh surface waters.[13,22] Hypothesized mechanisms affecting elements in the solid and dissolved loads are desorption, conservative seawater mixing, mineral dissolution, and ion-exchange. Characterizing the geochemical processes within the tidal channels will give important insights into elemental cycling and mobilization that can be applied to other estuaries around the world, particularly pristine ecosystems that may be exposed to increased inputs from anthropogenic perturbations upstream.

2 Methods

2.1 Sample collection

Water samples from the upper 1m of the water column were collected in metal (samples MD-TC-14 and MD-TC-15) and plastic buckets, which then filled 1L plastic HDPE bottles (with minimal headspace and with the bucket water well mixed to prevent sediment settling). No anomalous metal(loid) concentrations in the metal bucket samples were detected besides elevated dissolved Si in MD-TC-14 (Fig. B1). Samples were taken from the upper 1m of the water profile because the slow-settling sediments and coexisting water in the upper portion of the water column are what are likely being input into aquaculture ponds in the area via irrigation ditches. Additionally, sampling in the upper portion of the water column is much easier logistically, although future water/sediment sampling at various depths in the water column would be useful, since the composition and mineralogy of suspended sediments are known to change dramatically with depth.[23] Buckets were rinsed in-between each sample. Filtering of the samples was not performed in the field. Attempts were made to ensure representative samples,

with samples taken from a boat near mid-channel where river flow was constant and not stagnant. Samples were collected at the end of the dry season in May, 2019 and refrigerated upon return to Vanderbilt University.

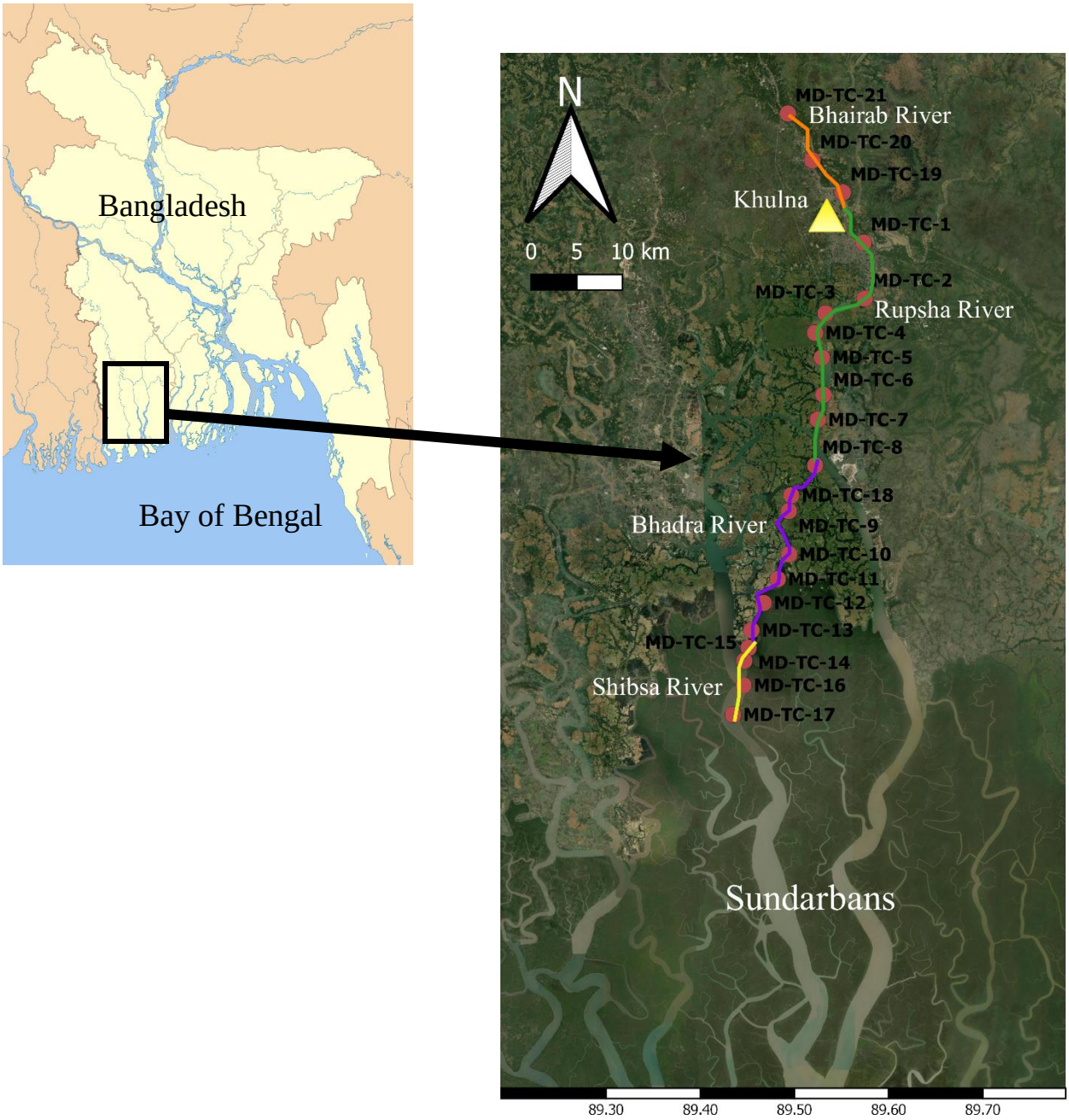

Figure 1: Map of the sample sites along the tidal channel transect (Bhairab-Rupsha-Bhadra-Shibsa as the main rivers) in Southwest Bangladesh, with the triangle representing the city of Khulna. The Sundarbans (natural mangrove forest) is the dark green area to the south of the sample locations. The Bay of Bengal is to the south of the Sundarbans. The colored lines along

the transect represent the main channels sampled from N-S as: Bhairab (orange), Rupsha (green), Bhadra (purple), and Shibsa (yellow).

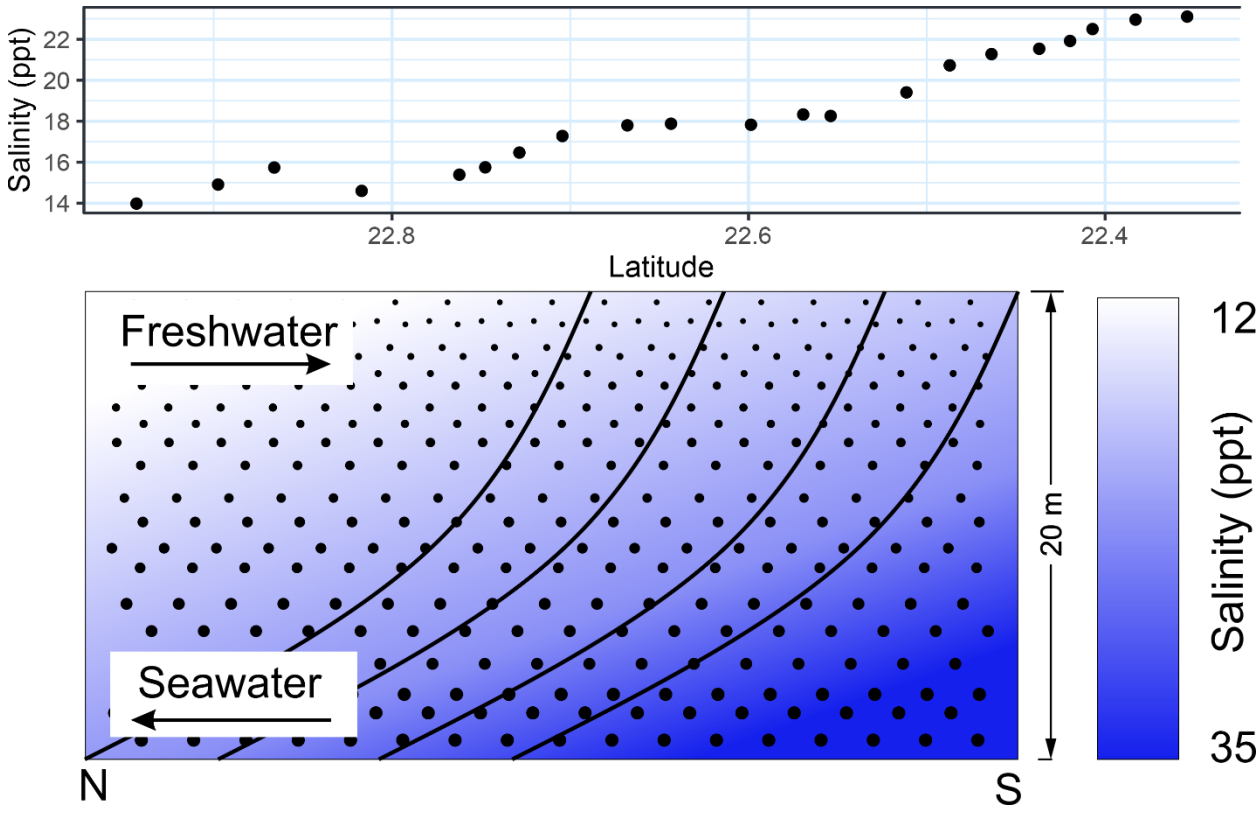

Figure 2: Conceptual diagram of seawater mixing along the river transect. The proportion of seawater in the tidal channel increases to the south. Solid black lines represent velocity profiles within the water column, and black dots represent suspended sediment. Above the conceptual diagram is a graph of measured salinity along the transect.

2.2 Field measurements

A Hach Hydrolab DS5 was used to gather in situ surface water measurements of pH, oxidation-reduction potential (ORP), turbidity (NTU), salinity (ppt), Eh in millivolts (mV), and specific conductivity (SpC) in microsiemens per centimeter (µS/cm) for all water samples. After sampling from the upper 1m of the water column with the bucket, the Hydrolab DS5 plastic sensor cover was filled about 80% after rinsing in-between samples, with the Hydrolab sensors then immersed into the water. For accurate turbidity measurements, the Hydrolab was filled before sediment settling could significantly occur in the bucket. However, turbidity would decline during the measurement because of sediment settling around the Hydrolab sensors. Calibration of the Hydrolab DS5 was performed before field use for ORP, pH, turbidity, and SpC with standard calibration solutions. In-situ ORP measurements are intended for differentiating

between oxic versus anoxic conditions instead of quantifying specific values, such as described in Ayers et al.[13,24] ORP (relative to the Ag/AgCl redox couple) was converted to Eh (relative to the standard hydrogen electrode (SHE)) in Table 1 by adding 187 mV to each field measurement. GPS coordinates were also recorded at each sample site and are listed in Table 1.

2.3 Sample analyses

2.3.1 Water/solid sample prep

Water samples were filtered with a 2.5 µm Whatman® ashless paper filter via a vacuum-suction device to collect the suspended sediment following refrigerated storage at Vanderbilt University (days from sampling to filtration shown in Table 1). Although the filter size was 2.5 µm, additional smaller particles were likely captured through cohesion of silty clay particles. Following filtration at 2.5 µm, a homogenized and well-mixed subset of each sample was filtered at 0.2 µm with a Nalgene Polyvinylidene Fluoride (PVDF) filter. 2mL of the 0.2 µm filtered samples were acidified with a drop of HNO_3 and diluted with deionized water to achieve a 5:1 dilution for inductively coupled plasma analyses (ICP-MS and ICP-OES). A 10:1 dilution was performed for a reanalysis of Na on the ICP-OES. A 20-30mL subset of the filtered undiluted water samples were used for ion chromatography (IC) and total organic carbon (TOC) analysis.

The filter paper full of the suspended sediment was dried overnight at ~45-50ºC following filtration. The filter and suspended sediment were then weighed to determine suspended sediment concentrations (SSC) from ~1L of the water that was filtered (to prevent headspace, slightly more than 1L of water filled each bottle that was filtered). The weight of the filter paper (weighed after drying at ~45-50ºC overnight before filtering the water sample) was subtracted from the dried filter + suspended sediment weight to determine SSC. Because sediment was uniformly distributed across the filter paper, splits between 0.25-0.5 grams of the filter paper + sediment were prepared for acid digestion.

2.3.2 Water sample analyses

All 5:1 diluted and acidified water samples were analyzed on a Perkin Elmer NexION 2000B ICP-MS in both standard and kinetic energy discrimination (KED) modes using EPA Method 6020B at Vanderbilt University for the elements As, Be, Cd, Co, Cr, Cu, Fe, Mn, Mo, Ni, Pb, Sb, Se, Ti, Tl, V, and Zn. All acidified surface water samples were also analyzed on an Agilent 5110 VDV ICP-OES using EPA Method 6010D at Vanderbilt University to report the ions: Al, As, B, Ba, Ca, Fe, K, Mg, Na, P, S, Si, and Sr. A rerun for Na at a 10:1 dilution was performed for the ICP-OES because of elevated Na concentrations from seawater mixing. Essentially, the same ICP methods were employed in previous investigations by the authors.[13,22] All filtered, unacidified surface water samples were analyzed for inorganic and organic carbon content via a Shimadzu model TOC-LCPH using EPA Method 9060A. Unacidified water samples were also analyzed for Cl, F, Br, NO_3, PO_4, and SO_4 with a Metrohm 881 Compact IC Pro using SW-846 EPA Method 9056. F, NO_3 and PO_4 were routinely below detection limit and thus not reported. The elements Fe and As are reported from the ICP-MS instead of ICP-OES,

because of improved precision on the ICP-MS for these elements due to lower detection limits compared to the ICP-OES. Method detection limits (MDLs) are listed in Table 2.

2.3.3 Solid sample analysis

0.25-0.5 grams of each filter paper + suspended sediment subsample were digested according to EPA Method 3051A at The Ohio State University Service Testing and Research Laboratory (STAR Lab) for analysis on an Agilent 5110 ICP-OES for the elements: Al, As, B, Ba, Be, Ca, Cd, Co, Cr, Cu, Fe, K, Li, Mg, Mn, Mo, Na, Ni, P, Pb, S, Sb, Se, Si, Sr, Tl, V and Zn. It is noted that EPA Method 3051A does not lead to complete digestion of silica, and thus Si was excluded in the reported values. Suspended sediment element concentrations were estimated using the "suspended sediment concentration factor," determined from the (blank filter + suspended sediment mass)/suspended sediment mass. This assumed a uniform ratio of suspended sediment distributed over the filters, which was observed consistently. This concentration factor was multiplied by the measured sediment-element concentrations to account for the weight dilution of the filter paper (filter paper element concentrations determined by running blanks are all very low (Table 3), but take up a significant mass comparable to the sample and are mainly comprised of unanalyzed elements such as C, O and H). The filter paper and suspended sediment digestion and filtering methods are similar to previous studies,[25,26] although the concentration dilution from the filter paper is explicitly described/addressed in this study. Approximate MDLs based on a 200x dilution factor for solid acid digestion are listed in Table 3.

2.3.4 Transmission electron microscopy (TEM)

A droplet from one unfiltered tidal channel sample taken in the upper 1m of the water column in the study area (P32-TC[22]) was mounted via drop-casting suspension on a lacey carbon-coated copper TEM grid, dried, then analyzed on a Tecnai Osiris equipped with SuperX quad EDS detectors with an accelerating voltage of 200kV. Suspended sediment from samples MD-TC-7 and MD-TC-11 were also analyzed on the Tecnai Osiris TEM after removing the sediment from the filter paper, mixing with isopropanol, sonicating for about 2 minutes, then placing a drop onto a carbon-coated copper TEM grid and wicking away the excess solvent. TEM and STEM-EDS maps were generated to characterize solid particulates that are present in tidal channel water, with STEM-EDS maps drift corrected with Bruker Esprit version 1.9 with a beam current of approximately 1nA. Wt. and at. % element quantification based on EDS spectra was performed using standardless cliff Lorimer approximation. TEM work was performed at the Vanderbilt Institute of Nanoscale Science and Engineering (VINSE).

2.3.5 Grain size analysis

A duplicate, unfiltered water sample of MD-TC-21 was analyzed for particle size via laser granulometry with a Malvern Mastersizer 2000 at Vanderbilt University. Most of the homogenized sample filled a 1L beaker after running deionized water through the instrument to establish background concentrations. The sample was then deflocculated via sonication before analysis. A homogenized subset of dried, filtered (>2.5µm) suspended sediment from several representative samples (including a replicate sample) along the transect were mixed in a 1L

beaker of water using the same procedures as above, but with a Malvern Mastersizer 3000 at Vanderbilt University.

2.3.6 Powder X-ray diffraction (XRD)

Dried, homogenized powder samples of suspended sediment from sample MD-TC-18 and deposited sediment adjacent to shrimp pond (sample site KA-4[22]) were dry cast on 20 x 20mm square sample glass holders with a 0.2mm indent. The samples were then analyzed with a Rigaku SmartLab powder X-ray diffractometer at Vanderbilt University with a Cu Kα (lambda = 0.154 nm) source at 40 kV and 44 mA. The detector was a D/teX Ultra 250 1D silicon strip detector. PDXL software identified the mineral phases associated with the intensity peaks.

2.4 Quality control

Samples were refrigerated upon arrival to Vanderbilt University, although it is noted that ~1-2 weeks of time passed without refrigeration of samples. Additionally, a significant amount of time passed between sampling and filtration. Thus, several checks were made to decipher whether storage time in general had any effect on suspended sediment and dissolved load composition due to element exchange. The days between sampling and filtering are displayed in Table 1, and results/discussion of possible element exchange over time between the dissolved load and suspended load within the 1L bottles are addressed in Sections 3.6 and 4.4.

Three 1L deionized water blanks were filtered under the same lab methodology as the tidal channel samples at the beginning, middle and end of the sample filtration process (with the same beakers that were cleaned in-between samples) for a total of 3 blanks with 0.2 µm filtered dissolved element concentrations and element concentrations of the filter paper itself. These values were routinely low or below detection limit, with the blanks' concentrations listed in Tables 2 and 3.

Filtered water samples analyzed with the ICP-MS, ICP-OES, IC and TOC analyzers at Vanderbilt University were run with standard solutions and blanks. Standards were required to be within 15% of the known value, while blanks were required to be below the MDL. The geometric mean charge balance error for water samples was approximately 7.7%, slightly higher than the charge balance errors for studies in the area that used similar methods (3.9%,[13] 4.6%[22]).

Additionally, duplicate samples that were filtered in the field at 0.45 µm and analyzed for the same water parameters[22] as this study were compared to the 1L duplicate subset of water samples filtered in the lab (in this study), for possible discrepancies between methodologies. It is noted that several trace elements such as Cr, Cu, Se, Zn, P, Co and Ni did not match well in several samples, possibly because of differences in filter size/methodology. The results are presented in Section 3.6 and discussion is elaborated in Section 4.3.3.

Overall, despite sampling/analytical challenges due to the logistics of our research in a remote coastal environment, contamination of samples should be minimal and post-sampling effects on element concentrations in the dissolved and suspended load should also be relatively minimal, thus not affecting our main data interpretations.

2.5 Data reduction

QGIS v.3.10.8 was utilized for map generation and ArcGIS Online was used for watershed maps. RStudio and Microsoft Excel were used for figure generation and statistical analyses. The Geochemist's Workbench 14.0 was used to calculate mineral saturation indices, dissolved HCO_3^- concentrations (from measured dissolved inorganic carbon (DIC)), and charge balance error using the default thermo.dat database.[27] Uncertainties are reported as sample standard deviation (1σ) for all elemental and geochemical results. Final reported element concentrations in the dissolved load from ICP analyses (Table 2) are based on the more precise 5.1:1 and 10.2:1 dilutions used, although the 2% difference of rounded values used in figure generation is deemed negligible and less than that of the figure lines/points. Reported Kd values (Table B1) use the original 5:1 and 10:1 dilution because they are log ratio values and the 2% change in dissolved concentrations is often negligible compared to the much greater concentrations in the suspended load.

3 Results

3.1 Grain size distribution and sediment mineralogy

Suspended sediment from an unfiltered duplicate water sample (MD-TC-21 duplicate; upstream in Bhairab River) had a median grain size of 12.2 μm and a volume-weighted mean grain size of 16.0 μm. Approximately 98.6 % of the particle volume was > 2.5 μm. Suspended sediment recovered from 2.5 μm filters for the samples MD-TC-18, MD-TC-5, MD-TC-9, and a replicate of MD-TC-9 (MD-TC-9-Dup) had median grain sizes of 14.8-16.9 μm; with volume-weighted mean grain sizes between 21.3 and 23.3 μm. These samples included both upstream and downstream portions of the transect, as MD-TC-18 and MD-TC-9 were taken >40 km downstream of MD-TC-21 near the confluence of the Bhadra and Dhaki rivers off the Rupsha (MD-TC-9) or within the confluence (MD-TC-18). Their approximate grain size distributions are shown in Fig. 3, which are unimodal, overlap significantly, and are similar to previously reported grain size distributions in the upper water column of the Ganges and Brahmaputra rivers.[23]

XRD data illustrate several noticeable peaks in the suspended sediment sample (MD-TC-18) and the sediment adjacent to a shrimp pond (KA-4[22]) (Fig. B2). These peaks are associated with minerals such as quartz, muscovite, dolomite, and clay minerals such as chlorite and illite. Qualitatively, the peaks between sample MD-TC-18 and KA-4 are quite similar and overlap significantly (Fig. B2).

3.2 Dissolved and suspended load concentrations (SSC) and geochemical parameters

Because not all geochemical results follow a normal distribution and are closest to being lognormally distributed, means are reported as geometric means, with variability reported as sample standard deviation. In general, tidal channel samples were near-neutral in pH with very little variation (7.61 ± 0.09) (Table 1). Conditions were generally oxidizing based on the positive measured Eh values (456 ± 10 mV), and suspended sediment concentrations varied significantly

along the tidal channel transect (0.49 ± 0.56 g/L). Although the mean SSC in this study is significantly less than the ~1.1 g/L averages in the Ganges and Brahmaputra rivers,[28] suspended sediment in this Asian river system can be quite variable by depth[23] and by season.[29] The mean SSC (0.49 g/L) in this study was still greater than the world average of 0.35 g/L.[28] Water samples were commonly saturated in: K-feldspar, kaolinite, muscovite, dolomite, illite, barite, albite, gibbsite and witherite (Table 1). Tidal channel samples have a high salinity of 18 ± 3 ppt, indicative of mixing with seawater from the Bay of Bengal (BoB).

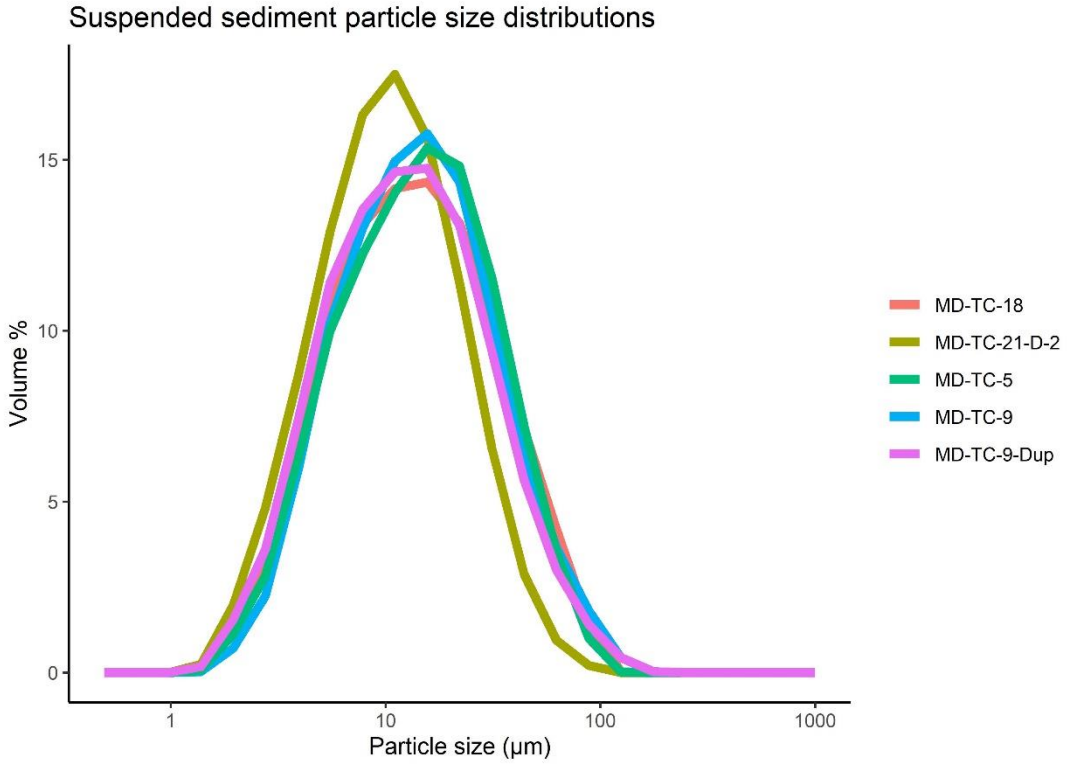

Figure 3: Approximate grain size distributions from suspended sediment samples along the sampled tidal channel transect, based on % volume of several grain size bins agglomerated together.

Due to the large seawater influence, major conservative ions in solution (e.g., Na, Cl, Mg, Ca, K, SO_4) were routinely elevated above world riverine dissolved concentrations[30] (Table 2). Dissolved organic carbon (DOC) (3.4 ± 0.6 mg/L) was within the lower range found in world river systems, similar to rivers such as the Connecticut, Fraser, Sanaga, and Yenisei rivers.[28] Most trace elements (i.e., V, Zn, Cr) are elevated well above average riverine dissolved element concentrations (Fig. B3), similar to other recent surface water studies in the area (Table B2). Dissolved Se and As are well above average river concentrations (0.07 µg/L and 0.62 µg/L, respectively).[28] The mean concentration for As in the dissolved load was 57 ± 17 µg/L, well above the WHO guideline of 10 µg/L, while the mean concentration for Se was 39 ± 63 µg/L, near the WHO guideline of 40 µg/L[31] and the U.S. Environmental Protection Agency (U.S. EPA) maximum contaminant level (MCL) of 50 µg/L.[32] Other elements of interest such as Ba (222 ± 71 µg/L), Co (1.0 ± 0.1 µg/L) and Ni (17 ± 4 µg/L) were significantly greater than average world

river dissolved concentrations (23 µg/L, 0.148 µg/L, and 0.801 µg/L, respectively),[28] but were below levels of health concern based on WHO guidelines or the lack of a guideline value (Co).[31] Some elements (i.e., Be, Pb, Tl) analyzed had very low concentrations close to or below detection limits, or negative values, and these elements were thus omitted from the reported results. Even though dissolved Cd values were quite low and sometimes below detection limit, none were negative, and were thus included for Kd calculations.

Table 1: Tidal channel physicochemical measured parameters and sampling locations

Sample ID	MD-TC-1	MD-TC-2	MD-TC-3	MD-TC-4	MD-TC-5	MD-TC-6
SpC (µS/cm)	24137.00	25313.00	25857.00	26922.00	28120.00	28893.00
Salinity (ppt)	14.60	15.39	15.75	16.47	17.28	17.80
TDS (g/L)	15.45	16.20	16.55	17.23	18.00	18.49
pH	7.36	7.60	7.64	7.69	7.70	7.71
Eh (mV)	473.00	449.00	450.00	459.00	466.00	472.00
Turbidity (NTU)	426.00	349.00	215.60	91.10	240.30	506.00
Suspended Sediment (g/L)	1.02	0.52	0.39	0.16	0.79	1.75
Date-Time[d]	5/5/2019 21:48	5/5/2019 22:21	5/5/2019 22:54	5/5/2019 23:21	5/5/2019 23:51	5/6/2019 0:23
Charge Imbalance[e]	8.93%	8.05%	8.66%	10.93%	9.34%	7.19%
Saturated Minerals[b]	*Ab, Brt, Kfs, Ilt, Kln, Ms, Dol, Gbs, Wth*	*Ab, Brt, Kfs, Ilt, Kln, Ms, Dol, Gbs, Wth, Tlc*	*Ab, Brt, Kfs, Ilt, Kln, Ms, Dol, Gbs, Wth, Tlc, Mgs*	*Ab, Brt, Kfs, Ilt, Kln, Ms, Dol, Gbs, Wth, Tlc, Mgs*	*Ab, Brt, Kfs, Ilt, Kln, Ms, Dol, Gbs, Wth, Tlc, Mgs*	*Ab, Brt, Kfs, Ilt, Kln, Ms, Dol, Gbs, Wth, Tlc, Mgs*
Days since sampling[c]	79	73	71	73	71	80
Latitude	22.81702538	22.76224381	22.74769729	22.72856242	22.70444525	22.66798745
Longitude	89.57321226	89.57451887	89.53284087	89.5218279	89.52907948	89.53078144

Sample ID	MD-TC-7	MD-TC-8	MD-TC-9	MD-TC-10	MD-TC-11	MD-TC-12
SpC (µS/cm)	29001.00	28936.00	29558.00	31243.00	33148.00	33933.00
Salinity (ppt)	17.88	17.83	18.26	19.41	20.73	21.28
TDS (g/L)	18.56	18.52	18.92	20.00	21.21	21.72
pH	7.71	7.72	7.71	7.66	7.57	7.49
Eh (mV)	475.00	455.00	464.00	463.00	464.00	453.00
Turbidity (NTU)	500.00	182.20	709.00	491.00	122.00	48.70
Suspended Sediment (g/L)	0.91	0.61	1.49	1.29	0.31	0.10
Date-Time[d]	5/6/2019 0:53	5/6/2019 6:48	5/6/2019 7:20	5/6/2019 7:50	5/6/2019 8:16	5/6/2019 8:51

Charge Imbalance[e]	8.64%	5.50%	10.60%	8.26%	5.62%	6.81%
Saturated Minerals[b]	*Ab, Brt, Kfs, Ilt, Kln, Ms, Dol, Gbs, Wth, Tlc, Mgs*	*Ab, Brt, Kfs, Ilt, Kln, Ms, Dol, Gbs, Wth, Tlc, Mgs*	*Ab, Brt, Kfs, Ilt, Kln, Ms, Dol, Gbs, Wth, Tlc, Mgs*	*Ab, Brt, Kfs, Ilt, Kln, Ms, Dol, Gbs, Wth, Tlc, Mgs*	*Ab, Brt, Kfs, Ilt, Kln, Ms, Dol, Gbs, Wth, Tlc*	*Ab, Brt, Kfs, Ilt, Kln, Ms, Dol, Gbs, Wth, Tlc*
Days since sampling[c]	80	78	93	94	87	94
Latitude	22.64350791	22.5986723	22.55395565	22.51145926	22.48714206	22.46372446
Longitude	89.52470658	89.52175022	89.4939169	89.49418736	89.48211993	89.4671845

Sample ID	**MD-TC-13**	**MD-TC-14**	**MD-TC-15**	**MD-TC-16**	**MD-TC-17**	**MD-TC-18**
SpC (µS/cm)	34298.00	34846.00	35681.00	36334.00	36537.00	29662.00
Salinity (ppt)	21.54	21.92	22.50	22.96	23.11	18.33
TDS (g/L)	21.95	22.30	22.84	23.25	23.38	18.98
pH	7.44	7.56	7.57	7.56	7.57	7.64
Eh (mV)	451.00	452.00	454.00	450.00	447.00	458.00
Turbidity (NTU)	176.10	141.80	200.40	195.20	125.60	836.00
Suspended Sediment (g/L)	0.48	0.33	0.48	0.31	0.22	2.07
Date-Time[d]	5/6/2019 9:22	5/6/2019 9:51	5/6/2019 10:25	5/6/2019 10:55	5/6/2019 11:27	5/7/2019 10:55
Charge Imbalance[e]	5.30%	7.13%	6.73%	5.15%	5.82%	7.76%
Saturated Minerals[b]	*Ab, Brt, Kfs, Ilt, Kln, Ms, Dol, Gbs, Wth*	*Ab, Brt, Kfs, Ilt, Kln, Ms, Dol, Gbs, Wth, Qz, Tlc*	*Ab, Brt, Kfs, Ilt, Kln, Ms, Dol, Gbs, Wth, Tlc*	*Ab, Brt, Kfs, Ilt, Kln, Ms, Dol, Gbs, Wth, Tlc*	*Ab, Brt, Kfs, Ilt, Kln, Ms, Dol, Gbs, Wth, Tlc*	*Ab, Brt, Kfs, Ilt, Kln, Ms, Dol, Gbs, Wth, Tlc, Mgs*
Days since sampling[c]	101	99	101	64	101	113
Latitude	22.4369582	22.41967732	22.40707043	22.38292227	22.35398457	22.56935935
Longitude	89.4542072	89.45118633	89.44664501	89.44586719	89.43466793	89.49654172

Sample ID	**MD-TC-19**	**MD-TC-20**	**MD-TC-21**	***Geometric Mean***	***Standard Deviation***
SpC (µS/cm)	25837.00	24607.00	23203.00	29521.25	4278.22
Salinity (ppt)	15.74	14.91	13.98	18.24	2.93
TDS (g/L)	16.54	15.75	14.85	18.89	2.74
pH	7.63	7.61	7.62	7.61	0.09
Eh (mV)	445.00	443.00	443.00	456.38	9.77
Turbidity (NTU)	225.10	193.40	143.00	230.87	210.54

Suspended Sediment (g/L)	0.46	0.19	0.18	0.49	0.56
Date-Time[d]	5/7/2019 15:27	5/7/2019 15:57	5/7/2019 16:30		
Charge Imbalance[e]	10.40%	9.54%	8.99%	7.67%[a]	1.79%
Saturated Minerals[b]	*Ab, Brt, Kfs, Ilt, Kln, Ms, Dol, Gbs, Wth, Tlc*	*Ab, Brt, Kfs, Ilt, Kln, Ms, Dol, Gbs, Wth, Tlc*	*Ab, Brt, Kfs, Ilt, Kln, Ms, Dol, Gbs, Wth, Tlc*		
Days since sampling[c]	113	107	107		
Latitude	22.86607737	22.89758088	22.94333535		
Longitude	89.55133013	89.5190009	89.49288593		

[a]Mean of absolute value of charge imbalance (%)

[b]Saturated minerals have saturation index >0 (log(Q/K)) - Ab albite; Brt barite; Kfs K-feldspar; Kln kaolinite; Ms muscovite; Wth witherite; Dol dolomite; Gbs gibbsite; Qz quartz; Ilt illite; Tlc talc; Mgs magnesite

[c]When the 1L refrigerated samples were filtered for suspended sediment for analyses following field sampling

[d]Bangladesh Standard Time (BST or GMT+6)

[e]Based on original dilution ratios of 5:1 and 10:1 for the ICP analyzed elements.

Table 2: Dissolved load concentrations in mg/L

Sample ID	MD-TC-1	MD-TC-2	MD-TC-3	MD-TC-4	MD-TC-5	MD-TC-6	MD-TC-7	MD-TC-8
Al[1]	0.14	0.14	0.15	0.15	0.16	0.15	0.15	0.15
As	0.073	0.069	0.036	0.065	0.044	0.073	0.070	0.072
B	2.29	2.30	2.43	2.48	2.54	2.58	2.63	2.65
Ba	0.31	0.29	0.30	0.28	0.28	0.26	0.27	0.27
Ca	208.6	205.7	218.2	218.3	229.8	231.0	234.1	236.0
Cd	0.00011	0.00009	0.00002	0.00010	0.00011	0.00009	0.00007	0.00006
Co	0.0009	0.0010	0.0009	0.0011	0.0010	0.0011	0.0010	0.0010
Cr	0.015	0.016	0.014	0.016	0.015	0.015	0.014	0.014
Cu	0.027	0.018	0.020	0.019	0.021	0.018	0.018	0.015
Fe	0.0009	0.0057	0.0051	0.0040	0.0024	0.0037	0.0037	0.0044
K	231.5	231.7	247.4	258.7	273.3	281.7	289.4	290.4
Mg	560.2	570.4	605.7	621.7	659.2	665.8	683.1	688.1

Mn	0.0013	0.0016	0.0011	0.0012	0.0009	0.0011	0.0008	0.0008
Mo	0.0041	0.0018	0.0049	0.0049	0.0055	0.0056	0.0049	0.0055
Na	6634.1	6789.1	7135.9	7664.3	8077.4	7727.5	8044.7	8292.6
Ni	0.011	0.014	0.013	0.013	0.016	0.016	0.017	0.017
P		0.041	0.088	0.006	0.001	0.005	0.020	0.009
S	427.0	434.4	462.1	481.2	504.4	513.2	524.6	526.3
Sb	0.0007	0.0007	0.0006	0.0007	0.0007	0.0006	0.0006	0.0007
Se	0.234	0.214	0.156	0.093	0.091	0.105	0.103	0.093
Si	2.02	2.00	1.93	1.76	1.65	1.55	1.57	1.59
Sr	3.63	3.64	3.92	4.02	4.24	4.29	4.36	4.42
Ti	0.011	0.011	0.010	0.009	0.010	0.011	0.011	0.011
V	0.016	0.017	0.015	0.018	0.017	0.016	0.015	0.015
Zn	0.029	0.013	0.011	0.010	0.012	0.011	0.009	0.012
Cl	9375.7	9765.7	10108.9	10305.4	11281.1	11352.4	11432.6	12485.5
Br	28.4	29.2	30.1	30.6	33.0	33.0	33.3	35.9
SO4	1101.5	1113.0	1241.8	1269.8	1290.0	1314.8	1368.5	1476.3
DIC	31.02	29.81	29.59	26.74	28.55	27.55	26.85	28.05
DOC	3.82	3.74	3.84	3.65	3.53	3.27	3.15	3.19
HCO_3^-	116.00	113.20	111.50	99.73	105.40	102.40	99.07	103.20

Sample ID	**MD-TC-9**	**MD-TC-10**	**MD-TC-11**	**MD-TC-12**	**MD-TC-13**	**MD-TC-14**	**MD-TC-15**	**MD-TC-16**
Al[1]	0.15	0.16	0.15	0.17	0.17	0.20	0.17	0.19
As	0.067	0.074	0.063	0.065	0.069	0.067	0.066	0.072
B	2.56	2.79	2.93	2.98	3.04	3.13	3.17	3.12
Ba	0.24	0.22	0.18	0.17	0.16	0.14	0.12	0.11
Ca	230.1	248.4	259.9	263.3	266.1	268.8	270.6	275.6
Cd	0.00010	0.00008	0.00004	0.00005	0.00012	0.00010	0.00006	0.00014
Co	0.0010	0.0010	0.0011	0.0012	0.0011	0.0012	0.0011	0.0012
Cr	0.014	0.013	0.013	0.013	0.013	0.013	0.013	0.013
Cu	0.015	0.020	0.014	0.018	0.021	0.023	0.022	0.025
Fe	0.0025	0.0025	0.0014	0.0013	0.0017	0.0038	0.0017	0.0012
K	287.8	317.1	342.3	352.0	358.8	374.0	380.2	387.3
Mg	675.5	743.3	786.5	800.5	817.9	850.1	864.2	886.0
Mn	0.0007	0.0008	0.0007	0.0009	0.0007	0.0006	0.0007	0.0008
Mo	0.0054	0.0056	0.0054	0.0061	0.0062	0.0066	0.0064	0.0064
Na	9036.2	8919.9	9541.1	10622.3	10076.6	10374.4	10062.3	10803.8
Ni	0.016	0.017	0.019	0.020	0.021	0.022	0.021	0.024
P	0.001	0.016	0.013	0.030	0.004	0.002	0.022	0.003
S	517.1	568.4	604.5	616.8	625.3	647.5	653.7	666.7
Sb	0.0006	0.0006	0.0006	0.0005	0.0005	0.0005	0.0004	0.0004
Se	0.082	0.077	0.067	0.063	0.054	0.056	0.040	0.041
Si	1.52	1.45	1.41	1.43	1.41	6.92	1.22	1.27

Sr	4.30	4.75	5.05	5.17	5.22	5.37	5.48	5.60
Ti	0.011	0.011	0.011	0.012	0.011	0.012	0.012	0.012
V	0.015	0.014	0.014	0.015	0.014	0.014	0.019	0.018
Zn	0.011	0.012	0.009	0.010	0.020	0.035	0.028	0.029
Cl	12098.8	12783.2	14419.2	15434.2	15242.6	15197.8	14948.6	16464.0
Br	34.8	42.4	46.2	48.4	48.2	48.2	47.4	51.0
SO4	1448.7	1447.1	1554.6	1710.8	1707.6	1658.2	1666.0	1766.2
DIC	27.53	26.77	29.24	27.53	28.55	24.97	26.49	25.70
DOC	2.86	2.84	3.16	3.05	2.99	2.60	3.36	3.36
HCO_3^-	99.96	96.75	104.10	95.83	99.84	87.19	92.90	89.00

Sample ID	**MD-TC-17**	**MD-TC-18**	**MD-TC-19**	**MD-TC-20**	**MD-TC-21**	***Geometric Mean***	***Standard Deviation***
Al[1]	0.17	0.19	0.16	0.14	0.14	0.16	0.02
As	0.075	0.060	0.027	0.031	0.025	0.057	0.017
B	3.17	2.55	2.06	1.92	1.76	2.59	0.41
Ba	0.11	0.27	0.30	0.31	0.32	0.22	0.07
Ca	273.4	248.3	210.9	202.9	194.7	236.5	26.0
Cd	0.00155	0.00009	0.00011	0.00004	0.00010	0.00009	0.00032
Co	0.0011	0.0010	0.0008	0.0007	0.0008	0.0010	0.0001
Cr	0.013	0.013	0.012	0.013	0.012	0.014	0.001
Cu	0.026	0.025	0.023	0.021	0.022	0.020	0.004
Fe	0.0023	0.0027	0.0052	0.0031	0.0029	0.0026	0.0014
K	387.8	300.4	238.5	230.9	213.0	293.5	57.8
Mg	883.5	711.2	586.9	549.6	518.8	692.0	117.2
Mn	0.0008	0.0004	0.0004	0.0002	0.0003	0.0007	0.0003
Mo	0.0069	0.0058	0.0054	0.0047	0.0046	0.0052	0.0011
Na	10952.8	8935.2	7400.1	6816.7	6767.7	8485.9	1463.2
Ni	0.023	0.019	0.014	0.013	0.012	0.017	0.004
P	0.003	0.015	0.005	0.009	0.003	0.008	0.020
S	668.0	538.1	442.1	421.7	393.6	528.1	88.3
Sb	0.0005	0.0006	0.0006	0.0006	0.0006	0.0006	0.0001
Se	0.035	0.008	0.001	0.001	0.001	0.039	0.063
Si	1.21	1.62	1.85	1.95	1.99	1.72	1.19
Sr	5.60	4.59	3.76	3.58	3.38	4.44	0.72
Ti	0.011	0.008	0.005	0.005	0.004	0.010	0.002
V	0.016	0.013	0.012	0.011	0.011	0.015	0.002
Zn	0.031	0.020	0.020	0.024	0.039	0.017	0.010
Cl	16361.0	12868.4	10058.7	9480.8	9399.4	12195.3	2453.2
Br	50.4	42.6	29.8	28.6	28.3	37.2	8.5
SO4	1856.6	1403.0	1169.4	1066.7	1106.7	1396.2	243.3
DIC	26.33	30.47	27.77	26.66	27.64	27.76	1.56
DOC	3.06	3.58	4.20	3.14	5.58	3.38	0.63
HCO_3^-	91.04	110.30	104.20	101.30	105.60	101.08	7.70

Blanks	DI_B_1	DI_B_2	DI_B_3	MDL[2]
Al[1]	0.0132	0.0160	0.0029	0.0034
As	0.00066	0.00057	0.00038	0.00018
B	2.65	2.15	1.75	0.0023
Ba		0.0003		0.0016
Ca				0.0065
Cd	0.00022	0.00015	0.00005	0.00009
Co	0.0004	0.0003	0.0002	0.00011
Cr	0.0017	0.0016	0.0016	0.00026
Cu	0.0008	0.0004	0.0006	0.0002
Fe	0.0001	0.0002	0.0002	0.00073
K		0.008	0.005	0.0032
Mg	0.004			0.0035
Mn	0.0006	0.0006	0.0004	0.00016
Mo	0.0004	0.0004	0.0003	0.00016
Na				0.0056
Ni				0.00026
P				0.0068
S				0.0058
Sb	0.0003	0.0003	0.0002	0.00007
Se				0.00031
Si	0.14	0.09	0.06	0.0038
Sr	0.0043	0.0060	0.0033	0.0037
Ti	0.0030	0.0027	0.0025	0.00023
V	0.0001	0.0001	0.0001	0.00013
Zn	0.0002	0.0002	0.0002	0.00045
Cl	0.011			0.010
Br	0.000	0.000	0.000	0.0064
SO4	0.000	0.000	0.057	0.0254
DIC	0.004	0.003	0.005	0.15
DOC	0.011	0.018	0.036	0.18
HCO_3^-				

[1]Negative values are omitted for all elements.

[2]Method detection limit (MDL)

Suspended sediment element concentrations (Table 3) are often less than or close to that of average upper continental crust (UCC),[33] although several trace elements are notably enriched relative to UCC such as Sb, Se, and Cd (Fig. 4A). Concentrations are generally greater than UCC for the most mobile elements during transport/weathering (right portion of Fig. 4A), while concentrations are less than UCC for the least mobile elements during transport/weathering (left

portion of Fig. 4A). Suspended sediment barium concentrations are particularly low (72 ± 16 mg/kg; Table 3). Element concentrations (particularly major elements) may be slightly less than if they were measured on an anhydrous basis. For comparisons to UCC, trace elements with measurements below detection limit were replaced with their detection limit values, rather than omitting the values below the MDL to prevent bias towards larger mean values. However, this may still slightly inflate the actual mean concentrations of several trace elements, such as Cd and Se. Several elements analyzed in the suspended sediment were routinely below detection limit and were thus omitted from the reported results (i.e., Be, Mo, Tl).

Table 3: Suspended load concentrations in mg/kg

Sample ID	MD-TC-1	MD-TC-2	MD-TC-3	MD-TC-4	MD-TC-5	MD-TC-6	MD-TC-7	MD-TC-8
Al	26567.84	22975.51	26913.94	32199.62	17797.52	24306.58	23678.09	24203.80
As	8.33	8.31	9.86	9.08	7.93	11.72	11.74	12.96
B	9.63	9.62	12.76	18.71	7.15	9.64	9.50	10.83
Ba	85.73	75.66	83.87	98.11	60.68	72.67	71.18	78.89
Ca	9782.79	5836.48	6088.12	5957.90	8672.92	11054.43	8626.32	8757.89
Cd	1.97	1.87	2.13	2.90	1.71	1.92	2.01	2.08
Co	16.17	16.22	16.94	19.02	14.09	15.73	16.45	17.02
Cr	42.79	40.49	44.94	52.05	33.15	43.78	41.17	42.55
Cu	32.24	31.11	32.20	37.00	28.04	29.61	33.92	31.28
Fe	30803.74	31403.67	33489.86	37625.56	26372.69	29798.04	30712.39	32294.04
K	5881.22	5410.86	6169.50	7527.49	4527.69	5453.18	5350.73	5677.88
Li	21.10	12.06	19.23	15.72	15.17	19.65	20.18	18.96
Mg	12720.12	12339.92	13495.90	15476.54	11267.67	12393.00	12624.75	13145.76
Mn	662.23	681.32	698.10	774.20	597.08	638.49	674.98	697.31
Na	4644.78	6384.29	9809.38	15802.49	7280.16	4968.18	5945.55	7459.04
Ni	40.76	40.85	45.17	48.60	36.20	39.76	42.11	43.77
P	477.93	463.22	471.37	536.08	419.50	453.38	458.85	460.75
Pb	18.77	18.65	19.58	22.06	17.40	17.96	19.57	19.61
S	854.38	977.82	1309.65	1843.07	1071.34	894.23	975.64	1117.67
Sb	1.51	2.05	1.17	3.33	1.60	1.67	2.27	1.68
Se	3.73	9.06	12.09	**0.90**	**0.90**	2.48	**0.90**	4.19
Sr	34.19	29.07	33.67	40.29	31.30	34.60	32.49	34.41
V	48.47	45.93	51.27	60.23	39.17	45.68	46.86	49.07
Zn	73.79	74.89	82.51	93.54	65.75	68.67	78.87	78.18

Sample ID	MD-TC-9	MD-TC-10	MD-TC-11	MD-TC-12	MD-TC-13	MD-TC-14	MD-TC-15	MD-TC-16
Al	26106.98	15855.49	22097.53	23337.61	14811.00	28873.56	19292.24	27281.27
As	10.08	8.17	9.81	**0.85**	8.60	**0.85**	4.96	8.86

B	9.85	7.60	13.31	28.32	9.60	17.26	12.71	17.66
Ba	74.81	53.34	62.00	67.08	42.29	79.42	51.71	71.32
Ca	9561.59	7975.96	4987.37	5431.92	3948.46	7135.96	5335.59	5465.12
Cd	1.93	1.53	**0.85**	**0.85**	**0.85**	1.91	**0.85**	**0.85**
Co	16.11	13.57	14.71	13.48	10.88	16.99	12.09	15.80
Cr	42.10	30.64	38.02	39.97	27.37	46.12	32.27	44.12
Cu	30.59	26.04	26.34	19.81	20.47	28.36	21.80	28.25
Fe	29943.37	24894.96	28561.00	27622.86	21100.49	33156.55	23708.46	30876.86
K	5733.03	4211.99	5389.03	7142.16	3989.15	7027.62	4966.82	6801.88
Li	22.47	13.22	14.71	6.80	10.31	20.11	9.55	20.11
Mg	12487.10	10427.40	11913.24	15217.09	9192.88	14054.94	10652.52	13850.36
Mn	655.42	586.71	618.16	569.43	451.00	698.14	477.75	624.16
Na	5008.55	5368.31	11226.44	37690.68	10049.75	11612.34	12885.07	17238.57
Ni	40.63	33.42	38.23	33.13	28.15	41.75	29.71	41.22
P	444.00	394.87	391.96	382.76	311.86	468.87	330.59	423.16
Pb	18.14	16.67	19.13	14.23	13.97	17.89	13.55	16.56
S	944.58	999.70	1492.61	3982.91	1321.61	1754.94	1686.56	2115.27
Sb	2.40	0.61	1.54	**0.36**	1.30	1.12	**0.36**	1.92
Se	**0.90**	3.87	**0.90**	**0.90**	1.65	13.35	**0.90**	4.37
Sr	33.85	27.95	30.57	51.91	24.15	36.53	29.69	38.16
V	47.04	35.46	42.67	44.63	31.30	52.44	35.62	49.14
Zn	73.67	60.31	68.48	71.80	66.98	75.96	61.43	89.03

Sample ID	**MD-TC-17**	**MD-TC-18**	**MD-TC-19**	**MD-TC-20**	**MD-TC-21**	***Geometric Mean***	***Standard Deviation***
Al	25280.22	16640.24	28249.64	33811.23	28638.19	23675.78	5140.59
As	14.37	9.07	10.17	13.78	15.78	7.81	3.76
B	19.22	6.31	10.64	16.14	12.24	11.95	5.21
Ba	65.95	57.94	92.52	107.74	94.01	71.87	16.42
Ca	4718.54	9099.62	8477.63	6000.39	5326.80	6791.79	1999.87
Cd	**0.85**	1.61	2.15	**0.85**	**0.85**	1.42	0.62
Co	15.35	13.92	18.00	18.66	17.84	15.53	2.10
Cr	42.13	31.53	47.39	53.49	48.66	40.58	6.98
Cu	29.44	28.74	32.16	33.46	31.88	28.83	4.39
Fe	30623.52	25372.14	34565.28	37321.87	35656.18	29967.83	4369.25
K	6382.05	4336.53	6834.87	7846.07	6654.60	5769.55	1108.48
Li	10.46	15.14	21.16	19.61	11.74	15.34	4.61
Mg	13123.98	10896.26	14150.09	15095.35	14387.02	12695.73	1681.16
Mn	600.99	603.49	728.94	783.87	730.51	639.68	84.62
Na	15222.63	5319.67	6177.97	12184.65	11262.39	9134.13	7315.94
Ni	38.30	34.68	46.14	47.43	45.31	39.38	5.62
P	432.46	412.07	485.05	504.40	520.78	436.47	56.68
Pb	17.43	16.78	20.25	21.79	22.81	18.06	2.49
S	1911.37	1013.86	1056.91	1528.81	1439.62	1336.38	692.32

Sb	1.11	1.41	1.54	2.21	2.00	1.39	0.70
Se	**0.90**	5.55	2.66	**0.90**	4.47	2.30	3.70
Sr	34.00	29.85	35.08	38.69	35.14	33.68	5.59
V	47.88	36.93	54.75	61.63	55.92	46.09	8.02
Zn	85.55	67.86	91.77	103.65	129.46	77.82	16.03

Filter Blanks	**DI_B_1**	**DI_B_2**	**DI_B_3**	**MDL***
Al	4.962	3.937	4.696	0.138
As	<0.851	<0.851	<0.851	0.851
B	<0.851	<0.851	<0.851	0.851
Ba	<0.851	<0.851	<0.851	0.851
Ca	27.930	20.910	19.700	0.937
Cd	<0.851	<0.851	<0.851	0.851
Co	<0.851	<0.851	<0.851	0.851
Cr	<0.851	<0.851	<0.851	0.851
Cu	0.206	0.263	0.522	0.060
Fe	15.850	5.640	5.464	0.131
K	1.710	5.802	19.700	14.569
Li	<0.171	<0.171	<0.171	0.171
Mg	4.769	4.450	3.627	0.661
Mn	0.259	0.121	0.072	0.016
Na	35.350	27.430	17.160	6.371
Ni	0.230	0.217	<0.115	0.115
P	1.323	1.725	0.065	0.719
Pb	<0.418	0.494	0.446	0.418
S	6.197	8.311	10.780	2.402
Sb	<0.360	<0.360	<0.360	0.360
Se	<0.895	<0.895	<0.895	0.895
Sr	0.062	0.032	0.040	0.020
V	<1.000	<1.000	<1.000	1.000
Zn	3.639	4.188	3.624	0.271

*Approximate method detection limit (MDL) based on 200x acid digestion dilution factor.

Non-blank concentrations in bold are where detection limits were inserted for concentrations below detection limit for mean and standard deviation calculations. Values <MDL were not reported from STAR lab at OSU.

3.3 Partition coefficient values (Kd) between suspended and dissolved loads and the proportion in the dissolved load (D)

Partition coefficients, known as Kd values, represent the bulk suspended sediment element concentration/total dissolved element concentration in L/kg in this study (Table B1). Most element Kd values decrease from left to right along the x-axis in Fig. 4B, although there are several exceptions. Mn and several trace elements like Co, Sb, As, Se, and Cd show higher Kd values than expected based on mobility trends (Fig. 4B). It is noted that trace elements such as As, Sb, Se, and Cd also have suspended sediment average element concentrations greater than UCC (Fig. 4A).

If the suspended sediment concentration (SSC; kg/L) is known, along with the Kd value of an element (L/kg), the dissolved proportion of that element can be calculated by:

$$D = \frac{1}{1+K_D*SSC} \quad (1)$$

Where D is the proportion of the element in the dissolved load based on mass within a theoretical 1L parcel of water that contains suspended sediment.[28] The proportion of the element in the suspended load is 1-D. As element mobility during transport and weathering increases from left to right along the x-axis, the proportion of the elements in the dissolved load also increases (Fig. 4C). Notable elements strongly deviating from the general trend are Co, Mn, Sb and Cd. For about half of the elements, transport in the dissolved load is dominant. Several elements such as Ni, K, Ba, Na and Sr tend to have dissolved load proportions closer to the Rio Negro (typical low suspended sediment river) than the Rio Solimoes (a typical turbid river), although it is noted that the dissolved proportion of Co in this study is closer to that of the Rio Solimoes.[28]

3.4 Element correlations/relationships

Major ions in solution (e.g., Mg, Ca, K, Cl, Na, SO_4) that are derived predominantly from seawater are well correlated with one another. while some trace elements (e.g., As and Se) tend to poorly correlate with other elements in the dissolved load (Fig. B4). However, Ni and Co are well correlated with most conservative ions in solution.

Concentrations of many transition metals in the suspended sediment load display strong positive correlations (Fig. B5). In particular, trace metals are very well correlated with Fe and Al, likely because they are associated with Fe-oxides and Al-silicates or Al-oxides in the silty-clay suspended sediment. Many metals (and P) show very strong trends of increasing concentration with increasing Fe content in the suspended sediment (Fig. B6). The metalloid As shows a moderate positive correlation with Fe in the suspended load.

3.5 Element trends with increased seawater mixing along the transect

Despite slight tidal cycle variations during the sampling period, a relatively consistent salinity trend can be seen with latitude (Fig. 2). As latitude decreases with increasing proximity to the Bay of Bengal, salinity increases, indicative of greater seawater mixing. This is also seen with strong negative associations between latitude and conservative ions in solution (Fig. B4).

As seawater mixing and thus salinity increases, Ni and Co concentrations increase in the dissolved load while their Kd values simultaneously decrease (Fig. 5). Arsenic and selenium,

which have concentrations above health guidelines in the dissolved load, show moderate to no relationship between Kd values and salinity along the transect (Fig. B7).

Elements in the suspended load predominantly show moderate to weak positive correlations with latitude and thus negative correlations with salinity (Fig. B5) For example, Ni and Co specifically show moderate negative correlations with salinity (Fig. B8) and thus moderate positive correlations with latitude (Fig. B5). These negative correlations with suspended load Ni and Co versus salinity are similar to trends seen with Ni and Co Kd values versus salinity and opposite the trends seen with Ni and Co dissolved concentrations (Fig. 5).

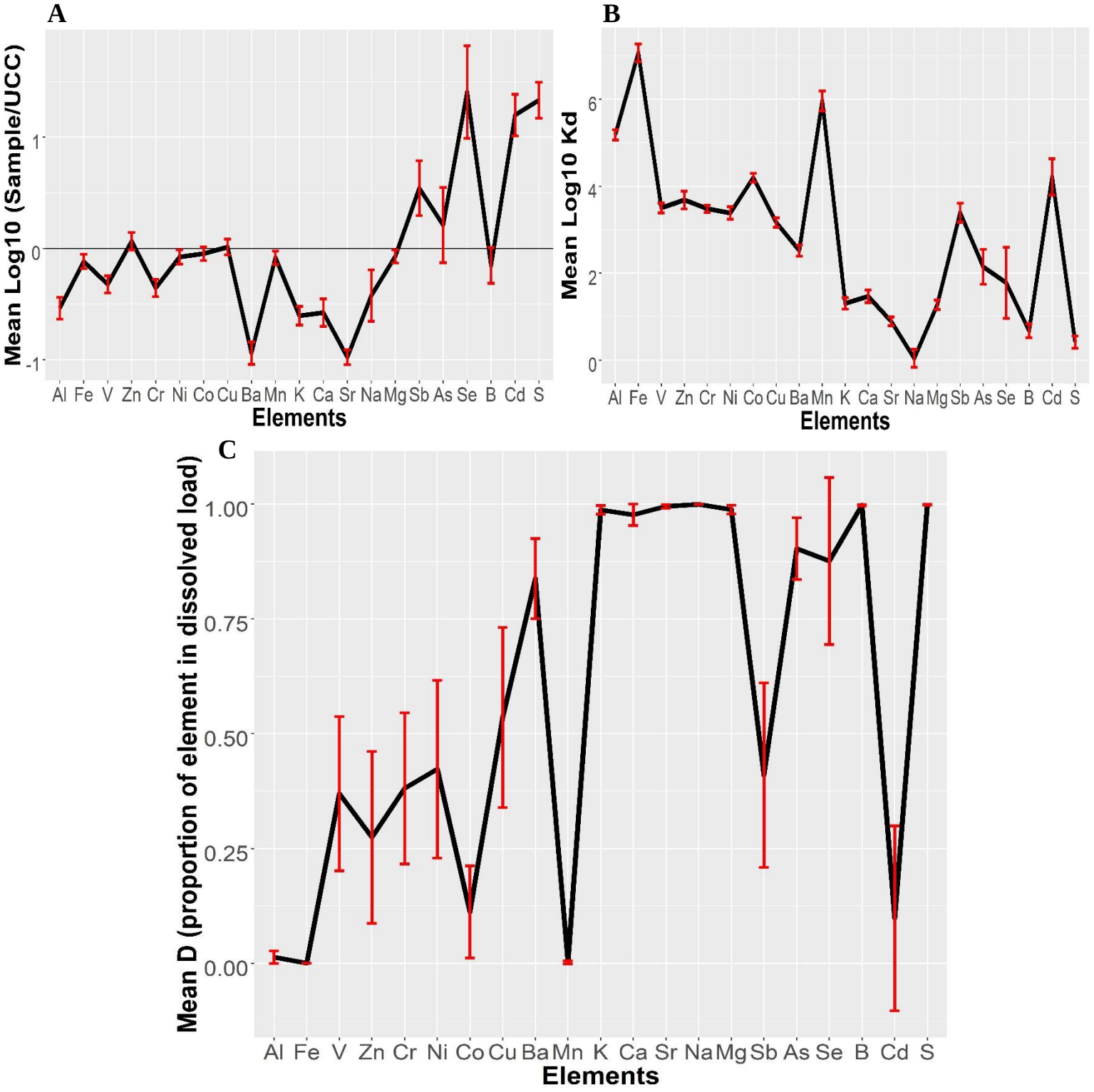

Figure 4: **(A)** Element concentrations in suspended sediment are normalized to upper continental crust (UCC),[33] with arithmetic mean log10 concentrations above 0 enriched relative to UCC and elements below 0 depleted relative to UCC. **(B)** Arithmetic mean log10 Kd values in

L/kg (bulk concentration solid-phase/concentration dissolved-phase). **(C)** Estimated geometric mean proportion of each element in the dissolved load (D) within the upper 1m of the water column. The remaining proportion is the proportion of the element in the suspended load. For all graphs, the elements included are arranged to show increasing mobility during weathering and transport from left to right along the x-axis.[28] The red bars are 1 standard deviation (1 σ) error bars and MDLs are inserted for solid-phase concentrations <MDL to prevent bias towards greater concentrations. n = 21.

Barium shows unique trends in both the dissolved and suspended load as seawater mixing increases along the transect (Fig. 6). Dissolved Ba decreases as latitude decreases and seawater mixing increases, but not in a singular linear fashion. Instead, two different linear slopes of best fit are apparent along the transect. Additionally, Ba has a moderate positive correlation with its suspended sediment concentration and latitude, albeit there is significant scatter. The Ba extracted from the suspended sediment through the EPA 3051A method (HNO_3 digestion) used in this study is strongly positively correlated with the extracted/measured Fe in the suspended load (Fig. 6). Barium Kd values are highest at lower latitudes close to the Bay of Bengal.

Both dissolved As and Se concentrations in the Bhairab River (that runs from the north of Khulna and meets the Rupsha River) are lower than values downstream of Khulna at lower latitudes (Fig. 7 & Fig. B9). While As does not show gradually decreasing concentrations south of Khulna towards the Bay of Bengal (Fig. B9), Se does (Fig. 7).

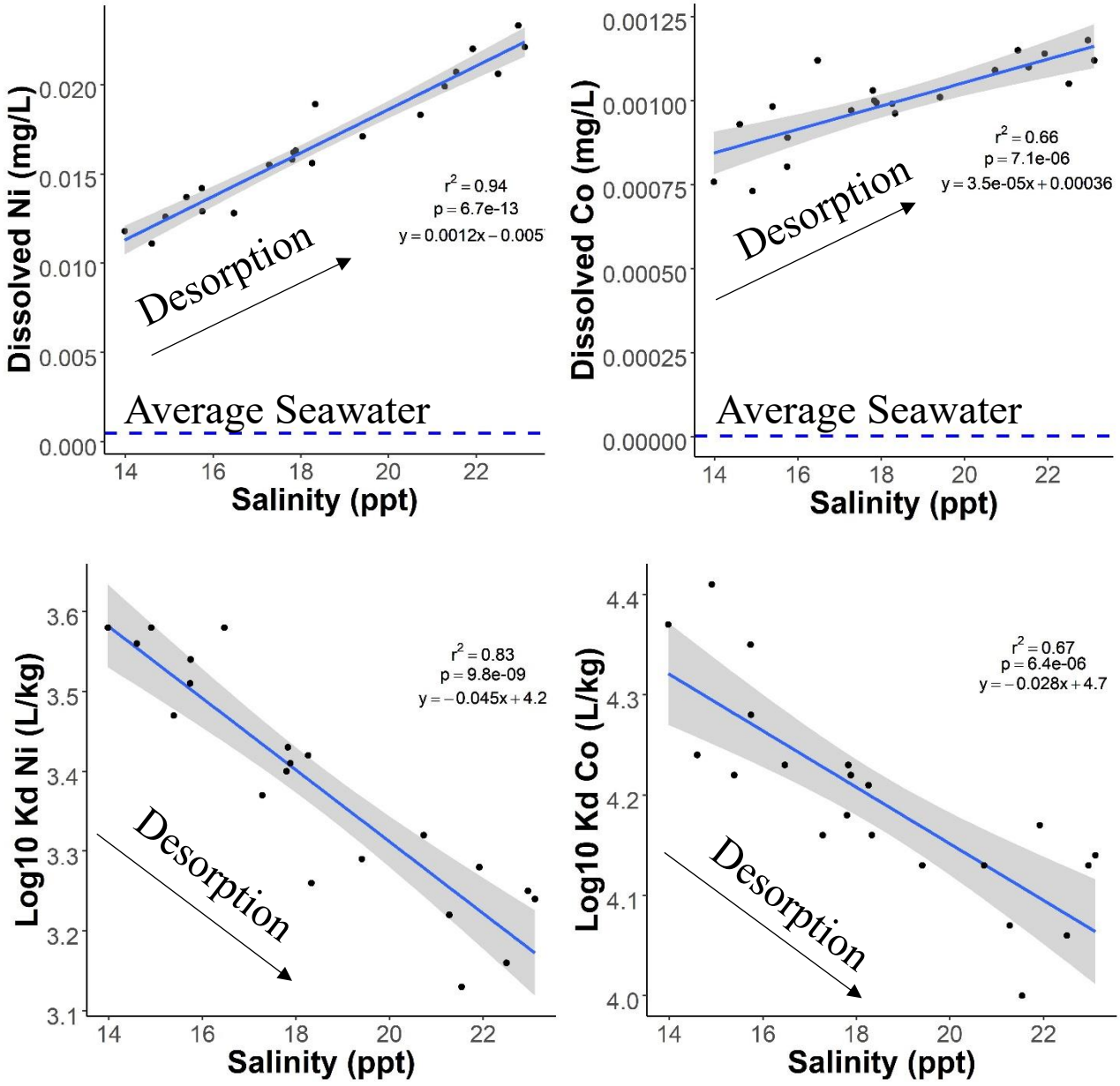

Figure 5: Salinity trends of Ni and Co Kd values (Log10 (L/kg)) with increased seawater mixing from higher to lower latitudes (upper row) and salinity trends of dissolved Co and Ni values (mg/L) with increased seawater mixing from higher to lower latitudes – dashed blue lines represent average open ocean concentrations (lower row).[34] Shaded regions represent the 95% confidence interval about the linear regression line.

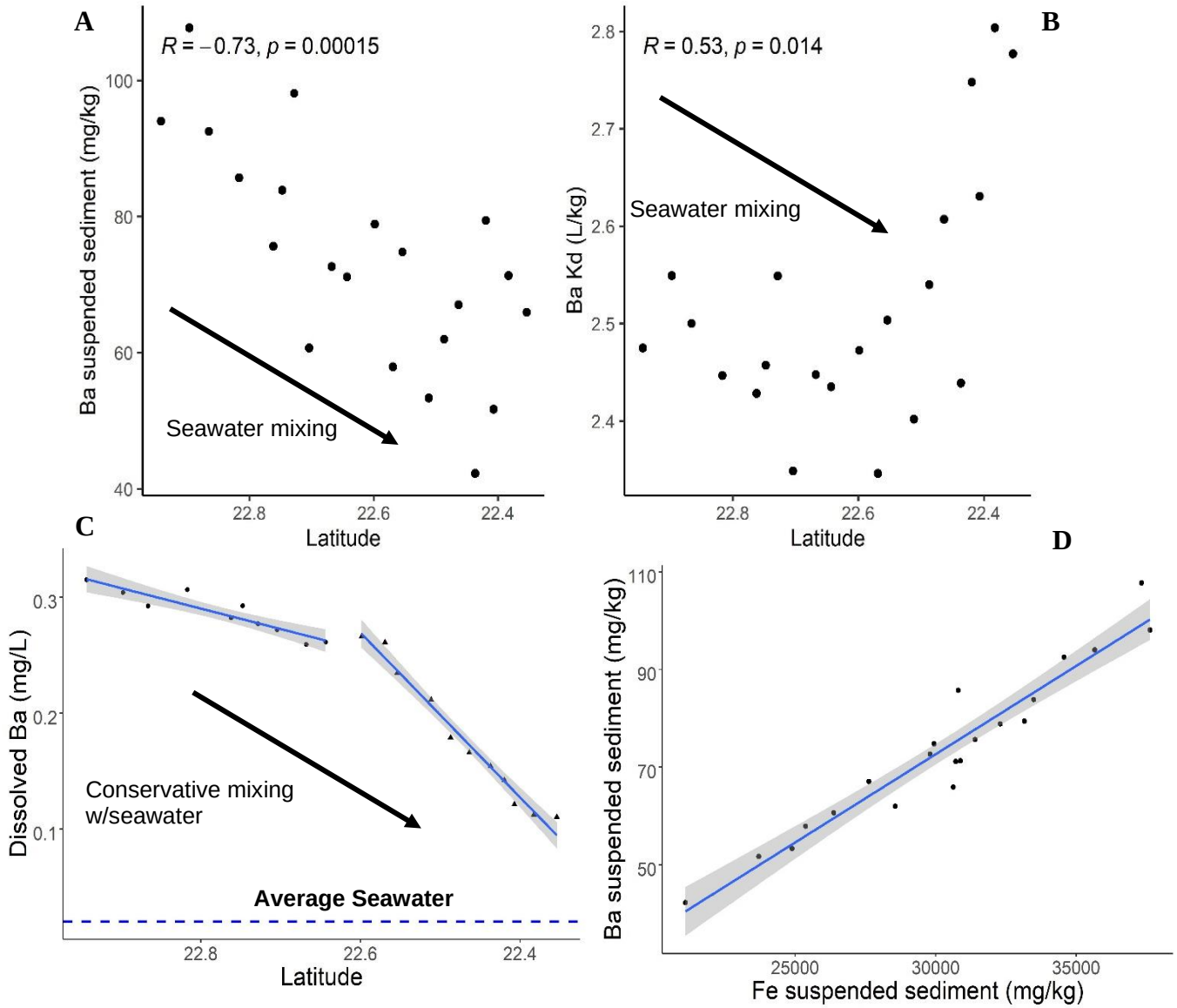

Figure 6: Various relationships of Ba with latitude and Fe, with (A) Ba concentration in the suspended load vs latitude, (B) Ba Kd values (L/kg) vs latitude, (C) Dissolved Ba vs latitude broken into two subpopulations with differing linear regression, and the blue dashed line representing average seawater,[35] (D) Suspended sediment Ba vs Fe concentrations in the suspended sediment load. Pearson correlation coefficient values are given with corresponding p-values in (A) and (B). Shaded regions are 95% confidence intervals about the linear regression lines in (C) and (D).

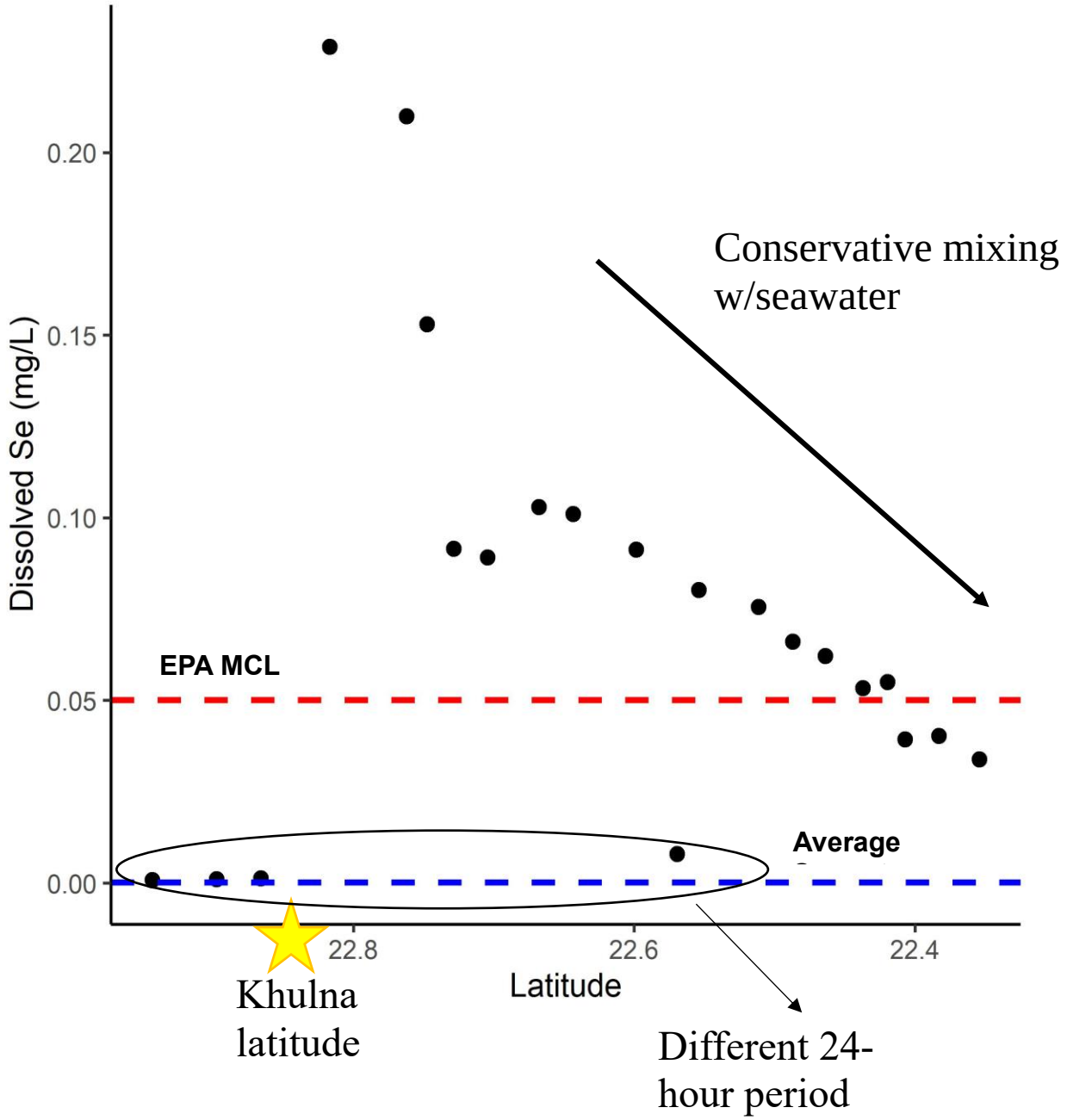

Figure 7: Dissolved selenium concentrations versus latitude, with the U.S. EPA drinking water maximum contaminant level (MCL) represented by the red dashed line, average open ocean concentration[34] represented by the blue dashed line, the approximate latitude of Khulna marked with a star, and samples circled that were collected in a separate 24-hour period.

3.6 Solid/dissolved phase disequilibrium and possible sample incubation effects

Due to the significant storage time of unfiltered samples, possible reactions such as sorption/desorption or dissolution may have occurred that changed the composition of both water and suspended sediment samples. There are mostly poor linear trends with significant scatter between element concentrations in the suspended and the dissolved load (Fig. B10). When comparing the lab filtered samples (0.2 µm) in this study with duplicates filtered in the field (0.45 µm) from a companion study,[22] Co and Ni in the lab filtered samples are significantly elevated in concentration, along with Cr, Zn and Cu (Fig. B11). Most other elements are similar in concentration. Additionally, Co and Ni have slight negative trends between the dissolved and solid load concentrations (Fig. B10). However, no trends are seen between Co and Ni Kd values and time from sampling to filtration (Fig. B12). There is little correlation between days from sampling to filtration and concentrations of almost all elements in the dissolved and solid load except for Se, Mn, Cr, and V in the dissolved load (Figs. B4 & B5). An element of interest in this study, Se, does show a moderate negative correlation between days from sampling to filtration and dissolved concentration (Fig. B13).

3.7 TEM particle imaging

TEM work on particulates from tidal channel suspended sediment within the study area (sample P32-TC)[22] and from this study (MD-TC-7 and MD-TC-11) routinely revealed small particles rich in Al and Si, likely to be clay minerals or other phyllosilicates (Figs. 8 & B14). Some of these particles had other elements such as Cu, Ti, and Fe associated with nanocrystals or coatings on their surfaces (mapped via STEM-EDS). A characteristic sample illustrates a striated surface containing several areas with higher concentrations of Fe and Cu, potentially attached to the larger particle surface as oxide nanoparticles (Fig. 8). Fe-rich particles <1µm were also common, including an Fe-particle near the filter size (0.2 µm) used in this study and several Fe-sulfide particles ~0.5 µm in diameter (Fig. B14). Several transition metals such as Mn, Ti, Ni, and Cu were found to be associated with these Fe-rich particles, although it is noted that the copper grid amplifies the Cu signal in EDS and elemental mapping, and the Ni EDS signal is weak (Fig. B14). Additionally, while mineralogical identification of the specific nanoparticles was difficult, a K-silicate particle with substantial K, Si and Al was identified that was likely a muscovite particle based on approximate wt.% and at.% proportions of Al, Si, O and K (Fig. B15).

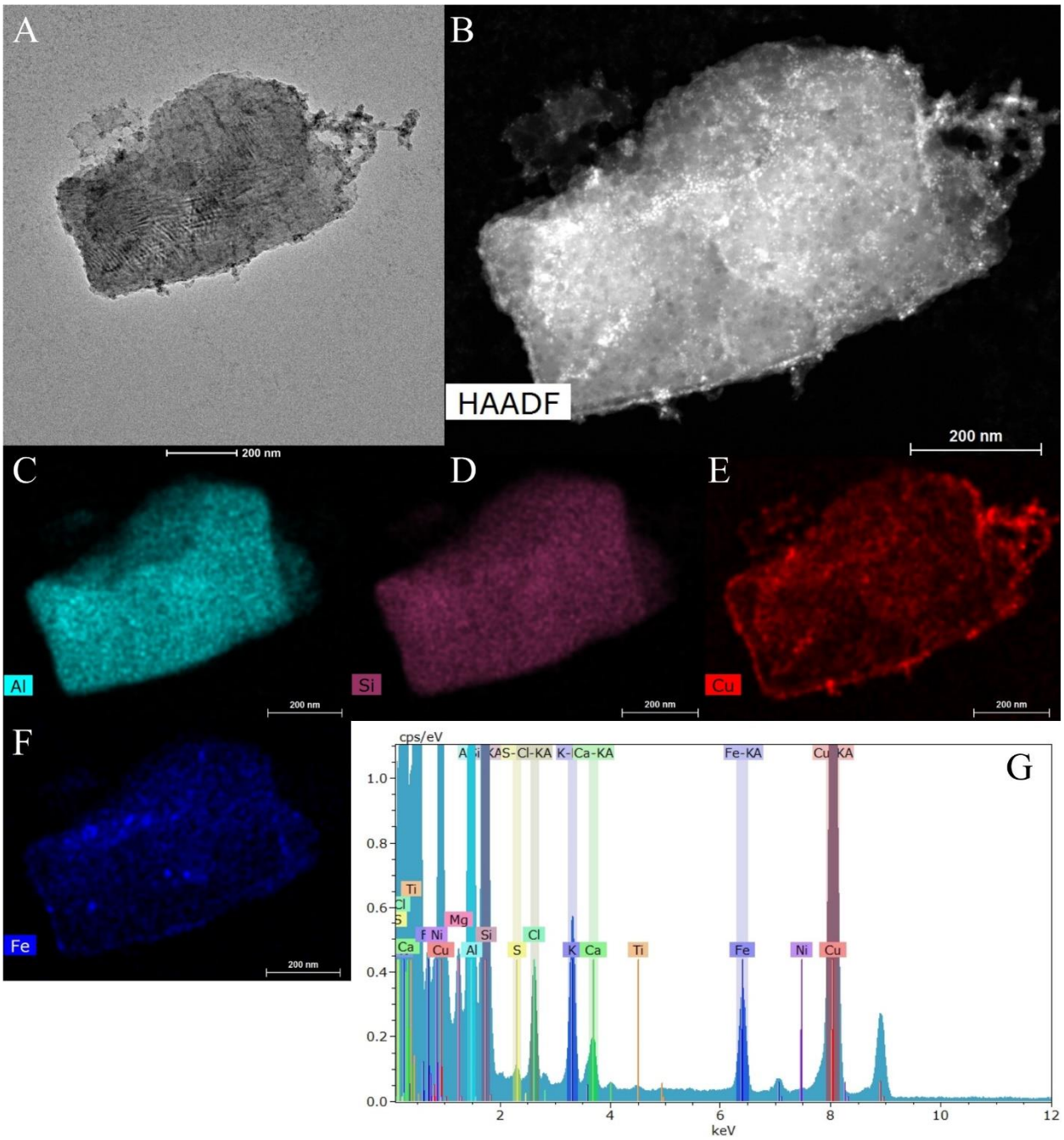

Figure 8: TEM analysis of a representative particulate from tidal channels in SW Bangladesh (Sample P32-TC).[22] (A) TEM image shows a plate-like particle with a striated surface about 1 μm in diameter. (B) High-angle annular dark-field (HAADF) imagery illustrates the heavier atoms through brighter luminescence. STEM-EDS maps are provided for the elements Al (C), Si (D), Cu (E), and Fe (F), which suggest an aluminum-silicate particle with Cu and Fe-rich nanoparticles or ferric oxide coatings potentially on the surface. (G) The EDS spectrum of the sample with large peaks for each of the elements mapped, with Cu amplified because of the Cu TEM grid.

4 Discussion

4.1 Element enrichment/depletion in the dissolved and suspended loads

4.1.1 The dissolved load

Several trace elements (Ba, Ni, Co, Se, As) (Table 2) normally seen in low concentrations in rivers' dissolved loads are elevated well above average world river dissolved load concentrations (Fig. B3). These element concentrations are similar to shrimp ponds and tidal channels from a previous study in the same region, which are also well above average seawater concentrations.[22] However, relative to other recent studies of surface waters in the region, mean As and Cu concentrations were much greater in this study, while Cd, Fe, Mn, Pb, and Zn were much lower than the other studies (Table B2). These differences may be in part due to temporal sampling variability, spatial variability, or analytical procedures.

Arsenic and Se are elevated above WHO drinking water guidelines in nearly all samples of this study, affirming that there must be a significant source contributing these elements to the river system. Possible sources of As include geogenic sources such as leaching from sediments that contain As originally derived from the Himalayas, or groundwater due to exfiltration or irrigation[13] because groundwater in the region contains elevated levels of As.[24] Arsenic can also be derived from anthropogenic sources, such as pesticides, herbicides, wood preservatives, and even animal feeds.[36] However, because of the prevalence of As-rich groundwater in the area, groundwater is deemed more likely as the ultimate source. This idea will be expanded upon in Section 4.3.3. While Se is less toxic than As and an essential micronutrient, it may still be harmful at elevated concentrations and may originate from fossil fuel burning,[36] municipal sewage or oil refinery effluent,[37] certain fertilizers[38] or the interaction of water with Se-rich rocks.[39] However, significant geogenic sourcing of Se thus far in Bangladesh has been shown to be limited, as soil concentrations are either typical of average world Se soil levels[40] or even lower,[41] and groundwater Se concentrations have been well below health standards thus far.[42–44] Possible anthropogenic sourcing of Se will also be discussed in more detail in Section 4.3.3.

While these tidal channels are not used for drinking water purposes during the dry season (i.e., early May) because of their high salinity, the WHO drinking water guidelines are still an effective benchmark to illustrate that these waterways are significantly enriched in Se and As in Southwest Bangladesh. For example, the high concentrations of dissolved Se and As may pose problems via accumulation in other biota, particularly because Southwest Bangladesh is an agricultural region that has been increasingly reliant upon shrimp aquaculture in recent years[45] and uses tidal channels extensively for agriculture/aquaculture irrigation.[13,22]

4.1.2 The suspended load

While most major elements (e.g., Al, Fe, K, Ca, Na) are depleted in the suspended sediment load relative to upper continental crust (UCC), several trace elements (Se, As, Sb, Cd) are enriched in most samples relative to UCC (Fig. 4A). Comparing elements in the suspended load to a reference material such as UCC can give insight into regional enrichment or depletion of solid-phase elements from transport, weathering or anthropogenic processes, assuming the

source material is similar in composition to the reference material (e.g., UCC). While the composition of the source material in this study (eroded Himalayan crust) is difficult to constrain with certainty,[46] average UCC can still provide a reasonable source comparison, as various Himalayan formations that may contribute to the source material have major element concentrations relatively similar to average UCC.[47]

The large depletion in Ca, Sr, Na, and K relative to UCC is likely representative of the significant weathering of mobile elements that occurs in the Ganges floodplain prior to deposition in the lower tidal plain,[46,48] or grain size sorting effects. This depletion should hold true even if the major element concentrations in this study are slightly lower than they would be on an anhydrous basis like those used in UCC calculations.[33] Previous work looking at deposited rice paddy and tidal channel sediment in Southwest Bangladesh also revealed depletion of mobile elements susceptible to weathering such as Sr, Na, and Ca, but saw enrichment of K relative to UCC.[49] The discrepancy between K concentrations between our study and Ayers et al.[49] is perhaps partly attributable to grain size sorting, because the volume-weighted mean grain size of the deposited sediments were oftentimes 2-3 times greater than the grain size of suspended sediment samples in this study. This is reflective of the upper portion of the water column (i.e., upper 1m used in this study) containing the finest grained sediment compared to the rest of the water column.[23] The coarser material in Ayers et al.[49] may have greater abundances of K-rich minerals, such as K-feldspar, which was seen in suspended sediment profiles in the Ganges and Brahmaputra rivers as grain size increases with depth.[23] However, mineralogical data in this study for both suspended sediment and shrimp pond sediment (Fig. B2) is remarkably similar to the sediment in Ayers et al.[49] based on qualitative observations of diffraction peaks, suggesting that grain size sorting within the silt sized range may not have a large effect on mineral abundance. This similar mineralogy is also consistent with the shrimp pond sediment being sourced from the tidal channel. Additionally, TEM analyses identified a K-silicate particle that is likely muscovite in our suspended sediment (Fig. B15), illustrating at least one of the K-phases present in sediment.

The enrichment of several trace elements such as Se, Cd, As and Sb and dissimilarities to the comparatively lower concentrations of several trace elements such as Sb, Cd and As in Ayers et al.[49] could be partly due to the finer grain size of the suspended sediments in the upper 1m of the water column. The smaller grain sizes (with presumably larger surface area) may be more effective at scavenging elements like Cd and As than the slightly coarser grains in Ayers et al.[49]. The elevated trace element concentrations may also be in part due to anthropogenic inputs,[23] such as from the city of Khulna, or because of volatilization of several trace elements during the $LiBO_2$ flux fusion procedures in Ayers et al.[49] leading to trace element depletion in that study. Enrichment of trace elements such as As, Se, Cd, and Sb relative to UCC was also reported in suspended sediment in the upper Ganges,[50] suggesting that the geogenic contribution of these trace elements from sediments in the Ganges river system may be greater than typical crustal values.

4.2 Fe solid phase correlations & element partitioning

Based on bulk chemistry suspended sediment correlations, it is apparent that most trace metals/metalloids are associated with Fe in the suspended sediment load (Fig. B6). Garzanti et

al.[23] proposes that many trace elements plotted in Fig. B6, such as As, Co, Ni, Cu and Pb are associated with the formation of secondary minerals (i.e., clays or oxyhydroxides) that are present in the shallow suspended loads of the Ganges and Brahmaputra rivers, which would include Fe minerals. The hypothesis of several trace elements associated with Fe-minerals is supported by TEM imaging, where aluminum silicate particles have metals such as Cu associated with Fe on their surface (Fig. 8), and <1µm particulate Fe-bearing minerals are associated with transition metals such as Mn, Ti, Ni and Cu (Fig. B14). However, besides the Fe coatings and likely presence of Fe-oxyhydroxides, Fe-sulfide particles were also identified (Fig. B14). Additionally, the metalloid As shows moderate correlations with Fe in the bulk suspended load (Fig. B6), suggesting some association between As and Fe-minerals such as Fe-oxyhydroxides, as proposed by previous researchers.[51–53] This also promotes the hypothesis that As in the Ganges floodplain sediments are derived from dissolution of primary minerals from the Himalaya, followed by sorption onto secondary mineral phases such as Fe-oxyhydroxides.[53,54] These secondary minerals are transported in rivers as suspended sediment and deposited throughout the floodplains in Bangladesh.

In general, as elements become more mobile in weathering and transport processes, their Kd values decrease and their dissolved proportions increase (Fig. 4C). However, several elements such as Mn, Co, Cd and Sb are exceptions to this trend, with all these elements partitioned into the solid load more than expected (Fig. 4C). Many of the most mobile elements also have elevated Kd values relative to what would be expected based on Kd values of less mobile elements (Fig. 4B).

One reason for elevated Kd values may be that several of the trace elements in the solid-phase were close to detection limit on the ICP-OES and may have concentrations artificially enhanced in the solid-load due to substitution of MDLs in Kd calculations for Figure 4B. Additionally, some Cd values were close to or below detection limit in the dissolved load, similar to values in blank samples (Table 2). However, this doesn't change the fact that Cd dissolved values are very low and thus make the Kd values large. A more likely explanation is that the abundance of Fe-oxides in the dominantly silt-sized suspended load leads to the enrichment of elements such as As and Cd that tend to sorb onto surfaces of these minerals. This may lead to increased Kd values because of greater concentrations of elements in the solid phase. Because of similar grain sizes in upstream and downstream samples along the transect (Fig. 3), grain size likely has a consistent effect on adsorption onto mineral surfaces.

The elements Mn, Co, Cd and Sb may have much lower proportions in the dissolved load than expected because of resistance to desorption processes and/or dissolution reactions occurring in estuary water, i.e., disequilibrium. Selenium and arsenic (likely as oxyanion species in most natural waters), however, may have greater concentrations in the dissolved load (and thus lower Kd values compared to Cd, Sb, Mn and Co) because of less affinity for Fe-oxides compared to trace metal cations in the oxidizing and slightly alkaline conditions of surface waters in this study (pH between 7.36-7.72; Table 1). This is seen with relatively weaker correlations (concentrations <MDL excluded) between Fe and Se ($r = 0.39$, $p = 0.21$) and Fe and As ($r = 0.58$; $p = 0.0092$) compared to metals often speciated as cations in solution (e.g., Co, Cd, Cr, Ni; Fig. B5), and is also supported by literature estimating the points of zero charge (PZC) and isoelectric points (IEP) of hydrous ferric oxides (HFOs) such as ferrihydrite and goethite

oftentimes between ~7.0-8.5.[55] If the pH of the waters in this study is above the PZC or IEP of the sorbing HFOs, then cations will be favored for sorption over dissolved anion species.

Several elements such as Ni, K, Ba, Na and Sr tend to plot closer to the dissolved element proportions of a typical low suspended sediment river (Rio Negro), while Co plots much closer to a typical high suspended sediment river (Rio Solimoes) (Fig. 4C).[28] However, the average suspended sediment loads of those rivers (Rio Negro <0.01 g/L; Rio Solimoes ~0.23 g/L[28]) are less than the average suspended sediment load in this study (0.49 g/L; Table 1). This is likely indicative of the large seawater influence of many soluble elements such as Ni, K, Na and Sr, which would increase the proportion of these elements in the dissolved load in Ganges tidal channels even if there is a relatively large amount of suspended sediment present. Barium may be primarily in the dissolved load even though its concentrations decrease with seawater mixing (Fig. 6C) because of previous desorption from suspended sediment upstream due to cation exchange, even where seawater influence was minimal,[9] or from groundwater input as suggested occurs significantly to the Bay of Bengal.[10,56]

4.3 Geochemical trends with increased seawater mixing

4.3.1 Evidence of trace metal desorption along the transect

As latitude decreases along the tidal channel transect and the sample locations approach the Bay of Bengal, salinity increases (Fig. 2). Thus, any spatial trends associated with latitude can also be interpreted as trends with salinity. The trace metals Ni and Co typically exhibit nonconservative behavior and have dissolved concentrations that are well above seawater[34] and increase linearly as salinity increases (Fig. 5). Thus, the increasing dissolved concentrations of these metals with increased seawater mixing cannot be explained by simple conservative mixing of seawater. A source other than seawater must be responsible for the increasing concentration of these trace metals.

A likely source of dissolved Ni and Co is suspended sediment, as desorption of Co and Ni from suspended sediment has been documented in a nearby estuary (Hooghly Estuary, ~100-150 km to the west of the study area) with increased seawater mixing.[1] That study saw the same linear trends of increasing dissolved Co and Ni with increasing salinity.[1] Furthermore, that study showed Kd values decreasing with salinity, suggestive of desorption from competitive cation interactions, which is consistent with the Kd trends of Ni and Co in our study (Fig. 5). Our lower suspended sediment concentrations of Ni and Co at higher salinities also supports some level of desorption occurring (Fig. B8). While the Kd values from Samanta and Dalai[1] were based on the exchangeable solid fractions of Ni and Co, the bulk Kd values used in this study can still provide a similar approximation of partitioning. However, Samanta and Dalai[1] also showed Cu exhibiting similar characteristics to Ni and Co with increased seawater mixing, which our study did not observe (Fig. B16). Additionally, Samanta and Dalai[1] attributed the desorption processes largely to competition with Na for sorption sites, which we did not see direct evidence of based on our Na concentrations. This may be because Samanta and Dalai[1] utilized data from suspended sediment that was rinsed with Milli-Q water, which may have removed some Na, Mg, and K from sea salt that was likely included in our suspended sediment analysis (the lack of rinsing

salts from our suspended sediment samples may also be the reason S is elevated relative to UCC (Fig. 4A), because of soluble sulfate minerals precipitating from seawater after drying).

4.3.2 Barium trends along the transect

Dissolved Ba in general exhibits decreasing concentration as salinity increases (Fig. 6C). This is indicative of conservative mixing with seawater, which is seen in other studies in the region at salinities equivalent to this study (>10 ppt).[8–10] However, a distinct change in linear regression slope is observed at a latitude of ~22.6 in this study (Fig. 6C), also when the transect transitions from the Rupsha River to the Bhadra River. This may indicate a decrease of Ba supplied to the dissolved load from sediment desorption (and thus increasing the rate/slope of conservative mixing), as both Ba Kd values and suspended sediment concentrations either remain stable or increase at lower latitudes (Figs. 6A & 6B). Other studies of Ba in the region indicate dissolved Ba increasing at low salinities due to sediment desorption from cation substitution,[8–10] which would explain the Ba concentrations in this study being well above average riverine Ba concentrations[28] if Ba desorption occurred upstream of our study area. Barium is strongly correlated with Fe in the sediment load as well (Fig. 6D), suggesting that the fraction of solid-phase Ba analyzed in this study is associated with Fe-minerals such as Fe-oxyhydroxides, which a large portion of labile Ba is associated with.[57]

Barium may also be introduced into tidal channels from groundwater exfiltration, particularly because average Ba (380 µg/L)[24] is elevated in groundwaters in the area relative to tidal channel samples in this study (~220 µg/L) and Ganges-Brahmaputra river representative values (~21 µg/L).[56] Moore[10] and Dowling et al.[56] insist that a large flux of the dissolved Ba in the Bay of Bengal is indeed from groundwater discharge. However, because desorption of Ba from tidal channel sediment or upstream river sediment is likely contributing substantial dissolved Ba[9] and the proportion of groundwater exfiltration to tidal channels is probably less than to the Bay of Bengal, groundwater Ba contribution to tidal channels is likely less than that of sediment desorption upstream.

4.3.3 Arsenic and selenium trends along the transect

Arsenic and selenium have been previously documented in concentrations above WHO guidelines in Southwest Bangladesh surface waters,[13,22] and thus this study set out to investigate whether the large city of Khulna could possibly be a source of these elements downstream. Previous work found several potential "hotspots" of Zn and U pollution in waterways near our study area through artificial mussel monitoring, albeit pollution was less in Khulna waterways compared to the Buriganga River in Dhaka.[21] However, that study did not analyze for Se or As, and As and Se were >WHO guidelines in the dissolved load in this study (Table 2).

Both selenium and arsenic exhibit the lowest concentrations in the Bhairab River along the more northern extent of Khulna at the highest latitudes in this study (Fig. 7 and Fig. B9). However, while As did not display any definitive mixing trends downstream (Fig. B9), Se showed conservative mixing with decreasing latitude and increased salinity for all samples but the three Bhairab River samples and another sample downstream (which was taken within a separate 24-hour sampling period at a similar time of day as previous nearby samples, and during

the same 24-hour sampling period as the three Bhairab River samples) (Fig. 7). Conservative mixing of dissolved Se with seawater has been documented before, specifically when it was anthropogenically sourced to San Francisco Bay in the U.S.[58] However, the dissolved Se concentrations in this study are much higher than in polluted estuary samples of other studies and are much closer to direct oil refinery effluent Se concentrations.[37,58] Khulna holds two large petroleum companies along the southern reaches of the Bhairab, which are a possible source of the downstream Se. However, based on watersheds of both the Bhairab and Rupsha rivers (Fig. B17), it is possible that Se may have been sourced upstream of Khulna. Selenium has no known geogenic sources of such high concentrations in the area, as soils[40,41] and groundwater[42–44] are not anomalously high in Se in Bangladesh. Thus, Se is likely anthropogenic. Our interpretations of anthropogenic Se support recent work in the Ganges river system in India, where trace element pollutant hotspots have been identified near cities, but typically do not persist downstream because of dilution from additional river tributaries.[50] In our case, the dilution is caused by seawater mixing in lieu of other river tributaries.

Because dissolved As is relatively ubiquitously elevated in samples irrespective of latitude with no definitive trends (Fig. B9), a possible source may be from groundwater during dry season low river flow, as previously suggested by Ayers et al.[13] However, assuming groundwater contribution was consistent along the transect, it would be expected that there would be conservative mixing of arsenic as the seawater fraction increases along the transect, unless some of the reworked tidal channel water from the Bay of Bengal contains As from submarine discharge. However, it is unlikely that the water from the Bay of Bengal would contain elevated As. Thus, either As is not sourced predominantly from groundwater or additional nonconservative processes are at work regarding As mobilization and transport, perhaps because of interactions of groundwater at redox zones between the sediment-water interface as suggested by Berube et al.[59] Arsenic from reducing groundwaters may sorb onto sediments in oxidizing environments before discharging into rivers, although if riverine dissolved As is sourced from groundwater, there must be exfiltration points where sorption is limited and redox conditions are thus not suitable for complete As sorption. Thus, variability in these redox transition zones of groundwater exfiltration may partially explain the nonconservative mixing seen between As and seawater (Fig. B9).

Samples with high concentrations of dissolved selenium that fall on a conservative mixing trend may specifically be sourced from an anthropogenic effluent flushing event (Fig. 7). The four samples with the lowest concentrations were taken in a different 24-hour period (Fig. 7). However, the relatively ubiquitously elevated Se concentrations in July shrimp ponds and May shrimp ponds in Southwest Bangladesh relative to average riverine concentrations[22] suggests that if the Se is ultimately sourced from effluent discharge, it is not from isolated events. Lastly, it is important to note that Se was an order of magnitude lower (1 µg/L vs 30 µg/L) in a sample of the Bhairab River in this study compared to Dietrich and Ayers[22] (Fig. B11), who field filtered at 0.45 µm at the same location. One likely cause of the discrepancy between samples is the filtration size difference (0.2 µm in this study versus 0.45 µm in Dietrich and Ayers[22]), where small, colloidal-like particles (organic or inorganic) may increase filtered "dissolved" concentrations.[28]

Both As and Se Kd values do not show any obvious trends with salinity (and therefore seawater mixing) along the transect (Fig. B7). This suggests that these elements are not strongly influenced by sorption or dissolution reactions along the transect as salinity increases. However, analysis of the extractable fractions of each element (at lower instrument detection limits) will provide better insight into possible element exchange, particularly for As, which is likely experiencing nonconservative processes based on the lack of conservative mixing seen along the transect (Fig. B9).

4.4 Possible sample incubation effects

Because several effects may occur during long incubation times of unfiltered water samples (i.e., dissolution, sorption reactions, biological reactions), the effect of incubation time on several geochemical parameters of interest was examined. Most dissolved and solid phase elements and geochemical parameters were not strongly correlated with days between sampling and lab filtration (Figs. B4 & B5). Additionally, most trace elements that may undergo desorption or dissolution processes showed significant scatter between the dissolved and suspended loads, suggesting disequilibrium partitioning (Fig. B10). Thus, even though the suspended sediments were in contact with the water for an extended period of time, slow kinetics likely prevented exchange equilibrium. Also, the residence time of water in the tidal channel during which reactions between sediment and water can occur was likely similar in magnitude to sample incubation time, because most water in this area is tidally reworked.[15] Lastly, because of the highly saline nature of the waters, lack of significant headspace in the sealed samples during storage, sample refrigeration, and relatively low DOC compared to world rivers,[28] biological reactions were also likely limited. This was additionally shown by poor correlation between DOC and days from sampling to filtration (Fig. B4).

Specifically regarding Ni and Co Kd values, the lack of any trends with days from sampling to filtration suggests that the desorption from salt cations occurred predominantly before the samples were stored (Fig. B12). Post-sampling effects of Se however, are possible, although there is lack of sufficient evidence to conclude that a significant amount of Se was sorbed, desorbed, or co-precipitated on suspended sediment during sample storage. The first line of insufficient evidence is the lack of exchange equilibrium between measurable dissolved and suspended Se (Fig. B10). Second, there is only a slight negative correlation ($r^2 = 0.48$; Fig. B13) between dissolved Se and the days from sampling to filtration. If there was a strong effect on the dissolved Se during sample storage, one would expect the correlation to be stronger, particularly if Se ranged 2 orders of magnitude in the dissolved load (Table 2). Third, when excluding four samples from the separate "non-effluent" 24-hour sampling period, Se is more strongly correlated with salinity ($r^2 = 0.76$) relative to days from sampling to filtration ($r^2 = 0.25$), implying the trends are indeed from mixing with seawater and not induced by sample incubation. Lastly, Se concentrations in duplicate samples filtered in the field for samples MD-TC-18 and MD-TC-19 were 15 µg/L and 30 µg/L, respectively, both less than any lab-filtered samples in this study taken during the proposed 24-hour effluent release event. Thus, even if some of the dissolved Se became immobilized in the solid phase during incubation (as suggested by the negative correlation between dissolved Se and days to filtering), the dissolved concentrations from the field filtrations (taken in the second, "non-effluent" 24-hr period) are still lower than all the Se concentrations in the main 24-hr sampling period, supporting our Se anthropogenic

effluent interpretations. However, slight sorption/desorption or coprecipitation of Se during sample storage cannot be fully discounted, particularly because of the differences in concentrations of Se in duplicate field filtered and lab filtered samples (Fig. B11) and that several other redox sensitive metals (Cr, V, and Mn) showed moderate negative correlations with days from sampling to filtration (Fig. B4).

4.5 Summary of geochemical mechanisms

The primary mechanisms hypothesized to affect the distribution and partitioning of elements along this study's transect were desorption, ion-exchange, and conservative mixing with seawater. Changes in pH and dissolution might also be expected to influence element partitioning in an estuarine environment, although direct evidence of these mechanisms causing changes along the transect is lacking. pH measurements showed very little variation along the transect ($1\sigma = 0.09$; Table 1), and although the pH values were lower than one might expect based on mixing with seawater, the lack of variation indicates that pH has little effect on changing element concentrations throughout the transect. However, the slightly alkaline pH (mean = 7.61) likely leads to preference for cation adsorption on HFOs as opposed to anion species such as arsenate, selenate, or selenite, because the points of zero charge and isoelectric points oftentimes are estimated as between ~7-8.5 for HFOs.[55] While dissolution can play an important role in element partitioning in coastal environments, it is difficult to deduce the extent it occurs in the natural environment, particularly in this study because of difficulty distinguishing dissolution processes in highly saline waters.[60] However, minerals that are major components of river sediments in Bangladesh[61] (Fig. B2) and are present in suspended sediment such as quartz, kaolinite and illite[60] have low laboratory dissolution rates and are saturated in our water samples, (Table 1) suggesting that dissolution of suspended sediments during transport was low in our study area. Furthermore, annual dissolution in seawater is estimated to be close to 0% for those minerals.[60] Lastly, Ayers et al.[49] classifies sediment weathering in this study region as likely transport limited, and thus dissolution reactions are slow if they are occurring.

Because of the focus of this study on trace elements rather than major elements, it is unclear to what extent major elements exchanged with one another on solid surface sites via ion exchange. However, there is evidence of saltwater major cation substitution leading to desorption of Ni and Co along the transect of this study with increased mixing of seawater. This may have significant impacts on dissolved estuarine fluxes into the ocean, particularly if there is an upstream pollution spill of Ni or Co, or a similar metal cation species. While these cations may adsorb effectively onto suspended sediment in lower salinity water, they may be mobilized in higher salinity water, which could pose a threat for biota in ecosystems such as the Sundarbans, or for farmers who irrigate with the saline tidal channel water for aquaculture. Lastly, while conservative mixing of elements such as saltwater ions may be obvious with increased seawater contribution, conservative mixing of other elements such as Ba and Se following a nonconservative input source (desorption or effluent) provides more insight into the dilution and behavior of these elements in estuarine environments. Thus, all hypothesized geochemical mechanisms affect element partitioning to some degree, but elements are affected in different ways. Better understanding of which elements are likely associated with certain processes can be useful for research in other estuary environments throughout the world, such as the Mississippi River delta or Red River delta.

5 Conclusions

Multiple processes affect element mobility and transport along tidal channels in Bangladesh, such as desorption, ion-exchange, and conservative mixing. The elements Ni and Co are affected by desorption processes induced by exchange with saltwater cations. Barium shows trends consistent with conservative mixing with seawater, although it too is likely affected by desorption processes, albeit largely upstream in lower salinity waters. Selenium and arsenic are elevated past drinking water guidelines in nearly all samples, with slight enrichment relative to upper continental crust in the suspended load as well. While Se is likely anthropogenically sourced from the city of Khulna or another site farther upstream, As is likely predominantly geogenic and may be partly sourced from groundwater exfiltration, like Ba.

Most trace elements are elevated above average dissolved river concentrations, and further monitoring of anthropogenic pollution sources upstream is needed to protect the Sundarbans natural mangrove forest. If there is any significant release of metal cations upstream such as Ni and Co, they may be increasingly mobilized in the saline, estuarine environment of the Sundarbans' tidal channels, particularly during the dry season.

Conflict of interest

There are no conflicts of interest to declare.

Acknowledgements

Funding supported by the NSF Coastal SEES Collaborative Research Grant OCE-1600319. We appreciate the thoughtful comments from Jessica Oster that helped improve the manuscript. Special thanks to Md. Zahidul Haque for his immense help in the field and to many others from the University of Dhaka, Khulna University and Pugmark Tours (Md Nazrul Islam (Bachchu)) who have helped with this ongoing research project. Thanks also goes out to Rossane DeLapp, James McBride and the Vanderbilt Institute of Nanoscale Science and Engineering (VINSE), Christopher Sharp, and Sunjeong Park and the Ohio State University Service Testing and Research Laboratory (STAR Lab) for analytical assistance.

References

1 S. Samanta and T. K. Dalai, Massive production of heavy metals in the Ganga (Hooghly) River estuary, India: Global importance of solute-particle interaction and enhanced metal fluxes to the oceans, *Geochim. Cosmochim. Acta*, 2018, **228**, 243–258.

2 A. A. de Souza Machado, K. Spencer, W. Kloas, M. Toffolon and C. Zarfl, Metal fate and effects in estuaries: A review and conceptual model for better understanding of toxicity, *Sci. Total Environ.*, 2016, **541**, 268–281.

3 V. Hatje, T. E. Payne, D. M. Hill, G. McOrist, G. F. Birch and R. Szymczak, Kinetics of trace element uptake and release by particles in estuarine waters: effects of pH, salinity, and particle loading, *Environ. Int.*, 2003, **29**, 619–629.

4 Y.-H. Li, L. Burkhardt and H. Teraoka, Desorption and coagulation of trace elements during estuarine mixing, *Geochim. Cosmochim. Acta*, 1984, **48**, 1879–1884.

5 G. E. Millward and Y. P. Liu, Modelling metal desorption kinetics in estuaries, *Sci. Total Environ.*, 2003, **314–316**, 613–623.

6 N. Thanh-Nho, E. Strady, T. Nhu-Trang, F. David and C. Marchand, Trace metals partitioning between particulate and dissolved phases along a tropical mangrove estuary (Can Gio, Vietnam), *Chemosphere*, 2018, **196**, 311–322.

7 E. Strady, Q. T. Dinh, J. Némery, T. N. Nguyen, S. Guédron, N. S. Nguyen, H. Denis and P. D. Nguyen, Spatial variation and risk assessment of trace metals in water and sediment of the Mekong Delta, *Chemosphere*, 2017, **179**, 367–378.

8 S. Samanta and T. K. Dalai, Dissolved and particulate Barium in the Ganga (Hooghly) River estuary, India: Solute-particle interactions and the enhanced dissolved flux to the oceans, *Geochim. Cosmochim. Acta*, 2016, **195**, 1–28.

9 J. Carroll, kelly K. Falkner, E. T. Brown and W. S. Moore, The role of the Ganges-Brahmaputra mixing zone in supplying barium and226Ra to the Bay of Bengal, *Geochim. Cosmochim. Acta*, 1993, **57**, 2981–2990.

10 W. S. Moore, High fluxes of radium and barium from the mouth of the Ganges-Brahmaputra River during low river discharge suggest a large groundwater source, *Earth Planet. Sci. Lett.*, 1997, **150**, 141–150.

11 N. T. Chowdhury, Water management in Bangladesh: an analytical review, *Water Policy*, 2010, **12**, 32–51.

12 S. Akter and K. R. Ahmed, Water chemistry and water quality of a tidal river system in relation with riverbank land use pattern and regional climate in the southwest Bengal Delta of Bangladesh, *Sustain. Water Resour. Manag.*, 2019, **5**, 1259–1279.

13 J. C. Ayers, G. George, D. Fry, L. Benneyworth, C. Wilson, L. Auerbach, K. Roy, Md. R. Karim, F. Akter and S. Goodbred, Salinization and arsenic contamination of surface water in southwest Bangladesh, *Geochem. Trans.*, 2017, **18**, 4.

14 H. Brammer, Bangladesh's dynamic coastal regions and sea-level rise, *Clim. Risk Manag.*, 2014, **1**, 51–62.

15 R. Hale, R. Bain, S. Goodbred Jr. and J. Best, Observations and scaling of tidal mass transport across the lower Ganges–Brahmaputra delta plain: implications for delta management and sustainability, *Earth Surf. Dyn.*, 2019, **7**, 231–245.

16 S. M. B. Rahaman, L. Sarder, M. S. Rahaman, A. K. Ghosh, S. K. Biswas, S. S. Siraj, K. A. Huq, A. F. M. Hasanuzzaman and S. S. Islam, Nutrient dynamics in the Sundarbans mangrove estuarine system of Bangladesh under different weather and tidal cycles, *Ecol. Process.*, 2013, **2**, 29.

17 S. M. Rahaman, S. K. Biswas, M. S. Rahaman, A. K. Ghosh, L. Sarder, S. Siraj and S. S. Islam, Seasonal nutrient distribution in the Rupsha-Passur tidal river system of the Sundarbans mangrove forest, Bangladesh, *Ecol. Process.*, 2014, **3**, 18.

18 K. Ahmed, Y. Mehedi, R. Haque and P. Mondol, Heavy metal concentrations in some macrobenthic fauna of the Sundarbans mangrove forest, south west coast of Bangladesh, *Environ. Monit. Assess.*, 2011, **177**, 505–514.

19 A. Kumar, AL. Ramanathan, M. B. K. Prasad, D. Datta, M. Kumar and S. M. Sappal, Distribution, enrichment, and potential toxicity of trace metals in the surface sediments of Sundarban mangrove ecosystem, Bangladesh: a baseline study before Sundarban oil spill of December, 2014, *Environ. Sci. Pollut. Res.*, 2016, **23**, 8985–8999.

20 D. K. Datta, P. K. Ghosh, Md. R. Karim and Md. M. Rahman, Geochemical options for water security in a coastal urban agglomerate of Lower Bengal Delta, Bangladesh, *J. Geochem. Explor.*, 2020, **209**, 106440.

21 G. Kibria, M. M. Hossain, D. Mallick, T. C. Lau and R. Wu, Monitoring of metal pollution in waterways across Bangladesh and ecological and public health implications of pollution, *Chemosphere*, 2016, **165**, 1–9.

22 M. Dietrich, and J. C. Ayers, Influences on tidal channel and aquaculture shrimp pond water chemical composition in Southwest Bangladesh. *Geochem. Trans.*, 2021, **22**, 1-22. https://doi.org/10.1186/s12932-021-00074-2

23 E. Garzanti, S. Andó, C. France-Lanord, P. Censi, P. Vignola, V. Galy and M. Lupker, Mineralogical and chemical variability of fluvial sediments 2. Suspended-load silt (Ganga–Brahmaputra, Bangladesh), *Earth Planet. Sci. Lett.*, 2011, **302**, 107–120.

24 J. C. Ayers, S. Goodbred, G. George, D. Fry, L. Benneyworth, G. Hornberger, K. Roy, Md. R. Karim and F. Akter, Sources of salinity and arsenic in groundwater in southwest Bangladesh, *Geochem. Trans.*, 2016, **17**, 4.

25 N. Weng and W.-X. Wang, Variations of trace metals in two estuarine environments with contrasting pollution histories, *Sci. Total Environ.*, 2014, **485–486**, 604–614.

26 W. Wang and W.-X. Wang, Phase partitioning of trace metals in a contaminated estuary influenced by industrial effluent discharge, *Environ. Pollut.*, 2016, **214**, 35–44.

27 C. M. Bethke, *Geochemical and Biogeochemical Reaction Modeling*, Cambridge University Press, 2007.

28 J. Gaillardet, J. Viers and B. Dupré, in *Treatise on Geochemistry*, eds. H. D. Holland and K. K. Turekian, Pergamon, Oxford, 2014, pp. 225–272.

29 V. Galy, C. France-Lanord and B. Lartiges, Loading and fate of particulate organic carbon from the Himalaya to the Ganga–Brahmaputra delta, *Geochim. Cosmochim. Acta*, 2008, **72**, 1767–1787.

30 J. Gaillardet, B. Dupré, P. Louvat and C. J. Allègre, Global silicate weathering and CO2 consumption rates deduced from the chemistry of large rivers, *Chem. Geol.*, 1999, **159**, 3–30.

31 World Health Organization, 2017.

32 U.S. EPA [U.S. Environmental Protection Agency], 2009.

33 R. L. Rudnick and S. Gao, Composition of the Continental Crust, *Treatise Geochem.*, 2003, **3**, 1–64.

34 R. Mason, in *Trace Metals in Aquatic Systems*, John Wiley & Sons, Ltd, 2013, pp. 219–309.

35 J. Wright and A. Colling, *Seawater: its Composition, Properties and Behaviour*, Elsevier, 1995.

36 B. P. Rosen and Z. Liu, Transport pathways for arsenic and selenium: A minireview, *Environ. Int.*, 2009, **35**, 512–515.

37 G. A. Cutter and M. L. C. San Diego-McGlone, Temporal variability of selenium fluxes in San Francisco Bay, *Sci. Total Environ.*, 1990, **97–98**, 235–250.

38 C. A. Girling, Selenium in agriculture and the environment, *Agric. Ecosyst. Environ.*, 1984, **11**, 37–65.

39 L. H. E. Winkel, C. A. Johnson, M. Lenz, T. Grundl, O. X. Leupin, M. Amini and L. Charlet, Environmental Selenium Research: From Microscopic Processes to Global Understanding, *Environ. Sci. Technol.*, 2012, **46**, 571–579.

40 P. N. Williams, S. Islam, R. Islam, M. Jahiruddin, E. Adomako, A. R. M. Soliaman, G. K. M. M. Rahman, Y. Lu, C. Deacon, Y.-G. Zhu and A. A. Meharg, Arsenic Limits Trace Mineral Nutrition (Selenium, Zinc, and Nickel) in Bangladesh Rice Grain, *Environ. Sci. Technol.*, 2009, **43**, 8430–8436.

41 J. E. Spallholz, L. Mallory Boylan and M. M. Rhaman, Environmental hypothesis: is poor dietary selenium intake an underlying factor for arsenicosis and cancer in Bangladesh and West Bengal, India?, *Sci. Total Environ.*, 2004, **323**, 21–32.

42 S. H. Frisbie, R. Ortega, D. M. Maynard and B. Sarkar, The concentrations of arsenic and other toxic elements in Bangladesh's drinking water., *Environ. Health Perspect.*, 2002, **110**, 1147–1153.

43 S. H. Frisbie, E. J. Mitchell, L. J. Mastera, D. M. Maynard, A. Z. Yusuf, M. Y. Siddiq, R. Ortega, R. K. Dunn, D. S. Westerman, T. Bacquart and B. Sarkar, Public Health Strategies for Western Bangladesh That Address Arsenic, Manganese, Uranium, and Other Toxic Elements in Drinking Water, *Environ. Health Perspect.*, 2009, **117**, 410–416.

44 M. M. Rahman, Z. Dong and R. Naidu, Concentrations of arsenic and other elements in groundwater of Bangladesh and West Bengal, India: Potential cancer risk, *Chemosphere*, 2015, **139**, 54–64.

45 M. M. H. Khan, I. Bryceson, K. N. Kolivras, F. Faruque, M. M. Rahman and U. Haque, Natural disasters and land-use/land-cover change in the southwest coastal areas of Bangladesh, *Reg. Environ. Change*, 2015, **15**, 241–250.

46 M. Lupker, C. France-Lanord, V. Galy, J. Lavé, J. Gaillardet, A. P. Gajurel, C. Guilmette, M. Rahman, S. K. Singh and R. Sinha, Predominant floodplain over mountain weathering of Himalayan sediments (Ganga basin), *Geochim. Cosmochim. Acta*, 2012, **84**, 410–432.

47 A. Galy and C. France-Lanord, Higher erosion rates in the Himalaya: Geochemical constraints on riverine fluxes, *Geology*, 2001, **29**, 23–26.

48 M. J. Bickle, H. J. Chapman, E. Tipper, A. Galy, C. L. De La Rocha and T. Ahmad, Chemical weathering outputs from the flood plain of the Ganga, *Geochim. Cosmochim. Acta*, 2018, **225**, 146–175.

49 J. C. Ayers, B. Patton and M. Dietrich, Preliminary Evidence of Transport-Limited Chemical Weathering and Element Immobility in the Ganges Tidal Delta Plain of Bangladesh, *Geochem. Geophys. Geosystems*, 2020, **21**, e2020GC009029.

50 S. Boral, I. S. Sen, A. Tripathi, B. Sharma and S. Dhar, Tracking Dissolved Trace and Heavy Metals in the Ganga River From Source to Sink: A Baseline to Judge Future Changes, *Geochem. Geophys. Geosystems*, 2020, **21**, e2020GC009203.

51 J. Akai, K. Izumi, H. Fukuhara, H. Masuda, S. Nakano, T. Yoshimura, H. Ohfuji, H. Md Anawar and K. Akai, Mineralogical and geomicrobiological investigations on groundwater arsenic enrichment in Bangladesh, *Appl. Geochem.*, 2004, **19**, 215–230.

52 H. M. Anawar, J. Akai, K. Komaki, H. Terao, T. Yoshioka, T. Ishizuka, S. Safiullah and K. Kato, Geochemical occurrence of arsenic in groundwater of Bangladesh: sources and mobilization processes, *J. Geochem. Explor.*, 2003, **77**, 109–131.

53 R. T. Nickson, J. M. McArthur, P. Ravenscroft, W. G. Burgess and K. M. Ahmed, Mechanism of arsenic release to groundwater, Bangladesh and West Bengal, *Appl. Geochem.*, 2000, **15**, 403–413.

54 S. Fendorf, H. A. Michael and A. van Geen, Spatial and Temporal Variations of Groundwater Arsenic in South and Southeast Asia, *Science*, 2010, **328**, 5.

55 M. Kosmulski, The pH dependent surface charging and points of zero charge. VII. Update, *Adv. Colloid Interface Sci.*, 2018, **251**, 115–138.

56 C. B. Dowling, R. J. Poreda and A. R. Basu, The groundwater geochemistry of the Bengal Basin: Weathering, chemsorption, and trace metal flux to the oceans, *Geochim. Cosmochim. Acta*, 2003, **67**, 2117–2136.

57 S. C. Carter, A. Paytan and E. M. Griffith, Toward an Improved Understanding of the Marine Barium Cycle and the Application of Marine Barite as a Paleoproductivity Proxy, *Minerals*, 2020, **10**, 421.

58 G. A. Cutter, The estuarine behaviour of selenium in San Francisco Bay, *Estuar. Coast. Shelf Sci.*, 1989, **28**, 13–34.

59 M. Berube, K. Jewell, K. D. Myers, P. S. K. Knappett, P. Shuai, A. Hossain, M. Lipsi, S. Hossain, A. Hossain, J. Aitkenhead-Peterson, K. M. Ahmed, S. Datta, M. Berube, K. Jewell, K. D. Myers, P. S. K. Knappett, P. Shuai, A. Hossain, M. Lipsi, S. Hossain, A. Hossain, J. Aitkenhead-Peterson, K. M. Ahmed and S. Datta, The fate of arsenic in groundwater discharged to the Meghna River, Bangladesh, *Environ. Chem.*, 2018, **15**, 29–45.

60 C. Jeandel and E. H. Oelkers, The influence of terrigenous particulate material dissolution on ocean chemistry and global element cycles, *Chem. Geol.*, 2015, **395**, 50–66.

61 D. K. Datta and V. Subramanian, Texture and mineralogy of sediments from the Ganges-Brahmaputra-Meghna river system in the Bengal Basin, Bangladesh and their environmental implications, *Environ. Geol.*, 1997, **30**, 181–188.

CHAPTER IV

GEOCHEMICAL PARTITIONING AND POSSIBLE HEAVY METAL(LOID) BIOACCUMULATION WITHIN AQUACULTURE SHRIMP PONDS[3]

Abstract:

Limited work has been conducted on trace metal(loid) exchange between sediment, water, feed, and shrimp, particularly in estuarine aquaculture environments. To identify metal(loid) sources and the processes controlling bioaccumulation in shrimp, we analyzed paired aquaculture water, sediment, and shrimp samples collected in Southwest Bangladesh in the late dry season (May), as well as several common artificial feeds. Additionally, we analyzed sediment extract samples from 24-hour laboratory batch experiments as an analogue for aquaculture pond sediment porewater to examine element mobilization from pond sediment. Weak correlations between element concentrations in extracts, pond water, and bulk sediment indicate equilibrium with sediment was not achieved in extract experiments or ponds, and that sediment composition has little influence on pond water or shrimp composition. Aquaculture shrimp metal(loid) concentrations were similar to artificial feed but not pond sediment or pond water, suggesting that shrimp composition is mostly influenced by diet. Although arsenic (As) and selenium (Se) were present at high concentrations in shrimp pond waters and sediment, they were often below detection in shrimp. However, the highly toxic metal thallium (Tl) was detected in shrimp at levels that pose significant human health risks based on calculated target hazard quotient (THQ) values. Thus, further research into potential Tl contamination in Bangladesh aquaculture environments is warranted.

Keyword: Trace elements, element partitioning, inorganic pollution, aquaculture, estuarine geochemistry

1. Introduction

A recent concern with shrimp farming is the possible accumulation of toxic heavy metals (in this work we are also referring to metalloids such as arsenic when mentioning inorganic metals) in shrimp, which may pose a health risk for consumers. Although worldwide there have been many surveys of heavy metal concentrations in aquaculture species (e.g., Jiang et al., 2014; Ju et al., 2017; Marriott et al., 2020; Martins et al., 2011; Mokhtar et al., 2009; Wu and Yang, 2011), there has been relatively limited examination of aquaculture species for heavy metal accumulation beyond routine surveys for risk assessment and metal bioaccumulation in shrimp (e.g., Biswas et al., 2021; Islam et al., 2017a; Mostafiz et al., 2020; Sarkar et al., 2016).

Even though previous research has pointed out potential health hazards of aquaculture shrimp consumption, minimal work has focused on the distribution of metals in aquaculture systems or

[3] Chapter published in "Science of the Total Environment" and reproduced with the permission of the publisher (Elsevier) and my co-author (Dr. John Ayers): Dietrich, M., & Ayers, J. Geochemical partitioning and possible heavy metal (loid) bioaccumulation within aquaculture shrimp ponds. *Science of the Total Environment*, 788, 147777. https://doi.org/10.1016/j.scitotenv.2021.147777

the processes that control the partitioning of metals between shrimp pond environmental media. Knowledge of the entire environmental system is essential for elucidating potential sources of heavy metals in shrimp. These sources include the water, sediment, fish feed, or natural biota within the ponds that the shrimp may eat.

What aquaculture shrimp consume depends largely on the intensity of the farming system, with traditional and extensive farming relying predominantly on natural or low-cost artificial feed, while more intensive aquaculture farms rely more upon nutritionally formulated feed (e.g., Paul and Vogl, 2011 and the references therein). Most Bangladesh shrimp farms are traditional/extensive farms (e.g., Paul and Vogl, 2011 and the references therein), which is representative of our sampling area in Southwest Bangladesh, where most farmers we sampled from used either natural or low-cost artificial fish feed, or a combination of both.

Most studies of aquaculture environments have not characterized all potential sources of metals in farmed species. For example, Guhathakurta and Kaviraj (2000) sampled sediment, water, shrimp (P. *monodon*), and mullet (L. *parsia*) from tidally irrigated ponds in the coastal Indian Sundarbans and found that shrimp and mullet consistently had elevated concentrations of lead (Pb) and zinc (Zn), but did not consider food sources. In Southwest Taiwan, aquaculture pond water sourced from groundwater with dissolved arsenic (As) > 10 µg/L (WHO guideline for safe drinking water) contributed to elevated total As in tilapia (*O. mossambicus*) and shrimp (*P. monodon*), but sediment and feed were not analyzed (Kar et al., 2011). Ju et al. (2017) measured heavy metals in aquaculture tilapia in Southwest Taiwan and found predominantly weak to no correlations between heavy metals in the water, sediment, and different body tissues of tilapia, but did not analyze any samples of fish feed. Mosafiz et al. 2020 estimated bioaccumulation factors of heavy metals based on the concentration ratio of the metal in giant freshwater prawn and water in coastal Bangladesh but did not examine any possible correlations between the shrimp and water, and did not sample feed or sediment in the ponds.

Ayers et al. (2017) and Dietrich and Ayers (2021) found elevated concentrations (>WHO drinking water guidelines) of dissolved As and selenium (Se) in Southwest Bangladesh aquaculture waters. Bioaccumulation of As and Se from water into shrimp may thus pose another health hazard for consumers (e.g., Kar et al., 2011).

Lastly, previous research (Ayers et al., 2020) suggests that the chemical weathering regime in Southwest Bangladesh is transport-limited and thus likely supporting a slow rate of trace metal exchange between waters and sediment because of the abundance of highly weathered materials and mineral-saturated waters. This suggests that direct or indirect trace metal exchange between aquaculture species and sediment may be limited.

The primary research objectives of this study are thus to: 1) Measure partition coefficients between pond sediments and water using 24-hr sediment extract experiments to determine if shrimp pond waters and sediments are in chemical equilibrium, which would suggest rapid element exchange between sediment and water and the potential indirect transfer of metals from sediment to shrimp, 2) Determine whether elevated concentrations of arsenic and selenium in aquaculture water or fish feed lead to elevated trace element concentrations in aquaculture shrimp, 3) Measure partition and correlation coefficients of major and trace elements between

water, feed, sediment, and shrimp to determine whether there are any dominant element transfer mechanisms in the environment, and 4) Estimate health risk for consumers who regularly consume Bangladesh aquaculture shrimp.

2. Methods and study area

2.1 *Southwest Bangladesh*

Coastal Southwest Bangladesh experiences a seasonal monsoonal climate, with the monsoon season contributing about 80% of the total annual rainfall between the months of June to September (Chowdhury, 2010). The distinct monsoon season in Bangladesh contributes to large compositional changes in tidal channel salinity in coastal areas depending on the season (e.g., Akter and Ahmed, 2019; Ayers et al., 2017), because riverine freshwater during the monsoon season dilutes saline tidal water from the Bay of Bengal. Coastal areas of Bangladesh are predominantly rural and agricultural, particularly focused around shrimp farming in recent decades (e.g., Benneyworth et al., 2016 and the references therein), with the two primary farmed species being giant tiger prawn (*P. monodon*) and giant freshwater prawn (*M. rosenbergii*) (e.g., Shamsuzzaman et al., 2017 and the references therein).

2.2 *Sampling*

Samples of paired shrimp, sediment, and water were collected in Southwest Bangladesh during May of 2019 at the end of the dry season within enclosed aquaculture ponds that were all irrigated with tidal channel water. Locations of the sample sites are provided in Fig. 1, which are just north of the Sundarbans natural mangrove forest and the Bay of Bengal, and the same May shrimp pond sample locations as used in Dietrich and Ayers (2021), which examined the shrimp pond waters' composition. At each site, a large scoop of sediment (> ~100 g.) was collected within the upper 10 cm of the sediment profile. For all sample sites except site KA-12, sediment samples were submerged underwater. Additionally, 50 mL of water was filtered at 0.45 µm in the field at each site, and at least one shrimp sample from each site was collected. All shrimp collected were giant tiger prawn (*P. monodon*) except for one chaka shrimp (*P. indicus*) and one harina shrimp (*M. monoceros*). Two samples of commonly used fish feed in the region [LSF-Shrimp feed for larger shrimp (Apon shrimp/prawn nursery feed), SSF- Shrimp feed for smaller shrimp (unidentified manufacturer)] were also collected near the city of Khulna. Two method blanks of water samples using deionized (DI) water were processed in the field (Dietrich and Ayers, 2021), sample duplicates of sediment and water were collected at site KA-21, and a sample of submerged and not submerged sediment were collected at site KA-13 for comparison.

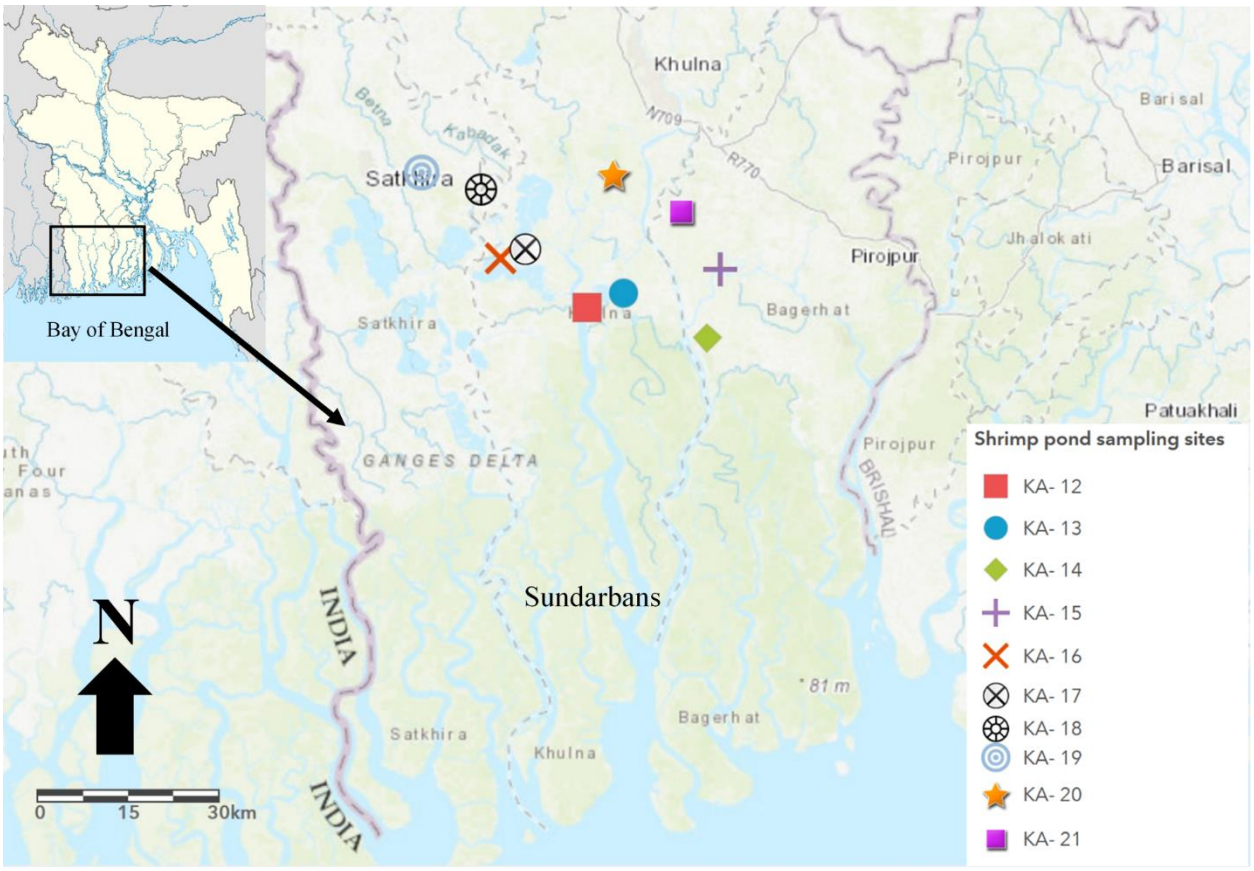

Figure 1: Location of shrimp pond sampling sites in Southwest Bangladesh, where paired soil, water, and shrimp samples were collected. GPS coordinates for sample sites are provided in Dietrich and Ayers (2021).

2.3 *Sample preparation*

All shrimp samples were kept in cold storage within several hours of sampling until they were rinsed with DI water and deshelled, with only the edible tissue portion (not the head or the tail) utilized for analysis. The shrimp tissues were cut into smaller pieces with a stainless-steel knife and first dried overnight in an oven at 105°C. A subset of each tissue sample was then ashed in a high-temperature muffle furnace for approximately 1 hour at 350°C, similar to methods employed by Sarkar et al. (2016), but at a lower temperature and for less time in order to minimize element volatilization. Fish feed samples were also prepared with the same drying/ashing methods as the shrimp.

Sediment samples were air-dried, then dried overnight at ~45°C before sieving at 1 mm and homogenizing before all analyses except total carbon (TC) analyses, where samples were just dried at <50°C and homogenized. Pond sediment batch experiments with a sediment-water slurry were performed to measure geochemical concentrations in the filtered extract as a proxy for porewater. The sediment extract experiments were based on EPA Method 1313, with an

approximate ratio of 1 g of dry sediment/10 mL DI water (water was measured based on mass, assuming 1 g = 1 mL). We chose to use only 5 g of sediment in our batch experiments instead of the EPA Method 1313 recommended minimum of 20 g because of the homogenous nature of the sediment and to maintain some consistency with extract experiments performed in Ayers et al. (2020). Consistent with EPA Method 1313, we chose 24 hours of contact time between the water and sediment, because >85% of each pond sediment sample was <300 μm in grain size (Table C1). Each slurry was mixed with magnetic stirrers for ~24 hours, then filtered with coarse filter paper before filtering at 0.45 μm to prepare the extract for complete chemical analysis. Each filtered extract sample was measured for pH with a Fisher Scientific accumet AB15 basic pH meter and a Fisher Scientific accumet pH probe. A subset of each extract (2 mL) was acidified with a drop of HNO_3 and then diluted to a ~5:1 ratio with DI water for inductively coupled plasma-optical emission spectroscopy (ICP-OES) and inductively coupled plasma-mass spectrometry (ICP-MS) analyses.

Approximately 2-3 g. of dried, sieved (<1 mm), and homogenized pond sediment from each sample was used for loss on ignition (LOI) in a high temperature muffle furnace to measure for adsorbed water content at 105°C (H2O-) and structural water content at 1000°C (H2O+) following methods used in Ayers et al. (2020). Following LOI, approximately 100 mg of sample was mixed with 600 mg of $LiBO_2$ and homogenized with mortar and pestle, then placed in a 1100°C muffle furnace for ~10 minutes to form a molten bead. The bead was then poured into 50 mL of heated 1M HNO_3 and stirred until fully dissolved. The solution was then poured into a 50 mL centrifuge tube and diluted with additional 1M HNO_3 until the volume again reached a total of 50 mL. The same methods were employed in Ayers et al. (2020).

Details of filtered pond surface water sample preparation can be found in Dietrich and Ayers (2021).

2.4 *Analyses*

All acidified, filtered sediment extract samples from the 24-hour batch experiments and the sediment solutions from $LiBO_2$ fusion were analyzed on a Perkin Elmer NexION 2000B ICP-MS in both standard and kinetic energy discrimination (KED) modes at Vanderbilt University using EPA Method is 6020B for the elements As, Ba (extracts only), Be, Cd, Co, Cr, Cu, Fe (extracts only), Mn, Mo, Ni, Pb, Sb, Se, Ti, Tl, V, Zn (extracts only). Seven-point calibration curves from 0.5 and 250 μg/L were used. All acidified extract and $LiBO_2$ sediment solution samples were also analyzed on an Agilent 5110 VDV ICP-OES using EPA Method is 6010D at Vanderbilt University to report the ions: Al, B, Ba (sediment samples only), Ca, Fe (sediment only), K, Mg, Na, P, S, Si, Sr, and Zn (sediment samples only). Five-point standard curves between 0.1 and 500 mg/L were utilized. Sediment extracts that were filtered and unacidified were analyzed for dissolved inorganic carbon (DIC) and dissolved organic carbon (DOC) content with a Shimadzu model TOC-LCPH using EPA Method 9060A. Unacidified extract samples were also analyzed for Cl, NO_3, PO_4, and SO_4 with a Metrohm 881 Compact IC Pro using SW-846 EPA Method 9056. Essentially, the same above methods were also employed in Dietrich and Ayers (2021) for all filtered water samples.

All ashed shrimp and fish feed samples were analyzed at the Ohio State University STAR Lab for the elements: Al, As, B, Ba, Be, Ca, Cd, Co, Cr, Cu, Fe, K, Li, Mg, Mn, Mo, Na, Ni, P, Pb, S, and Sb on the ICP-OES. Results for As, Be, Cd, and Co were omitted because all values were below method detection limit (MDL). 0.4-0.5 g. subsamples of shrimp/fish feed ash were dissolved in 15 mL HNO_3, and then samples were filtered at 0.45 µm and diluted 10-fold before running on an Agilent 5110 ICP-OES.

Analysis of ~50mg of sediment sample for total carbon (TC) and total inorganic carbon (TIC) in shrimp pond sediment samples was performed on a Shimadzu model TOC-LCPH combined with an SSM-5000A unit for solid samples at Vanderbilt University, with the difference between the two calculated as total organic carbon (TOC).

A dried, sieved (<1 mm), and homogenized subset of each sediment sample was analyzed for particle size via laser granulometry with a Malvern Mastersizer 3000 at Vanderbilt University. A 1L beaker of DI water was first run through the instrument to establish background concentrations, then each subset of sediment sample was mixed into a 1L beaker of DI water. The sample was then deflocculated via sonication before analysis. Sample measurements were averaged over three analyses.

Dried and homogenized powder samples of pond sediment samples KA-19, KA-21, and NIST SRM 2711 – Montana Soil were dry cast on 20 x 20 mm square sample glass holders with a 0.2 mm indent. The samples were then analyzed with a Rigaku SmartLab powder X-ray diffractometer at Vanderbilt University with a Cu Kα (lambda = 0.154 nm) source at 40 kV and 44 mA. The detector was a D/teX Ultra 250 1D silicon strip detector. Calculated intensities were reported using the default Rietveld method. “Match!” software identified the mineral phases associated with the intensity peaks.

Details on field-filtered pond water instrument analyses can be found in Dietrich and Ayers (2021).

2.5 *Quality control*

NIST 1566b – Oyster Tissue unashed (desiccator dried) reference material was analyzed at the Ohio State University STAR Lab on the ICP-OES (in a separate batch from shrimp samples) following standard microwave digestion procedures (Isaac et al., 1985; Jones et al., 1991) to measure precision of the instrument. Arithmetic mean element % recovery was 109.7% for 15 elements and can be viewed graphically in Fig. C1a with data in Table C2. Additionally, an ashed subset of NIST 1566b sample (heated at 350°C for ~1 hr) was simultaneously analyzed on the ICP-OES to determine how ashing an organism of a similar organic matrix with known reference values affected element concentrations through volatilization. A “volatilization correction factor” was then determined for each element based on the concentration of the element in the ashed NIST 1566b sample/concentration in the unashed NIST 1566b sample (Fig. C1b; Table C2). Final shrimp element concentrations were then calculated based on these volatilization correction factors to correct for volatilization during the ashing process, while elements without a volatilization correction factor had their concentrations calculated based on the original dry weight of the shrimp at 105°C. All final shrimp element concentrations carry

some degree of uncertainty because of volatilization, but the relative concentrations of volatilization corrected elements should be reasonably accurate.

For $LiBO_2$ fusion sediment samples, NIST SRM 2711 – Montana Soil was analyzed with triplicate samples prepared. Because significant volatilization of most elements occurred due to the high temperature of the furnace during $LiBO_2$ fusion (most element % recoveries <100% after correction to an anhydrous basis based on LOI, Table C3), a correction factor based on the average concentration of the NIST SRM 2711 standard after $LiBO_2$ and mass correction for LOI divided by the given value of the standard was calculated for each element (Table C3). It is noted that the Co and Cr reference values from NIST 2711 are noncertified values. These volatilization correction factors were used to generate the final table of pond sediment element concentrations (Table 1), because the Montana soil was likely of similar general composition as the Bangladesh samples in this study [i.e., similar H_2O+ (9.0%) and H_2O- (2.1%) values during LOI, and similar bulk mineralogy (Fig. C2)] and thus likely experienced similar effects of element volatilization. $LiBO_2$ fusion method blanks of only $LiBO_2$ powder and no sample were also prepared in triplicate, and all reported element values were either close to/less than MDL, or <8% of measured values. B and Mo were not reported because of high concentrations in the $LiBO_2$ method blanks.

Duplicate and replicate sediment samples showed consistency in element concentrations, with replicate samples for KA-16 having an arithmetic mean element concentration difference of 5.2% and duplicate samples each taken at site KA-21 having an arithmetic mean element concentration difference of 4.8%. At site KA-13, the submerged sample was similar in composition to the unsubmerged sample, with an arithmetic mean element concentration difference of 10.1%, although Ca, S and Al were three major elements (>100 mg/kg) with noticeably higher concentrations (>10%) in the submerged sample. Thus, both the submerged and non-submerged sample were included in all generated results except for paired sediment-shrimp correlations (where submerged KA-13 was included).

Water pond sample method blanks (DI water) collected in the field were consistently near or below method detection limit (MDL) for analyzed elements, and May pond water samples had a geometric mean charge balance error of ~6% (Dietrich and Ayers, 2021).

A method blank for the 24-hour sediment extract batch experiment that used DI water contained element concentrations and DOC/DIC concentrations that were consistently close to or below MDL on the analytical instruments, although P, Sr, and B were measured at concentrations 10% or greater of their sample geometric means.

For samples run on the ICP-MS, ICP-OES, IC and TOC analyzers at Vanderbilt University, periodically measured concentrations in standards were required to be within 15% of the known value and blanks were required to be below the method detection limit (MDL).

Approximate MDLs for all samples analyzed at Vanderbilt University and The Ohio State University (shrimp and oyster tissue) are listed in the supplementary (Table C4).

2.6 *Health risk calculations and bioaccumulation factor (BAF) calculations*

Health-based risk assessment for consumption of aquaculture shrimp containing potentially hazardous inorganic metals was based on the target hazard quotient (THQ) equation often used for seafood (e.g., Ravanbakhsh et al., 2020; Storelli, 2008) and which was originally developed in the U.S. EPA Region III risk-based concentration table (Smith, 1995).

$$THQ = (EF \times ED \times FIR \times C)/(RfD \times WAB \times TA) \times 10^{-3} \quad (1)$$

A THQ >1 indicates a greater likelihood that an individual will experience adverse health effects from consumption of the food (e.g., Wang et al., 2005). EF is exposure frequency (365 days/year); ED is the exposure duration (70 years); FIR is the food ingestion rate (crustaceans: 5.42 g/person/day for adults; Storelli, 2008 and the references therein; and 2.71 g/person/day for children because children consume less than adults — ~50%, i.e., 54% was used in Ravanbakhsh et al., 2020); C is the metal concentration in the aquaculture shrimp (mg/kg); RfD is the oral reference dose in mg/kg/day, which is 1.0E-5 for Tl (Soluble salts, U.S. EPA, 2020), 1.4E-01 for Mn (Diet, U.S. EPA, 2020), 2.0E-01 for Ba (U.S. EPA, 2020), 4.0E-02 for Cu (U.S., EPA, 2020), 3.0E-01 for Zn (Zinc and Compounds, U.S., EPA, 2020); WAB is average body weight (adults 70 kg; children 16 kg), and TA is the averaging time for non-carcinogens (365 days/year x ED). The MDL of Tl was used for sample KA-15 to calculate the THQ for Tl.

Bioaccumulation factors (BAFs) are commonly used in the literature to estimate the uptake of an element in shrimp or fish compared to their environmental surroundings, such as the water (e.g., Kar et al., 2011; Mostafiz et al., 2020; Ravanbakhsh et al., 2020), which is calculated by:

$$BAF = C_{shrimp}/C_{water} \quad (2)$$

Where C_{shrimp} is the concentration of the element in the shrimp (mg/kg) and C_{water} is the concentration of the element in the water (mg/L).

2.7 *Partition coefficient (Kd) calculations*

Bulk partition coefficients (Kd) values were calculated based on bulk element concentrations in the standing pond water, sediment extracts, and pond sediment. Kd values are a ratio of the concentration of the element in the solid phase (i.e., pond sediment) over the concentration of the element in the dissolved phase (i.e., filtered extract solution or filtered pond water overlying the submerged paired sediment sample), conveyed in the equation:

$$Kd = C_{solid}/C_{water\text{-}extract} \quad (3)$$

Where C_{solid} is the concentration of the element in the solid phase, while $C_{water\text{-}extract}$ is the concentration of the element in the dissolved phase (water or sediment extract solution). Because the original solid sediment sample must equilibrate with DI water in the extract batch experiments, we assume C_{solid} is slightly affected by equilibration and thus calculate a “residual solid” element concentration ($C_{solid\text{-}res}$) based on mass balance correction:

$$C_{solid\text{-}res} = (C_{bulk} - X_{extract}C_{extract})/X_{solid\text{-}res} \quad (4)$$

Where $X_{extract}$ and $C_{extract}$ are the mass fraction of the extract and concentration in the extract solution, respectively, C_{bulk} is the element concentration in the entire 55 g. DI water-sediment experimental setup, and $X_{solid\text{-}res}$ is the mass fraction of the residual solid. Thus, all calculated Kd values for sediment extract solutions (except S) are mass balanced corrected, similar to Ayers et al. (2020) even though Kd values hardly change after the correction. Sulfur was not mass balance corrected because due to its high variability and highly mobile nature, $C_{solid\text{-}res}$ values were often negative.

2.8 *Data processing*

All data was compiled and analyzed in Microsoft Excel and RStudio, with the study site map generated using ArcGIS Online. The principal component analysis (PCA) plot (code available on GitHub--https://github.com/dietrimj/bangladesh-geochem-code/blob/3502c2d8c9b66ad4fee4e1c539819e84bc53c0a9/Ch3_PCA_code.R) was created in R using the "factoextra" package (Kassambara and Mundt, 2020) and a heatmap (code available on GitHub--https://github.com/dietrimj/bangladesh-geochem-code/blob/3502c2d8c9b66ad4fee4e1c539819e84bc53c0a9/Ch3_heatmap_code.R) was generated with the "ComplexHeatmap" package in R (Gu et al., 2016). Saturation indices [log (Q/K)] for minerals in sediment extract solutions were calculated with The Geochemist's Workbench SpecE8 v. 14 software and the default thermo.dat database (Bethke, 2007). Unless specified, all reported means are geometric means due to the non-normality of several element distributions, and 1σ uncertainties are reported as sample standard deviation.

3. Results

Element concentrations, partition coefficients (Kds), and other geochemical parameters (i.e., pH, DOC) across all collected environmental media were measured to help assess: 1) Whether 24-hr batch experiment Kd (sediment/extract) values differ from in situ Kd(sediment/pond water) values, 2) Whether arsenic and selenium or any other trace elements of concern accumulate in shrimp, 3) What the relationships between element concentrations in different environmental media are, and 4) Whether a health-risk assessment of Bangladesh aquaculture shrimp reveals significant consumption risk.

3.1 *Extract and shrimp pond partition coefficients*

Kd (sediment/extract) and Kd (sediment/pond water) partition coefficient values are reported in Table C5 and sediment extract concentrations in Table C6. Kd values show trends consistent with the relative mobility of elements during weathering and transport, with highly mobile elements having low Kd values because of a greater proportion of the element in the dissolved load (Fig. 2). Several elements across both Kd types in this study that noticeably deviate from this trend are Si, Cd, Se, As, Sb, and Mg (Fig. 2a), with greater proportions of each element in the solid load than would be expected based on Kd values of adjacent elements. Sediment extract Kd values were broadly similar with shrimp pond standing water Kd values and showed similar trends (Fig. 2a). Sediment extract Kd values in this study are very similar to

those in Ayers et al. (2020) with nearly all mean values within 1σ variation, even though the batch experiments were only 15 minutes in that study compared to 24 hours in this study (Fig. 2b). Filtered sediment extract solutions were commonly saturated in the minerals: albite, barite, calcite, dolomite, gibbsite, illite, K-feldspar, kaolinite, microcline, muscovite, and quartz.

3.2 *Shrimp pond sediment concentrations and pond water general composition*

Shrimp pond sediment concentrations (Table 1) were similar to upper continental crust (UCC) for most elements, although samples were notably enriched in Cu, As, Se, Cd and S and depleted in Zn, Ca, Sr, and Na relative to UCC (Fig. 3a). Shrimp pond sediment was also compared to tidal channel and Sundarbans sediment samples taken in the same general study area with similar grain size (Ayers et al., 2020) to help evaluate whether there were unique processes affecting element concentrations in shrimp pond sediment. Most element ratios of shrimp pond sediment/tidal channel or Sundarbans sediment were within 1σ sample variation, although there was distinct depletion of Zn and Na in shrimp pond sediment and enrichment of several trace elements such as Ni, Co, Cu, and Se (Fig. 3b). TOC concentrations in sediment were consistent with low variability (mean = 2.0 ± 0.4 %), while TIC was generally low in sediment (mean = 0.07 ± 0.02%) (Table S1). H_2O+ was consistent among sediment samples as well (mean = 9.6 ± 1.5%), while H_2O- was always lower than H_2O+ (mean = 2.2 ± 0.4%) (Table C1).

Pond waters are highly saline, with the water type being Na-Cl type during the dry season (May), plotting near seawater on a Piper diagram (Dietrich and Ayers, 2021). Mean salinity was 15.2 ± 4.4 ppt. The pH range was generally narrow within pond waters (mean = 8.3 ± 0.4), and Se and As concentrations were commonly >WHO drinking water guidelines (Dietrich and Ayers, 2021).

3.3 *Shrimp and fish feed element concentrations*

Shrimp and fish feed were both depleted in As (all values < MDL despite significant enhanced concentration during ashing of oyster tissue and thus likely shrimp tissue as well; Fig. C1b). Mn and Cr were much higher in both types of fish feed compared to any shrimp samples, with Cr particularly elevated in the SSF sample (23.1 mg/kg; Table 2). Only one shrimp sample contained detectible Se, despite the LSF fish feed sample containing approximately 8.1 mg/kg of Se. Zinc was >38 mg/kg in all shrimp and fish feed samples, while Tl was >0.95 mg/kg in all samples except KA-15 (Table 2).

3.4 *Sediment-water-shrimp geochemical correlations and relationships*

Nearly all correlations between concentrations in shrimp, water, and sediment are weak to moderate, with no discernable trends or geochemical relationships based on non-parametric Spearman's rank correlation coefficients (used instead of Pearson correlation coefficient due to the common non-normality of the data) (Figs. C3, C4, C5). However, P in pond water and P in sediment have a distinctive moderate negative correlation (ρ = -0.69, p = 0.018) while Mn in pond water and pond sediment display a strong positive correlation (ρ = 0.78, p = 0.0047).

The bioaccumulation factor (BAF) is equal to Kd(shrimp/water). Bioaccumulation factors for shrimp reveal P, Zn, and Cu are elements that bioaccumulate significantly more than other elements when assuming their source is solely from water, with means of 168,621 ± 94,760, 10,628 ± 3,233, and 5,695 ± 3,924, respectively (Table C7). If using the MDL of Tl in water (0.0001 mg/L) because of values <MDL for TL in water, and Tl values based on dry weight of shrimp at 105°C, the mean BAF is 48,738 ± 34,804 when excluding the shrimp sample <MDL.

For each sample type there were several strong correlations between elements. In pond water, most elements that tend to behave conservatively in solution were strongly positively correlated (Ca, K, Mg, Na, S, Sr; Fig. C3), which is also indicative of their ultimate derivation from seawater. In pond sediment, strong negative correlations occurred between Mg and Pb, Ca and Pb, Sr and Pb, As and Ca, Sr and Cd, and Cd and Ca; while strong positive correlations occurred between Cr and Al, Co and Al, Ba and K, Ba and Si, Al and Fe, Ba and Fe, Ba and Mg, and Ba and Na (Fig. C4). In sediment extracts, most conservative elements in solution such as Mg, K, Ca, Sr and S are strongly positively correlated, while Al, Fe and Ti are strongly positively correlated with each other as well (Fig. C6). Fe and Mn are moderately negatively correlated in extract solutions (Fig. C6).

There was weak-moderate to no relationship between grain size (median grain size = 20.5 µm ± 7.2 µm), LOI, and carbon content in soils with sediment-element concentrations (Figs. C7, C8). TOC in pond sediment and DOC in sediment extracts show a weak positive correlation (ρ = 0.41), albeit not significant based on a high p-value (0.21) (Fig. C9). TOC in pond sediment and DOC in pond water showed no relationship (ρ = 0.023, p = 0.95) and DOC in pond water and sediment extract associated with the same sediment samples also showed no significant relationship (ρ = -0.19, p = 0.57).

Based on principal component analysis (PCA) of log10 transformed element concentrations, which reduces dimensionality of the data and illustrates variance, all three species of shrimp plotted generally together, close to fish feed and distinct from other sample media (Fig. 4a). When looking at heat maps for all sample types based on log10 transformed concentrations and groupings based on hierarchical clustering on both axes, there are distinct sample type groupings (Fig. 4b). Sediment has comparatively high Al and Si concentrations, fish feed and shrimp have high P, S, and K, and water and extracts have high Na relative to concentrations of other elements (Fig. 4b). PCA vector loadings also make it clear that the variance and distinct grouping of aqueous (water and extract) samples is mostly due to lower concentrations of elements than in solid samples (Fig. 4a), although the concentrations of soluble cations in waters and extracts such as Na are still higher than typically insoluble elements like Al and Si (Fig. 4b).

Table 1: Pond sediment element concentrations

	KA-12	KA-13	KA-13-U	KA-14	KA-15	KA-16	KA-17	KA-18	KA-19
Al[a]	72385.3	77756.8	89679.7	72583.8	85156.6	81490.9	83465.1	76856.6	64554.4
Ba	449.6	500.1	503.1	470.4	521.0	471.7	512.0	495.1	412.7
Ca	7018.1	11542.4	13203.6	7371.3	6121.6	13887.3	14003.6	9340.4	6262.6

Fe	39879.6	44054.6	45316.2	33221.8	47582.5	43850.5	45626.8	44187.1	35990.7
K	23313.2	25889.2	26724.9	25432.5	27361.9	27260.1	28895.2	26758.4	22671.9
Mg	13197.2	15122.5	15724.2	12302.7	15882.8	16773.3	16354.2	15335.7	12749.6
Na	10535.1	11227.1	12011.4	11632.0	11083.2	10787.5	12027.9	8209.1	7114.9
P	551.2	505.7	528.5	533.3	630.5	521.6	533.7	529.7	480.4
S	406.9	373.1	415.9	383.7	509.5	401.5	562.5	410.6	372.9
Si	238263.5	245212.2	268185.0	244682.2	247818.5	236687.6	271486.9	253561.5	199117.3
Sr	73.9	88.9	95.2	91.8	82.5	99.2	97.9	79.4	69.3
As	14.9	13.6	15.0	19.9	17.0	10.3	11.4	11.1	20.2
Cd	11.5	12.6	15.3	10.7	16.4	6.4	6.8	21.7	13.8
Co	15.0	18.9	19.4	15.3	18.5	17.5	17.7	16.3	14.1
Cr	85.3	108.3	111.3	88.0	110.0	99.5	98.5	88.7	79.8
Cu	51.4	63.6	65.0	57.9	74.8	56.4	69.9	63.0	45.9
Mn	515.2	721.9	766.4	501.2	426.6	640.6	525.0	483.5	459.4
Ni	33.0	45.3	53.4	31.6	55.7	37.2	52.5	61.2	33.1
Pb	12.1	12.5	14.7	24.2	21.8	6.7	4.7	17.9	23.8
Sb	1.7	0.8	0.9	0.6	0.3	0.2			
Se	1.1	1.2	0.8	9.3	5.0	14.7	21.9	30.8	24.3
Ti	4152.4	4394.5	4826.7	4435.8	4748.9	4401.9	4618.6	4450.4	3738.3
V	89.2	93.0	97.2	86.1	106.2	86.4	85.1	72.1	60.1
Zn	20.2	26.3	34.7	20.2	40.8	25.0	38.1	18.4	25.9

	KA-20	**KA-21**	**Geometric mean**	**Std Dev**
Al[a]	80627.4	89137.4	79082.8	7624.0
Ba	543.0	571.4	493.7	43.8
Ca	16962.8	11287.5	10045.5	3670.3
Fe	43709.8	48199.7	42623.8	4672.9
K	27896.7	29456.3	26436.3	2102.0
Mg	16778.9	18031.0	15192.2	1827.3
Na	12073.1	12365.2	10684.8	1684.0
P	624.1	549.3	542.7	45.5
S	565.3	416.9	433.1	72.3
Si	293929.7	285071.9	251824.9	26114.6
Sr	103.4	99.7	88.5	11.4
As	10.1	12.5	13.8	3.6
Cd	5.0	7.2	10.6	5.1
Co	15.8	17.6	16.8	1.7
Cr	88.8	106.0	96.2	11.1
Cu	47.6	54.9	58.5	9.1
Mn	470.3	595.1	545.6	111.7
Ni	34.5	40.1	42.3	10.7
Pb	4.4	4.7	11.2	7.7

Sb		0.1	0.5	0.6
Se	14.0	27.6	7.6	11.1
Ti	4743.8	5155.2	4500.6	373.8
V	71.6	88.3	84.1	12.9
Zn	34.3	38.9	28.3	8.2

[a]Concentrations in mg/kg calculated based on the NIST SRM 2711 – Montana Soil volatilization correction factor (Table C3) and LOI adjustment

Table 2: Shrimp and fish feed element concentrations

	KA-12	**KA-13**	**KA-14**	**KA-15**	**KA-16**	**KA-17**	**KA-18**	**KA-19**	**KA-20**
Al[a]	**25.0**	**29.5**	**99.6**	**9.3**	**33.0**	**36.5**	**27.7**	**27.4**	**22.5**
B	*2.2*	*1.8*	*1.1*	*1.7*	*1.8*	*5.3*	*3.2*	*1.7*	*3.5*
Ba	**0.5**	**0.9**	**2.5**	**0.9**	**1.0**	**0.7**	**0.9**	**1.3**	**0.8**
Ca	**1319.4**	**4325.0**	**6350.6**	**1269.7**	**1599.9**	**1224.2**	**1065.0**	**3251.5**	**2098.5**
Cr									
Cu	**13.9**	**45.3**	**39.3**	**39.0**	**31.5**	**42.4**	**51.8**	**16.5**	**18.2**
Fe	**5.2**	**15.3**	**153.5**	**4.9**	**21.0**	**23.5**	**14.7**	**33.0**	**12.9**
K	**10971.5**	**11309.0**	**10816.3**	**10187.8**	**10265.4**	**10866.7**	**8573.9**	**12084.9**	**10288.7**
Li	*0.2*	*0.2*	*0.3*			*0.1*		*0.2*	*0.1*
Mg	**1058.4**	**1305.5**	**1251.6**	**1215.1**	**1266.7**	**1147.6**	**990.8**	**1150.3**	**1316.3**
Mn	**0.8**	**1.4**	**9.4**	**0.9**	**1.8**	**1.0**	**0.9**	**2.1**	**2.0**
Mo						*0.3*			
Na	**5506.8**	**4895.5**	**4149.3**	**3760.1**	**3753.8**	**4540.8**	**4002.2**	**6695.5**	**3959.1**
Ni									
P	**7131.8**	**7608.1**	**7516.1**	**7311.9**	**7644.1**	**7051.8**	**6467.5**	**7231.9**	**7416.0**
Pb		*0.5*							
S	**8387.3**	**6014.5**	**8800.9**	**5897.1**	**6330.3**	**8647.2**	**7940.1**	**8532.6**	**5357.7**
Sb								*0.5*	*0.4*
Se							*0.9*		
Si	**630.7**	**675.9**	**1088.4**	**633.4**	**700.8**	**619.9**	**621.6**	**697.3**	**677.5**
Sr	**11.9**	**33.0**	**38.0**	**12.2**	**15.4**	**14.1**	**8.9**	**26.2**	**23.8**
Tl	*9.4*	*9.0*	*1.0*		*10.6*	*3.5*	*8.8*	*4.5*	*5.1*
V			*0.7*						
Zn	**41.0**	**46.9**	**40.2**	**42.9**	**45.1**	**45.4**	**38.7**	**46.1**	**42.1**

	KA-21	LSF	SSF	Shrimp geometric mean	Shrimp std dev
Al[a]	**38.3**	**99.6**	**106.8**	**29.7**	**24.2**
B	*3.2*	*10.4*	*15.3*	*2.3*	*1.3*
Ba	**0.9**	**4.4**	**7.7**	**0.9**	**0.6**
Ca	**1311.0**	**4623.9**	**10999.8**	**1965.0**	**1750.0**
Cr		*0.7*	*23.1*		
Cu	**37.9**	**191.4**	**14.9**	**30.8**	**13.1**
Fe	**34.6**	**148.3**	**242.8**	**19.1**	**43.9**
K	**10773.6**	**9291.6**	**9497.2**	**10576.6**	**911.4**
Li		*0.2*	*0.3*	*0.2*	*0.1*
Mg	**1240.7**	**2629.2**	**2115.9**	**1189.8**	**106.6**
Mn	**1.9**	**90.3**	**68.0**	**1.6**	**2.6**
Mo				*0.3*	
Na	**3013.4**	**2376.4**	**1755.4**	**4325.4**	**1049.7**
Ni		**0.5**	**0.4**		
P	**8136.4**	**7716.2**	**10153.5**	**7339.6**	**439.0**
Pb			*0.4*	*0.5*	
S	**6883.7**	**12339.2**	**9466.1**	**7168.0**	**1320.0**
Sb		*0.3*	*0.3*	*0.4*	*0.1*
Se		*8.1*		*0.9*	
Si	**652.1**	**1117.7**	**954.6**	**690.0**	**139.9**
Sr	**11.2**	**10.2**	**33.2**	**17.3**	**10.2**
Tl	*2.5*	*1.5*	*8.4*	*4.9*	*3.5*
V		*0.7*	*0.9*	*0.7*	
Zn	**45.2**	**76.0**	**51.5**	**43.3**	**2.8**

Bold = based on NIST oyster concentration ratio @350°C

Italicized = based on mass at 105°C prior to ashing

[a]All element concentrations in mg/kg based on either the calculated NIST 1566b – Oyster Tissue volatilization correction factor or the mass of the shrimp at 105°C

3.5 *Partitioning between different environmental media and pond water*

Comparing mean element concentrations in feed, shrimp, and sediment to mean element concentrations in water allows for general Kd value calculations (mean sample/mean water; Table C8), which reveal that sediment tends to have the greatest concentrations of elements relative to water, with feed and shrimp exhibiting very similar Kd values (Fig. 5). Some of the more mobile elements during weathering and transport (i.e., Sr, Na, Mg, B) tend to have the lowest Kd values (Fig. 5), indicative of a greater proportion of the element in water.

3.6 *Health-risk assessment of aquaculture shrimp*

THQ evaluations of non-carcinogenic hazardous risk was completed for the elements Ba, Cu, Mn, Zn, and Tl (Fig. C10). For Tl, because there was no volatilization or volatilization correction factor based on standard NIST oyster tissue, concentrations were converted for risk assessment based on the volatilization correction factor of As. This was because As had one of the highest volatilization correction factors of all elements analyzed (Fig. C1b) due to little volatilization at 350°C (and thus easily becomes concentrated in the sample) compared to other elements, and we wanted to ensure we initially did not overestimate risk. Although our reported THQ values for Tl are a conservative estimate, they are still > the THQ threshold of 1 for all samples except two adult calculations, and are >5 in children in all but two shrimp samples (Fig. C10). If using the mass loss adjusted Tl values based on initial sample weight at 105°C (Table 2) instead for THQ calculations and not including KA-15, which was <MDL, the mean THQ values would increase 6.9-fold. All other elements were well below THQ thresholds of 1 in all samples, although Cu THQs in children had a geometric mean of 0.13. In general, child THQ values were much larger than adult THQ values (Fig. C10) because of a body weight for children in the THQ calculation that is proportionally less than the adjusted rate of food intake.

4. Discussion

4.1 *Sediment-water element partitioning and equilibration in shrimp ponds*

Prior research within the Ganges tidal delta in Southwest Bangladesh concluded that the area is likely a transport-limited weathering regime, where chemical weathering is limited by the supply of fresh, unweathered material (Ayers et al., 2020). Weathering is minimal in the timescale of years-decades, with little sediment compositional alteration. The results in our study generally support this, as concentrations in shrimp pond sediments are predominantly within 1σ variation of concentrations in freshly deposited tidal channel and Sundarbans sediments of similar grain size (Fig. 3b). Tidal channel and Sundarbans sediment are likely at least several years younger than aquaculture pond sediment because ponds receive minimal sediment deposition following excavation except for embankment failures or tidal river management, while average fresh sediment deposition in the Sundarbans island interiors/Southwest Bangladesh tidal delta plain is ~1cm/yr when not sediment-starved from embankment construction (Bomer et al., 2020a; Rogers et al., 2013).

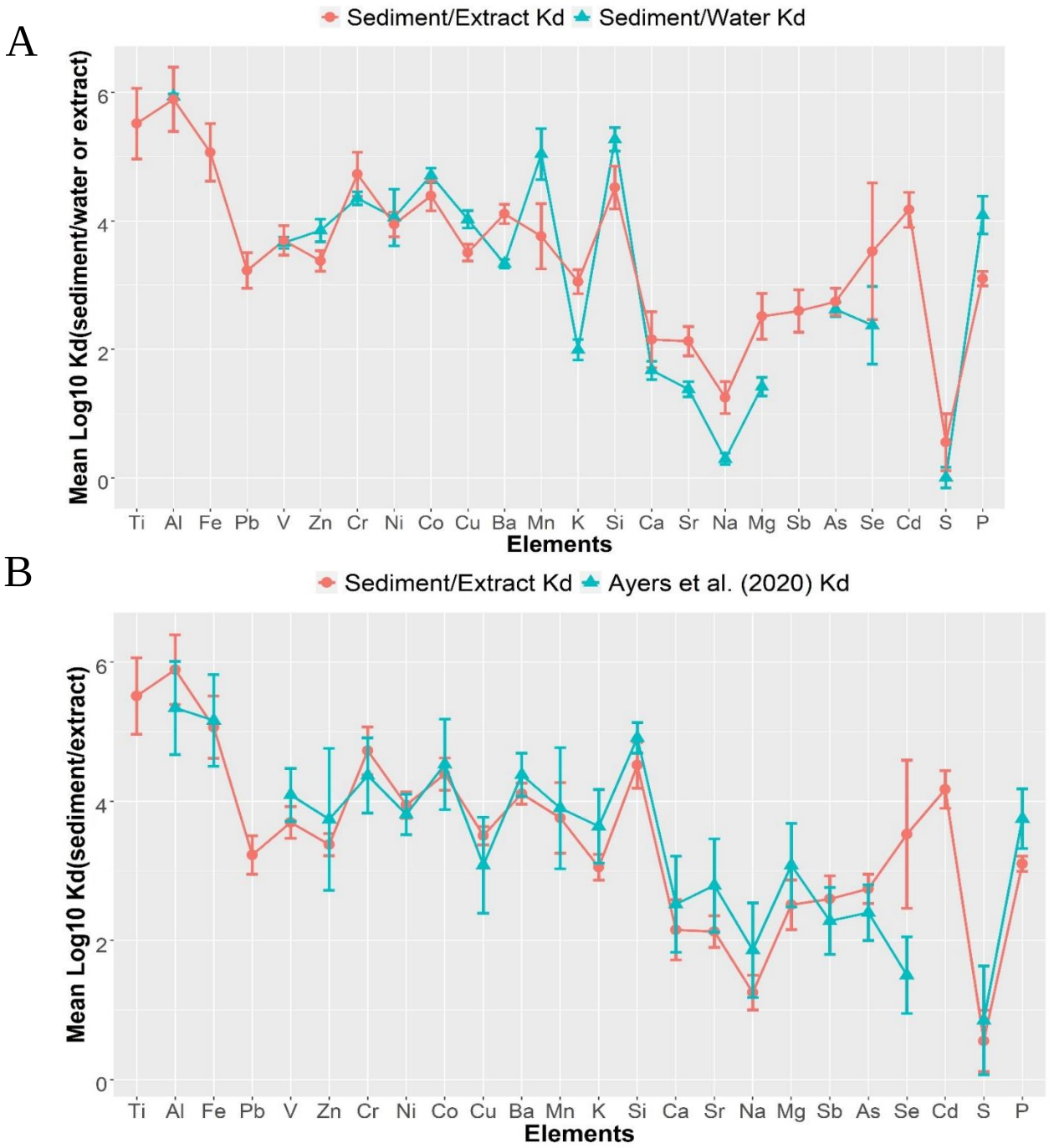

Figure 2: Spidergram figures of arithmetic mean bulk log10(Kd) values, with elements arranged in order of increasing mobility during weathering and transport from left to right along the x-axis (Gaillardet et al., 2014), with P also added. Several elements have omitted values depending on the sample type. The top figure (A) compares sediment/pond water Kd values with 24-hr sediment/extract Kd values (n=11 both types, both samples at KA-13--underwater and not submerged--are included), while the bottom figure (B) compares sediment/extract Kd values from this study to Ayers et al. (2020) (all sample types, mean values and 1σ from their Table S3), where 15-minute batch experiments instead of 24-hr batch experiments were performed. 1σ sample variation error bars are provided.

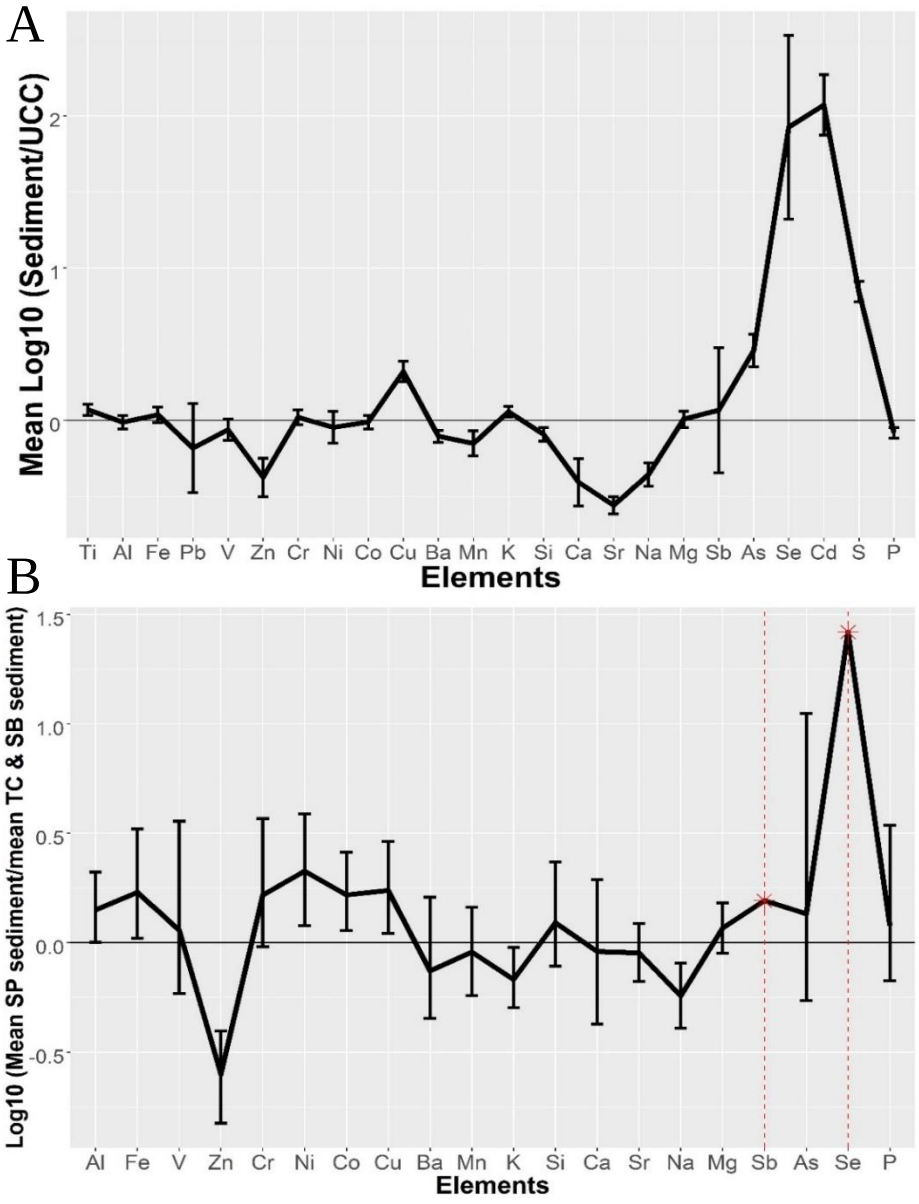

Figure 3: (A) Log-normalized arithmetic mean element concentrations in shrimp pond sediment (n=11, both samples at site KA-13--underwater and not submerged--are included) relative to upper continental crust (UCC) (Rudnick and Gao, 2003). 1σ sample variation error bars are provided. Concentrations in sediment are volatilization corrected for the $LiBO_2$ fusion analytical method based on NIST 2711 Montana soil element recoveries from three replicate samples and are also corrected for loss-on-ignition (LOI) mass loss. (B) Log-normalized ratios of non-LOI or volatilization corrected shrimp pond sediment (SP) element geometric mean concentrations (n=11), normalized to tidal channel (TC) and Sundarbans (SB) sediment samples (n=15; Ayers et al., 2020). Sulfur was omitted because of anomalous variance in Ayers et al. (2020) (1σ for S was >2x the geometric mean) and Sb and Se upper and lower 1σ sample variation error bar limits were omitted and marked with an asterisk and vertical dotted red line because sample standard deviations of each element were greater than the sample geometric means.

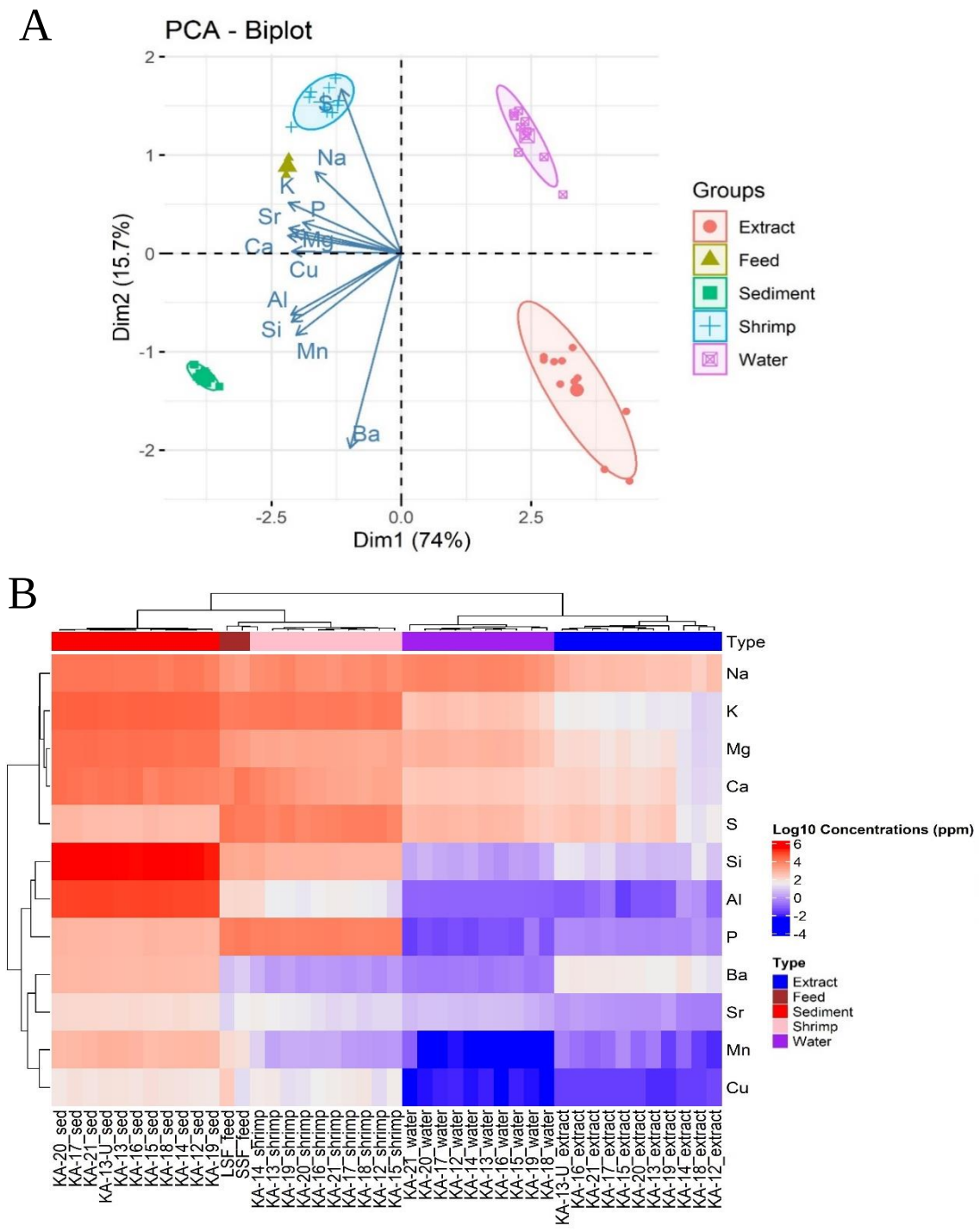

Figure 4: (A) Principal component analysis (PCA) biplot for sediment (volatilization corrected values), fish feed, water, sediment extracts, and shrimp based on log10 element concentrations (ppm) where all values were >MDL for each sample type (Al, Ba, Ca, Cu, K, Mg, Mn, Na, P, S, Si, Sr). 80% confidence intervals are provided for ellipses. (B) Heatmap with dendrograms on each axis made using complete linkage and Euclidean distance based on log10 element concentrations (ppm). The same elements as plot (A) were used in plot (B).

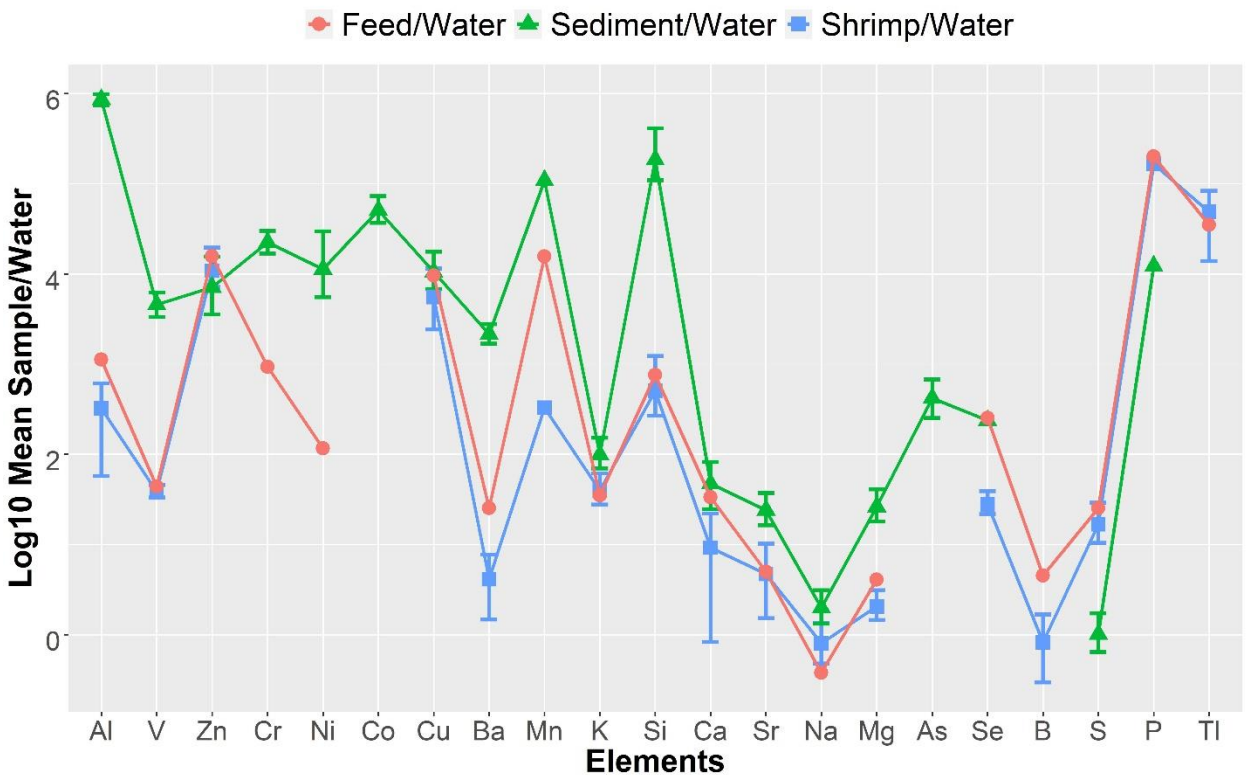

Figure 5: Log10 Kd values (mean sample/mean water element concentrations) in L/kg. 1σ sample variation error bars are provided when both the upper and lower limits could be calculated. Because there were only two feed samples, no sample variation is included.

The highly weathered state of the sediment contributes to slow exchange reaction kinetics, as even after 24 hours batch experiments did not reveal any strong correlations between element concentrations in the extracts and sediment (Fig. C6). This suggests disequilibrium is pervasive in the shrimp pond environment. However, Kd values in 24-hr batch experiments overlap substantially with 15-min batch experiments of similar sediments in the area (Fig. 2b), implying that elements associated with surface layer sites on the silty clay sediments are rapidly leached into solution. The low correlations between element concentrations in extracts and sediment may be due to the slow equilibration of elements that are essential structural constituents of minerals in the sediment, or ions that substitute for them (co-precipitation). Thus, influence of sediment composition on pond water or pond shrimp composition appears minimal unless there are abnormal amounts of trace metals on sediment surface layer sites that can exchange rapidly with solution.

In addition to the highly weathered nature of material in this area, the fact that most extract waters and pond waters are saturated in minerals common in sediment in the study area such as K-feldspar, illite, dolomite, muscovite, and quartz (e.g., Ayers et al., 2020; Dietrich and Ayers, under review, and Fig. C2) means that dissolution of these minerals should not occur. Kd values for most major elements that form these minerals are thus not true Kd values because their equilibrium concentrations can vary in the solid phase but not the aqueous phase. Thus, these "apparent" Kd values for major elements are affected more by the element concentration in the

sediment than in the water, although disequilibrium in the system allows for seawater ion concentration in the dissolved load to also significantly affect apparent Kd values. For example, the high salinity of the pondwater significantly lowers major element pond Kd values (e.g., Na, Mg, K) relative to batch experiments that use DI water (Fig. 2a). However, the relatively homogenous nature of sediment in the area and similar composition of pond waters in May keeps major element Kd values relatively stable in both extract experiments and shrimp ponds even though disequilibrium is prevalent.

pH often strongly influences element partitioning between solid and dissolved phases (e.g., Sansalone and Buchberger, 1997), but the pH range in pond waters was quite narrow (1σ = 0.4, min = 7.8, max = 8.9), and there was little to no correlation between pH and pond Kd values (Fig. C11). Additionally, narrow pH ranges in sediment extracts (mean = 8.4 ± 0.4) likely resulted in little to no correlation of pH with extract Kd values (Fig. C12). The lack of Kd-pH dependency may also be indicative of disequilibrium exchange. However, it does not mean that pH does not influence partitioning in our study samples. For example, the alkaline pH values likely favor desorption of anion species to solution over desorption of cation species, resulting in lower Kd values for elements often present as oxyanions such as S, Se and As.

Lastly, several elements such as Zn, Cu, Mn, Si, and P have greater sediment/water than sediment/extract Kd values (Fig. 2a). Elements like Mn, Cu, Zn, Si and P may have greater Kd values in the field as opposed to batch experiments because they may be more associated with colloidal material (<0.45 μm) in sediment batch experiments, and are thus included in the measured "dissolved" load. Sediment batch experiments may have more colloidal (<0.45 μm) material than pond water samples because of a greater sediment/water ratio, and thus a greater likelihood of higher colloidal density in solution. The inclusion of colloidal material rich in certain elements in the "dissolved load" would thus lower those elements' Kd values.

4.2 *Pond sediment element depletion and enrichment*

Relative to UCC, Zn and the mobile cations Ca, Sr, and Na are depleted beyond 1σ sample variation in samples (Fig. 3a). The elements Ca, Sr and Na were also depleted in rice paddy, tidal channel and Sundarbans sediment samples relative to UCC in Ayers et al. (2020), as well as suspended tidal channel sediment samples taken in the same study area by Dietrich and Ayers (under review). This is likely a product of both the highly weathered material being depleted in more mobile cations, as well as grain size sorting effects, with finer sediment likely containing less abundance of plagioclase feldspar (e.g., Garzanti et al., 2011). Depletion of Na in shrimp pond sediments relative to Ayers et al. (2020) (Fig. 3b) may be related to physical factors that affect leaching of mobile cations, such as differences in water exchange in the shrimp ponds compared to the tidal channel and Sundarbans sediments. However, the mechanisms behind this are unclear, as the rates of water exchange in tidal channels should be even greater than that of shrimp ponds.

The significant depletion of Zn in shrimp pond sediment samples (Figs. 3a and 3b) is unique to this study and not seen in nearby Sundarbans river sediment samples (Islam et al., 2017b) or tidal channel and suspended sediment samples in the study area (Ayers et al, 2020; Dietrich and Ayers, under review) where Zn concentrations more closely resemble average upper

continental crust. It is unclear what may have caused such substantial depletion in Zn concentrations, as even correcting for potential volatilization processes during $LiBO_2$ fusion still resulted in low Zn values.

The enrichment of Se, As, Cd and Cu relative to UCC in aquaculture shrimp pond sediments may be partly attributed to anthropogenic inputs into shrimp ponds, such as fish feed or agrochemicals (e.g., Paul and Vogl, 2011). The elements Ni, Co, and Cu are also slightly enriched in shrimp pond sediment relative to tidal channel and Sundarbans sediment, albeit close to 1σ variation (Fig. 3b), pointing to anthropogenic sourcing in the pond environment. For example, fish feed in our study contained Cr, Cu, Se, Ni, and Sb (Table 2) while fish feed analyzed by Islam et al. (2017a) contained Cd and Co. However, if fish feed is contributing to enrichment of trace elements in pond sediment, it may be from leaching into the water column and then subsequent sorption to sediment, as farmers in Bangladesh often measure out their fish feed carefully to avoid significant solid waste. Future work with batch leaching experiments of fish feed would be useful to determine element mobility from the feed.

4.3 *Pond sediment element relationships with other sediment parameters*

Pond sediment element concentrations are not strongly correlated with sediment parameters such as grain size, TOC, or TIC (Fig. C7), mainly because the variance (1σ) for these parameters was low (Table C1). Pond sediment TOC was about double that seen in Sundarbans near-surface sediment samples (Bomer et al., 2020b), which is likely related to higher DOC content in shrimp pond waters relative to tidal channels in the area and accumulation of dead vegetation at the bottom of the ponds (Dietrich and Ayers, 2021). Although TIC was low in sediment, it was still detected in trace amounts (Table C1), which is likely indicative of carbonate minerals present that help buffer both pond water and extract solutions to alkaline pH values. This is also consistent with mineralogy work in the area where dolomite has been detected in solid samples and is almost always saturated in water samples (e.g., Ayers et al., 2020; Dietrich and Ayers, under review).

4.4 *Arsenic and selenium potential bioaccumulation*

Two elements of initial focus of possible shrimp bioaccumulation were As and Se, because of their previously documented concentrations >WHO drinking water guidelines in the shrimp ponds sampled in this study (Dietrich and Ayers, 2021). Of particularly interest was As, for As bioaccumulation throughout the food chain is an established concern in aquatic environments where there is high As in water and/or sediment (e.g., Hull et al., 2021; Kar et al., 2011). Even if As tends to be in the less toxic organic forms in shrimp and fish species (e.g., Dietrich, 2018; Kar et al., 2011), it is still important to document for understanding environmental cycling and assessing any additional health risks to consumers.

Our results indicate all shrimp contained As <MDL (0.851 mg/kg), and because As concentration in ashed oyster tissue was 11.8 times the original non-ashed composition (Fig. C1b), this suggests that the As content in the unashed shrimp was likely far less than 0.851 mg/kg. Arsenic was also <MDL in fish feed samples (Fig. C13). Collectively, this suggests that As accumulation was not significant in shrimp even though both water and sediment contained

As enriched relative to drinking water guidelines, average seawater, or upper continental crust. Thus, the concentration of As in shrimp diet may be the ultimate indicator of whether or not there is bioaccumulation, even though Kar et al. (2011) saw a linear relationship between aquaculture tilapia As and pond water As. Differences between tilapia and shrimp diet/physiology likely affect the direct comparison of the two (e.g., Mokhtar et al., 2009). Our results do support those of Martins et al. (2011) though, which found that increased metal concentrations in aquaculture pond waters did not seem to influence concentrations in Nile tilapia liver and muscle tissue.

Selenium, also enriched in pond sediment and pond waters (Fig. 3 & Dietrich and Ayers, 2021), was only detected in one shrimp sample (Table 2). Selenium was also measured at ~8.1 mg/kg in LSF fish feed (Fig. C13). However, unlike As, Se was significantly volatilized in our ashing procedure based on the oyster tissue unashed and ashed sample comparison (Table C2). Thus, Se may be more prevalent in shrimp than As, although future research with non-volatilizing digestion methods and lower instrument detection limits would be needed to discern this. Additionally, because Se shrimp bioaccumulation can show temporal variance in natural lake systems (Wright et al., 2020), more frequent sampling throughout the year can help elucidate whether temporal variance in shrimp Se accumulation also occurs in aquaculture systems. Ultimately, it is difficult to conclude whether Se is being transferred to shrimp in significant quantities in this study because of methodology volatilization concerns, and thus if Se is primarily being transferred from the sediment, water, or feed.

4.5 *Geochemical distributions between water, feed, sediment, and shrimp in aquaculture ponds*

Shrimp element concentrations do not appear strongly influenced by sediment or water within aquaculture ponds. Comparison of O and H isotopes (from Dietrich and Ayers, 2021) and element concentrations in shrimp pond sediment, waters, and shrimp did not reveal any strong correlations (Figs. C3, C4, C5), suggesting that there is no significant geochemical exchange between these environmental media, at least on the timescales of our measurements. However, this does not mean there is no element exchange between media over longer timescales. For example, over time, significantly elevated concentrations of Se and As in pond water may lead to accumulation in pond sediment, even if concentrations between contemporaneous sediment and water are not strongly correlated, because influxes may be slightly larger than outfluxes. Additionally, if shrimp diets change or aquaculture species change within a pond, bioaccumulation and thus element transfer from water or sediment to organism may change.

While shrimp food used at each pond was not sampled in this study (i.e., natural or artificial feed) and it was difficult to acquire precise feeding habits/history for every pond, commonly used market fish feed had generally similar inorganic element content as that in the aquaculture shrimp (Fig. 4). Their elemental compositions were distinct from that of other sample media (pond water, sediment, and extracts). Because fish feed is usually predominantly fish meal (i.e., our SSF sample was 40% fish meal) and other organic material, it makes sense that the general elemental compositions are similar between fish feed and shrimp as opposed to water and sediment extracts that are rich in soluble cations or pond sediment rich in aluminum silicates and other minerals. The difference in relative proportions of elements among sample

types is visually evident in Fig. 4b groupings, as Al and Si concentrations are particularly high in sediment, and Na has relatively higher concentrations within water and extract samples. Another way to visualize the differences between sample types is through Kd values of sample/water, where Kd(sediment/water) is commonly greater than feed and shrimp, albeit all sample types follow relatively similar trends (Fig. 5). The large overlap between sample/water Kd values for feed and shrimp (Fig. 5) further illustrate the similarities in element composition within these samples, and how certain elements such as S and P are higher in feed and shrimp relative to sediment in the ponds.

Most shrimp accumulated substantial Ba, Fe, Zn, Cu, Mn and Tl, which was also present in fish feed (Table 2). The fact that all these elements are in fish feed, sometimes even at concentrations greater than that of pond sediment (Tl, Zn), suggests feed may be an important source of these metals in most shrimp. Additionally, some shrimp contained detectible Se, Pb, Sb, and V, which were also each present in at least one of the fish feed samples (Table 2). However, because shrimp in several ponds that we sampled were fed significant "natural" feed (i.e., vegetation) in their pond environment, sediment and water may also be sources of some of these elements. It is difficult to deduce whether some elements that are enriched >UCC in sediment such as Cu or Sb came from sediment, water, or fish feed, particularly because some elements such as Zn, Cu, Ba and V are also enriched in pond water greater than that of typical seawater or river water (Dietrich and Ayers, 2021). Furthermore, shrimp sample KA-18 was supposedly given no artificial fish feed, yet still had significant Se and Tl accumulation (Table 2), which was also found in fish feed samples. This begs to question whether the shrimp were indeed only fed natural feed within their environment, or if whatever the shrimp are eating is somehow bioaccumulating trace elements very effectively. Regardless, because shrimp elemental composition is not strongly correlated with pond water or sediment element concentrations and fish feed contains several unique trace elements found in shrimp, it is reasonable to conclude that fish feed is at least partly contributing to the uptake of several trace metals such as Tl, Zn, Mn, and Cu in shrimp. Thus, it is most important for farmers to monitor feed for toxic metals that may bioaccumulate in shrimp.

While most elements in shrimp are predominantly sourced from feed and not water, shrimp likely exchange elements with water directly through waste excretion and indirectly through consumption of vegetation, which would influence values of bioaccumulation factors (BAFs) between water and shrimp (Table C7). BAFs are useful for identifying elements that hyperaccumulate in shrimp compared to their natural surroundings, and likely represent steady state values that reflect a dynamic equilibrium. Thus, regardless of source, it is apparent that P, Zn, Cu, and Tl accumulate significantly in shrimp relative to their ambient environmental surroundings (water) based on mean BAF values >5000, well above other measured elements (Table C7). Other elements such as Ba, Ca, K, Mg, and Na have much lower BAFs (mean values <50), implying relatively minimal accumulation of these elements in shrimp from their environmental surroundings.

4.6 *Health-based risk assessment for consumers of Bangladesh aquaculture shrimp*

Thallium was detected in much higher concentrations in both shrimp and fish feed (Table 2) than anticipated, because nearly all pond sediment and water Tl concentrations were <MDL

and thus not reported (Fig. C13). This was likely not due to high background concentrations or interferences, as Tl was <MDL in both the ashed and unashed NIST oyster sample. Thallium is a highly toxic metal, with a toxicity considered even greater than that of Hg, Cd, and Pb (e.g., Karbowska, 2016). Thus, THQ calculations were performed to assess noncarcinogenic health risk of consuming the aquaculture shrimp from the region, particularly with Tl in mind. Most shrimp are exported out of Bangladesh and consumed elsewhere and not by aquaculture farmers in the region.

Even when using arsenic's "volatilization correction factor" to conservatively estimate concentrations of Tl in shrimp (since we could not find an organic standard with a certified Tl value), THQ values are >1 in almost all samples for both children and adults (Fig. C10), indicating a greater likelihood of adverse health effects occurring from regular consumption of the shrimp. The actual concentrations of Tl in the shrimp using volatilization correction for Tl and not As may be even greater, for when combusting sewage sludge, Tl began to volatilize at <800°C, lower than the minimum volatilization temperature of As (Folgueras, et al., 2003). Thus, this indicates a significant potential health risk not considered by any prior study on shrimp in the region.

However, it is important to note that due to an elevated method detection limit for Tl in shrimp and fish feed analyses (1.034 mg/kg), there is an added measure of uncertainty with our values. Analysis of three paper filter method blanks in Dietrich and Ayers (under review) using the same ICP-OES and a similar digestion method also measured 1.15 mg/kg of Tl in one sample blank. However, the fact that nearly all our shrimp and feed samples were well above the MDL indicates that there is some level of Tl accumulation in shrimp, likely from the feed, and that further research into the health risks and accumulation of this toxic element in Bangladesh aquaculture shrimp ponds is clearly warranted.

5. Conclusion

Partitioning of elements between pond water, sediment extracts and pond sediment in Southwest Bangladesh suggests that chemical steady state is achieved rather quickly as elements on surface sites of sediment partition into the dissolved load. However, attainment of chemical equilibrium appears to be a slow process, as even 24-hr sediment batch experiments did not reveal any strong correlations between element concentrations in extracts and sediment. Thus, significant sourcing or leaching of trace elements to water or shrimp from aquaculture pond sediment is unlikely. There are predominantly weak to no element correlations between paired pond sediment, water, and shrimp, suggesting limited element exchange between these environmental media. In contrast, the similarity of shrimp and fish feed compositions and several unique metals in each suggests that the feed is an important source of metal uptake in shrimp. Thus, aquaculture farmers in Southwest Bangladesh should be more concerned about what is in shrimp feed than what is in water or sediment. Although As and Se were not significantly detected in shrimp despite relatively high concentrations in water and sediment, Tl was found in shrimp at levels that may lead to an increased likelihood of adverse health effects for shrimp consumers based on target hazard quotient values, and more research on Tl is warranted. Lastly, it is recommended that aquaculture feed and shrimp be periodically sampled and analyzed to avoid metal bioaccumulation in shrimp.

Acknowledgements

Funding supported by the NSF Coastal SEES Collaborative Research Grant OCE-1600319. Special thanks to Md. Zahidul Haque for his immense help in the field and to many others from the University of Dhaka (especially Md. Saddam Hossain and Abrar Hossain), Khulna University and Pugmark Tours (Md Nazrul Islam (Bachchu)) who have helped with this ongoing research project. Thanks also goes out to Rossane DeLapp, Sunjeong Park and the Ohio State University Service Testing and Research Laboratory (STAR Lab) for analytical assistance, and Christopher Sharp for support on the powder XRD.

References

Akter, S., & Ahmed, K. R. (2019). Water chemistry and water quality of a tidal river system in relation with riverbank land use pattern and regional climate in the southwest Bengal Delta of Bangladesh. *Sustainable Water Resources Management*, 1–21. https://doi.org/10.1007/s40899-019-00308-3

Ayers, J. C., George, G., Fry, D., Benneyworth, L., Wilson, C., Auerbach, L., Roy, K., Karim, M. R., Akter, F., & Goodbred, S. (2017). Salinization and arsenic contamination of surface water in southwest Bangladesh. *Geochemical Transactions*, *18*(1), 4. https://doi.org/10.1186/s12932-017-0042-3

Ayers, J., Patton, B., & Dietrich, M. (2020). Preliminary Evidence of Transport-Limited Chemical Weathering and Element Immobility in the Ganges Tidal Delta Plain of Bangladesh. *Geochemistry, Geophysics, Geosystems*, *21*(8), 1–22. https://doi.org/10.1002/essoar.10502497.1

Benneyworth, L., Gilligan, J., Ayers, J. C., Goodbred, S., George, G., Carrico, A., Karim, M. R., Akter, F., Fry, D., Donato, K., & Piya, B. (2016). Drinking water insecurity: water quality and access in coastal south-western Bangladesh. *International Journal of Environmental Health Research*, *3123*(July), 1–17. https://doi.org/10.1080/09603123.2016.1194383

Bethke C. M. (2007) *Geochemical and biogeochemical reaction modeling*., Cambridge University Press.

Biswas, C., Soma, S. S., Rohani, M. F., Rahman, M. H., Bashar, A., & Hossain, M. S. (2021). Assessment of heavy metals in farmed shrimp, Penaeus monodon sampled from Khulna, Bangladesh: An inimical to food safety aspects. *Heliyon*, *7*(3), e06587.

Bomer, E. J., Wilson, C. A., Hale, R. P., Hossain, A. N. M., & Rahman, F. A. (2020a). Surface elevation and sedimentation dynamics in the Ganges-Brahmaputra tidal delta plain, Bangladesh: Evidence for mangrove adaptation to human-induced tidal amplification. *Catena*, *187*, 104312.

Bomer, E. J., Wilson, C. A., & Elsey-Quirk, T. (2020b). Process Controls of the Live Root Zone and Carbon Sequestration Capacity of the Sundarbans Mangrove Forest, Bangladesh. *Sci*, *2*(3), 51.

Chowdhury, N. T. (2010). Water management in Bangladesh: An analytical review. *Water Policy*, *12*(1), 32–51. https://doi.org/10.2166/wp.2009.112

Dietrich, M. (2018). In response to," Systematic review and health risk assessment of arsenic and lead in the fished shrimps from the Persian Gulf," by Fakhri et al. *Food and Chemical Toxicology*, *121*, 715-716.

Dietrich, M., & Ayers, J. C. (2021). Influences on tidal channel and aquaculture shrimp pond water chemical composition in Southwest Bangladesh. *Geochemical Transactions*, 22(1), 1-22. https://doi.org/10.1186/s12932-021-00074-2

Dietrich, M., Ayers, J. (under review). Element transport and partitioning along tidal channels in Southwest Bangladesh. *Environmental Science: Processes & Impacts*.

Folgueras, M. B., Díaz, R. M., Xiberta, J., & Prieto, I. (2003). Volatilisation of trace elements for coal–sewage sludge blends during their combustion. *Fuel*, *82*(15-17), 1939-1948.

Gaillardet, J., Viers, J., & Dupré, B. (2014). Trace Elements in River Waters in: Surface and Ground Water, Weathering and Soils. In *Treatise on Geochemistry*. https://doi.org/10.1016/B978-0-08-095975-7.00507-6

Garzanti, E., Andó, S., France-Lanord, C., Censi, P., Vignola, P., Galy, V., & Lupker, M. (2011). Mineralogical and chemical variability of fluvial sediments 2. Suspended-load silt (Ganga–Brahmaputra, Bangladesh). *Earth and Planetary Science Letters*, *302*(1-2), 107-120.

Gu, Z., Eils, R., & Schlesner, M. (2016). Complex heatmaps reveal patterns and correlations in multidimensional genomic data. *Bioinformatics*, *32*(18), 2847-2849.

Guhathakurta, H., & Kaviraj, A. (2000). Heavy metal concentration in water, sediment, shrimp (Penaeus monodon) and Mullet (Liza parsia) in some brackish water ponds of Sunderban, India. *Marine Pollution Bulletin*, *40*(11), 914–920. https://doi.org/10.1016/S0025-326X(00)00028-X

Hull, E.A., Barajas, M., Burkart, K.A., Fung, S.R., Jackson, B.P., Barrett, P.M., Neumann, R.B., Olden, J.D. and Gawel, J.E. (2021). Human health risk from consumption of aquatic species in arsenic-contaminated shallow urban lakes. *Science of The Total Environment*, 145318.

Isaac, R.A. and W.A. Johnson. 1985. Elemental analysis of plant tissue by plasma emission spectroscopy: Collaborative study. Journal of Association of Official Analytical Chemists 68:499-505.

Islam, G. M., Habib, M. R., Waid, J. L., Rahman, M. S., Kabir, J., Akter, S., & Jolly, Y. N. (2017a). Heavy metal contamination of freshwater prawn (Macrobrachium rosenbergii) and prawn feed in Bangladesh: A market-based study to highlight probable health risks. *Chemosphere*, *170*, 282–289. https://doi.org/10.1016/j.chemosphere.2016.11.163

Islam, M. A., Al-Mamun, A., Hossain, F., Quraishi, S. B., Naher, K., Khan, R., et al. (2017b). Contamination and ecological risk assessment of trace elements in sediments of the rivers of Sundarban mangrove forest, Bangladesh. *Marine Pollution Bulletin*, *124*(1), 356–366. https://doi.org/10.1016/j.marpolbul.2017.07.059

Jiang, D., Hu, Z., Liu, F., Zhang, R., Duo, B., Fu, J., Cui, Y. and Li, M. (2014). Heavy metals levels in fish from aquaculture farms and risk assessment in Lhasa, Tibetan Autonomous Region of China. *Ecotoxicology*, *23*(4), 577-583.

Jones, J. B. Sr., B. Wolf and H. A. Mills. 1991. Microwave Digestion Using CEM Microwave Digestion System. In: Plant Analysis Handbook. Micro-Macro Publishing. Athens, GA.

Ju, Y. R., Chen, C. W., Chen, C. F., Chuang, X. Y., & Dong, C. Di. (2017). Assessment of heavy metals in aquaculture fishes collected from southwest coast of Taiwan and human consumption risk. *International Biodeterioration and Biodegradation*, *124*, 314–325. https://doi.org/10.1016/j.ibiod.2017.04.003

Kar, S., Maity, J. P., Jean, J. S., Liu, C. C., Liu, C. W., Bundschuh, J., & Lu, H. Y. (2011). Health risks for human intake of aquacultural fish: Arsenic bioaccumulation and contamination. *Journal of Environmental Science and Health - Part A Toxic/Hazardous Substances and Environmental Engineering*, *46*(11), 1266–1273. https://doi.org/10.1080/10934529.2011.598814

Karbowska, B. (2016). Presence of thallium in the environment : sources of contaminations , distribution and monitoring methods. *Environmental Monitoring and Assessment*. https://doi.org/10.1007/s10661-016-5647-y

Kassambara, A., & Mundt, F. (2020). Package 'factoextra'. *Extract and visualize the results of multivariate data analyses*. https://cran.r-project.org/web/packages/factoextra/factoextra.pdf

Marriott, A. L., Kelly, T. J., Sarkar, S. K., Chenery, S. R. N., Rakshit, D., Bhattacharya, B. D., & Watts, M. J. (2020). Elemental composition of aquaculture fish from West Bengal, India: nutrition versus food safety. *Environmental Geochemistry and Health*, *42*(4), 1211–1228. https://doi.org/10.1007/s10653-019-00401-8

Martins, C. I. M., Eding, E. H., & Verreth, J. A. J. (2011). The effect of recirculating aquaculture systems on the concentrations of heavy metals in culture water and tissues of Nile tilapia Oreochromis niloticus. *Food Chemistry*, *126*(3), 1001–1005. https://doi.org/10.1016/j.foodchem.2010.11.108

Mokhtar, M. B., Aris, A. Z., Munusamy, V., & Praveena, S. M. (2009). Assessment level of heavy metals in Penaeus monodon and Oreochromis spp. in selected aquaculture ponds of high densities development area. *European Journal of Scientific Research*, *30*(3), 348-360.

Mostafiz, F., Islam, M. M., Saha, B., Hossain, M. K., Moniruzzaman, M., & Habibullah-Al-Mamun, M. (2020). Bioaccumulation of trace metals in freshwater prawn, Macrobrachium rosenbergii from farmed and wild sources and human health risk assessment in Bangladesh. *Environmental Science and Pollution Research*, *27*(14), 16426–16438. https://doi.org/10.1007/s11356-020-08028-4

Paul, B. G., & Vogl, C. R. (2011). Impacts of shrimp farming in Bangladesh: Challenges and alternatives. *Ocean and Coastal Management*, *54*(3), 201–211. https://doi.org/10.1016/j.ocecoaman.2010.12.001

Ravanbakhsh, M., Zare Javid, A., Hadi, M., & Jaafarzadeh Haghighi Fard, N. (2020). Heavy metals risk assessment in fish species (Johnius Belangerii (C) and Cynoglossus Arel) in Musa Estuary, Persian Gulf. *Environmental Research*, *188*(March), 109560. https://doi.org/10.1016/j.envres.2020.109560

Rogers, K. G., Goodbred Jr, S. L., & Mondal, D. R. (2013). Monsoon sedimentation on the 'abandoned'tide-influenced Ganges–Brahmaputra delta plain. *Estuarine, Coastal and Shelf Science*, *131*, 297-309.

Rudnick, R. L., & Gao, S. (2003). Composition of the continental crust. *Treatise on Geochemistry*, vol. 3.

Sansalone, J. J., & Buchberger, S. G. (1997). Partitioning and first flush of metals in urban roadway storm water. *Journal of Environmental engineering*, *123*(2), 134-143.

Sarkar, T., Alam, M. M., Parvin, N., Fardous, Z., Chowdhury, A. Z., Hossain, S., Haque, M. E., & Biswas, N. (2016). Assessment of heavy metals contamination and human health risk in shrimp collected from different farms and rivers at Khulna-Satkhira region, Bangladesh. *Toxicology Reports*, *3*, 346–350. https://doi.org/10.1016/j.toxrep.2016.03.003

Shamsuzzaman, M. M., Islam, M. M., Tania, N. J., Abdullah Al-Mamun, M., Barman, P. P., & Xu, X. (2017). Fisheries resources of Bangladesh: Present status and future direction. *Aquaculture and Fisheries*, *2*(4), 145–156. https://doi.org/10.1016/j.aaf.2017.03.006

Smith, R. L. (1995). EPA Region III Risk Based Concentration Table. *United States Environmental Protection Agency, Region III*. https://hwbdocuments.env.nm.gov/Los%20Alamos%20National%20Labs/References/9642.PDF

Storelli, M. M. (2008). Potential human health risks from metals (Hg, Cd, and Pb) and polychlorinated biphenyls (PCBs) via seafood consumption: Estimation of target hazard

quotients (THQs) and toxic equivalents (TEQs). *Food and Chemical Toxicology*, *46*(8), 2782–2788. https://doi.org/10.1016/j.fct.2008.05.011

U.S. EPA [U.S. Environmental Protection Agency]. (2020). *Regional Screening Level (RSL) Summary Table (TR=1E-06, HQ=1) November 2020*. https://semspub.epa.gov/work/HQ/400431.pdf

Wang, X., Sato, T., Xing, B., & Tao, S. (2005). Health risks of heavy metals to the general public in Tianjin, China via consumption of vegetables and fish. *Science of the total environment*, *350*(1-3), 28-37.

Wright, J., Yang, S., Johnson, W.P., Black, F.J., McVey, J., Epler, A., Scott, A.F., Trentman, M.P., Martin, A.R., Pandey, G. and Piskadlo, A.M. (2020). Temporal correspondence of selenium and mercury, among brine shrimp and water in Great Salt Lake, Utah, USA. *Science of The Total Environment*, *749*, 141273.

Wu, X. Y., & Yang, Y. F. (2011). Heavy metal (Pb, Co, Cd, Cr, Cu, Fe, Mn and Zn) concentrations in harvest-size white shrimp Litopenaeus vannamei tissues from aquaculture and wild source. *Journal of Food Composition and Analysis*, *24*(1), 62-65.

CHAPTER V

SYNTHESIS

5.1 Overall implications

Both major and trace elements are important constituents of biological, lithological, and aqueous environmental media. Trace elements in particular are important to quantify because many are essential nutrients, some are toxic, and their natural concentrations are highly variable. Thus, organisms are especially sensitive to fluctuations of these elements. Additionally, trace elements can be effective proxies for important processes occurring in the environment, such as sorption, mineral precipitation, and pollution. This dissertation has attempted to tie together various geochemical relationships between the lithosphere, hydrosphere, and biosphere in Southwest Bangladesh to better elucidate the cycling of trace elements, particularly ones of toxicological concern such as As and Se.

This research has helped gain a better understanding of how processes in shrimp ponds and tidal channels affect the concentrations of trace elements in the dissolved and solid phases. Evaporation in dry season shrimp ponds in Southwest Bangladesh occurs at quantifiable levels, but it affects concentrations of dissolved trace and major elements less than tidal fluctuations. However, evaporation causes increases in DOC concentrations greater than that of trace or major elements, which may reflect DOC being more sensitive to endogenous (biological) processes in shrimp ponds as opposed to trace element and major element concentrations, which are more sensitive to exogenous changes.

The predominant exogenous influence on shrimp ponds is irrigation source, which means that tidal channel inputs dominate shrimp pond inputs. However, element compositions of shrimp and sediment in the ponds do not seem largely affected by the concentrations of elements in the aqueous phase, illustrating some disconnect between the exchange of elements in the system. Furthermore, shrimp element concentrations are more closely related to the composition of fish feed than water, sediment, or pore water (as measured from sediment extracts). Thus, other sources of elements such as fish feed likely have larger influences on shrimp composition relative to water or sediment. Farmers in the region should therefore more closely monitor the quality of their feed as opposed to water or sediment quality.

The highly weathered nature of most sediment in Southwest Bangladesh results in slow chemical exchange between water and sediment, particularly because most waters are saturated in the minerals that dominate the sediments. However, a relative steady state appears to be achieved quickly between water and sediment in the area, likely indicative of sorbed elements on surface layer sites being released quickly into solution.

Arsenic, selenium, and many other trace elements such as nickel and cobalt are much higher than average riverine dissolved concentrations in both shrimp ponds and tidal channels, which could have long-term implications for agricultural lands or the Sundarbans natural mangrove forest. Most elements are affected by either conservative mixing with seawater, or saltwater ion induced competitive desorption, which releases large proportions of the elements,

particularly the metal cations Ni and Co, into the dissolved load. Arsenic and selenium are oftentimes higher than drinking water guidelines in late dry season and early monsoon shrimp pond and tidal channel waters, which could be problematic even if people in the area are not directly drinking this water. The As and Se from elevated surface waters may accumulate in sediment, groundwater, or other organisms, and thus eventually prove problematic for both human and ecological health. However, the antagonistic toxicological nature of As and Se may alleviate possible adverse health outcomes of these elements if both are consumed simultaneously.

While prediction and understanding of dissolved As and Se concentrations in shrimp pond and tidal channel waters is difficult, both can be reasonably modeled through multiple linear regression. Several important geochemical parameters such as Ni, P, and V dominate these models, which indicates that the behavior of dissolved As and Se is similar to several chemical analogs. Furthermore, through closer examination of the main irrigation source of shrimp ponds in Southwest Bangladesh, tidal channels, there is strong evidence of Se being ultimately sourced from anthropogenic processes upstream, while As may be geogenic in origin. Regardless of the source, As, Se, and other trace elements remain at elevated concentrations in the dissolved load even under highly oxidizing surface water conditions, reflecting their high mobility in transport.

Farmers in the area and wildlife conservation officials need to continually monitor surface water concentrations of trace elements, particularly ones that can be harmful to humans and wildlife such as As and Se. Without better pollution monitoring upstream, dissolved concentrations of most trace elements will likely continue to be greater than average riverine values, which may have long term ramifications for agriculture and ecology in Southwest Bangladesh due to bioaccumulation in plants and organisms. Of immediate concern from a human consumption standpoint is the further evaluation of aquaculture shrimp for the toxic metal thallium, as we detected it in very high concentrations in three different commercially distributed shrimp species and two fish feed varieties. This could pose a large health risk to consumers of shrimp in Bangladesh and abroad, particularly children.

Although surface water is rarely used for drinking in Southwest Bangladesh and therefore may not be regarded with as much importance for inorganic contaminant monitoring as groundwater, surface water monitoring is still paramount for understanding both geogenic and anthropogenic influences on surface processes in the environment. Non-drinking water sources in the environment still affect not only ecological life but may adversely affect certain agricultural products if not properly understood or assessed.

5.2 Future research endeavors

Because of the general lack of comprehensive surface water studies in Bangladesh beyond simple reporting of dissolved element concentrations, a more holistic evaluation of additional environmental media (e.g., sediment, agricultural products, fish, etc.) is needed to properly understand the distribution and partitioning of elements in the environment. Due to the growing of crops oftentimes in the same plots of land as aquaculture ponds, it is urged that all agricultural products be analyzed for potentially harmful levels of Tl, As and Se, among other elements. Furthermore, long-term aquaculture pond and tidal channel river measurements of both

major and trace elements will help better explain the cycling of these elements and may give insight into the times of year when waters are lowest in harmful trace elements and thus most suitable for irrigation purposes. More insight into trace element speciation is also necessary to better predict how they will be cycled throughout the environment. For example, while As and Se occur predominantly as oxyanion species in the oxidizing surface water environment, actual quantification of this will enable better prediction of how much of these elements may eventually sorb or become immobilized on other environmental media such as sediment. Lastly, better constraining the actual sources of trace elements in this environment is greatly needed, particularly for As. While surface water As may ultimately be coming from groundwater, some may be anthropogenic or in the form of colloidal material mobilized from riverbank natural reactive barriers, and thus included in the measured dissolved load. Pinpointing the source of As in Bangladesh surface waters is vital for understanding its cycling in the environment and connection to the groundwater that so many people drink and are poisoned by in Bangladesh.

Only through a holistic examination of the total environment can we truly understand both natural and anthropogenic sourcing of potentially harmful elements in the environment. Through using a complete geochemical perspective, we can then begin to identify effective remediation strategies to reduce risks to both the human and natural environment.

Chapter I & Chapter V References

Akter, S., Ahmed, K.R., 2019. Water chemistry and water quality of a tidal river system in relation with riverbank land use pattern and regional climate in the southwest Bengal Delta of Bangladesh. Sustain. Water Resour. Manag. 1–21. https://doi.org/10.1007/s40899-019-00308-3

Anawar, H.M., Akai, J., Komaki, K., Terao, H., Yoshioka, T., Ishizuka, T., Safiullah, S., Kato, K., 2003. Geochemical occurrence of arsenic in groundwater of Bangladesh: Sources and mobilization processes. J. Geochemical Explor. 77, 109–131. https://doi.org/10.1016/S0375-6742(02)00273-X

Ayers, J.C., George, G., Fry, D., Benneyworth, L., Wilson, C., Auerbach, L., Roy, K., Karim, M.R., Akter, F., Goodbred, S., 2017. Salinization and arsenic contamination of surface water in southwest Bangladesh. Geochem. Trans. 18, 4. https://doi.org/10.1186/s12932-017-0042-3

Ayers, J.C., George, G., Fry, D., Benneyworth, L., Wilson, C., Wallace Auerbach, L., Roy, K., Karim, M.R., Akhter, F., Goodbred, S., 2016. Sources of Salinity and Arsenic in groundwater in Southwest Bangladesh. Geochem. Trans. 1–22. https://doi.org/10.1186/s12932-016-0036-6

Azad, A.K., Jensen, K.R., Lin, C.K., 2009. Coastal Aquaculture Development in Bangladesh: Unsustainable and Sustainable Experiences. Environ. Manage. 44, 800–809. https://doi.org/10.1007/s00267-009-9356-y

Barai, K.R., Harashina, K., Satta, N., Annaka, T., 2019. Comparative analysis of land-use pattern and socioeconomic status between shrimp- and rice- production areas in southwestern coastal Bangladesh: a land-use/cover change analysis over 30 years. J. Coast. Conserv. https://doi.org/10.1007/s11852-019-00682-2

Benneyworth, L., Gilligan, J., Ayers, J.C., Goodbred, S., George, G., Carrico, A., Karim, M.R., Akter, F., Fry, D., Donato, K., Piya, B., 2016. Drinking water insecurity: water quality and access in coastal south-western Bangladesh. Int. J. Environ. Health Res. 3123, 1–17. https://doi.org/10.1080/09603123.2016.1194383

Bhuiyan, M.A.H., Dampare, S.B., Islam, M.A., Suzuki, S., 2015. Source apportionment and pollution evaluation of heavy metals in water and sediments of Buriganga River, Bangladesh, using multivariate analysis and pollution evaluation indices. Environ. Monit. Assess. 187. https://doi.org/10.1007/s10661-014-4075-0

Bowell, R.J., Alpers, C.N., Jamieson, H.E., Nordstrom, D.K., Majzlan, J., 2014. The Environmental Geochemistry of Arsenic -- An Overview --. Rev. Mineral. Geochemistry 79, 1–16. https://doi.org/10.2138/rmg.2014.79.1

Chowdhury, N.T., 2010. Water management in Bangladesh: An analytical review. Water Policy

12, 32–51. https://doi.org/10.2166/wp.2009.112

Eisler, R. (1994). Arsenic in the Environment. Part II: Human Health and Ecosystem Effects: A review of arsenic hazards to plants and animals with emphasis on fishery and wildlife resources. 185-259.

Frisbie, S.H., Mitchell, E.J., Dustin, H., Maynard, D.M., Sarkar, B., 2012. World health organization discontinues its drinking-water guideline for manganese. Environ. Health Perspect. 120, 775–778. https://doi.org/10.1289/ehp.1104693

Gooddy, D.C., Shand, P., Kinniburgh, D.G., Riemsdijk, W.H., 1995. Field-based partition coefficients for trace elements in soil solutions. Eur. J. Soil Sci. 46, 265–285. https://doi.org/doi:10.1111/j.1365-2389.1995.tb01835.x

Hamilton, S. J. (2004). Review of selenium toxicity in the aquatic food chain. Science of the Total Environment, 326(1-3), 1-31.

Hasan, S., Ashraf Ali, M., 2010. Occurrence of manganese in groundwater of Bangladesh and its implications on safe water supply. J. Civ. Eng. 38, 121–128.

Hughes, M.F., 2002. Arsenic toxicity and potential mechanisms of action. Toxicol. Lett. 133, 1–16.

Janssen, R.P.T., Peijnenburg, W., Posthuma, L., VandenHoop, M., 1997. Equilibrium partitioning of heavy metals in Dutch field soils .1. Relationship between metal partition coefficients and soil characteristics. Environ. Toxicol. Chem. 16, 2470–2478. https://doi.org/10.1897/1551-5028(1997)016<2470:epohmi>2.3.co;2

Kabir, M.J., Cramb, R., Alauddin, M., Roth, C., 2016. Farming adaptation to environmental change in coastal Bangladesh: shrimp culture versus crop diversification. Environ. Dev. Sustain. 18, 1195–1216. https://doi.org/10.1007/s10668-015-9697-z

Neumann, R.B., Ashfaque, K.N., Badruzzaman, a. B.M., Ashraf Ali, M., Shoemaker, J.K., Harvey, C.F., 2009. Anthropogenic influences on groundwater arsenic concentrations in Bangladesh. Nat. Geosci. 3, 46–52. https://doi.org/10.1038/ngeo685

Rahman, S.M., Kippler, M., Tofail, F., Bölte, S., Hamadani, J.D., Vahter, M., 2017. Manganese in drinking water and cognitive abilities and behavior at 10 years of age: A prospective cohort study. Environ. Health Perspect. 125, 1–8. https://doi.org/10.1289/EHP631

Roy, K., Karim, M.R., Akter, F., Islam, M.S., Ahmed, K., Rahman, M., Datta, D.K., Khan, M.S.A., 2018. Hydrochemistry, water quality and land use signatures in an ephemeral tidal river: implications in water management in the southwestern coastal region of Bangladesh. Appl. Water Sci. 8, 78. https://doi.org/10.1007/s13201-018-0706-x

Saha, N., Rahman, M.S., Ahmed, M.B., Zhou, J.L., Ngo, H.H., Guo, W., 2017. Industrial metal

pollution in water and probabilistic assessment of human health risk. J. Environ. Manage. 185, 70–78. https://doi.org/10.1016/j.jenvman.2016.10.023

Shammi, M., Rahman, M.M., Islam, M.A., Bodrud-Doza, M., Zahid, A., Akter, Y., Quaiyum, S., Kurasaki, M., 2017. Spatio-temporal assessment and trend analysis of surface water salinity in the coastal region of Bangladesh. Environ. Sci. Pollut. Res. 24, 14273–14290. https://doi.org/10.1007/s11356-017-8976-7

Smedley, P.L., Kinniburgh, D.G., 2002. Source and behaviour of arsenic in natural waters. Appl. Geochemistry 17, 517–568.

Uddin, M. N., Islam, A. S., Bala, S. K., Islam, G. T., Adhikary, S., Saha, D., ... & Akter, R. (2019). Mapping of climate vulnerability of the coastal region of Bangladesh using principal component analysis. Applied geography, 102, 47-57.

Van den Hoop, M. A. G. T. 1995. Metal speciation in Dutch soils: Field-based partition coefficients for heavy metals at background levels. National Institute of Public Health and the Environment.

Supporting Information for Chapter II

Detailed Sampling Information:

All acidified water samples (including blanks) except for rainwater underwent a 5:1 dilution with deionized water for ICP-MS analysis because of high salinity. The May 2019 water samples did not undergo dilution for the ICP-OES analysis, although July 2018 (excluding rainwater) and July 2019 water samples did undergo the 5:1 dilution. Non-diluted samples were still within the dynamic range of the ICP-OES. Figures/models contain data based on a 5:1 dilution, but reported data (Table 2) was updated for better precision based on the more specific 5.1:1 dilution. However, the 2% difference is less than the width of lines and points in the plots, and the dilution ratio change would not impact correlation matrices, nor evaporation and regression models.

Samples from 2019 were refrigerated after arrival to Vanderbilt University, while samples from 2018 were not, although they were analyzed within ~2 months for TOC/IC and the original ICP-OES run was completed within ~2 months as well. Ayers et al., 2017 did not see any significant changes in DIC or DOC over a period of 12-38 days, although nitrate did decrease, but is excluded in this study. Samples from 2019 were completely analyzed within ~2 months of sample collection, while ICP-MS and ICP-OES reanalysis for July 2018 final reported sample values was conducted ~15 months after sample collection because of initial concerns with potentially pushing the upper range of the ICP-OES quantification range for Na. However, the ICP-OES reanalysis concentrations were in excellent agreement for the major cations from the July 2018 samples' original run, indicating evaporative concentration or precipitation of elements was unlikely, and volatilization of elements via atmospheric contact was also unlikely. It is noted though that absolute Na concentrations were consistently higher in the initial OES run.

The July 2018 tidal channel sample was not filtered for TOC or IC analyses. ICP-MS results are listed for As, because of better quantification with lower detection limits on the ICP-MS versus the ICP-OES.

Because shrimp pond KA-10 was not irrigated via tidal channels, it was excluded for all grouped shrimp pond comparisons. Although KA-3 was included because it was irrigated by a tidal channel, it may have an inaccurate SpC value (Table 1). Shrimp pond water samples in May were taken in close spatial proximity to shrimp pond sites in July (Fig. 2), so that spatial salinity gradients are unlikely to largely affect the interpretation of Fig. A3 or Fig. 4. It is noted that tidal channel sample Site-1 was more saline than any other samples (as seen through Na and Cl concentrations), but was likely under slightly different tidal influence and freshwater-seawater mixing dynamics than other samples (collected in the Kobodak cross channel), and was thus only included in isotope figures.

Additionally, the tidal channel sample (MD-TC-22) that was used in the evaporation models was sampled close to the time of high tide at the Pusur River mouth. This could mean the salinity values and isotopic values of the tidal channel sample were towards the upper range within daily fluctuating tidal cycles (higher tide means an isotope ratio enriched towards

seawater and also greater seawater conservative ion concentrations) and thus provides an upper estimate of those measured inputs into the shrimp pond (and a minimum evaporation estimation).

Multiple Linear Regression Modeling:

Variables were selected for inclusion into multiple linear regression analyses initially based on selecting several elements showing moderate correlations with As or Se, such as V, Mn, DOC and Co (Fig. A1), or hypothesized geochemical relationships. For example, because Se shows distinct variance based on slight saltwater ion/salinity seasonality (Fig. 4; Fig. A3), Cl was included as a representative salt ion in modeling to determine whether it could serve as a predictive variable for Se. Rainwater was excluded in the modeling because it is not affected by local geochemical processes besides very minor atmospheric inputs, and thus most element concentrations are relatively negligible relative to seawater, tidal channel water, and groundwater (e.g., Ayers et al., 2017).

V and Cl are strongly positively correlated (Fig. A1), violating the assumption of no multicollinearity in multiple linear regression. When removing Cl from the predictive model of Cl, V, Ni, and DOC, the adjusted R^2 becomes 0.67 ($p < 0.0001$) with each variable (V, Ni and DOC) having a p-value <0.01 (Table A5), which is greater than the adjusted R^2 (0.64, $n = 30$, $p < 0.0001$) for Co, Ba and DOC even though these variables appear to be the best predictive variables for a 3 variable model when 25 samples are considered (Fig. 8). Only four samples with missing values for any of the As predictive variables ($n = 26$) and only one sample with missing values for any of the Se predictive variables ($n = 29$) were omitted from the aforementioned models (Tables A3, A4, and A5).

Using the variable subset of Se, P, V, Ni, $\delta^{18}O$, and pH resulted in an adjusted R^2 of 0.70 for As ($p = 0.016$) (Table A6), and selecting the variables Al, Co, P, Ba, Ni, $\delta^{18}O$, $\delta^{2}H$ and pH resulted in an adjusted R^2 of 0.90 for Se ($p = 0.0041$) (Table A7). However, when including isotopes, 16 sample observations must be omitted due to missing variables, making a sample size of $n = 14$. Furthermore, having both $\delta^{18}O$ and $\delta^{2}H$ as predictor variables clearly violates the assumption of no multicollinearity for multiple linear regression. When omitting $\delta^{18}O$ from the Se model, the adjusted R^2 drops to 0.45 ($p = 0.14$) and omitting $\delta^{2}H$ reduces the R^2 to 0.42 ($p = 0.16$).

Tables and Figures

Table A1: Concentrations of elements in seawater compiled from the literature: Pilson, 1998 ([a]), Sarma et al., 2012 – MN Transect ([b]), Ogawa and Tanoue, 2003 – Upper range of Indian Ocean values ([c]), Srichandan et al., 2016 – Upper limit off NW Bay of Bengal ([d]), Mason, 2013 ([e]), and Wright and Colling, 1995 ([f]). For simplicity, all elements are listed at total concentrations, although major elements ([a]) and DIC ([b]) in seawater are derived from their predominant ion concentrations in mg/kg but written here as mg/L because the density conversion is negligible (~1.02) for an already generic estimation.

	Seawater Concentration (mg/L)		Seawater Concentration (mg/L)
Cl[a]	**19353**	**Ba[f]**	**0.02**
Na[a]	**10781**	**Al[e]**	**0.00054**
SO4[a]	**2712**	**P[f]**	**0.06**
Mg[a]	**1284**	**As[e]**	**0.0017**
S[f]	**905**	**Se[e]**	**0.00013**
K[a]	**399**	**V[e]**	**0.0015**
Ca[a]	**411.9**	**Mn[d]**	**0.00734**
DIC[b]	**19.1**	**Zn[e]**	**0.00033**
DOC[c]	**0.84**	**Cu[e]**	**0.00025**
Sr[a]	**7.94**	**Ni[e]**	**0.00047**
B[a]	**25.7**	**Cr[e]**	**0.00021**
Si[f]	**2**	**Co[e]**	**0.0000012**

Table A2: Geochemist's Workbench React program script for a surface water evaporation model, modeling evaporation of tidal channel input water while in the irrigated shrimp pond.

```
data = thermo.tdat verify
conductivity = conductivity-USGS.dat
temperature = 25 C
H2O      = 1 free kg
Al+++    = 93.7 ug/l
V+++     = 18.1 ug/l as V
Cr+++    = 4.4 ug/l as Cr
Mn++     = 4.1 ug/l as Mn
Co++     = .36 ug/l as Co
```

Ni++ = 5.6 ug/l as Ni
Cu+ = 5.9 ug/l as Cu
Zn++ = 4.1 ug/l as Zn
As(OH)4- = 42.6 ug/l as As
SeO3-- = 11.7 ug/l as Se
B(OH)3 = 2.5 mg/l as B
Ba++ = .25 mg/l as Ba
Ca++ = 198.6 mg/l as Ca
K+ = 278.2 mg/l as K
Mg++ = 567 mg/l as Mg
Na+ = 5405 mg/l as Na
HPO4-- = .054 mg/l as P
SO4-- = 1337 mg/l
SiO2(aq) = 2.12 mg/l as Si
Sr++ = 3.65 mg/l as Sr
Cl- = 8869 mg/l
Br- = 44.86 mg/l
pH = 7.67
swap e- for O2(aq)
Eh = 267 mV
HCO3- = 112.5 mg/l
balance off
react -100 g/l of H2O

Table A3: Multiple linear regression output for selected primary predictor variables based on multiple linear subset regression for As.

```
Call:
lm(formula = As ~ Cu + P + V + Ni, data = data)

Residuals:
      Min        1Q    Median        3Q       Max
-0.020069 -0.008693 -0.002284  0.005545  0.048094

Coefficients:
            Estimate Std. Error t value Pr(>|t|)
(Intercept) -0.006741   0.012124  -0.556   0.5841
Cu           1.718763   0.687983   2.498   0.0209 *
P            0.077547   0.051316   1.511   0.1456
V            2.041054   0.575027   3.549   0.0019 **
Ni          -1.863999   0.753860  -2.473   0.0220 *
---
Signif. codes:  0 ‘***’ 0.001 ‘**’ 0.01 ‘*’ 0.05 ‘.’ 0.1 ‘ ’ 1

Residual standard error: 0.01448 on 21 degrees of freedom
  (4 observations deleted due to missingness)
Multiple R-squared:  0.4839,  Adjusted R-squared:  0.3855
F-statistic: 4.922 on 4 and 21 DF,  p-value: 0.005861
```

Table A4: Multiple linear regression output for selected primary predictor variables based on multiple linear subset regression for Se.

```
Call:
lm(formula = Se ~ V + Ni + DOC + Cl, data = data)

Residuals:
      Min        1Q    Median        3Q       Max
-0.032661 -0.019022 -0.002155  0.013897  0.040920

Coefficients:
             Estimate Std. Error t value Pr(>|t|)
(Intercept)  1.416e-02  1.317e-02   1.075 0.292912
V           -5.476e+00  1.327e+00  -4.127 0.000382 ***
Ni           3.178e+00  9.707e-01   3.274 0.003212 **
DOC          5.713e-03  1.232e-03   4.638 0.000104 ***
Cl           7.832e-06  2.706e-06   2.895 0.007962 **
---
Signif. codes:  0 ‘***’ 0.001 ‘**’ 0.01 ‘*’ 0.05 ‘.’ 0.1 ‘ ’ 1

Residual standard error: 0.02211 on 24 degrees of freedom
  (1 observation deleted due to missingness)
Multiple R-squared:  0.7802,   Adjusted R-squared:  0.7436
F-statistic:  21.3 on 4 and 24 DF,  p-value: 1.317e-07
```

Table A5: Multiple linear regression output for selected primary predictor variables based on multiple linear subset regression for Se.

```
Call:
lm(formula = Se ~ V + Ni + DOC, data = data)

Residuals:
      Min        1Q    Median        3Q       Max
-0.039108 -0.019917 -0.003914  0.013867  0.059160

Coefficients:
             Estimate Std. Error t value Pr(>|t|)
(Intercept)  0.028225   0.013932   2.026  0.05358 .
V           -2.183840   0.777885  -2.807  0.00954 **
Ni           4.782861   0.906714   5.275 1.83e-05 ***
DOC          0.003774   0.001176   3.208  0.00364 **
---
Signif. codes:  0 ‘***’ 0.001 ‘**’ 0.01 ‘*’ 0.05 ‘.’ 0.1 ‘ ’ 1

Residual standard error: 0.02516 on 25 degrees of freedom
  (1 observation deleted due to missingness)
Multiple R-squared:  0.7035,   Adjusted R-squared:  0.6679
F-statistic: 19.77 on 3 and 25 DF,  p-value: 8.798e-07
```

Table A6: Multiple linear regression output including an isotope predictor variable for As.

```
Call:
lm(formula = As ~ Se + P + V + Ni + d18O + pH, data = data)

Residuals:
       Min         1Q     Median         3Q        Max
-0.0059425 -0.0008563  0.0000130  0.0007339  0.0047557

Coefficients:
             Estimate Std. Error t value Pr(>|t|)
(Intercept)  0.133264   0.043684   3.051  0.01857 *
Se          -0.281884   0.123210  -2.288  0.05599 .
P            0.099795   0.022593   4.417  0.00309 **
V            2.113018   0.601300   3.514  0.00981 **
Ni           2.184351   0.863182   2.531  0.03920 *
d18O         0.004651   0.001765   2.635  0.03367 *
pH          -0.017973   0.005586  -3.218  0.01470 *
---
Signif. codes:  0 ‘***’ 0.001 ‘**’ 0.01 ‘*’ 0.05 ‘.’ 0.1 ‘ ’ 1

Residual standard error: 0.003919 on 7 degrees of freedom
  (16 observations deleted due to missingness)
Multiple R-squared:  0.8387,   Adjusted R-squared:  0.7005
F-statistic: 6.068 on 6 and 7 DF,  p-value: 0.01596
```

Table A7: Multiple linear regression output including isotope predictor variables for Se.

```
Call:
lm(formula = Se ~ Al + Co + P + Ba + Ni + d18O + d2H + pH, data = data)

Residuals:
        13         14         15         16         17         18         19
 3.579e-03  1.681e-03  4.400e-03  6.696e-05 -3.326e-03 -5.290e-04 -2.544e-03
        20         21         22         23         24         25         26
-4.228e-03  2.542e-04 -8.720e-04 -5.446e-04  9.332e-04 -1.351e-03  2.481e-03

Coefficients:
             Estimate Std. Error t value Pr(>|t|)
(Intercept)  6.138e-01  8.430e-02   7.281 0.000764 ***
Al          -9.558e-01  2.329e-01  -4.104 0.009316 **
Co          -4.591e+02  7.981e+01  -5.753 0.002227 **
P           -8.565e-01  1.430e-01  -5.991 0.001858 **
Ba           1.629e-01  6.939e-02   2.347 0.065798 .
Ni           3.139e+00  8.493e-01   3.697 0.014048 *
d18O        -2.140e-01  4.105e-02  -5.213 0.003429 **
d2H          3.773e-02  7.052e-03   5.350 0.003064 **
pH          -3.119e-02  5.868e-03  -5.315 0.003152 **
---
Signif. codes:  0 ‘***’ 0.001 ‘**’ 0.01 ‘*’ 0.05 ‘.’ 0.1 ‘ ’ 1

Residual standard error: 0.004016 on 5 degrees of freedom
  (16 observations deleted due to missingness)
Multiple R-squared:  0.9604,   Adjusted R-squared:  0.8969
F-statistic: 15.14 on 8 and 5 DF,  p-value: 0.004144
```

Table A8: Multiple linear regression output for important predictor variables for As from data in Table S4 in Boral et al. (2020), from the upper Ganges.

```
Call:
lm(formula = As ~ Cu + V + Ni, data = PredictD)

Residuals:
     Min       1Q   Median       3Q      Max
-11.8380  -2.8581  -0.0012   2.5799  14.2559

Coefficients:
            Estimate Std. Error t value Pr(>|t|)
(Intercept) -1.65994    1.30592  -1.271  0.20830
Cu           4.75747    0.52821   9.007  5.5e-13 ***
V           -0.27914    0.09889  -2.823  0.00634 **
Ni          -0.81865    0.50824  -1.611  0.11216
---
Signif. codes:  0 ‘***’ 0.001 ‘**’ 0.01 ‘*’ 0.05 ‘.’ 0.1 ‘ ’ 1

Residual standard error: 4.771 on 64 degrees of freedom
Multiple R-squared:  0.6569,   Adjusted R-squared:  0.6408
F-statistic: 40.84 on 3 and 64 DF,  p-value: 7.19e-15
```

Table A9: Multiple linear regression output for important predictor variables for As from tidal channel surface water data (including a duplicate sample) in Ayers et al. (2020), from lower Ganges tidal tributaries.

```
Call:
lm(formula = As ~ Cu + V + Ni + P, data = Ayers_TC)

Residuals:
         1          3          4          5          6          7         10
-1.645e-04 -1.880e-04  3.680e-04  8.622e-06 -3.094e-04 -1.952e-04 -5.321e-04
        11         12         13
-6.370e-04  4.793e-04  1.170e-03

Coefficients:
             Estimate Std. Error t value Pr(>|t|)
(Intercept)  0.0044004  0.0003822  11.513 8.67e-05 ***
Cu          -0.2447471  0.0814662  -3.004  0.02995 *
V            0.4528870  0.1766426   2.564  0.05041 .
Ni          -1.0276585  0.6569294  -1.564  0.17851
P           -0.1493359  0.0316770  -4.714  0.00527 **
---
Signif. codes:  0 ‘***’ 0.001 ‘**’ 0.01 ‘*’ 0.05 ‘.’ 0.1 ‘ ’ 1

Residual standard error: 0.0007238 on 5 degrees of freedom
  (5 observations deleted due to missingness)
Multiple R-squared:  0.8576,   Adjusted R-squared:  0.7436
F-statistic: 7.526 on 4 and 5 DF,  p-value: 0.02407
```

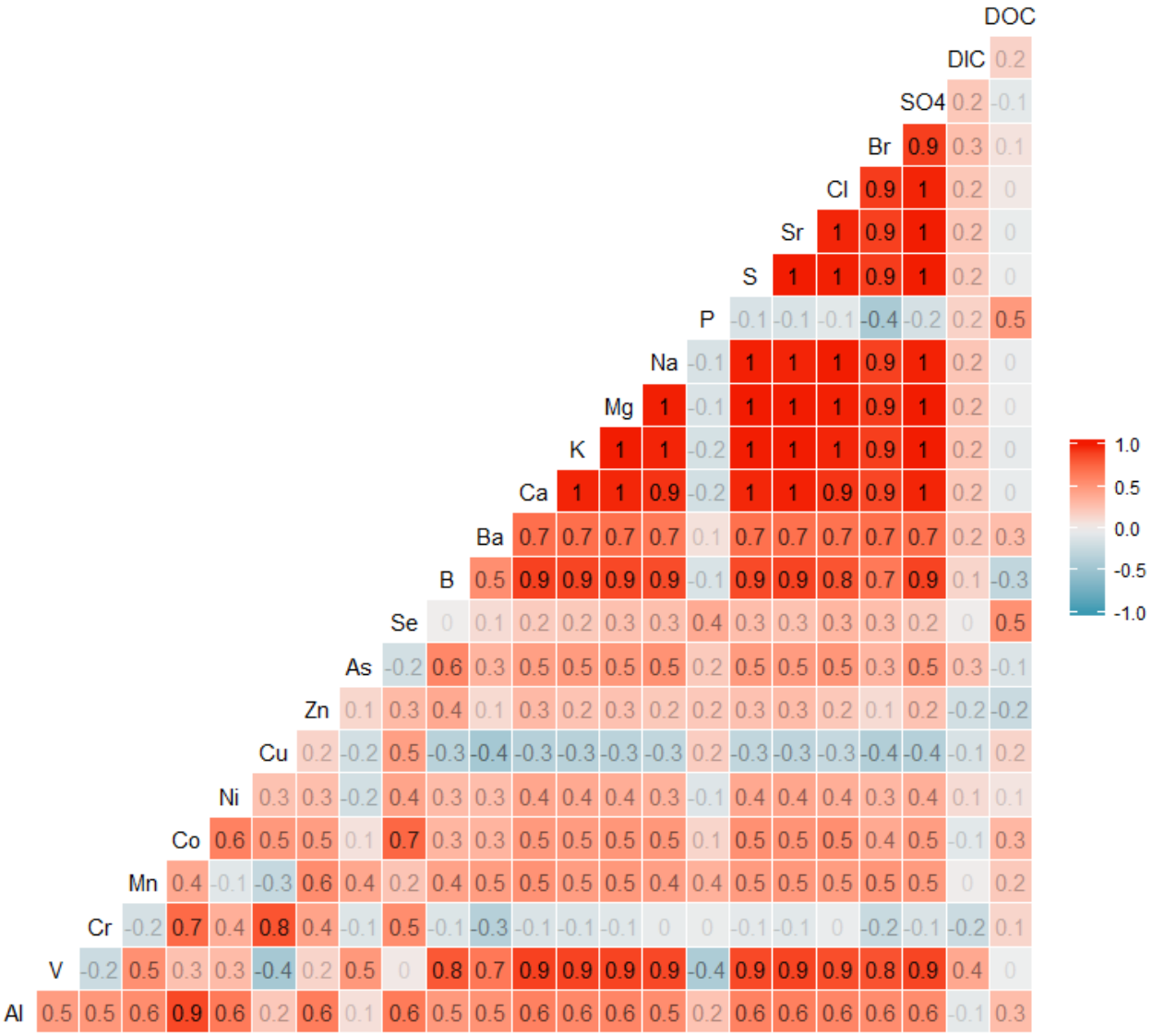

Figure A1: Pearson correlation coefficient matrix between log10 transformed dissolved element concentrations in surface water samples, excluding rainwater (Si omitted because of several negative values, and pH, ORP (Eh) and SpC omitted because of missing values).

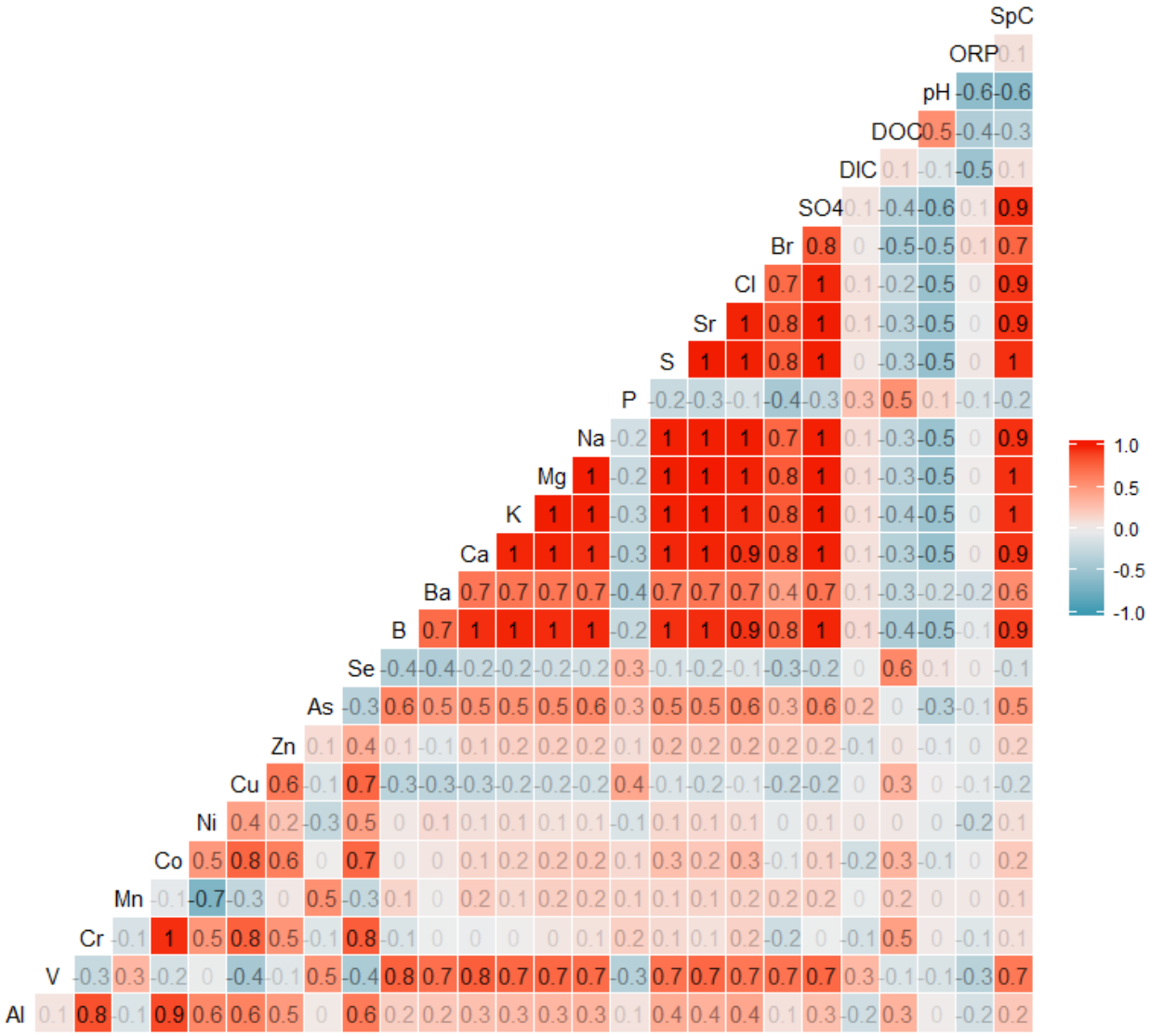

Figure A2: Pearson correlation coefficient matrix between log10 transformed dissolved element concentrations in shrimp pond samples (Si omitted because of several negative values). For the correlation matrix, ORP (relative to Ag/AgCl redox couple) is interchangeable with Eh even though Eh values relative to the standard hydrogen electrode (SHE) are +187 mV compared to ORP values.

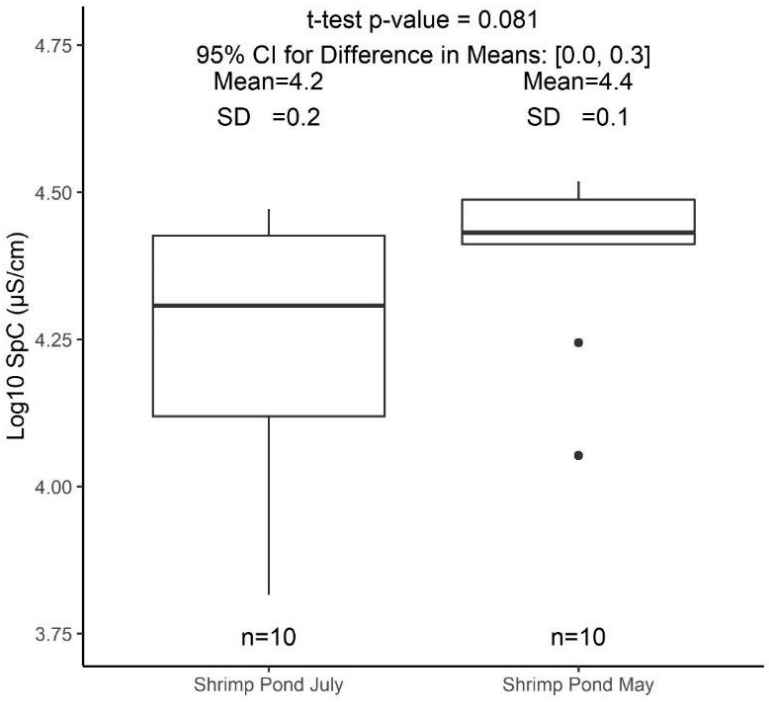

Figure A3: Comparative box plot illustrating the slight seasonality seen between July and May shrimp ponds irrigated with tidal channels via log transformed SpC data.

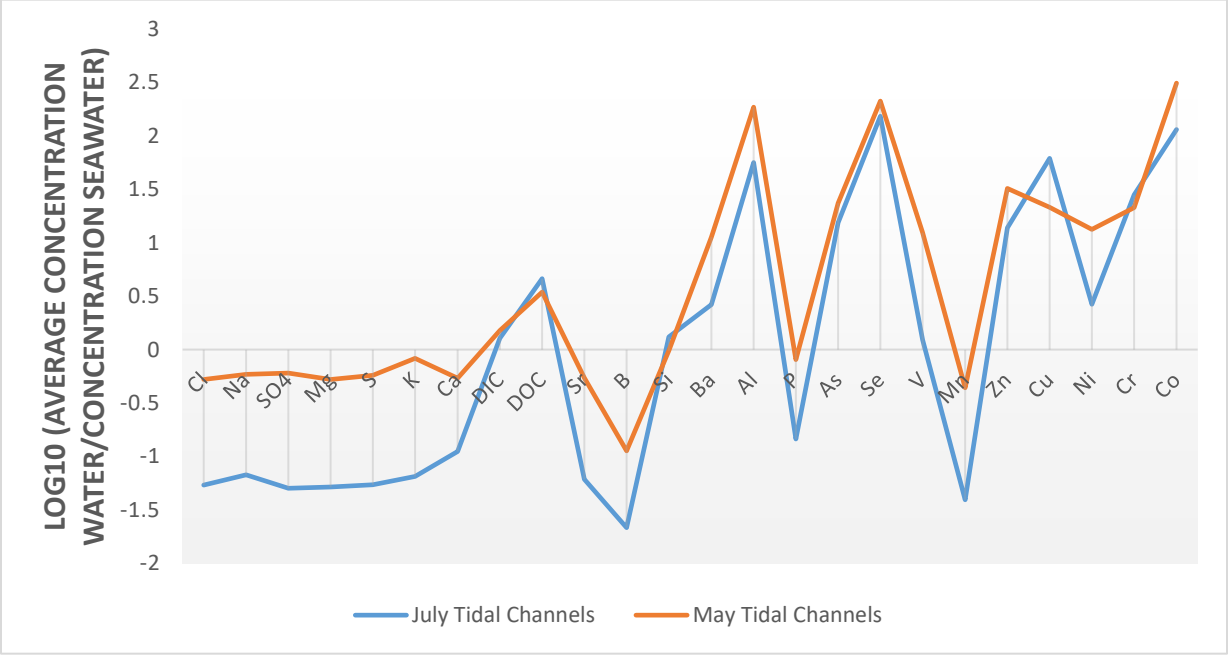

Figure A4: Spider diagram showing relative enrichment or depletion of elements in tidal channel water when normalized to average seawater concentrations (Table A1; values above 0 are enriched relative to seawater, values <0 are relatively depleted).

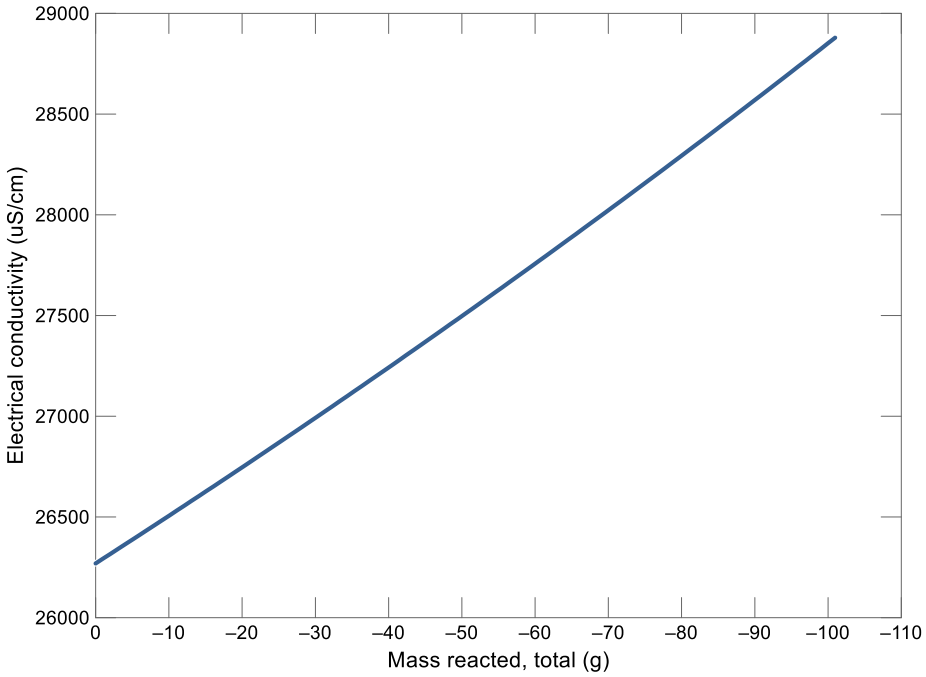

Figure A5: Geochemist's Workbench evaporation model output, depicting specific conductivity (SpC) in solution during evaporation of a tidal channel sample towards the composition of the irrigated shrimp pond sample. The model's initial SpC values calculated from the analysis are slightly different from the field-measured value, likely because of discrepancies between the Geochemist's Workbench SpC calculation and greater uncertainty of field measurements at high salinity.

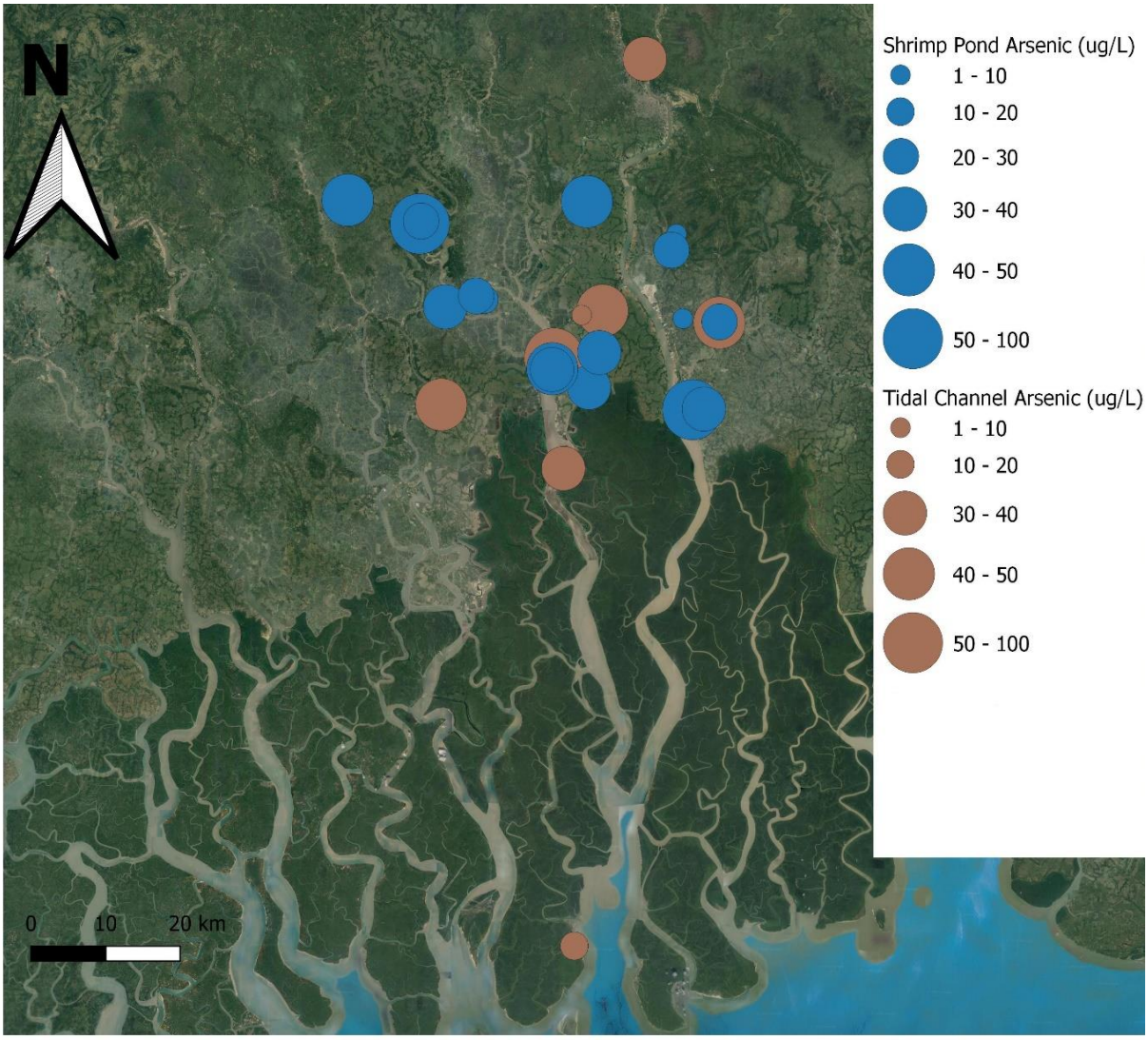

Figure A6: Arsenic concentrations in shrimp ponds and tidal channels from May and July 2018-2019. Large spatial heterogeneity is seen, with most concentrations over the WHO guideline value of 10 $\mu g.L^{-1}$.

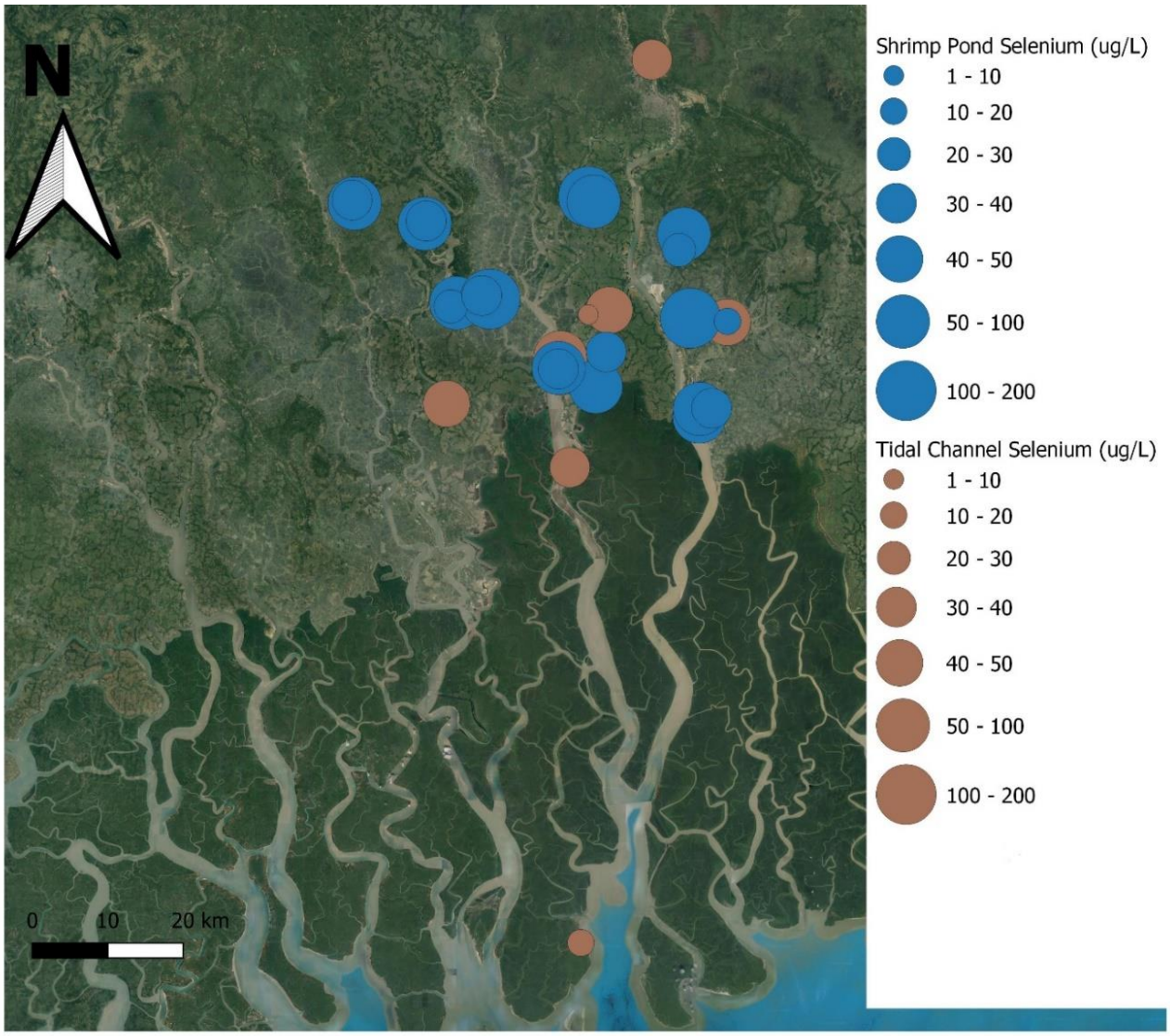

Figure A7: Selenium concentrations in shrimp ponds and tidal channels from May and July 2018-2019. Large spatial heterogeneity is seen, with many samples over the EPA MCL of 50 $\mu g.L^{-1}$.

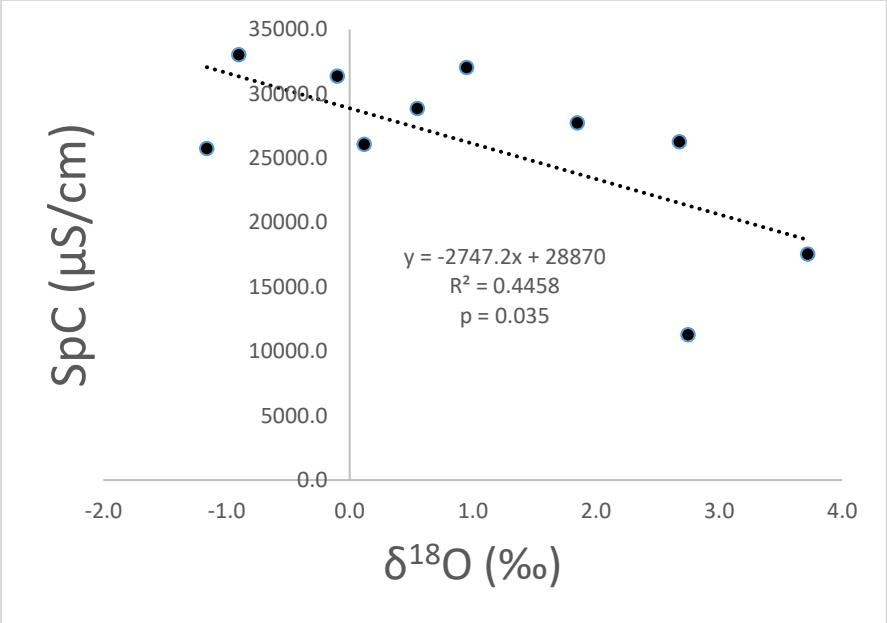

Figure A8: Bivariate plot between SpC and $\delta^{18}O$ in May shrimp ponds.

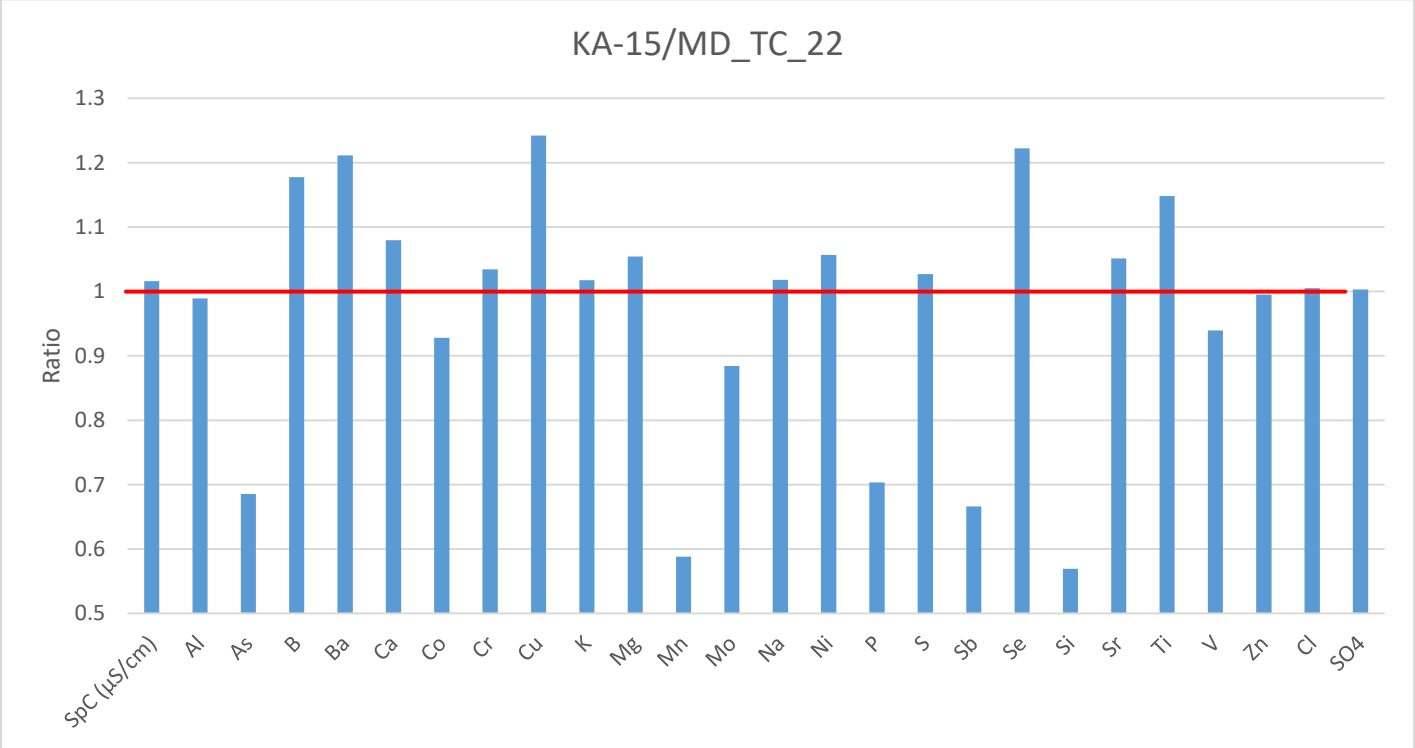

Figure A9: Bar chart plot of ratio between concentration in shrimp pond and a tidal channel directly adjacent to it as an irrigation source. All values >1 (red line) indicate higher shrimp pond values than tidal channel values.

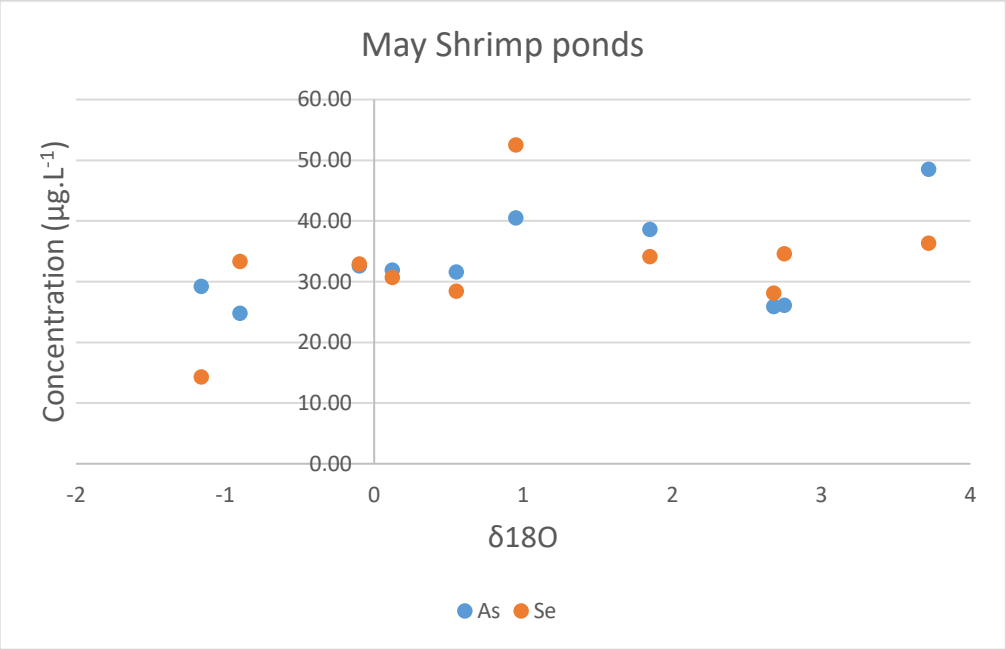

Figure A10: Bivariate plot of As and Se ($\mu g.L^{-1}$) with $\delta^{18}O$, showing little to no relationship.

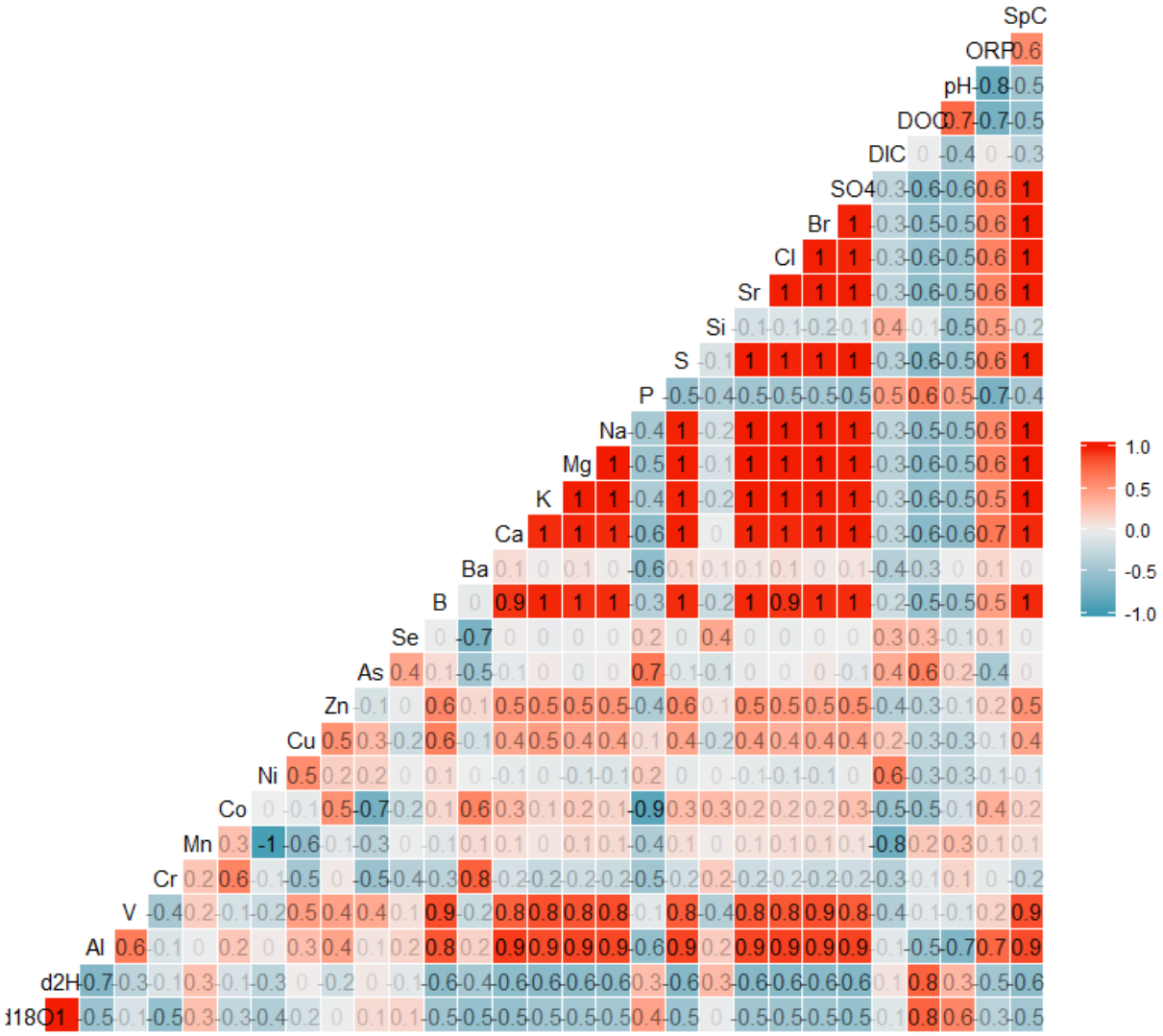

Figure A11: Log10 transformed Pearson correlation coefficient matrix between $\delta^{18}O$ and $\delta^{2}H$, elements and other geochemical parameters in May shrimp pond water samples. For the correlation matrix, ORP (relative to Ag/AgCl redox couple) is interchangeable with Eh even though Eh values relative to the standard hydrogen electrode (SHE) are +187 mV compared to ORP values.

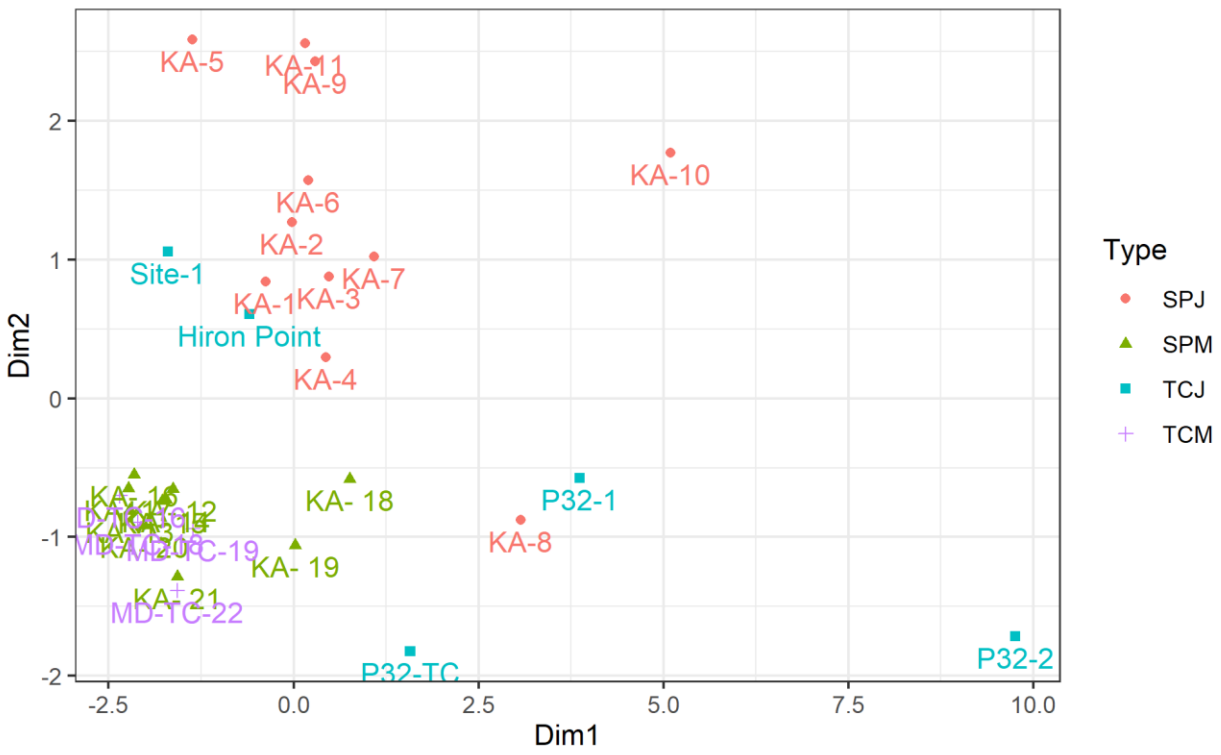

Figure A12: Multidimensional scaling (MDS) plot by Aitchison distance (using the classical method) of July shrimp ponds (SPJ), May shrimp ponds (SPM), July tidal channels (TCJ), and May tidal channels (TCM) for all geochemical variables except stable isotopes, with missing data replaced via the "mice" package (van Buuren, 2020) and MDS completed via the "provenance" package (Vermeesch, 2020). In addition to illustrating the compositional difference between July and May samples, MDS shows the similarity in May tidal channel and shrimp pond composition, and the disconnect among July shrimp ponds and tidal channels. MDS is useful because it plots samples based on multiple compositional variables in abstract Cartesian space, where samples that are more similar plot closer together.

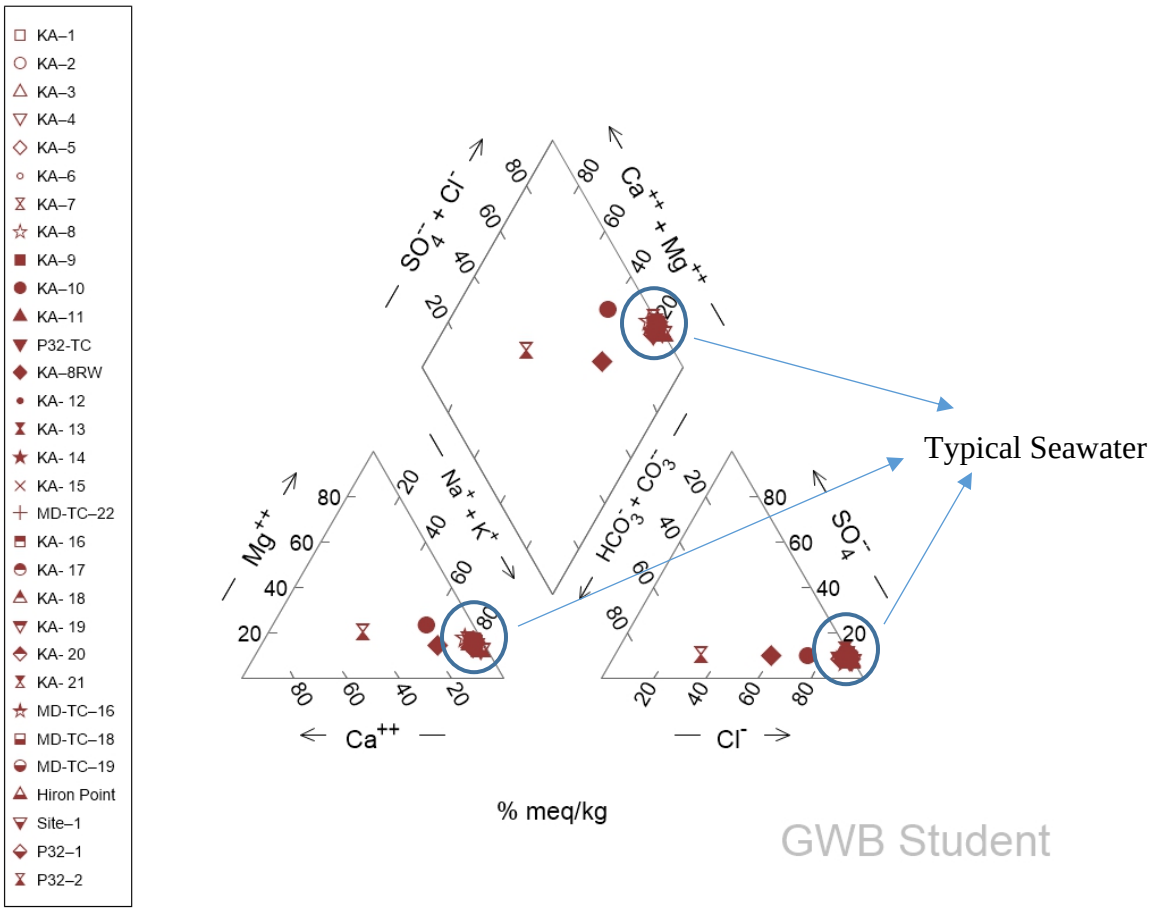

Figure A13: Piper diagram created in The Geochemist's Workbench, illustrating how most water samples plot within typical seawater composition.

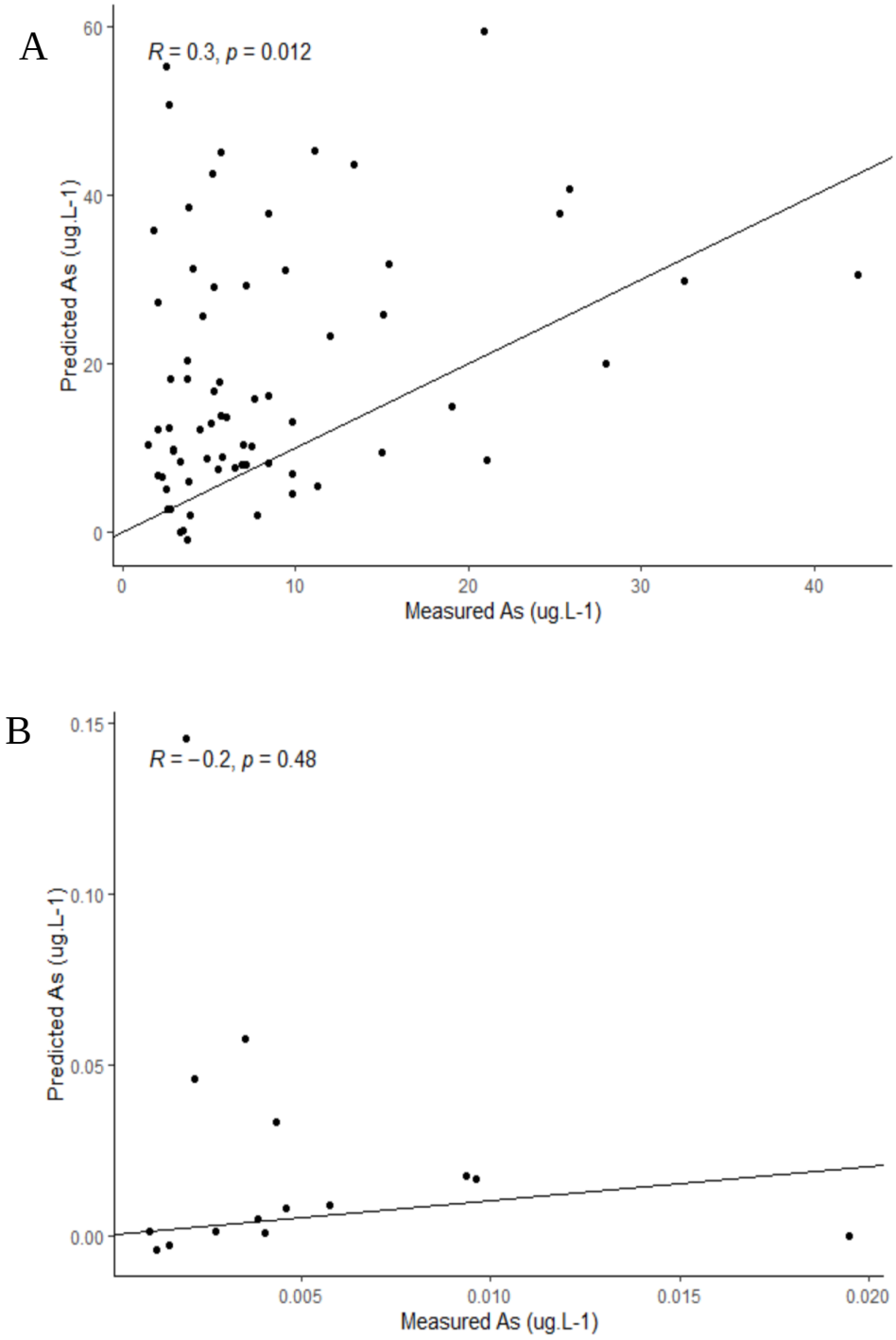

Figure A14: Predicted versus measured As in surface water samples in (A) the Ganges River (Boral et al., 2020) and (B) Ganges tidal channel tributaries (Ayers et al., 2020), with the solid black line representing a 1:1 ratio. A Pearson correlation coefficient is also provided for each plot.

References

Ayers, J.C., George, G., Fry, D., Benneyworth, L., Wilson, C., Auerbach, L., Roy, K., Karim, M.R., Akter, F., Goodbred, S., 2017. Salinization and arsenic contamination of surface water in southwest Bangladesh. Geochem. Trans. 18, 4. https://doi.org/10.1186/s12932-017-0042-3

Ayers, J. C., Patton, B., & Dietrich, M., 2020. Preliminary Evidence of Transport-Limited Chemical Weathering and Element Immobility in the Ganges Tidal Delta Plain of Bangladesh. *Geochemistry, Geophysics, Geosystems*, *21*(8), e2020GC009029. https://doi.org/10.1029/2020GC009029

Boral, S., Sen, I.S., Tripathi, A., Sharma, B., Dhar, S., 2020. Tracking dissolved trace and heavy metals in the Ganga River from source to sink: A baseline to judge future changes. Geochemistry, Geophys. Geosystems 1–22. https://doi.org/10.1029/2020GC009203

van Buuren, S., 2020. Multivariate Imputation by Chained Equations. https://cran.r-project.org/web/packages/mice/mice.pdf

Mason, R. P., 2013. Trace metals in aquatic systems. John Wiley & Sons.

Ogawa, H., Tanoue, E., 2003. Dissolved Organic Matter in Freshwaters. J. Oceanogr. 59, 129–147. https://doi.org/10.1023/A:1025528919771

Wright, J., Colling, A., 1995. Seawater: Its Composition, Properties and Behaviour. Elsevier. https://linkinghub.elsevier.com/retrieve/pii/C20130102085

Pilson, M. E. Q., 1998. Major constituents of seawater. An Introduction to the Chemistry of the Sea, 58-65.

Sarma, V.V.S.S., Krishna, M.S., Rao, V.D., Viswanadham, R., Kumar, N.A., Kumari, T.R., Gawade, L., Ghatkar, S., Tari, A., 2012. Sources and sinks of CO 2 in the west coast of Bay of Bengal. Tellus, Ser. B Chem. Phys. Meteorol. 64. https://doi.org/10.3402/tellusb.v64i0.10961

Srichandan, S., Panigrahy, R.C., Baliarsingh, S.K., Rao B., S., Pati, P., Sahu, B.K., Sahu, K.C., 2016. Distribution of trace metals in surface seawater and zooplankton of the Bay of Bengal, off Rushikulya estuary, East Coast of India. Mar. Pollut. Bull. 111, 468–475. https://doi.org/10.1016/j.marpolbul.2016.06.099

Vermeesch, P., 2020. provenance: Statistical Toolbox for Sedimentary Provenance Analysis. https://cran.r-project.org/package=provenance

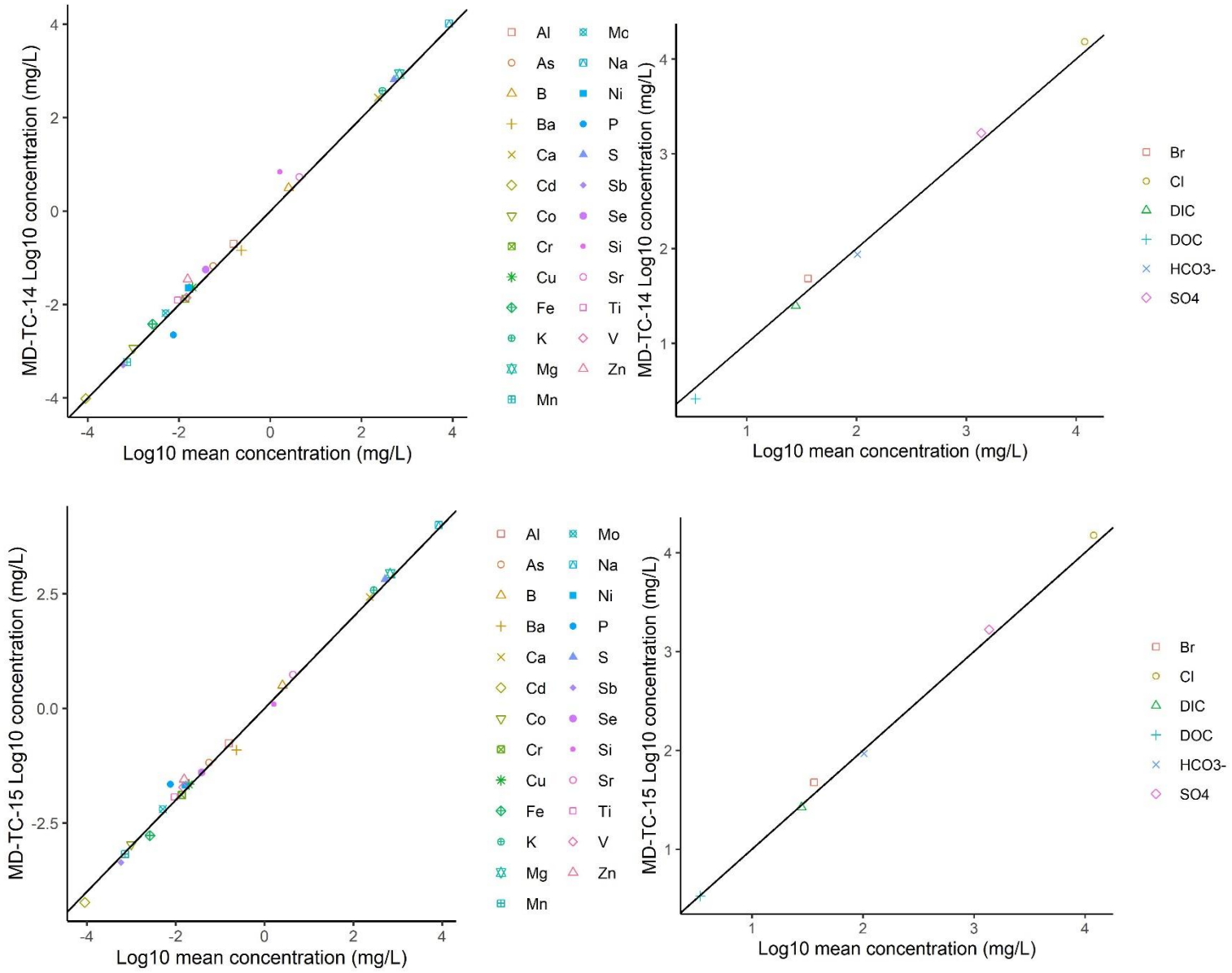

Figure B1: Log10 element concentrations in metal buckets versus log10 mean concentrations of elements in plastic buckets, with a 1:1 ratio line inserted in black.

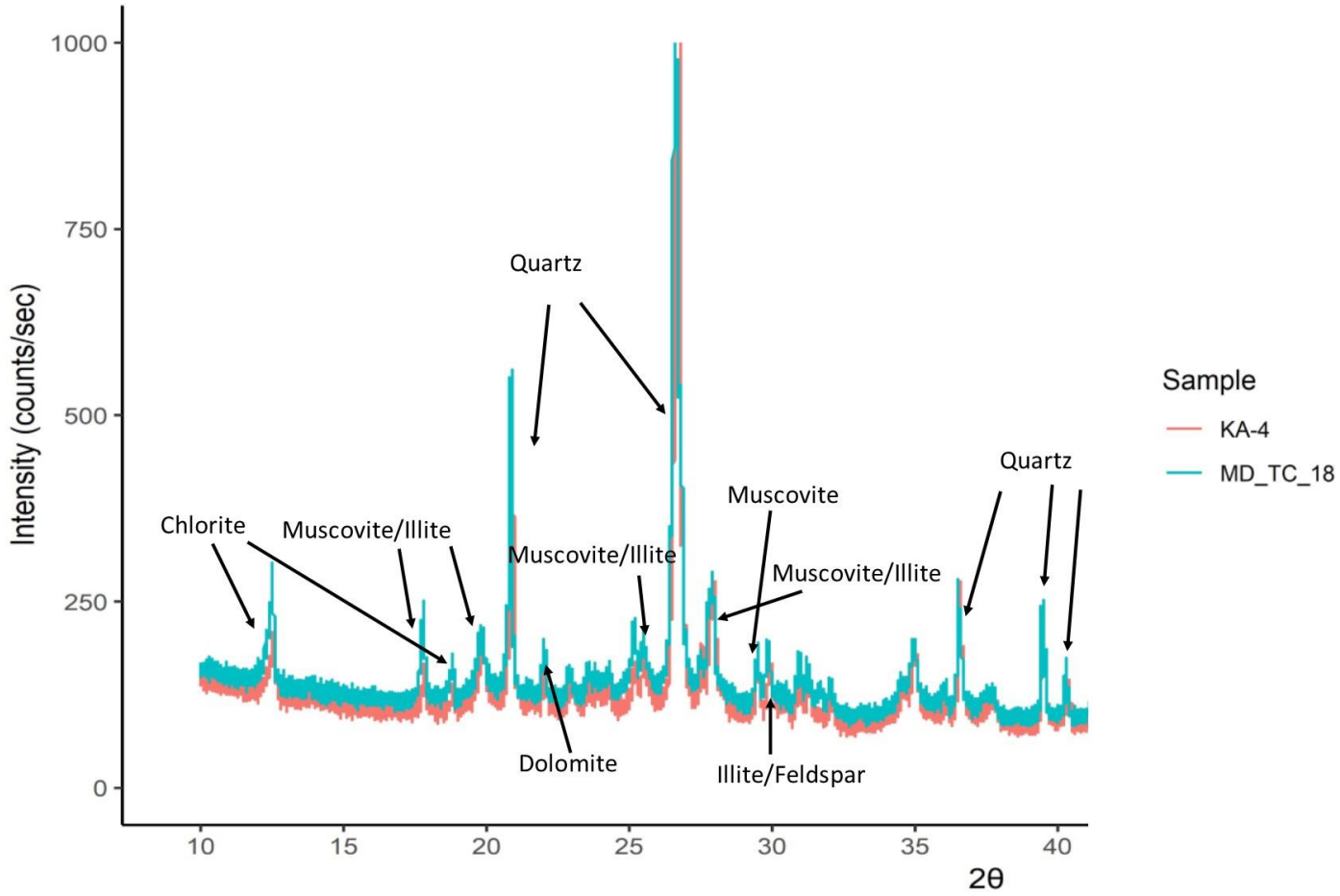

Figure B2: Powder XRD analysis of suspended sediment (>2.5µm) in the upper 1m of a tidal channel (MD-TC-18) and a shrimp pond sediment sample (Location KA-4; Dietrich and Ayers, 2021) in Southwest Bangladesh. Major mineral phases are identified with their corresponding peaks. Feldspar is a K-component of Feldspar – K (Al Si3 O8). The y-axis depicts observed intensity and is truncated for better visualization.

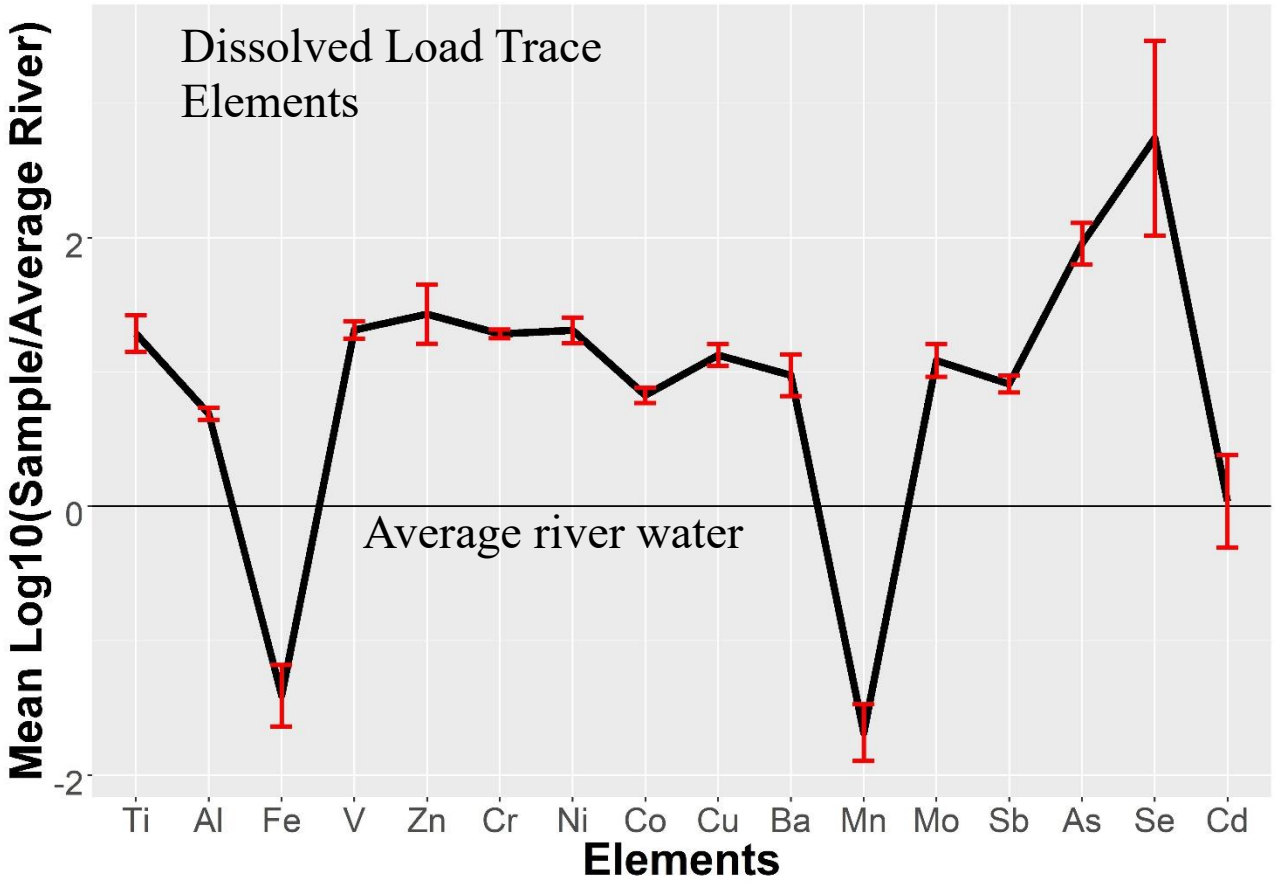

Figure B3: Dissolved element concentrations normalized to average riverine element concentrations (Gaillardet et al., 2014) with 1σ variation error bars.

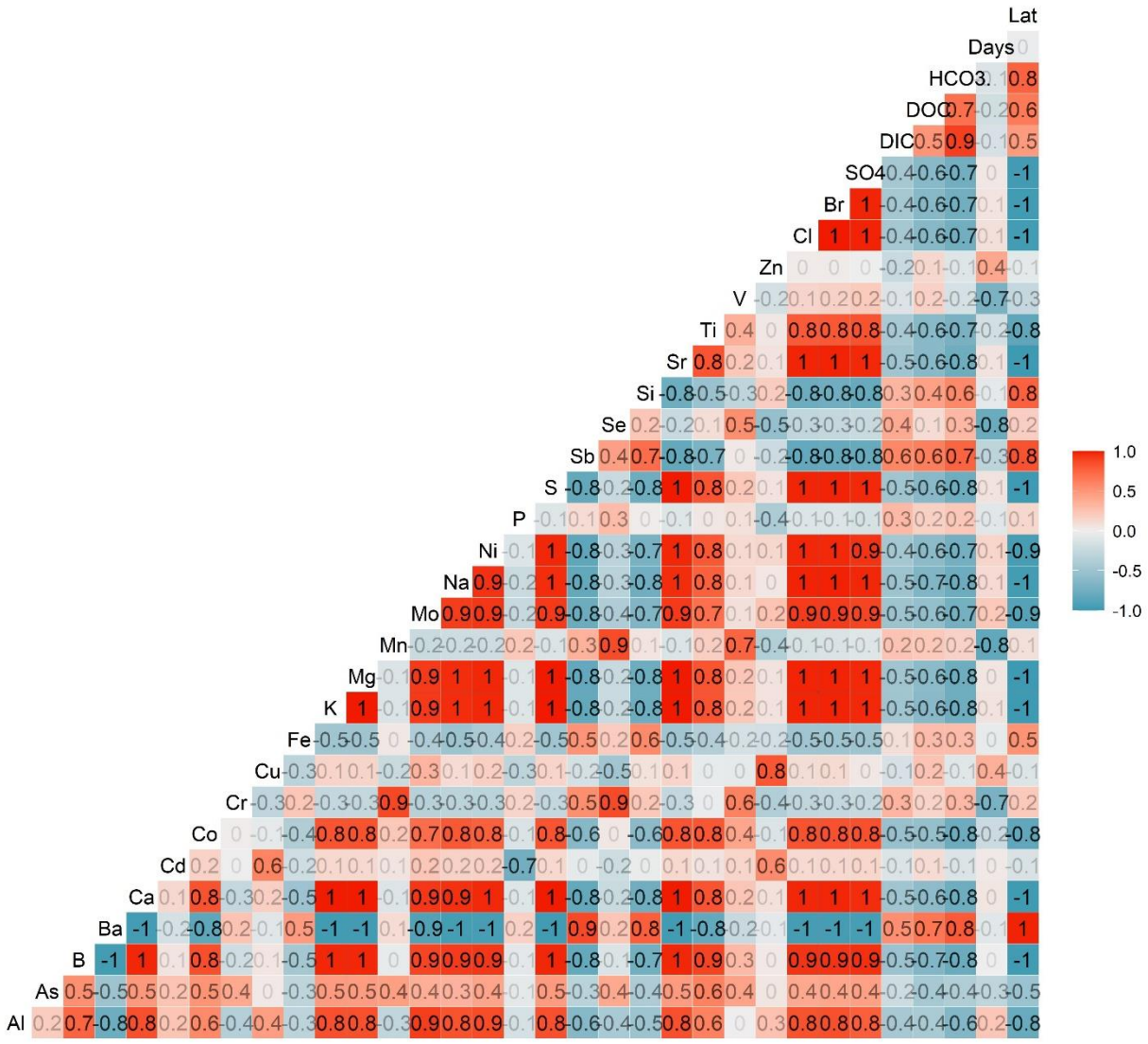

Figure B4: Dissolved load Spearman Rank correlation matrix (several elements are non-normally distributed) with color bar scale. "Days" stands for days from sampling to lab filtration and "Lat" for latitude. The MDL for one negative P reported concentration was inserted.

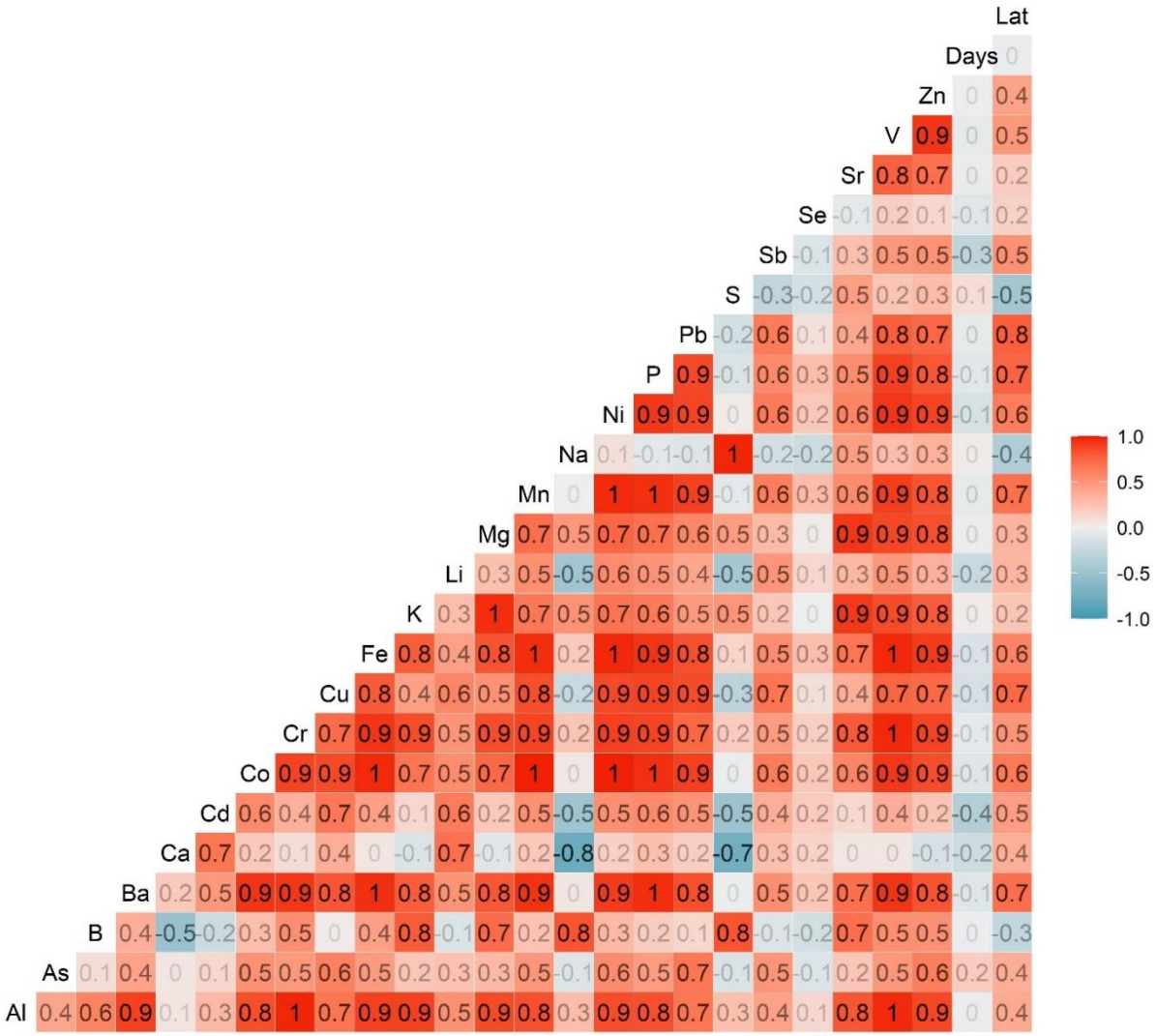

Figure B5: Suspended sediment load Spearman Rank correlation matrix (several elements are non-normally distributed) with color bar scale (detection limit values substituted in for element values <MDL). "Days" stands for days from sampling to lab filtration and "Lat" for latitude.

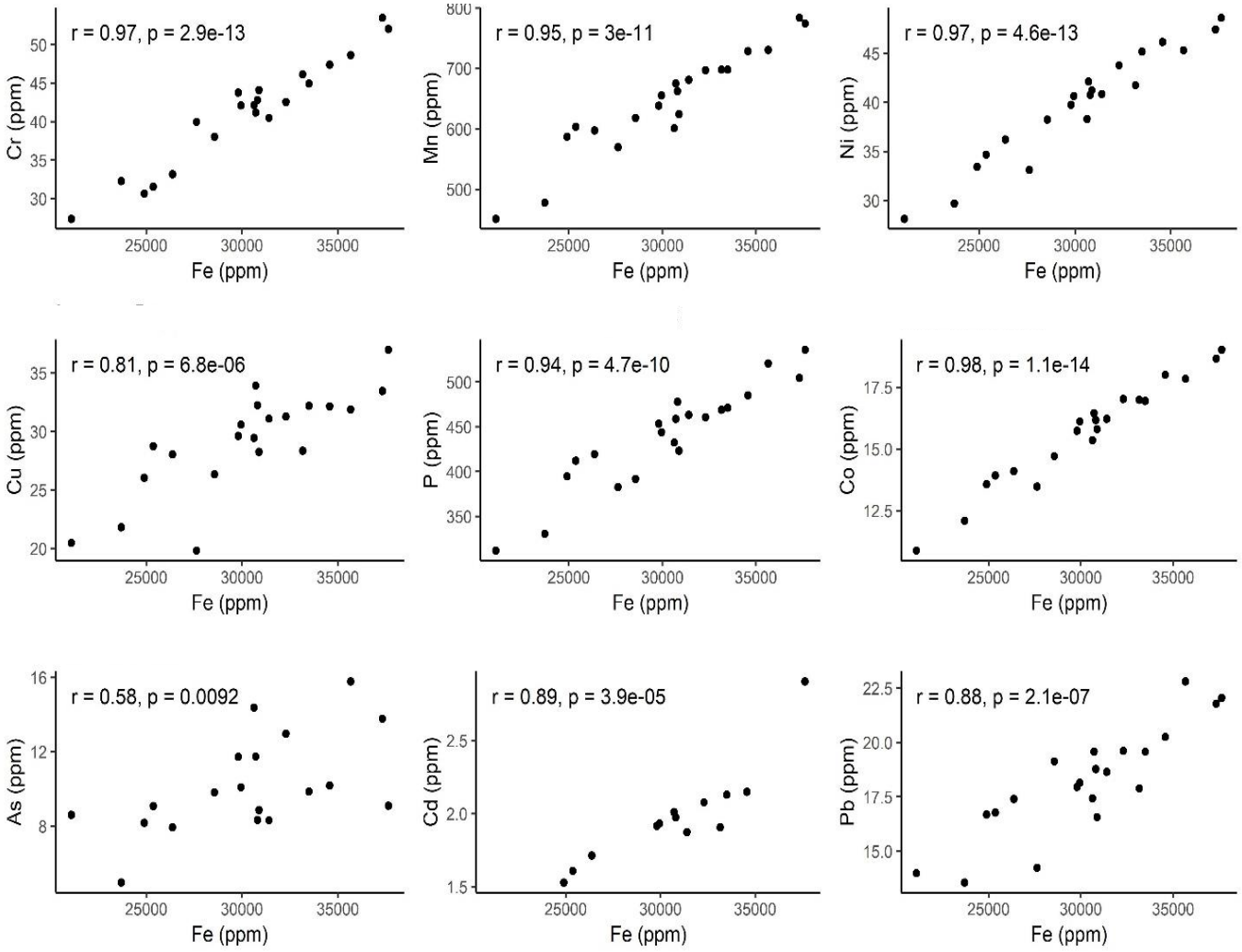

Figure B6: Several elements that showed significant positive correlations with Fe in the suspended sediment load. Concentrations <MDL are excluded. Pearson correlation coefficients and p-values are given.

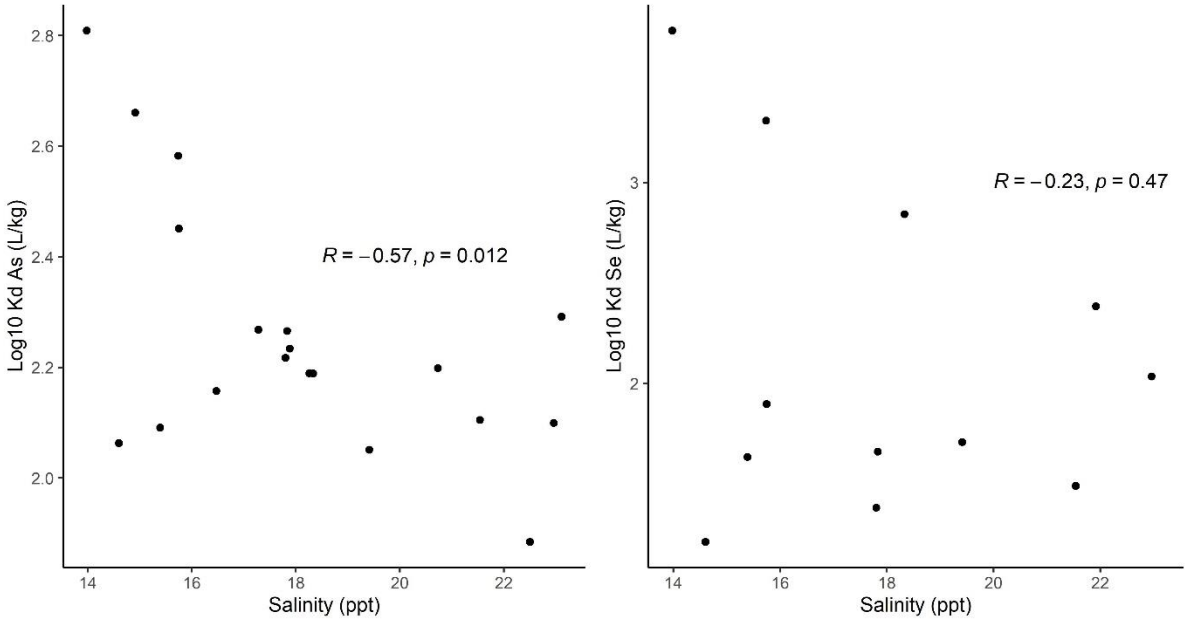

Figure B7: Salinity trends of As and Se Kd values in Log10 (L/kg) (results <MDL excluded) along the transect with increased seawater mixing. Pearson correlation coefficients and p-values are given.

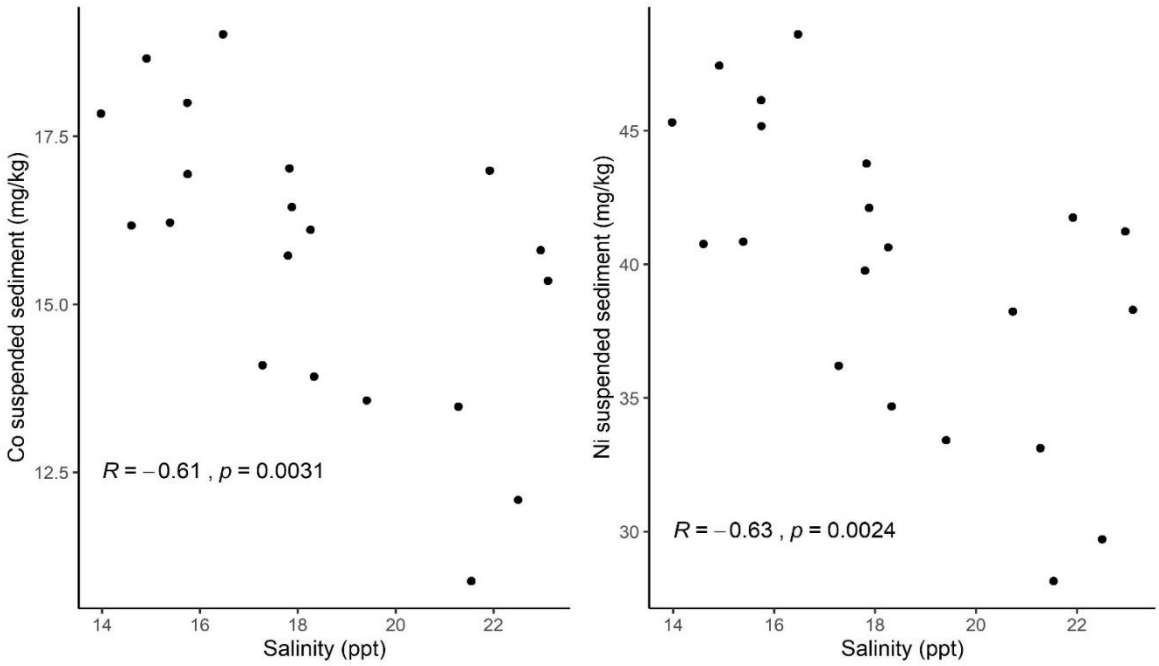

Figure B8: Cobalt and nickel suspended sediment concentration plotted against salinity, with Pearson correlation coefficients and p-values.

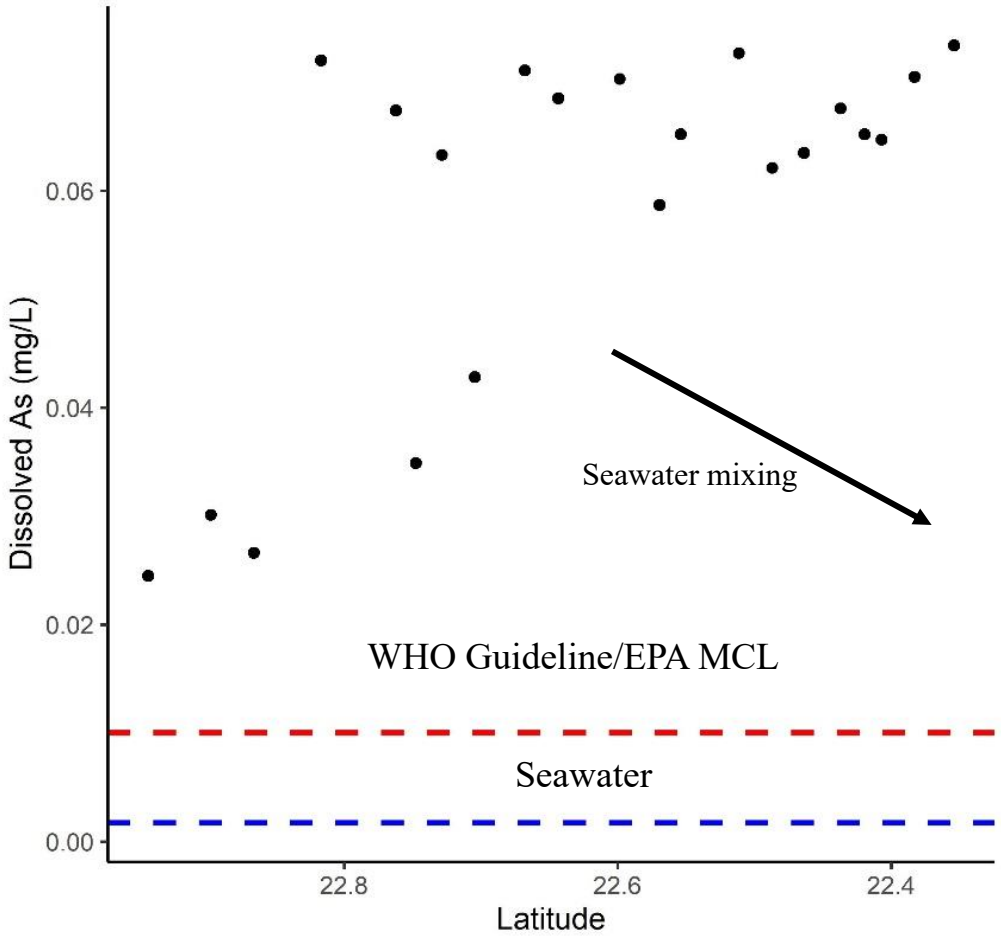

Figure B9: Dissolved As versus latitude. Correlation coefficients are ommitted because of the anchoring effect of the three high latitude values in the Bhairab River. Large scatter with no definitive trend is apparent between all other samples. Average open seawater As is 0.0017 mg/L (Mason, 2013) and is marked by the blue dashed line, while the WHO guideline/EPA MCL (0.01 mg/L) is marked by the red dashed line.

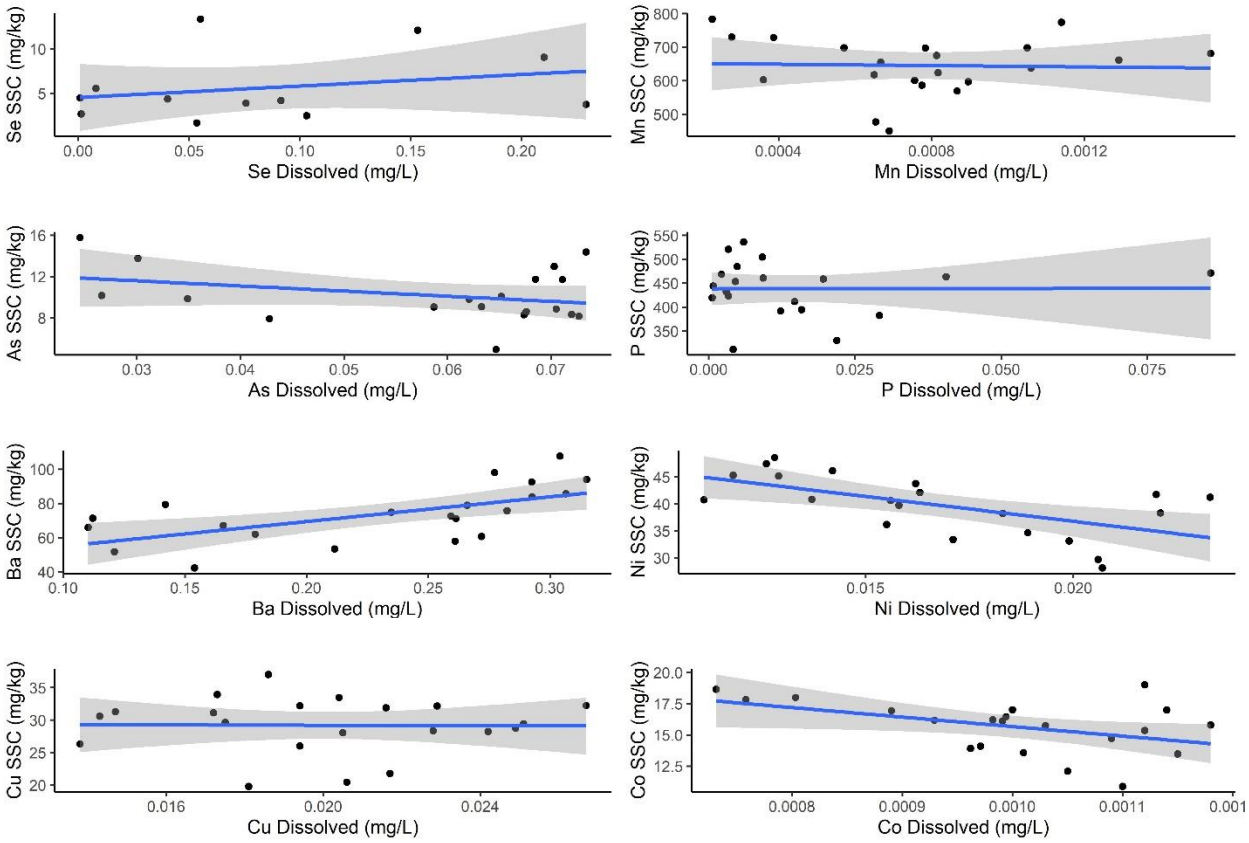

Figure B10: Element concentrations in the suspended sediment (SSC) load versus concentrations in the dissolved load. Values <MDL are omitted. The shaded gray regions represent the 95% confidence interval about the linear regression line, with linear regression statistics omitted because of the large scatter in the data (as seen with large confidence intervals).

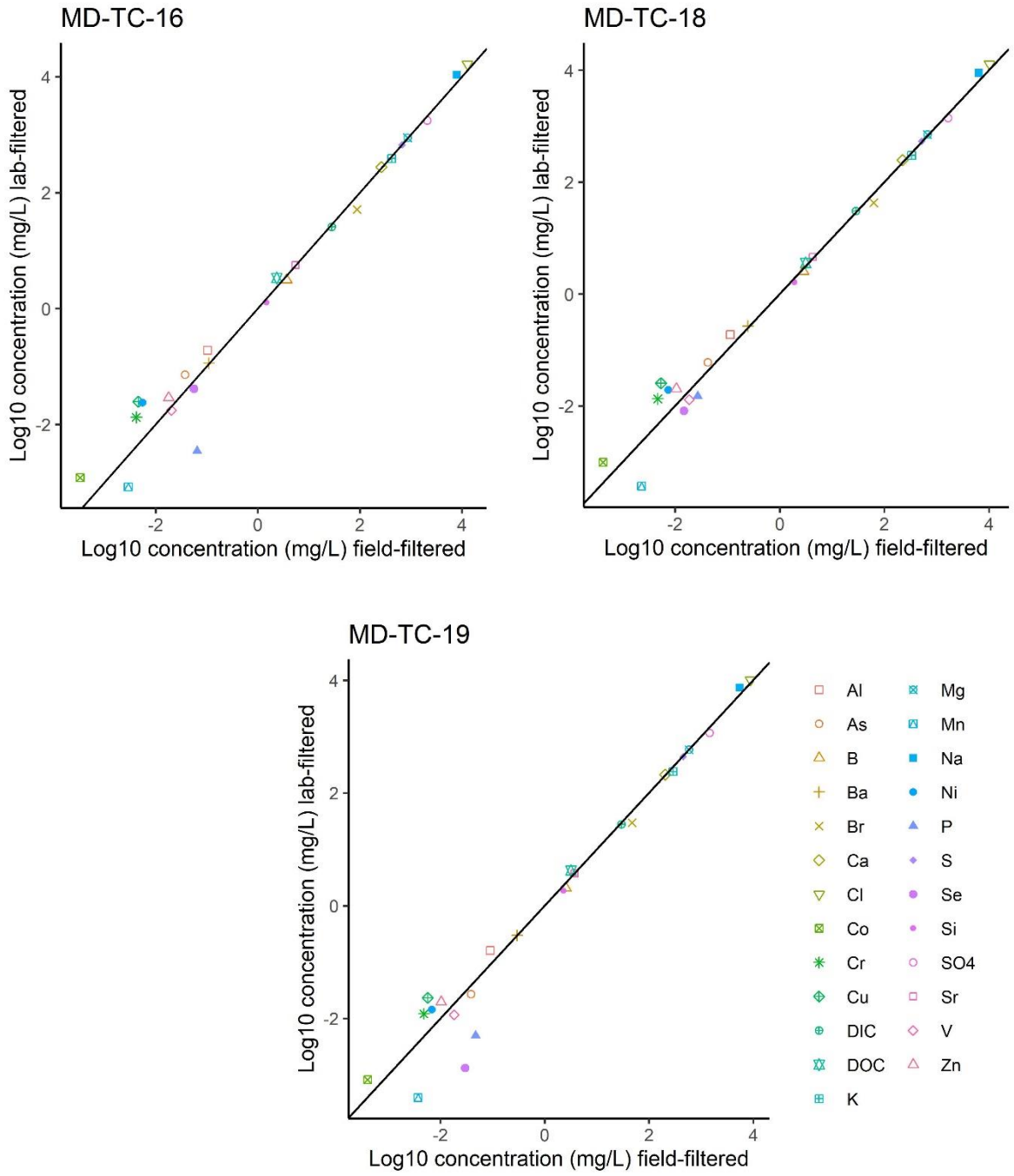

Figure B11: Comparison of field filtered dissolved load concentrations (0.45µm; Dietrich and Ayers, 2021) with lab filtered dissolved concentrations (0.2 µm; This study). Each set of samples were at the same study site. Black lines are for 1:1 comparison between sample types, with a slope of 1 and y-intercept of 0. Samples falling on the black line indicate the same concentrations in both sets of samples.

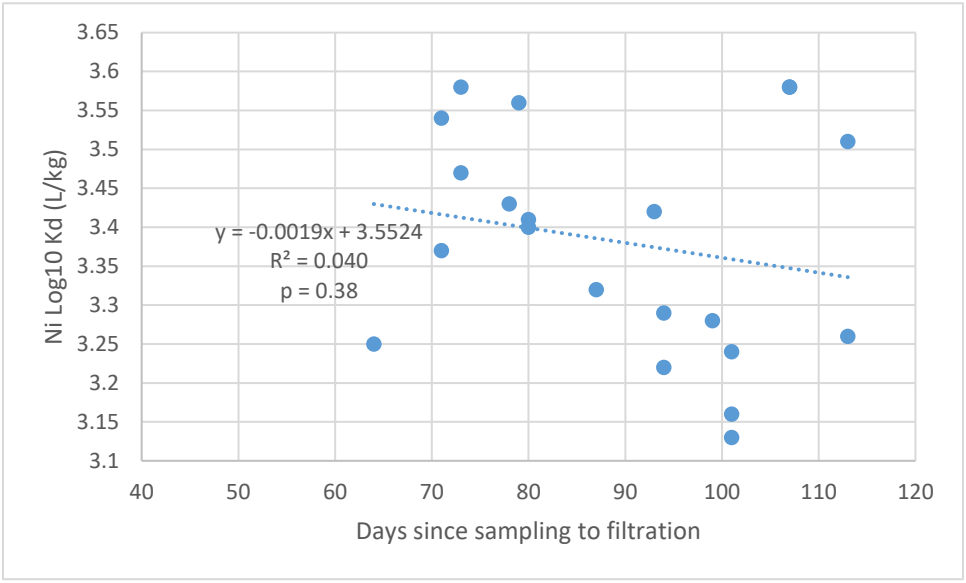

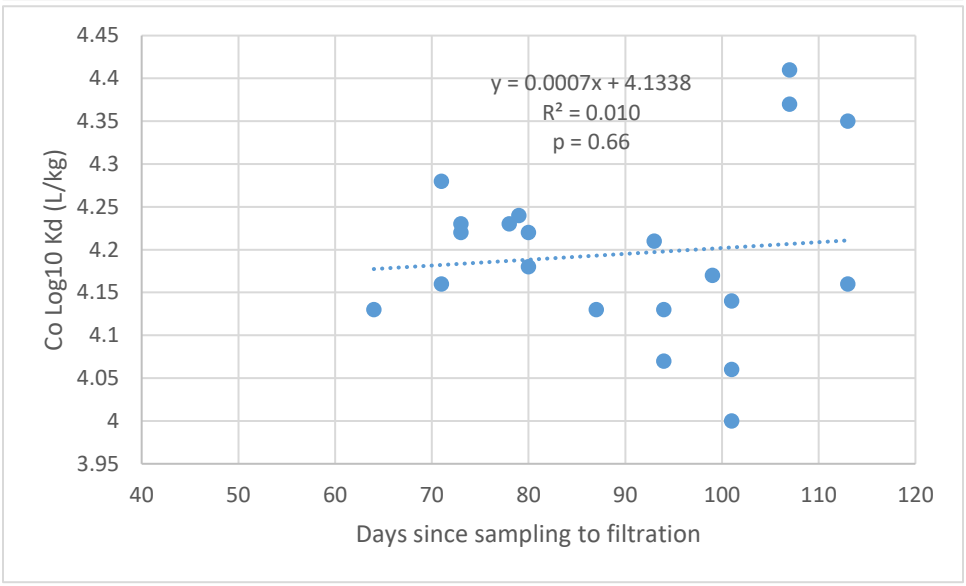

Figure B12: Days since sampling to lab filtration versus Co and Ni Kd values. Linear regression lines are provided.

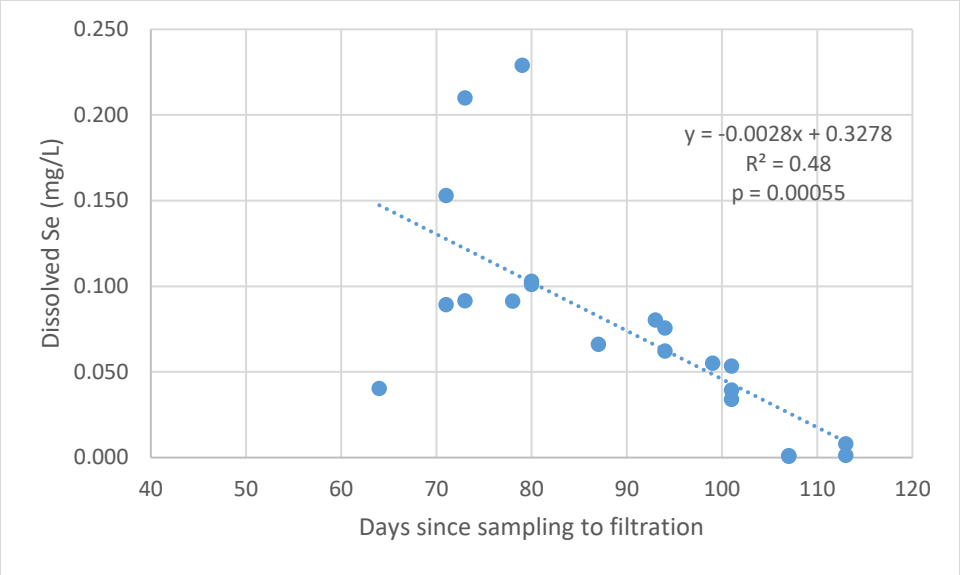

Figure B13: Days since sampling to lab filtration versus the dissolved Se concentration. The linear regression line is provided.

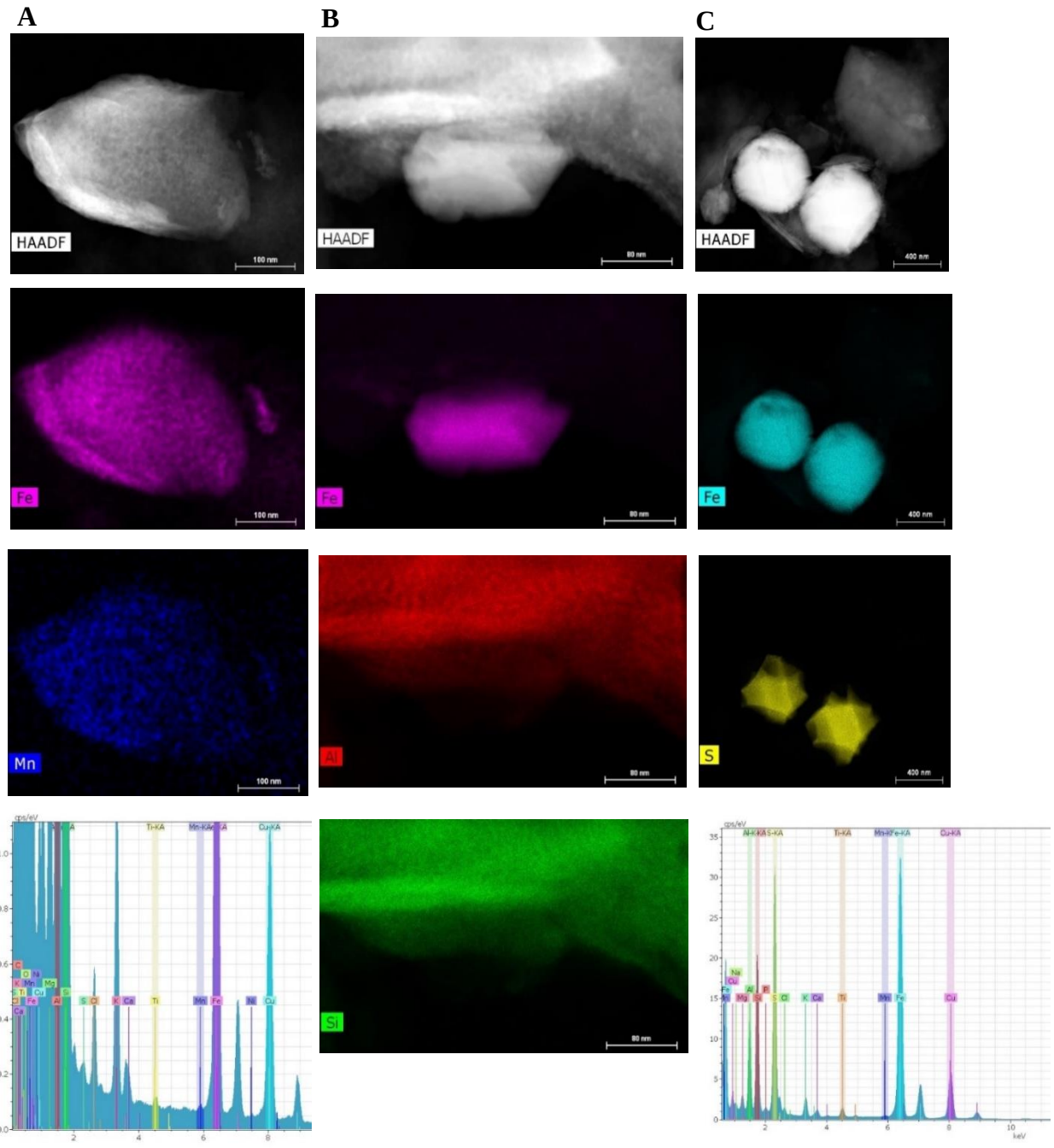

Figure B14: TEM analysis of several Fe-rich particles from samples MD-TC-7 (first two columns) and MD-TC-11 (third column), specifically showing: Column (**A**) – High-angle annular dark-field (HAADF) image, STEM-EDS maps, and EDS spectra with several element peaks identified for an Fe-rich particle (about 0.5 μm in diameter) associated with several transition metals such as Mn, Ti, Cu, and potentially Ni; Column (**B**) – HAADF image and STEM-EDS maps of Al, Si and Fe, showing the Fe-rich nanoparticle (~0.2 μm in diameter) associated with the larger aluminum silicate particle; Column (**C**) – HAADF image, STEM-EDS maps and EDS spectra, showing an Fe-sulfide particles ~0.5μm in diameter.

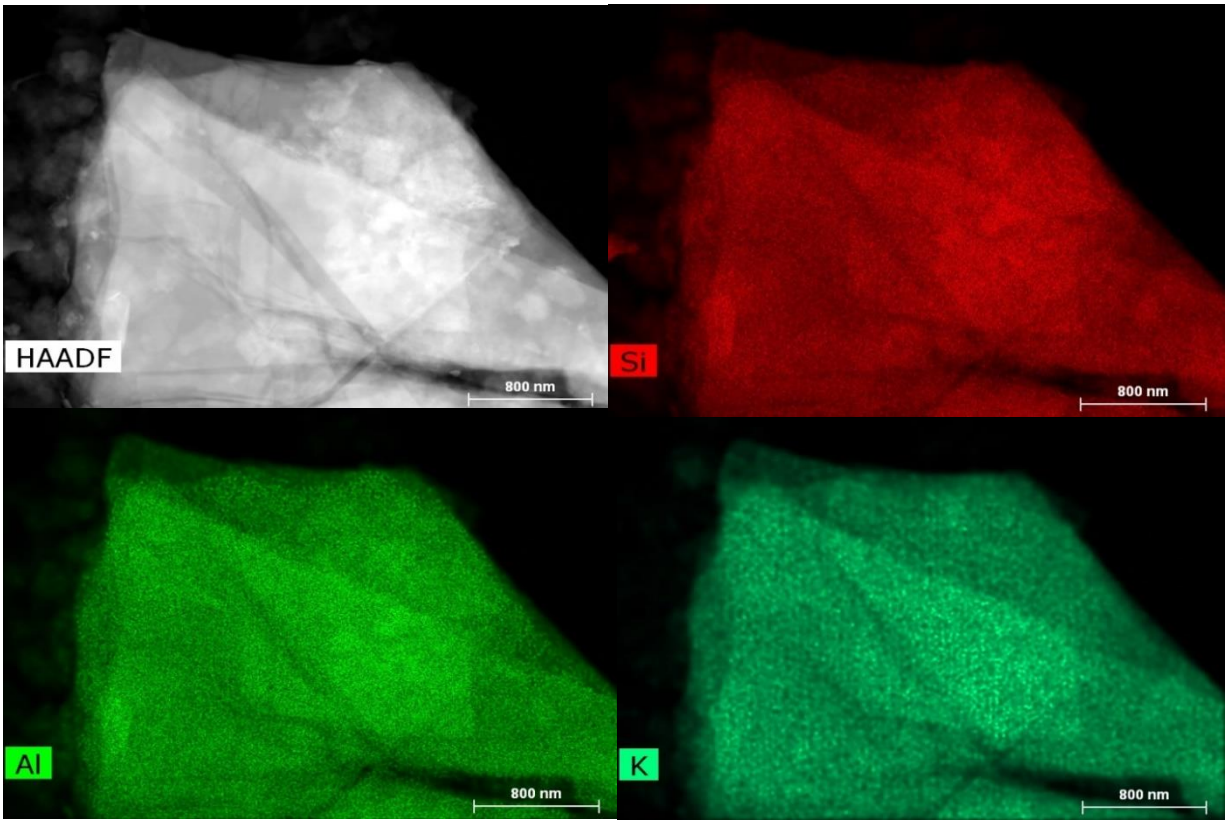

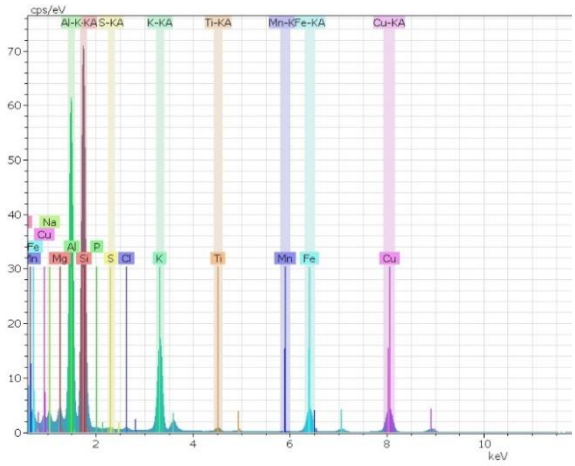

Element	series	Net	[wt.%]	[norm. wt.%]	[norm. at.%]	Error in wt.% (3 Sigma)
Silicon	K-series	298063	27.35	27.35	21.33	0.23
Aluminium	K-series	250267	22.88	22.88	18.57	2.14
Potassium	K-series	104185	9.93	9.93	5.56	0.97
Oxygen	K-series	447671	39.84	39.84	54.54	3.67
		Sum:	100	100	100	

Figure B15: TEM imaging of a K-silicate particle, potentially muscovite with other small crystals/oxides present, from sample MD-TC-11 with: a high-angle annular dark-field (HAADF) image, STEM-EDS maps, EDS spectra, and approximate wt.% and at. % concentrations of major elements present, assuming other contributions are relatively negligible.

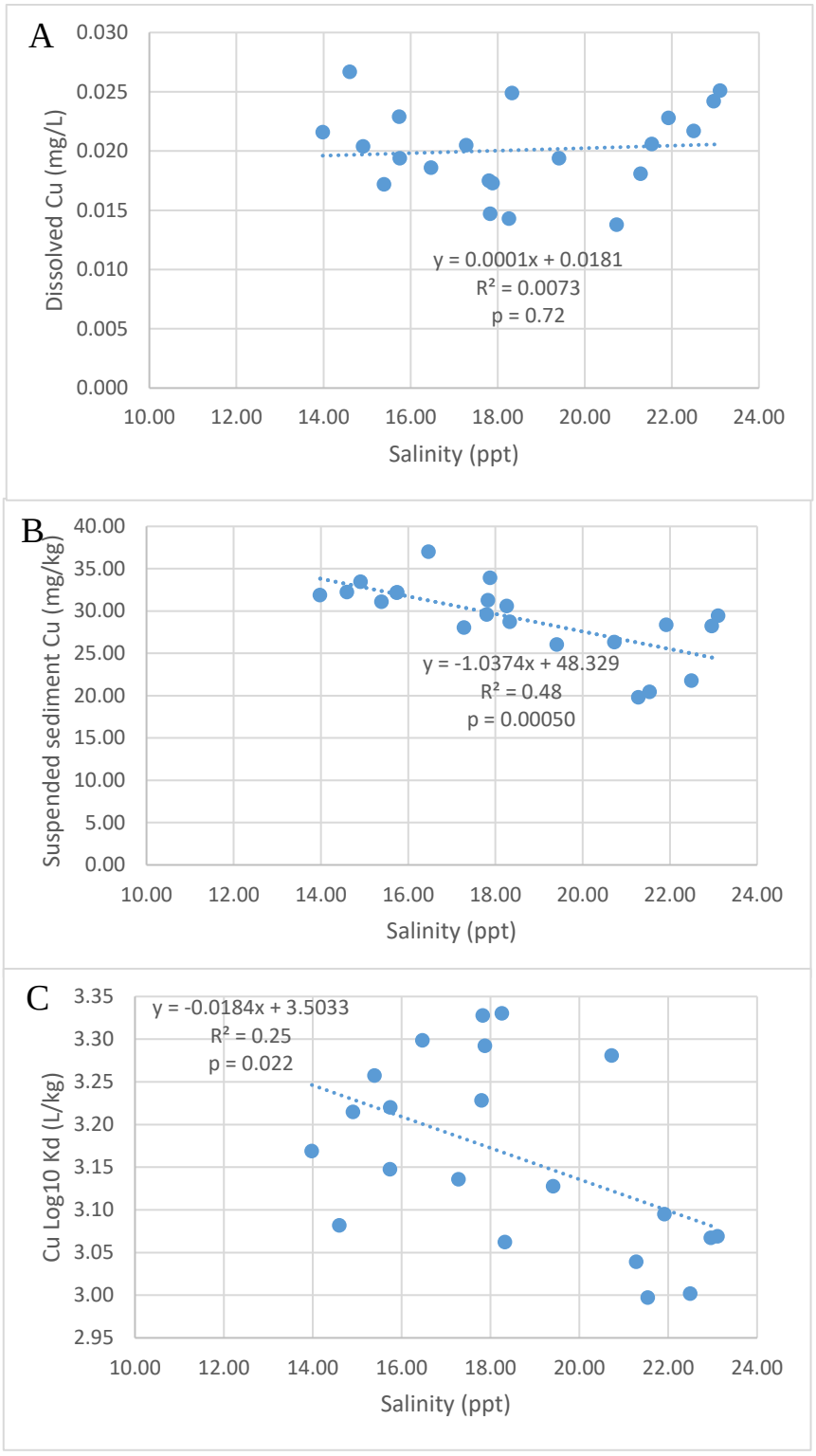

Figure B16: Dissolved (A), solid-phase suspended sediment (B), and Kd values of Cu (C) plotted against salinity. Linear regression lines are provided for each plot.

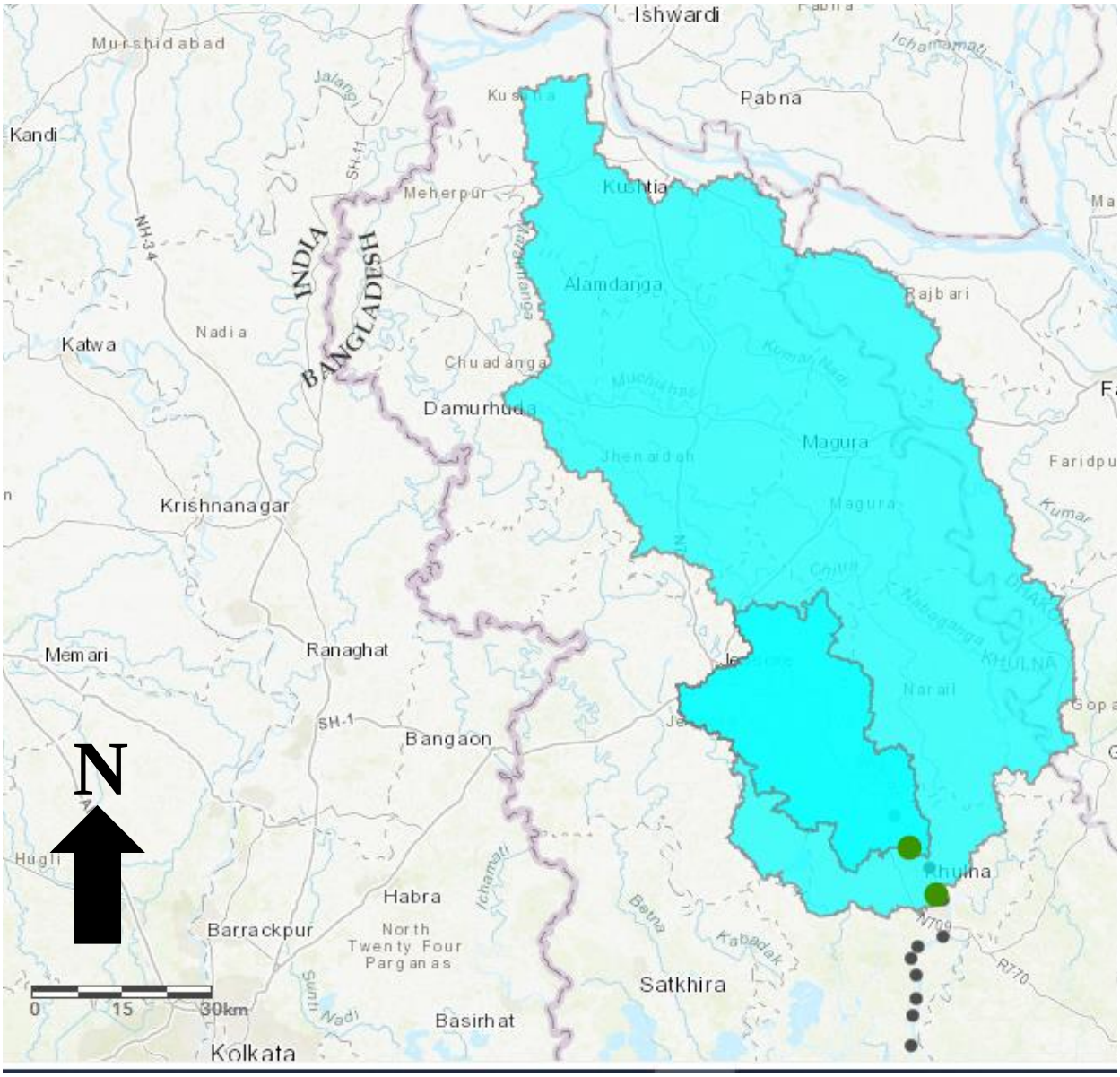

Figure B17: Watershed map for samples north of Khulna along the Bhairab River (smaller outlined watershed) and for samples south of Khulna along the Rupsha River (larger outlined watershed). Several sample sites are depicted as black dots, and the green dots represent the watershed drainage point.

Table B1: Calculated Log10 Kd (bulk solid concentration/dissolved concentration) values (L/kg) used in this study (with MDLs used when suspended sediment values <MDL). The medians and standard deviations are also provided.

Sample ID	Al	Fe	V	Zn	Cr	Ni	Co	Cu	Ba	Mn	K	Ca	Sr	Na	Mg	Sb	As	Se	B	Cd	S
MD-TC-1	5.28	7.56	3.48	3.42	3.46	3.56	4.24	3.08	2.45	5.71	1.41	1.68	0.98	-0.15	1.36	3.36	2.06	1.21	0.63	4.28	0.31
MD-TC-2	5.23	6.75	3.45	3.78	3.40	3.47	4.22	3.26	2.43	5.65	1.38	1.46	0.91	-0.02	1.34	3.51	2.09	1.63	0.63	4.32	0.36
MD-TC-3	5.25	6.83	3.54	3.90	3.51	3.54	4.28	3.22	2.46	5.82	1.41	1.45	0.94	0.15	1.36	3.27	2.45	1.90	0.73	4.99	0.46
MD-TC-4	5.33	6.98	3.53	3.99	3.53	3.58	4.23	3.30	2.55	5.83	1.47	1.44	1.01	0.32	1.40	3.66	2.16	0.99	0.89	4.48	0.59
MD-TC-5	5.06	7.05	3.38	3.75	3.37	3.37	4.16	3.14	2.35	5.82	1.23	1.59	0.88	-0.04	1.24	3.39	2.27	1.00	0.46	4.19	0.34
MD-TC-6	5.23	6.91	3.46	3.81	3.47	3.40	4.18	3.23	2.45	5.78	1.30	1.69	0.92	-0.18	1.28	3.46	2.22	1.38	0.58	4.36	0.25
MD-TC-7	5.19	6.93	3.50	3.93	3.48	3.41	4.22	3.29	2.44	5.92	1.28	1.58	0.88	-0.12	1.28	3.59	2.23	0.95	0.57	4.49	0.28
MD-TC-8	5.20	6.88	3.52	3.84	3.49	3.43	4.23	3.33	2.47	5.95	1.30	1.58	0.90	-0.04	1.29	3.42	2.27	1.66	0.62	4.55	0.34
MD-TC-9	5.24	7.09	3.51	3.85	3.49	3.42	4.21	3.33	2.50	5.99	1.31	1.63	0.90	-0.25	1.28	3.63	2.19	1.05	0.59	4.31	0.27
MD-TC-10	5.00	7.01	3.40	3.72	3.37	3.29	4.13	3.13	2.40	5.88	1.13	1.52	0.78	-0.21	1.16	3.04	2.05	1.71	0.44	4.27	0.25
MD-TC-11	5.17	7.33	3.48	3.90	3.48	3.32	4.13	3.28	2.54	5.98	1.21	1.29	0.79	0.08	1.19	3.45	2.20	1.13	0.67	4.33	0.40
MD-TC-12	5.14	7.33	3.49	3.87	3.48	3.22	4.07	3.04	2.61	5.82	1.32	1.32	1.01	0.56	1.29	2.83	1.13	1.16	0.99	4.26	0.82
MD-TC-13	4.96	7.11	3.34	3.54	3.32	3.13	4.00	3.00	2.44	5.82	1.05	1.18	0.67	0.01	1.06	3.42	2.10	1.49	0.51	3.84	0.33
MD-TC-14	5.17	6.95	3.58	3.35	3.56	3.28	4.17	3.09	2.75	6.09	1.28	1.43	0.84	0.06	1.23	3.35	1.12	2.38	0.75	4.30	0.44
MD-TC-15	5.05	7.16	3.28	3.35	3.41	3.16	4.06	3.00	2.63	5.86	1.12	1.30	0.74	0.12	1.10	2.93	1.88	1.36	0.61	4.17	0.42
MD-TC-16	5.16	7.42	3.46	3.50	3.53	3.25	4.13	3.07	2.80	5.88	1.25	1.31	0.84	0.21	1.20	3.65	2.10	2.04	0.76	3.78	0.51
MD-TC-17	5.17	7.13	3.48	3.45	3.51	3.24	4.14	3.07	2.78	5.90	1.22	1.25	0.79	0.15	1.18	3.38	2.29	1.42	0.79	2.75	0.47
MD-TC-18	4.95	6.98	3.46	3.53	3.38	3.26	4.16	3.06	2.35	6.22	1.17	1.57	0.82	-0.22	1.19	3.37	2.19	2.84	0.40	4.28	0.28
MD-TC-19	5.26	6.83	3.68	3.67	3.60	3.51	4.35	3.15	2.50	6.27	1.47	1.61	0.98	-0.07	1.39	3.38	2.58	3.31	0.72	4.30	0.39
MD-TC-20	5.38	7.09	3.74	3.64	3.62	3.58	4.41	3.21	2.55	6.54	1.54	1.48	1.04	0.26	1.45	3.57	2.66	2.93	0.93	4.32	0.57
MD-TC-21	5.32	7.10	3.72	3.53	3.61	3.58	4.37	3.17	2.47	6.42	1.50	1.45	1.03	0.23	1.45	3.51	2.81	3.76	0.85	3.94	0.57
Median	5.19	7.05	3.48	3.72	3.48	3.40	4.18	3.15	2.47	5.88	1.30	1.46	0.90	0.01	1.28	3.42	2.19	1.49	0.63	4.30	0.39
Standard Deviation	0.12	0.21	0.11	0.20	0.08	0.14	0.10	0.11	0.13	0.23	0.13	0.15	0.10	0.21	0.11	0.22	0.40	0.82	0.16	0.42	0.14

Table B2: Trace element concentrations in surface water samples in recent studies in Southwest Bangladesh.

As[1]	**Cd**	**Cu**	**Cr**	**Fe**	**Mn**	**Ni**	**Pb**	**Zn**	**Months of sampling**	**Location**	**Study**
57.0	0.1	20.2	13.7	2.6	0.7	16.7	<MDL	16.5	May	Bhairab-Rupsha-Bhadra-Shibsa Rivers	This study
8.0				98.0					June-Aug	Ponds/Lakes in Rupsha Upazila	Ahmed et al. (2020)
3.5	6.5		45.2	976.6	288.5	18.7	18.4	68.4	March-May	Rupsha River Basin	Islam et al. (2020)
12.3	9.8		40.0	2062.0	65.4	21.4	26.6	33.8	March-May	Pasur River Basin	Islam et al. (2020)
5.5	1.0	5.4	7.2			3.9	7.1		Aug-Sept	Rupsha River	Proshad et al. (2020)
6.1	1.4	6.0	8.9			5.5	7.3		Jan-Feb	Rupsha River	Proshad et al. (2020)

[1]All concentrations are mean values, in µg/L.

References

Ahmed, A., Ghosh, P. K., Hasan, M., & Rahman, A. (2020). Surface and groundwater quality assessment and identification of hydrochemical characteristics of a south-western coastal area of Bangladesh. Environmental monitoring and assessment, 192(4), 1-15.

Dietrich, M., & Ayers, J. C. (2021). Influences on tidal channel and aquaculture shrimp pond water chemical composition in Southwest Bangladesh. *Geochemical Transactions*, 22(1), 1-22. https://doi.org/10.1186/s12932-021-00074-2

Gaillardet, J., Viers, J., Dupré, B. (2014). Trace Elements in River Waters in: Surface and Ground Water, Weathering and Soils, *Treatise on Geochemistry*. https://doi.org/10.1016/B978-0-08-095975-7.00507-6

Islam, A. R. M. T., Islam, H. T., Mia, M. U., Khan, R., Habib, M. A., Bodrud-Doza, M., ... & Chu, R. (2020). Co-distribution, possible origins, status and potential health risk of trace elements in surface water sources from six major river basins, Bangladesh. Chemosphere, 249, 126180.

Mason, R. P. (2013). Trace metals in aquatic systems. John Wiley & Sons.

Proshad, R., Islam, S., Tusher, T. R., Zhang, D., Khadka, S., Gao, J., & Kundu, S. (2020). Appraisal of heavy metal toxicity in surface water with human health risk by a novel approach: a study on an urban river in vicinity to industrial areas of Bangladesh. Toxin Reviews, 1-17.

Supporting Information for Chapter IV

Table C1: Additional pond sediment physiochemical data

Aquaculture pond sediment data for grain size (in μm) from laser granulometry (Dx values refer to the percentile of the sample grain size distribution data, thus Dx (50) is the median), total carbon (TC), total inorganic carbon (TIC), total organic carbon (TOC), and loss on ignition data for adsorbed water (H2O-) and structural water content (H2O+).

	KA-12	KA-13	KA-13U	KA-14	KA-15	KA-16	KA-17
Surface area moment mean	10.80	10.89	12.39	13.62	19.41	14.45	12.16
Volume moment mean	19.66	26.12	24.92	25.15	69.71	29.81	23.73
Dx (5)	3.98	3.87	4.34	4.63	5.27	4.75	4.36
Dx (16)	6.21	6.21	7.05	7.75	10.15	7.99	6.94
Dx (25)	8.01	8.08	9.39	10.69	15.53	11.04	9.12
Dx (50)	15.31	15.30	18.13	21.36	39.87	23.43	17.42
Dx (75)	27.79	29.19	32.91	35.94	97.87	43.67	32.19
Dx (84)	34.64	39.29	42.80	43.62	138.94	54.39	41.90
Dx (95)	49.37	74.51	70.39	59.16	235.43	75.45	65.55
Mode	24.40	15.99	21.87	31.61	39.58	42.02	20.14
TC (%)	1.62	1.76	1.85	1.59	2.61	2.34	2.17
TIC (%)	0.06	0.07	0.09	0.05	0.04	0.08	0.07
TOC (%)	1.56	1.69	1.76	1.54	2.57	2.26	2.10
H2O- (%)	2.10	2.65	1.98	1.68	2.91	2.37	2.08
H2O+ (%)	8.81	10.65	9.44	7.13	12.57	11.24	10.76

	KA-18	KA-19	KA-20	KA-21	*Geometric mean*	*Standard deviation*
Surface area moment mean	11.04	11.82	14.75	16.05	13.18	2.64
Volume moment mean	24.30	26.79	28.06	33.94	28.44	13.60
Dx (5)	3.79	4.00	4.94	5.11	4.43	0.52
Dx (16)	6.21	6.59	8.31	8.76	7.38	1.26

Dx (25)	8.18	8.80	11.53	12.43	10.04	2.31
Dx (50)	16.17	17.75	23.35	27.23	20.50	7.24
Dx (75)	31.73	35.40	40.33	49.62	38.76	19.78
Dx (84)	43.02	48.57	49.33	61.31	50.18	29.00
Dx (95)	74.68	82.88	67.47	85.15	77.83	50.77
Mode	18.23	19.55	35.73	46.90	26.93	10.85
TC (%)	1.86	2.03	2.87	2.17	2.04	0.41
TIC (%)	0.06	0.07	0.11	0.06	0.07	0.02
TOC (%)	1.80	1.96	2.76	2.11	1.98	0.40
H2O- (%)	2.22	2.29	1.87	2.22	2.19	0.35
H2O+ (%)	8.66	9.53	9.52	8.09	9.56	1.54

Table C2: NIST 1566b – Oyster Tissue concentrations and volatilization correction factors

NIST 1566b – Oyster Tissue reference material element concentrations of regular digested material and ashed material compared to the NIST standard values, with % recovery for un-ashed material on the ICP-OES, and the Ash/Raw digested ratio representing the "volatilization correction factor" of the elements in the ashing process for 1 hour @ 350°C. All concentrations in mg/kg.

	Digested	**Ash***	**NIST value**	**% Recovery**	**Digested% deviation from NIST digested standard value**	**Ash/Digested**
Al	124.3	172.3	197.2	63.03	-36.97	1.39
As	8.931	105.4	7.65	116.75	16.75	11.80
B	7.78	<0.851				
Ba	8.073	17.23				2.13
Be	<0.851	<0.851				
Ca	861.2	2045	838	102.77	2.77	2.37
Cd	2.721	5.978	2.48	109.72	9.72	2.20
Co	<0.851	0.9311	0.371			
Cr	<0.851	<0.851				
Cu	79.62	58.02	71.6	111.20	11.20	0.73
Fe	219.9	338.6	205.8	106.85	6.85	1.54
K	7156	15950	6520	109.75	9.75	2.23
Li	<0.171	1.134				
Mg	1089	2807	1085	100.37	0.37	2.58
Mn	20.99	51.9	18.5	113.46	13.46	2.47
Mo	0.3049	8.992				29.49

Na	3110	6410	3297	94.33	-5.67	2.06
Ni	1.27	14.3	1.04	122.12	22.12	11.26
P	7416	18530				2.50
Pb	<0.418	<0.418	0.308			
S	6593	2359	6890	95.69	-4.31	0.36
Sb	0.5669	<0.360				
Se	4.055	<0.895	2.06	196.84	96.84	
Si	319.2	24.18				0.08
Sr	6.785	12.54				1.85
Tl	<1.034	<1.034				
V	0.5202	<0.117	0.577	90.16	-9.84	
Zn	1599	3861	1424	112.29	12.29	2.41

*based on ash weight (not by raw material weight)

Table C3: NIST 2711 – Montana Soil concentrations and volatilization correction factors

NIST 2711 – Montana Soil reference material results (3 replicates) following $LiBO_2$ fusion methods and solution analysis on the ICP-OES and ICP-MS. Arithmetic mean and standard deviations of % recovery are provided, along with "volatilization correction factor" results, which are the concentrations of the $LiBO_2$ fusion samples/reference value of the reference standard, and essentially the same as NIST oyster "volatilization correction factors," although because of the higher temperatures in the $LiBO_2$ fusion method, nearly all elements were volatilized significantly.

	NIST 2711 Mean % recovery	**NIST 2711 STDEV % recovery**	**NIST 2711 Mean volatilization correction factor**	**NIST 2711 STDEV volatilization correction factor**
Al	89.40	8.46	1.12	0.08
Ba	84.61	2.71	1.18	0.03
Ca	92.52	3.19	1.08	0.03
Fe	92.07	3.06	1.09	0.03
K	75.86	2.97	1.32	0.03
Mg	74.64	3.39	1.34	0.03
Na	46.49	1.52	2.15	0.02
P	63.60	2.94	1.57	0.03
Si	78.06	1.53	1.28	0.02
Sr	81.42	2.51	1.23	0.03
As	11.63	3.79	8.60	0.04
Cd	4.60	5.37	21.74	0.05
Co	77.04	2.45	1.30	0.02
Cr	66.83	4.11	1.50	0.04
Cu	72.91	2.34	1.37	0.02

Mn	76.86	1.45	1.30	0.01
Ni	106.22	7.35	0.94	0.07
Pb	31.84	11.68	3.14	0.12
Sb	45.52	4.67	2.20	0.05
Se	67.94	51.38	1.47	0.51
Ti	73.59	2.22	1.36	0.02
V	62.46	2.57	1.60	0.03
Zn	55.47	6.72	1.80	0.07
S	73.90	2.86	1.35	0.03

Table C4: **Instrument method detection limits (MDLs)**

Method detection limits (MDLs) for all analytical instruments used in this study in µg/L. OSU stands for Ohio State University.

Elements	**ICP-OES (OSU)**	**ICP-OES**	**ICP-MS**	***Species***	**IC**	**TOC**
Al	137.73	6.40		Cl	9.80	
As	851.00	8.20	0.18	NO3-	10.20	
B	851.00	5.90		PO4---	22.00	
Ba	851.00	4.90	0.36	SO4--	19.60	
Be	851.00		0.17	DIC		79.00
Ca	936.58	10.10		DOC		96.00
Cd	851.00		0.09			
Co	851.00		0.11			
Cr	851.00		0.26			
Cu	60.10		0.20			
Fe	131.11	8.90	0.73			
K	14569.12	8.10				
Li	171.00					
Mg	660.71	5.10				
Mn	16.48		0.16			
Mo	159.00		0.16			
Na	6371.27	9.50				
Ni	115.00		0.26			
P	719.17	11.00				
Pb	418.00		0.09			
S	2401.92	9.60				
Si		8.40				
Sb	360.00		0.07			
Se	895.00		0.31			
Sr	20.38	5.20				

Ti			0.23			
Tl	1034.00		0.10			
V	1000.00		0.13			
Zn	271.36		0.45			

Table C5: **Log10 Kd values**

Calculated log10 Kd values of shrimp pond data and sediment extract data, with arithmetic means and standard deviations also provided. Units are in L/kg.

Kd Residual Sediment/Extract	**KA-12**	**KA-13**	**KA-13-U**	**KA-14**	**KA-15**	**KA-16**	**KA-17**
Al	5.82	6.22	6.17	4.93	6.59	6.14	5.62
Ba	4.43	4.17	4.06	3.85	4.11	3.96	4.06
Ca	2.70	2.03	1.94	2.57	1.65	1.91	2.22
Fe	4.82	5.40	5.36	3.90	5.46	5.34	4.88
K	3.30	3.08	2.94	3.04	3.04	2.86	3.00
Mg	3.05	2.44	2.21	2.82	2.24	2.20	2.46
Na	1.25	1.47	0.70	1.50	1.22	1.05	1.19
P	3.11	3.16	3.03	3.15	3.24	3.04	3.05
S[1]	1.05	0.32	0.26	1.16	0.28	0.13	0.55
Si	4.66	4.92	4.10	4.82	4.77	4.11	4.28
Sr	2.41	2.09	2.05	2.45	2.04	1.90	2.08
As	2.94	2.89	2.77	2.96	2.87	2.44	2.47
Cd	3.94	4.26	4.32	4.21	4.47	3.88	4.03
Co	4.25	4.57	4.59	3.95	4.03	4.39	4.33
Cr	4.72	5.00	4.99	3.98	5.31	4.65	4.53
Cu	3.23	3.74	3.50	3.45	3.51	3.39	3.51
Mn	4.70	3.46	3.39	3.67	2.91	3.60	3.57
Ni	3.81	4.05	3.95	3.65	4.00	3.78	4.05
Pb	3.13	3.30	3.34	3.43	3.55	3.04	2.87
Sb	2.99	2.87	2.71	2.76	2.53	2.12	
Se	2.01	2.54	2.33	4.03	3.08	3.46	3.83
Ti	5.22	5.97	5.83	4.15	5.93	5.64	5.19
V	4.20	3.90	3.79	3.48	3.83	3.58	3.38
Zn	3.30	3.50	3.42	3.17	3.36	3.22	3.58

Kd Residual Sediment/Extract	**KA-18**	**KA-19**	**KA-20**	**KA-21**	**Arithmetic mean**	**Std dev**
Al	5.10	6.04	6.20	5.97	5.89	0.50
Ba	4.28	4.08	4.09	4.09	4.11	0.15
Ca	2.92	1.54	2.29	1.90	2.15	0.43

Fe	4.88	5.24	5.20	5.24	5.06	0.45
K	3.49	2.95	2.94	2.92	3.05	0.19
Mg	3.20	2.23	2.52	2.26	2.51	0.36
Na	1.62	1.13	1.34	1.30	1.25	0.25
P	2.85	3.08	3.24	3.15	3.10	0.11
S[1]	1.38	0.17	0.60	0.22	0.55	0.44
Si	4.03	4.75	4.77	4.48	4.52	0.33
Sr	2.44	1.75	2.19	2.00	2.13	0.23
As	2.52	3.03	2.60	2.67	2.74	0.21
Cd	4.56	4.50	3.81	3.91	4.17	0.27
Co	4.67	4.54	4.46	4.49	4.39	0.23
Cr	4.76	4.90	4.58	4.57	4.73	0.34
Cu	3.55	3.63	3.46	3.56	3.50	0.13
Mn	4.37	4.30	3.62	3.75	3.76	0.51
Ni	4.39	3.87	3.89	3.94	3.94	0.19
Pb	3.46	3.61	2.87	2.91	3.23	0.28
Sb				2.20	2.60	0.33
Se	5.90	3.79	3.73	4.09	3.53	1.06
Ti	5.17	5.75	5.87	5.92	5.51	0.55
V	3.55	3.64	3.59	3.71	3.69	0.23
Zn	3.12	3.40	3.48	3.59	3.38	0.16

[1]Non-residual sediment values.

Kd Pond Sediment/Pond Water	**KA-12**	**KA-13**	**KA-13-U**	**KA-14**	**KA-15**	**KA-16**	**KA-17**	**KA-18**
Al	5.89	5.93	5.99	5.89	5.96	5.94	5.95	5.96
Ba	3.28	3.42	3.43	3.26	3.23	3.26	3.37	3.31
Ca	1.47	1.67	1.73	1.50	1.46	1.80	1.75	1.88
K	1.90	1.88	1.89	1.97	1.99	1.94	1.89	2.42
Mg	1.32	1.33	1.35	1.32	1.42	1.40	1.32	1.80
Na	0.26	0.23	0.26	0.32	0.30	0.25	0.23	0.54
P	4.20	3.99	4.01	4.31	4.22	4.02	4.25	4.03
S	-0.09	-0.17	-0.12	-0.06	0.06	-0.10	-0.02	0.38
Si	5.22	5.43	5.47	5.10	5.31	5.60	5.19	5.03
Sr	1.26	1.29	1.32	1.39	1.33	1.37	1.29	1.69
As	2.58	2.61	2.66	2.79	2.76	2.50	2.65	2.62
Co	4.53	4.82	4.83	4.59	4.73	4.71	4.63	4.62
Cr	4.31	4.52	4.53	4.20	4.38	4.31	4.34	4.25
Cu	3.79	3.95	3.95	4.03	4.00	4.12	4.02	4.24
Mn	5.05	5.21	5.24	5.09	5.24	5.18	5.15	5.14
Ni	3.74	4.04	4.11	3.69	3.96	3.82	3.96	3.94

Se	1.49	1.56	1.39	2.47	2.53	2.71	2.81	2.94
V	3.61	3.65	3.67	3.70	3.79	3.65	3.66	3.82
Zn	3.43	3.91	4.03	3.77	3.99	3.79	3.71	3.80

Kd Pond Sediment/Pond Water	**KA-19**	**KA-20**	**KA-21**	**Arithmetic mean**	**Std dev**
Al	5.88	5.91	5.99	5.93	0.04
Ba	3.34	3.39	3.35	3.33	0.07
Ca	1.65	1.80	1.71	1.67	0.14
K	2.11	1.90	2.05	1.99	0.16
Mg	1.54	1.34	1.46	1.42	0.14
Na	0.28	0.24	0.33	0.30	0.09
P	3.30	4.24	4.41	4.09	0.30
S	0.21	0.00	-0.03	0.01	0.16
Si	5.30	5.01	5.27	5.27	0.18
Sr	1.46	1.34	1.42	1.38	0.12
As	2.61	2.39	2.68	2.62	0.11
Co	4.90	4.75	4.64	4.71	0.11
Cr	4.32	4.36	4.33	4.35	0.10
Cu	3.92	3.99	4.24	4.02	0.14
Mn	5.11	5.14	3.85	5.04	0.40
Ni	4.06	3.94	5.32	4.05	0.44
Se	2.82	2.42	2.98	2.37	0.60
V	3.51	3.55	3.66	3.66	0.09
Zn	3.94	3.95	4.02	3.85	0.18

Table C6: **Batch extract concentrations**

24-hr sediment extract concentrations in mg/L after filtration at 0.45 µm.

Sample ID	**BLANK**	**KA-12**	**KA-13**	**KA-13-U**	**KA-14**	**KA-15**	**KA-16**	**KA-17**	**KA-18**
Al	0.00	0.11	0.05	0.06	0.86	0.02	0.06	0.20	0.62
B	0.48	2.36	1.37	4.89	0.92	0.84	6.63	5.65	7.32
Ba	0.00	0.02	0.03	0.04	0.07	0.04	0.05	0.04	0.03
Ca	0.85	13.88	99.24	134.77	19.47	111.15	151.40	79.95	11.16
K	0.55	11.52	21.21	30.63	23.19	24.61	37.41	28.58	8.67
Mg	0.19	11.69	52.64	90.64	18.18	85.91	99.95	55.03	9.61
Na	0.36	376.67	285.94	799.52	279.49	415.88	510.07	474.76	158.60
P	0.24	0.43	0.35	0.49	0.38	0.36	0.47	0.47	0.73

S	0.57	36.29	180.51	229.27	26.74	270.35	294.79	159.35	17.15
Si	0.39	5.21	2.98	21.06	3.68	4.20	18.39	14.23	23.82
Sr	0.19	0.28	0.67	0.79	0.32	0.69	1.10	0.75	0.28
As	0.000	0.017	0.017	0.025	0.022	0.023	0.036	0.037	0.032
Cd	0.000	0.001	0.001	0.001	0.001	0.001	0.001	0.001	0.001
Co	0.000	0.001	0.001	0.000	0.002	0.002	0.001	0.001	0.000
Cr	0.000	0.002	0.001	0.001	0.009	0.001	0.002	0.003	0.002
Cu	0.000	0.030	0.011	0.020	0.020	0.023	0.023	0.021	0.018
Fe	0.00	0.61	0.18	0.20	4.21	0.16	0.20	0.61	0.58
Mn	0.00	0.01	0.25	0.31	0.11	0.52	0.16	0.14	0.02
Mo	0.000	0.014	0.008	0.011	0.004	0.004	0.004	0.013	0.007
Ni	0.000	0.005	0.004	0.006	0.007	0.006	0.006	0.005	0.002
Pb	0.000	0.009	0.006	0.007	0.009	0.006	0.006	0.006	0.006
Sb		0.002	0.001	0.002	0.001	0.001	0.001	0.002	0.001
Se	0.000	0.010	0.003	0.004	0.001	0.004	0.005	0.003	0.000
Ti	0.000	0.025	0.005	0.007	0.317	0.006	0.010	0.030	0.030
Tl	0.000	0.007	0.004	0.004	0.004	0.004	0.003	0.003	0.003
V	0.000	0.006	0.012	0.016	0.029	0.016	0.022	0.035	0.020
Zn	0.000	0.010	0.008	0.013	0.014	0.018	0.015	0.010	0.014
Cl^-	0.58	563.86	452.76	1,281.18	438.09	671.18	823.93	716.98	255.59
NO_3^-	0.00	0.44	0.20	0.48	0.11	0.17	0.17	0.14	0.09
PO_4^{3-}	0.00	1.33	1.20	1.88	1.24	1.18	1.50	1.55	2.60
SO_4^{2-}	0.00	118.55	591.71	755.52	85.04	945.83	971.29	464.71	54.38
DIC	0.06	25.09	14.69	14.89	18.01	10.54	19.90	22.42	29.40
DOC	0.44	14.97	11.62	11.88	10.59	18.19	15.14	14.33	10.52
pH	6.41	8.73	8.51	8.35	8.44	7.25	8.42	8.60	8.78

Sample ID	KA-19	KA-20	KA-21	Geometric mean	Std dev
Al	0.06	0.05	0.10	0.10	0.28
B	1.34	2.71	4.38	2.69	2.38
Ba	0.03	0.04	0.05	0.04	0.01
Ca	140.12	82.13	126.46	64.40	52.21
K	25.00	31.62	34.60	23.27	8.95
Mg	70.65	49.12	93.78	44.91	33.52
Na	304.84	376.26	415.21	370.96	165.46
P	0.40	0.36	0.39	0.43	0.11
S	252.91	142.33	254.05	120.81	102.88
Si	3.58	4.94	9.42	7.65	7.84
Sr	1.05	0.63	0.90	0.61	0.29
As	0.019	0.025	0.026	0.025	0.007
Cd	0.000	0.001	0.001	0.001	0.000
Co	0.000	0.001	0.001	0.001	0.000

Cr	0.001	0.002	0.003	0.002	0.002
Cu	0.011	0.017	0.015	0.018	0.006
Fe	0.21	0.28	0.28	0.37	1.18
Mn	0.02	0.11	0.10	0.09	0.15
Mo	0.006	0.008	0.007	0.007	0.003
Ni	0.004	0.004	0.005	0.005	0.001
Pb	0.006	0.006	0.006	0.007	0.001
Sb	0.001	0.001	0.001	0.001	0.000
Se	0.004	0.003	0.002	0.002	0.002
Ti	0.007	0.006	0.006	0.014	0.092
Tl	0.003	0.003	0.004	0.004	0.001
V	0.014	0.019	0.017	0.017	0.008
Zn	0.010	0.011	0.010	0.012	0.003
Cl^-	455.91	593.89	662.48	582.19	267.65
NO_3^-	0.25	0.19	0.32	0.20	0.13
PO_4^{3-}	1.28	1.09	1.22	1.41	0.44
SO_4^{2-}	836.15	434.48	836.62	390.06	347.94
DIC	13.31	17.30	15.94	17.60	5.53
DOC	10.32	11.65	14.37	12.84	2.51
pH	8.38	8.43	8.48	8.39	0.40

Table C7: Bioaccumulation factors (BAFs)

Calculated bioaccumulation factors (BAFs) of shrimp/water element concentrations. Elements included when there was not a significant abundance of missing values due to concentrations <MDL.

Sample	KA-12	KA-13	KA-14	KA-15	KA-16	KA-17	KA-18
Al	267.5	319.8	1067.8	100.4	354.5	389.7	327.3
B	0.6	0.5	0.4	0.6	0.6	1.5	2.2
Ba	2.3	4.8	9.7	3.0	3.8	3.1	3.6
Ca	5.5	17.5	27.3	5.9	7.2	4.9	8.7
K	37.3	33.0	39.8	36.0	32.9	29.2	84.6
Mg	1.7	1.9	2.1	2.0	1.9	1.5	4.1
Na	1.0	0.7	0.8	0.7	0.6	0.6	1.7
P	203186.5	146028.9	290195.1	193950.8	152577.3	232732.8	132259.5
Si	442.0	742.9	561.0	524.8	1166.5	354.0	265.2
Sr	2.9	7.3	10.1	3.2	3.7	2.8	5.4
Cu	1656.0	6277.8	7322.8	5214.7	7323.1	6405.6	14387.5
Mn	177.9	315.6	2332.1	382.1	429.9	277.2	262.3

S	16.8	10.9	19.9	13.2	12.6	14.7	46.2
Zn	5469.7	14591.0	11662.9	10325.1	11222.3	6177.6	13327.5
Tl[a]	94254.8	90288.8	9575.6		106357.6	35155.8	87878.5

Sample	KA-19	KA-20	KA-21	Geometric mean	Std dev
Al	319.5	224.2	417.7	323.1	258.3
B	0.8	1.1	1.3	0.8	0.6
Ba	7.0	3.5	3.4	4.0	2.2
Ca	22.9	7.9	6.0	9.4	8.1
K	68.9	29.3	40.6	40.5	18.5
Mg	3.1	1.7	2.0	2.1	0.8
Na	1.8	0.6	0.5	0.8	0.5
P	30360.6	204297.5	381990.1	168621.0	94760.0
Si	695.2	234.3	421.5	485.5	276.0
Sr	11.0	5.0	3.0	4.8	3.1
Cu	3013.9	3700.5	12012.6	5695.1	3924.1
Mn	593.3	595.8	22.9	323.8	654.0
S	36.9	9.6	15.5	17.2	12.1
Zn	15423.3	10942.1	12270.6	10628.1	3233.2
Tl[a]	45438.7	50934.0	25038.1	48737.7	34804.4

[a]Based on Tl water method detection limit (MDL) of 0.0001 mg/L.

Table C8: Average water concentration (mg/L) and log10 Kd (L/kg) values for shrimp, sediment, and feed

Kd values (partition coefficients) between mean solid-phase element concentrations in feed, sediment, and shrimp over mean water element concentrations. Bioaccumulation factor is the same as the Kd value of shrimp/water. The method detection limit (MDL) was inserted for Tl in water.

Elements	Shrimp/water	1σ upper limit	1σ lower limit	Sediment/water	1σ upper limit	1σ lower limit
Al	2.51	2.79	1.76	5.93	5.99	5.87
V	1.58	1.66	1.52	3.66	3.80	3.52
Zn	4.04	4.29	3.86	3.85	4.19	3.55
Cr				4.35	4.48	4.23
Ni				4.05	4.47	3.74
Co				4.71	4.86	4.57
Cu	3.74	4.06	3.39	4.02	4.25	3.83
Ba	0.61	0.89	0.17	3.33	3.44	3.23
Mn	2.52			5.04		4.17

K	1.60	1.79	1.44	1.99	2.18	1.84
Si	2.70	3.09	2.43	5.27	5.61	5.04
Ca	0.96	1.35	-0.08	1.67	1.91	1.39
Sr	0.67	1.01	0.18	1.38	1.57	1.21
Na	-0.10	0.13	-0.32	0.30	0.49	0.12
Mg	0.31	0.49	0.16	1.42	1.61	1.26
As				2.62	2.83	2.40
Se	1.45	1.59	1.34	2.37	2.91	
B	-0.09	0.22	-0.53			
S	1.22	1.46	1.02	0.01	0.24	-0.19
P	5.22		4.82	4.09		3.67
Tl	4.69	4.92	4.14			

Elements	Feed/water	Mean water	1σ
Al	3.05	0.09	0.00
V	1.64	0.02	0.00
Zn	4.20	0.00	0.00
Cr	2.97	0.00	0.00
Ni	2.06	0.00	0.00
Co		0.00	0.00
Cu	3.98	0.01	0.00
Ba	1.40	0.23	0.04
Mn	4.19	0.01	0.02
K	1.54	267.87	81.04
Si	2.88	1.36	0.69
Ca	1.52	213.02	45.56
Sr	0.70	3.69	1.01
Na	-0.42	5408.15	1430.20
Mg	0.61	579.72	162.96
As		0.03	0.01
Se	2.40	0.03	0.01
B	0.65	2.80	0.67
S	1.40	427.70	135.02
P	5.30	0.04	0.06
Tl	4.54	0.00	

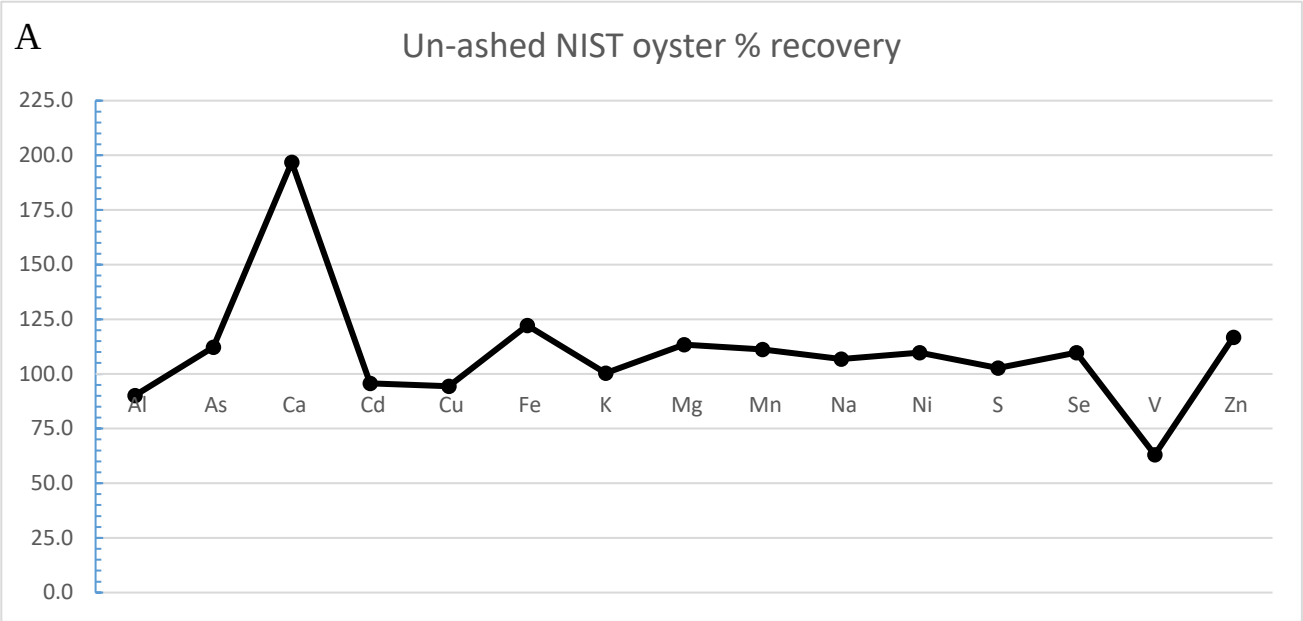

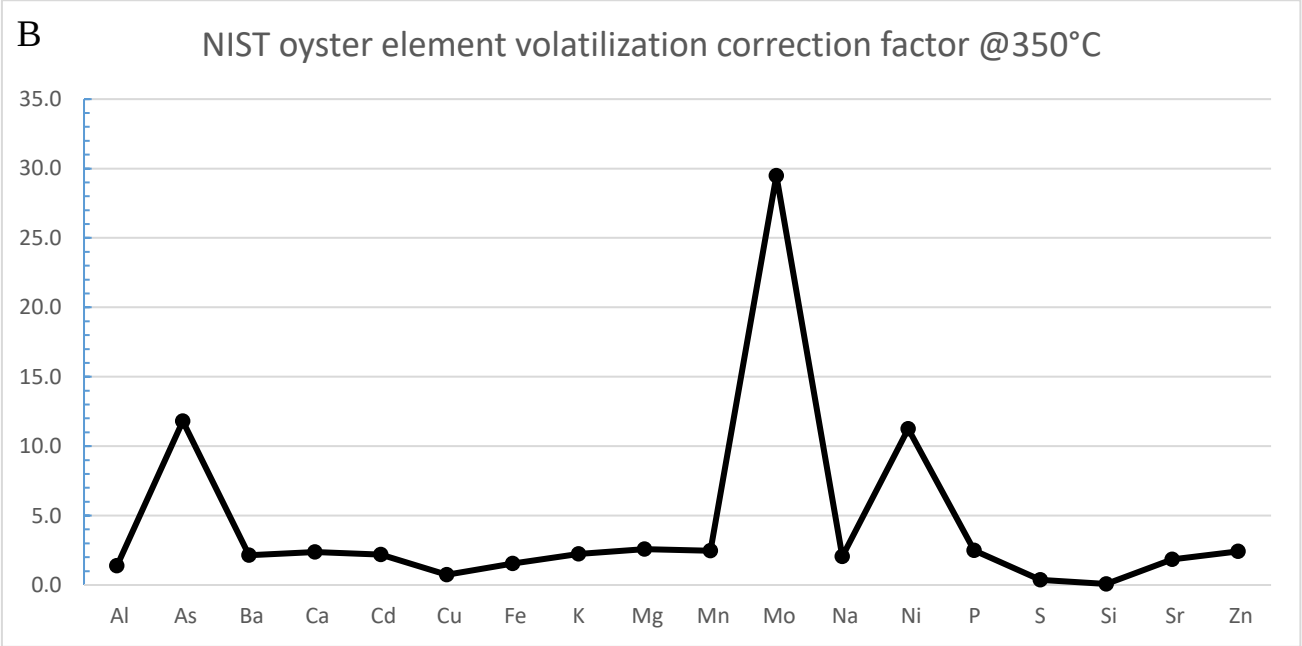

Figure C1: NIST 1566b – Oyster Tissue reference material % recovery for un-ashed material on the ICP-OES (A), and the "volatilization correction factor" of the reference material's element concentrations in ashed/un-ashed sample type (B). Several elements that were <MDL in either the ashed or unashed oyster tissue did not have volatilization correction factors calculated, although it is important to note that Sb, Se, B, and V underwent significant volatilization while Co and Li were concentrated in ash significantly enough to raise concentrations >MDL.

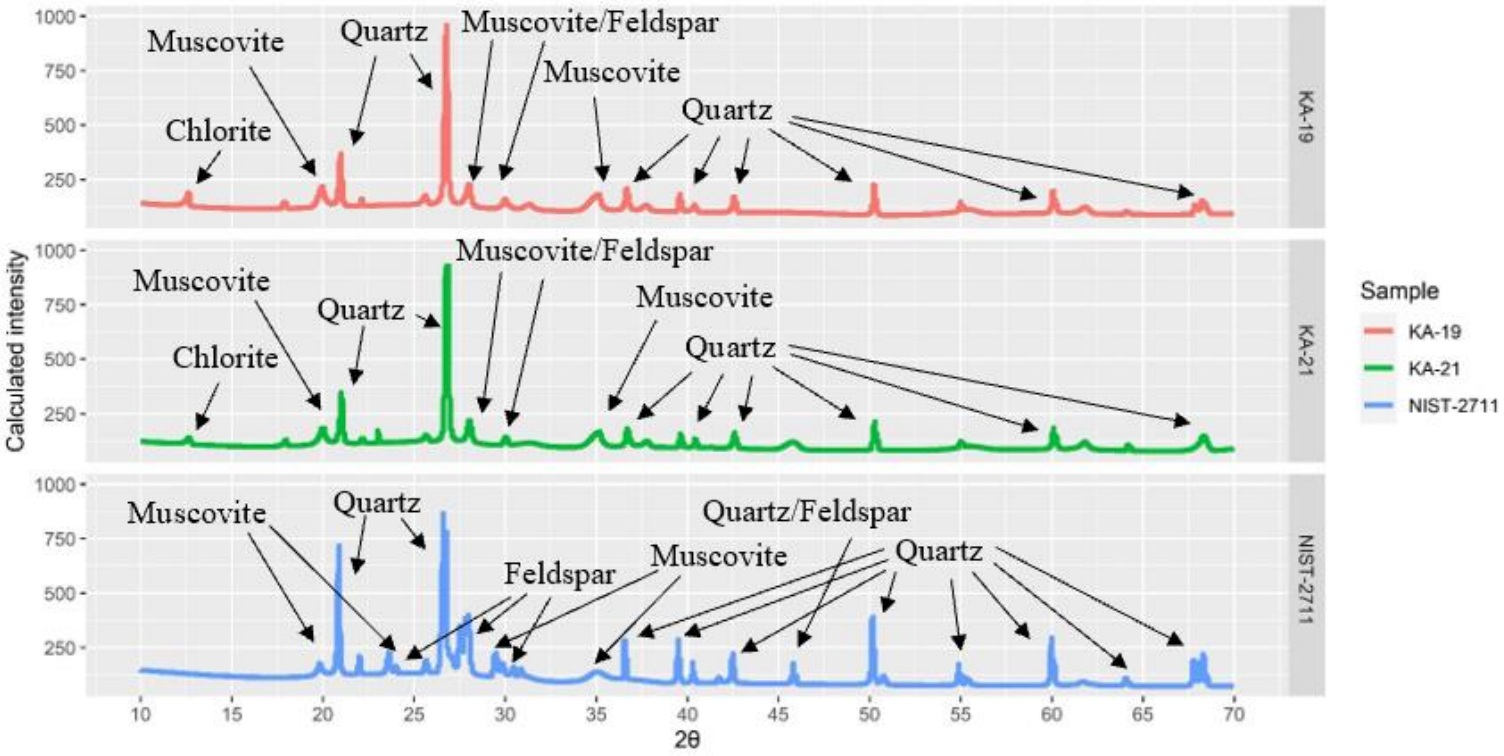

Figure C2: Powder XRD Rietveld method calculated intensities (y-axis truncated for better visualization) for two May shrimp pond sediment samples and the NIST 2711 Montana soil standard. Major minerals corresponding with diffraction peaks are also indicated. Phyllosilicates are difficult to differentiate with powder XRD, but the general presence/predominance of Al-Si sheet minerals and quartz in all three samples is likely. 2θ range was 10°-70°, with measurements every 0.01°.

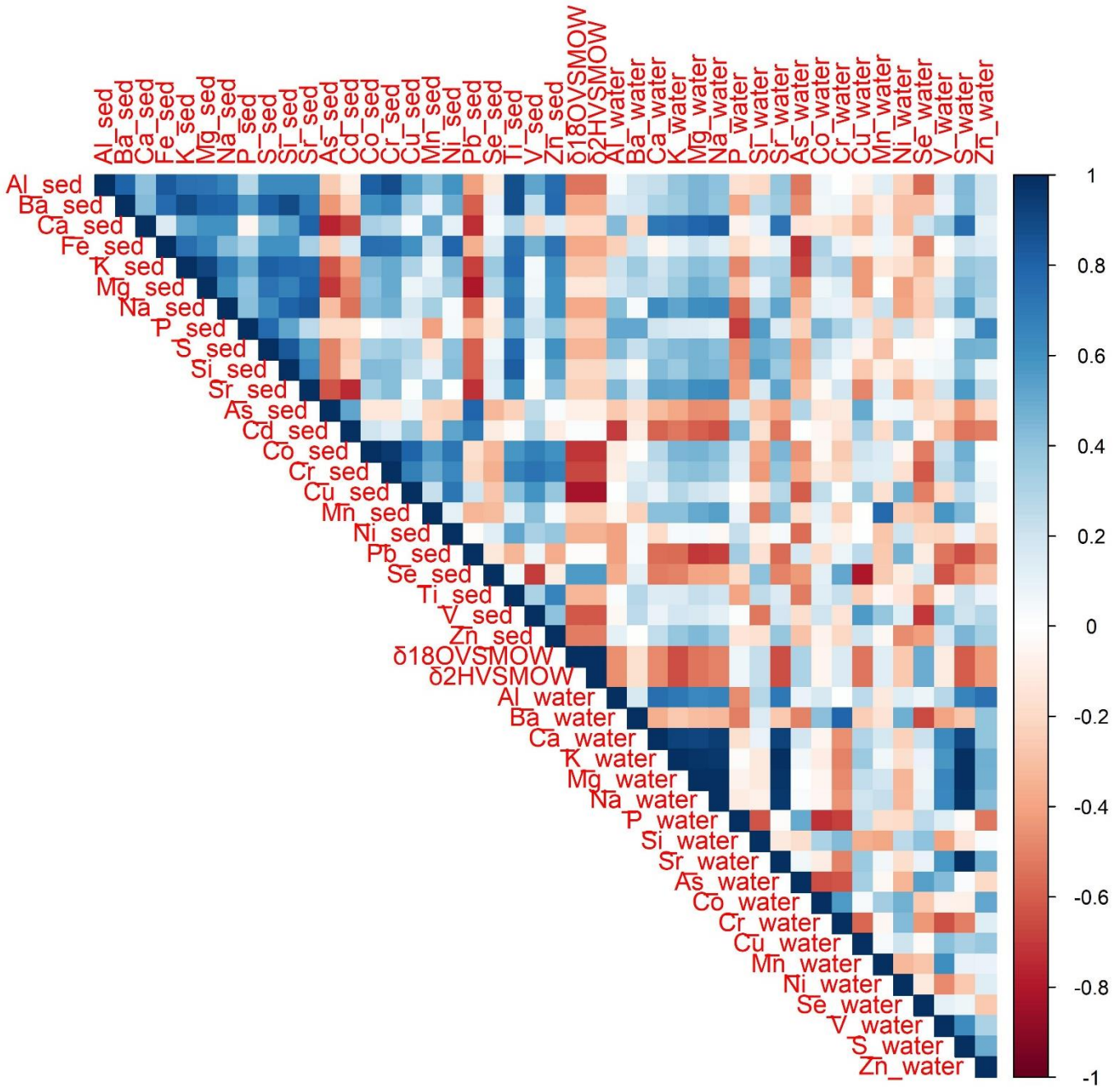

Figure C3: Spearman correlation coefficient matrix for paired water and volatilization corrected sediment data in shrimp ponds.

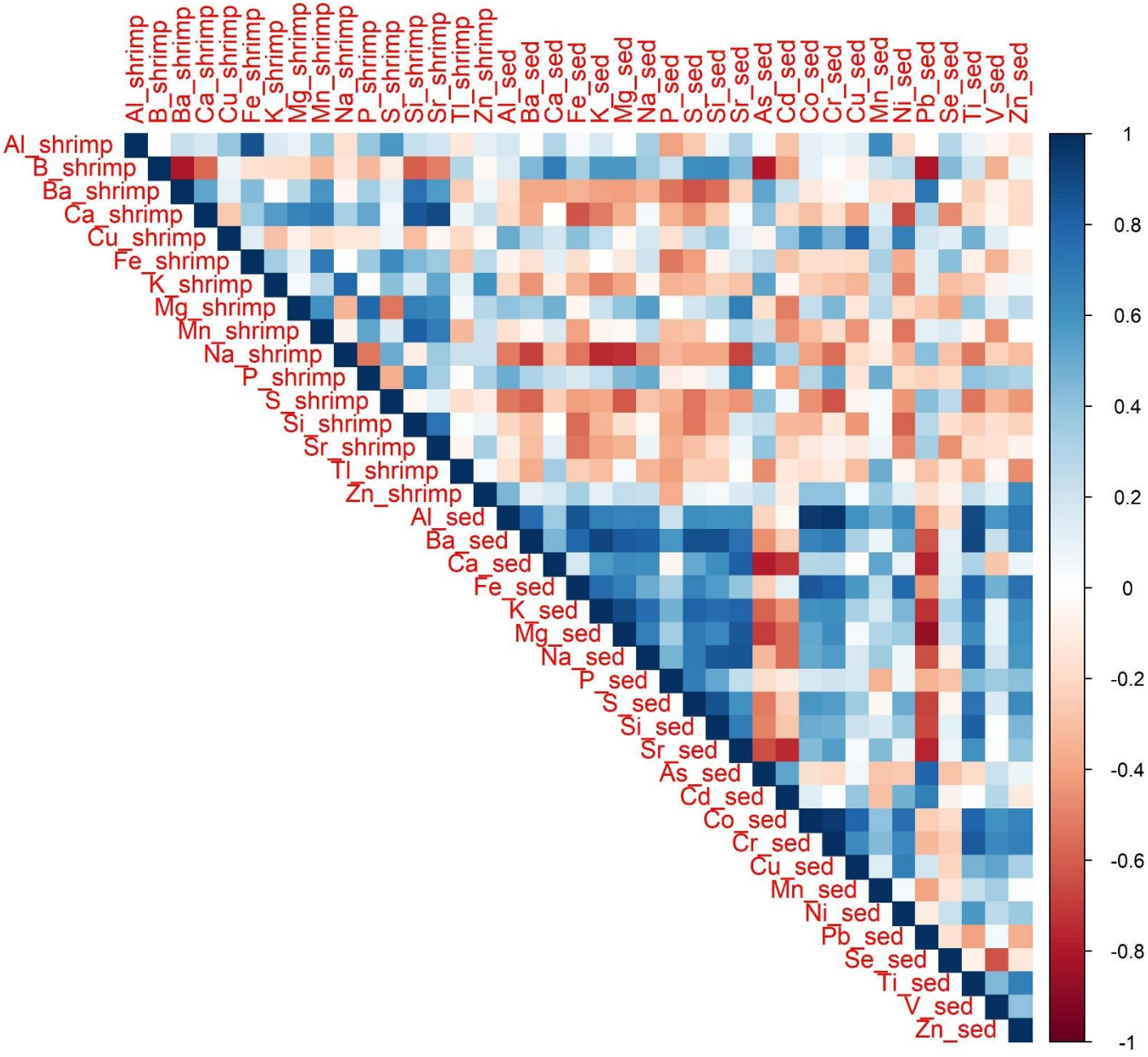

Figure C4: Spearman correlation coefficient matrix for paired shrimp and volatilization corrected sediment data in shrimp ponds. KA-13U (submerged sediment sample) was paired with shrimp sample KA-13.

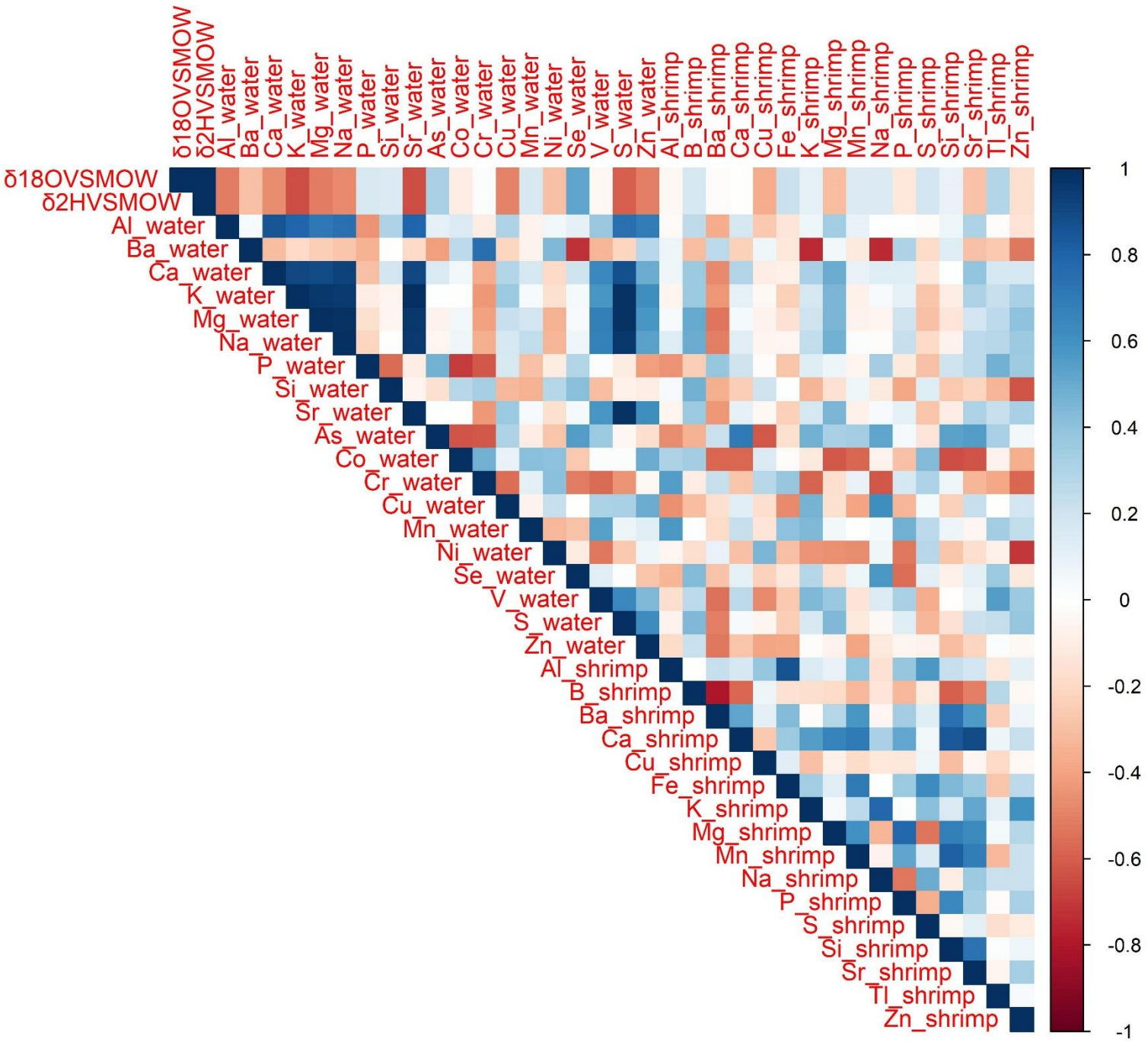

Figure C5: Spearman correlation coefficient matrix for paired shrimp and water data in shrimp ponds.

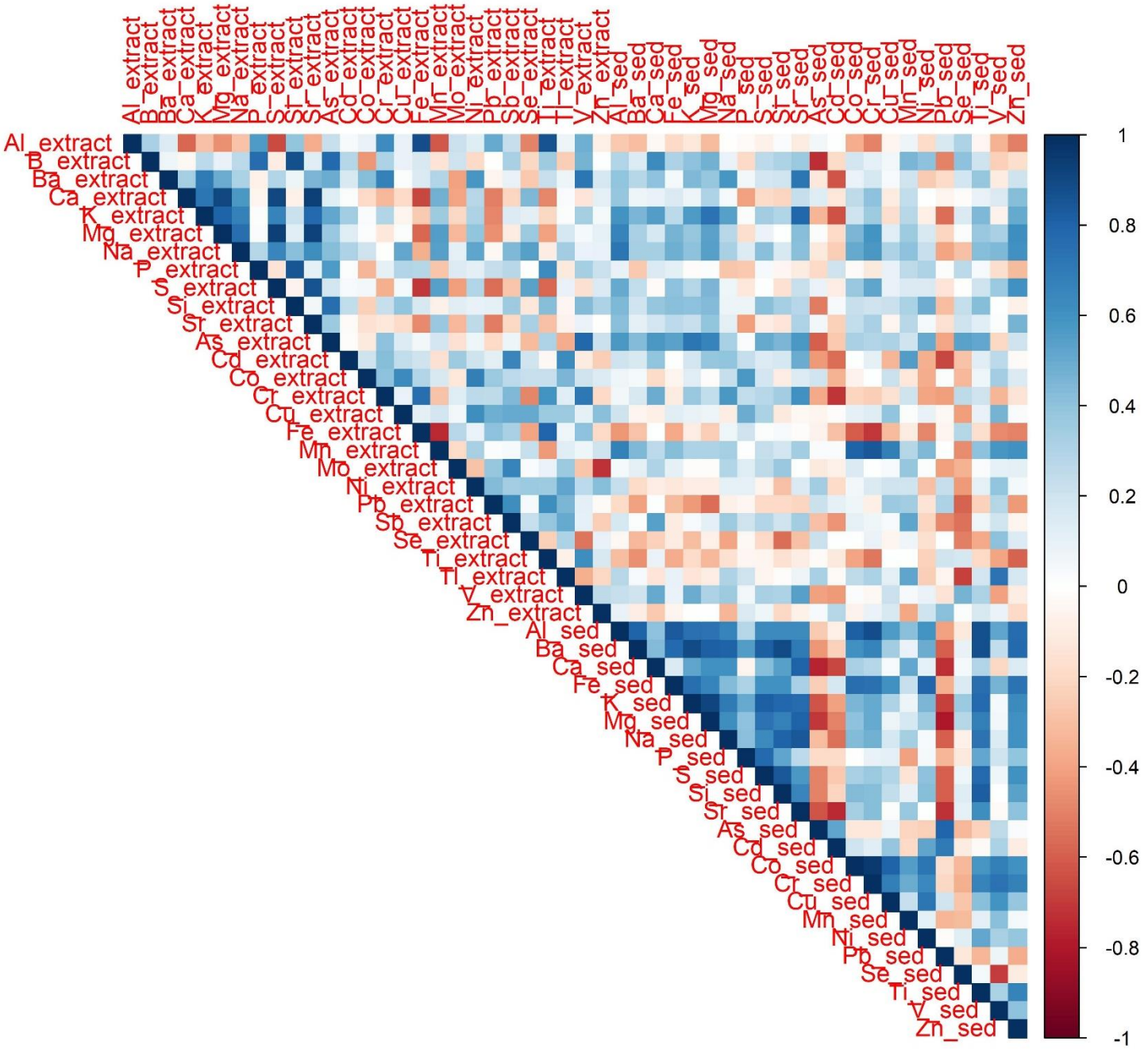

Figure C6: Spearman correlation coefficient matrix between 24-hr sediment batch extract element concentrations and volatilization corrected sediment element concentrations in paired samples.

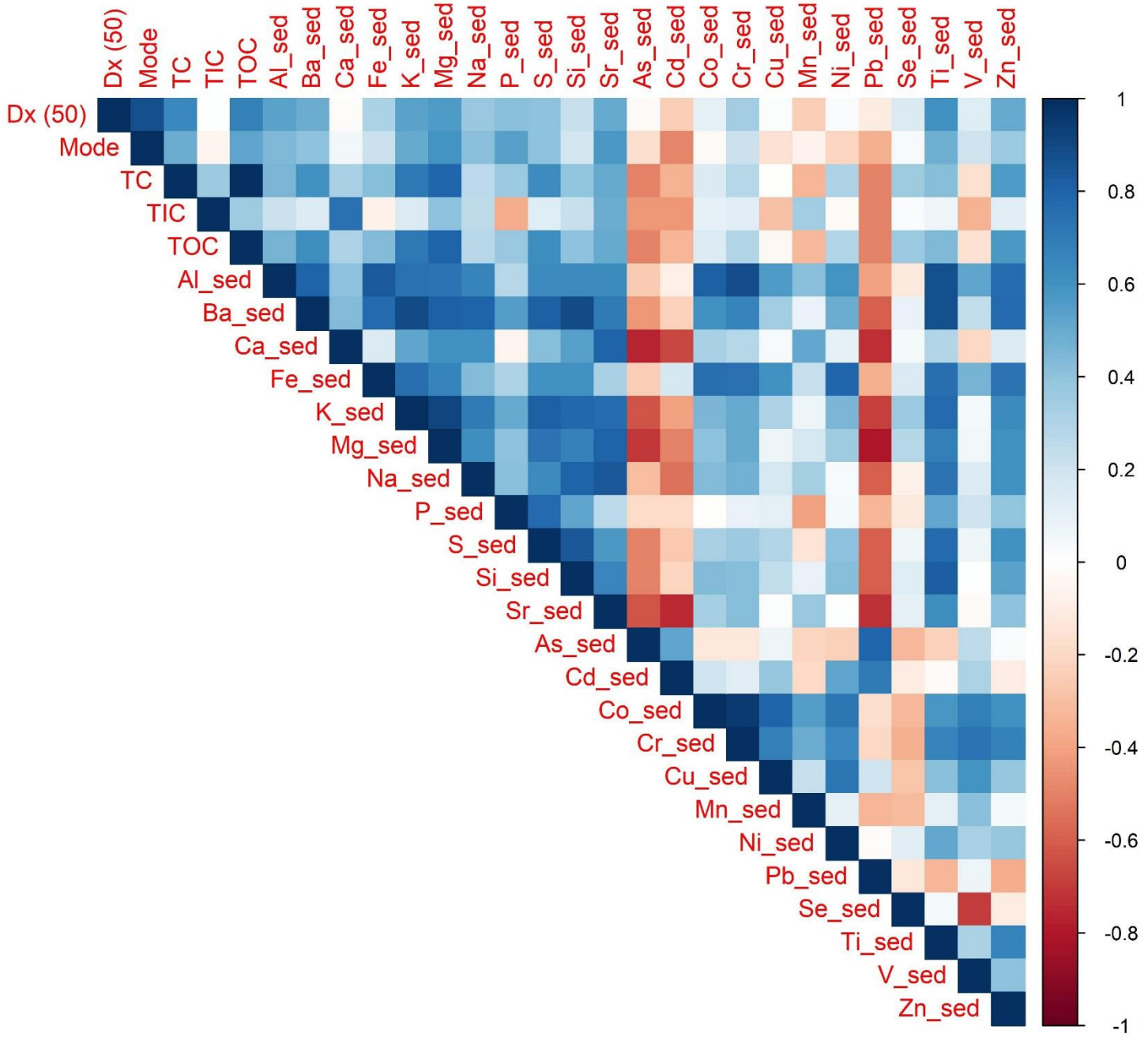

Figure C7: Spearman correlation coefficient matrix for select paired sediment data (volatilization corrected element values) in shrimp ponds, including median grain size in µm [Dx (50)], mode grain size in µm (Mode), total % carbon (TC), total % inorganic carbon (TIC), and total % organic carbon (TOC).

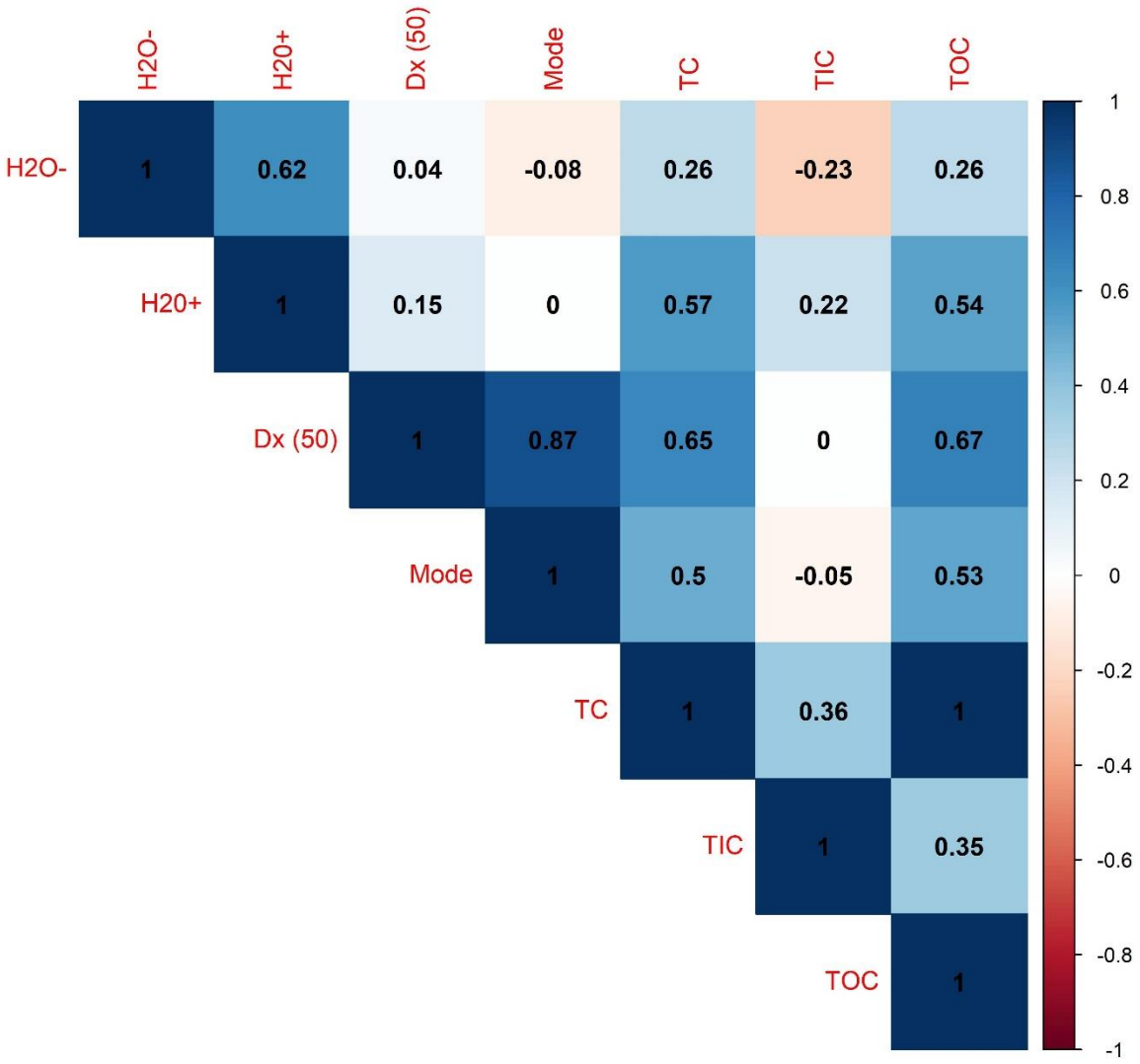

Figure C8: Spearman correlation coefficient matrix for select paired sediment data in shrimp ponds, including median grain size in µm [Dx (50)], mode grain size in µm (Mode), total % carbon (TC), total % inorganic carbon (TIC), and total % organic carbon (TOC), adsorbed water content (H2O-), and structural water content (H2O+).

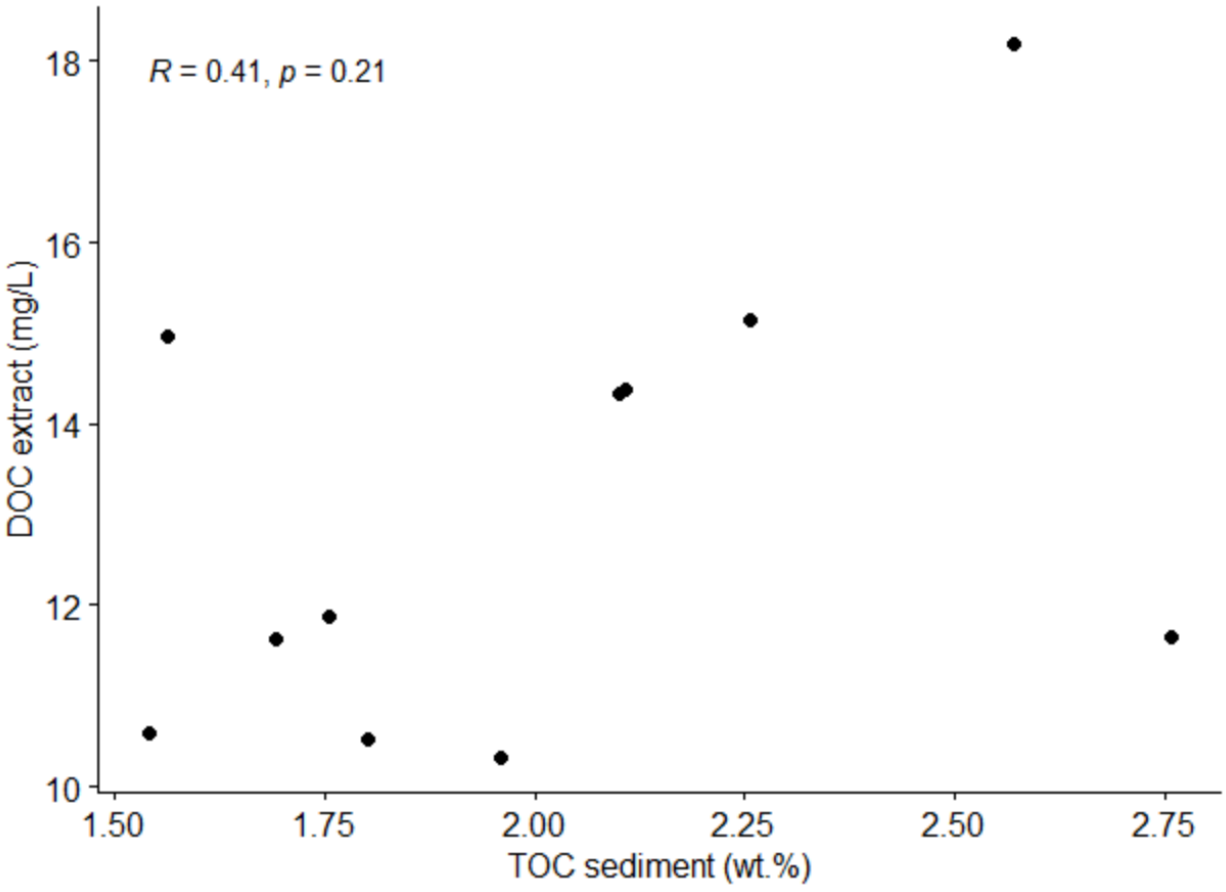

Figure C9: Bivariate comparison between total organic carbon (TOC) in the solid sediment samples and the dissolved organic carbon (DOC) in the 24-hr sediment extract samples. The Spearman correlation coefficient and p-value are provided.

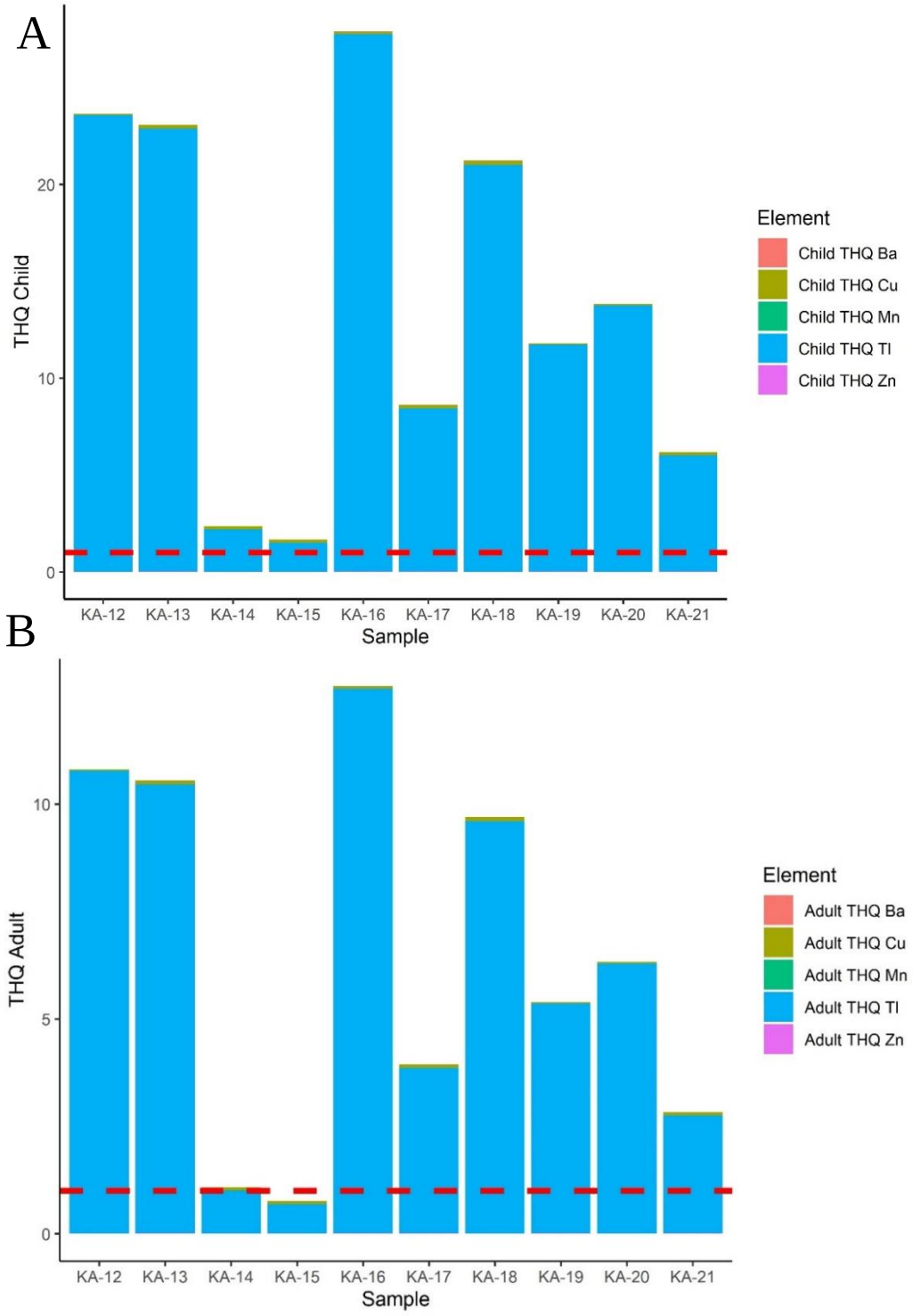

Figure C10: Target hazard quotient (THQ) values for each shrimp sample for each element of health concern in children (A) and adults (B). Thallium makes up the vast proportion of calculated health risk. The horizontal dotted red line represents a THQ value of 1, above which adverse health effects are more likely to occur. The stacked THQ values of all metals combined represents the total THQ, although Tl is clearly the element of greatest THQ contribution.

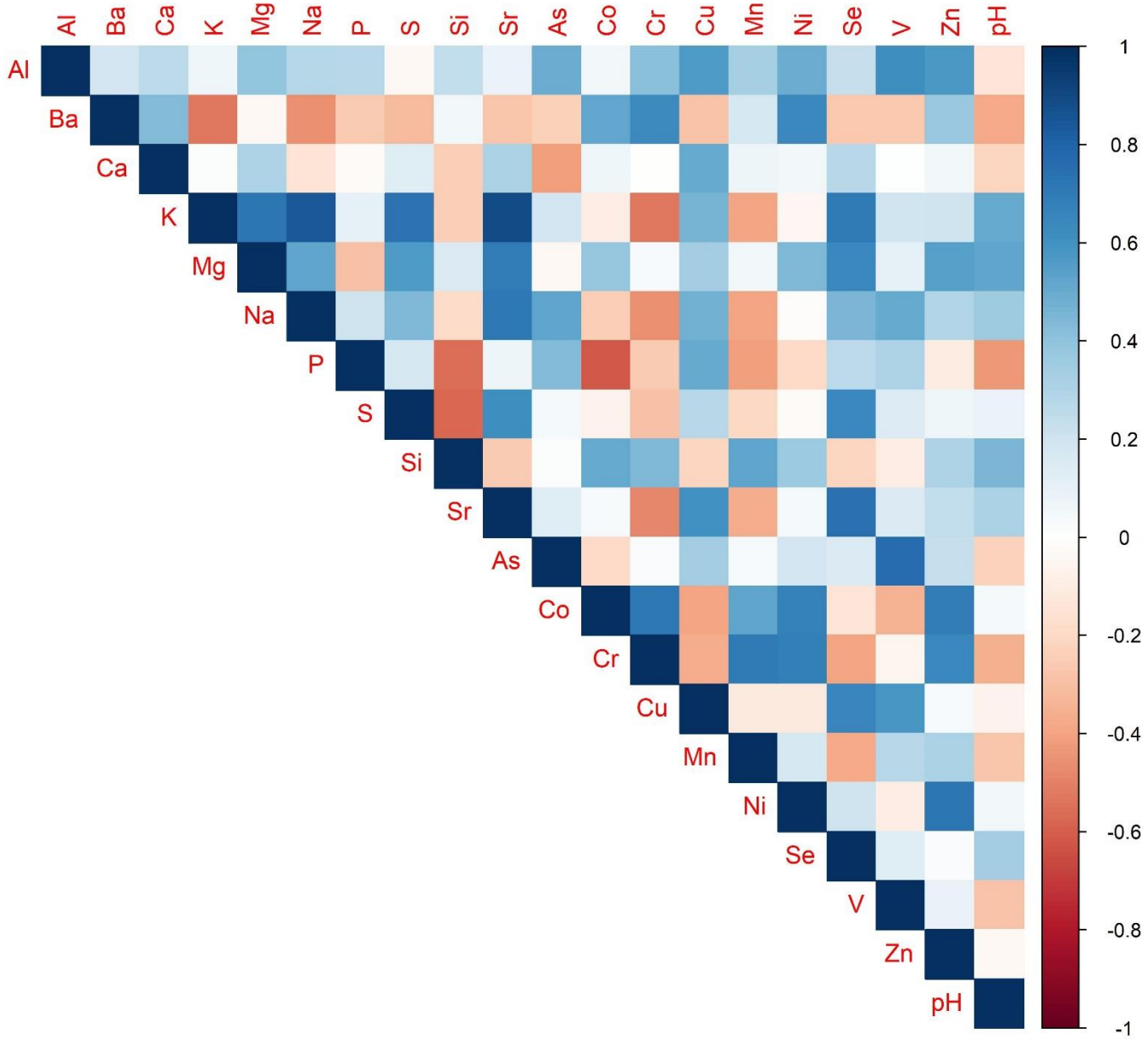

Figure C11: Spearman correlation coefficient matrix between pond sediment Kd values and pond water pH.

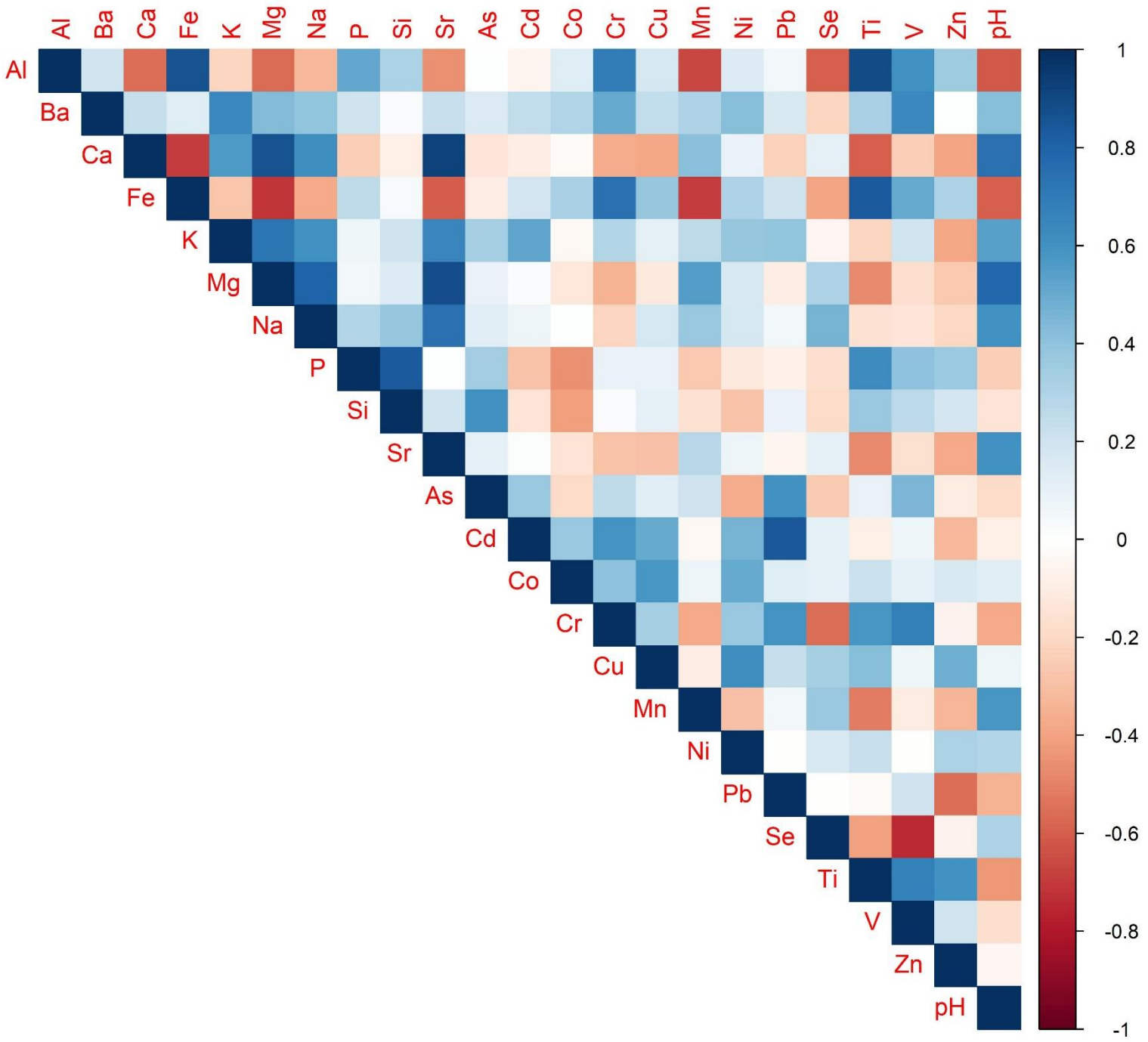

Figure C12: Spearman correlation coefficient matrix between 24-hr sediment batch extract Kd values and filtered extract pH. S and Sb excluded because of missing values.

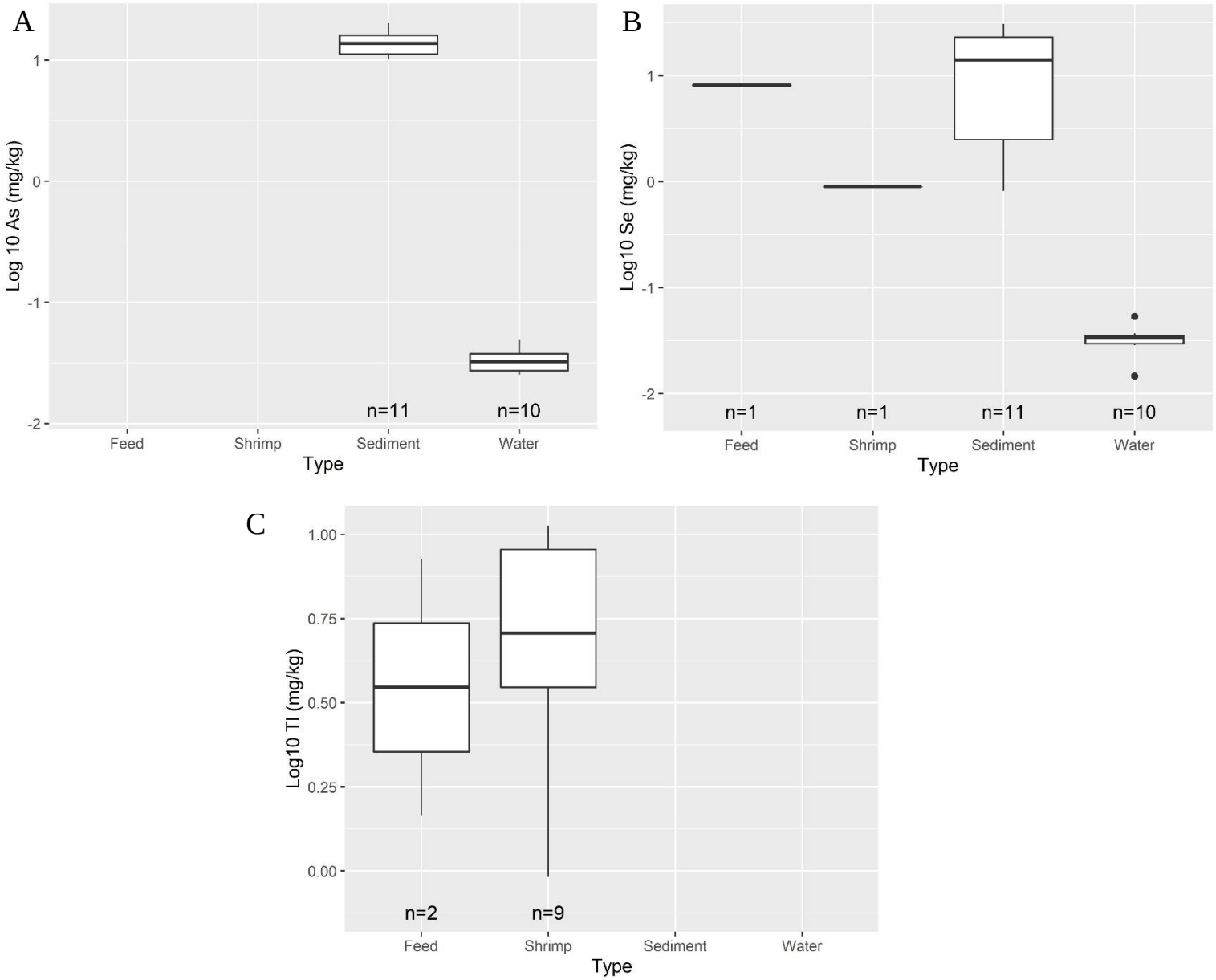

Figure C13: Concentrations of (A) As, (B) Se, and (C) Tl in different pond media shown through box and whisker plots. Concentrations <MDL and those not reported (because of nearly all values <MDL in water and sediment) were omitted.